DESIGN OF RAILWAY POWER CONDITIONER IN AUTOTRANSFORMER-FED TRACTION POWER SUPPLY SYSTEM

Kritsada Mongkoldee

A Thesis Submitted in Partial Fulfillment of the Requirements for the Degree of Doctor of Philosophy in Electrical Engineering

Suranaree University of Technology

Academic Year 2020

การออกแบบอุปกรณ์ปรับสภาพกำลังไฟฟ้าในระบบจ่ายไฟฟ้าขับเคลื่อนแบบหม้อแปลงออโตสำหรับรถไฟ

นายกฤษดา มงคลดี

วิทยานิพนธ์นี้เป็นส่วนหนึ่งของการศึกษาตามหลักสูตรปริญญาวิศวกรรมศาสตรดุษฎีบัณฑิต
สาขาวิชาวิศวกรรมไฟฟ้า
มหาวิทยาลัยเทคโนโลยีสุรนารี
ปีการศึกษา 2563

DESIGN OF RAILWAY POWER CONDITIONER IN AUTOTRANSFORMER-FED TRACTION POWER SUPPLY SYSTEM

Suranaree University of Technology has approved this thesis submitted in partial fulfillment of the requirements for the Degree of Doctor of Philosophy.

Thesis Examining Committee

(Assoc. Prof. Dr.Mongkol Konghirun)

Chairperson

(Assoc. Prof. Dr.Thanatchai Kulworawanichpong)

Member (Thesis Advisor)

(Prof. Wg. Cdr. Dr.Sarawut Sujitjorn)

Member

(Assoc. Prof. Dr.Keerati Chayakulkeeree)

Member

(Dr.Tosaphol Ratniyomchai)

Member

(Assoc. Prof. Flt. Lt. Dr.Kontorn Chamniprasart)

Vice Rector for Academic Affairs

and Internationalization

(Assoc. Prof. Dr.Pornsiri Jongkol)

Dean of Institute of Engineering

กฤษดา มงคลดี : การออกแบบอุปกรณ์ปรับสภาพกำลังไฟฟ้าในระบบจ่ายไฟฟ้าขับเคลื่อนแบบหม้อแปลงออโตสำหรับรถไฟ (DESIGN OF RAILWAY POWER CONDITIONER IN AUTOTRANSFORMER-FED TRACTION POWER SUPPLY SYSTEM) อาจารย์ที่ปรึกษา : รองศาสตราจารย์ ดร.ธนัดชัย กุลวรวานิชพงษ์, 312 หน้า.

ปัญหาคุณภาพกำลังไฟฟ้า เช่น ความไม่สมดุลแรงดันไฟฟ้า ในระบบจ่ายไฟฟ้ากระแสสลับสำหรับรถไฟมักเกิดขึ้นจากการรับไฟฟ้าจากแหล่งจ่ายไฟฟ้าสามเฟสที่มีค่ากำลังไฟฟ้าลัดวงจรต่ำเมื่อเทียบกับโหลด ดังนั้น อุปกรณ์ปรับสภาพกำลังไฟฟ้า (Railway Power Conditioner: RPC) จึงมีความจำเป็นและการติดตั้งอุปกรณ์ดังกล่าวยังคุ้มค่ากว่าการสร้างระบบจ่ายไฟฟ้าใหม่ เนื่องจากอุปกรณ์ปรับสภาพกำลังไฟฟ้ามีราคาสูง การเลือกขนาดที่เหมาะสมกับระบบจะสามารถช่วยลดค่าใช้จ่ายได้มาก นอกจากนี้แบบจำลองในคอมพิวเตอร์ของอุปกรณ์ดังกล่าวยังมีความสำคัญต่อการออกแบบและการดำเนินงาน งานวิจัยนี้จึงศึกษาและนำเสนอกระบวนการหาขนาดที่เหมาะสมที่สุดของอุปกรณ์ปรับสภาพกำลังไฟฟ้าโดยใช้วิธีการหาค่าเหมาะสมที่สุดแบบกลุ่มอนุภาค (Particle Swarm Optimisation: PSO) และหลักการชดเชยบางส่วน (partial compensation) รวมถึงใช้วิธีการหาค่าเหมาะสมที่สุดแบบวิธีเชิงพันธุกรรม (Genetic Algorithm: GA) เพื่อการเปรียบเทียบ สร้างแบบจำลองทางคณิตศาสตร์ของอุปกรณ์ปรับสภาพกำลังไฟฟ้าและอุปกรณ์อื่น ๆ สำหรับระบบจ่ายไฟฟ้าแบบหม้อแปลงออโตโดยใช้วิธีการคำนวณการไหลกำลังไฟฟ้าแบบนิวตันราฟสันที่ใช้กระแสเป็นฐาน (current-based Newton-Raphson power flow calculation) และศึกษาการนำหม้อแปลงออโตแบบปรับแท็ปได้มาใช้ในระบบจ่ายไฟฟ้าของรถไฟ การศึกษานี้ใช้รถไฟฟ้าสายตะวันออกที่วิ่งให้บริการในเมืองเดนเวอร์ รัฐโคโลราโด ประเทศสหรัฐอเมริกา เป็นกรณีศึกษา

วิธีการหาขนาดเหมาะสมที่สุดของ RPC ที่นำเสนอสามารถหาขนาดพิกัดและจุดทำงานของ RPC ในกรณีศึกษาที่ใช้ข้อมูลระบบจ่ายไฟฟ้าขับเคลื่อนและการทำงานของรถไฟจากรถไฟฟ้าสายตะวันออก (East Corridor Line) ในเมืองเดนเวอร์ รัฐโคโลราโด ประเทศสหรัฐอเมริกา ได้อย่างมีประสิทธิผล ผลลัพธ์ที่ได้แสดงให้เห็นว่า วิธีการที่นำเสนอสามารถลดขนาดของ RPC เมื่อเทียบกับพิกัดการชดเชยแบบสมบูรณ์ (full compensation capacity) ได้ร้อยละ 15 ในกรณีตัวประกอบกำลังเป้าหมายเท่ากับ 0.95 และลดได้ถึงร้อยละ 25 ในกรณีตัวประกอบกำลังเป้าหมายเท่ากับ 0.90 ทั้งกรณีที่ใช้กับหม้อแปลงแบบวีและหม้อแปลงแบบสกอตต์ ส่วนตัวประกอบความไม่สมดุลแรงดันไฟฟ้าหลังการชดเชยได้รับการปรับปรุงให้มีค่าไม่เกินร้อยละ 2 ดังนั้น ขนาดที่เหมาะสมที่สุดที่หาได้จึงสามารถนำไปใช้เป็นแนวทางในการเลือกพิกัดติดตั้งของ RPC ในสถานีไฟฟ้าขับเคลื่อนได้

นอกจากนี้ ผลลัพธ์จากการศึกษาการใช้หม้อแปลงออโตแบบปรับแท็ปได้ในระบบจ่ายไฟฟ้าสำหรับรถไฟแสดงให้เห็นว่า การปรับแท็ปหม้อแปลงออโตพร้อมกันทุกลูกตลอดช่วงการจ่ายไฟจะก่อให้เกิดกำลังไฟฟ้าสูญเสียมากขึ้นในทุกกรณี ถึงแม้ว่าการปรับแท็ปที่เหมาะสมที่สุดในแต่ละหม้อแปลงออโตจะสามารถลดกำลังสูญเสียและความไม่สมดุลแรงดันไฟฟ้าให้น้อยที่สุด และเพิ่มตัวประกอบกำลังให้มากที่สุดได้ แต่ปริมาณที่ได้นั้นอยู่ในระดับที่น้อยมาก ด้วยเหตุนั้น แนวคิดการประยุกต์ใช้การปรับแท็ปของหม้อแปลงออโตจึงมีความเป็นไปได้ยากและอาจไม่คุ้มกับการลงทุน

สาขาวิชา วิศวกรรมไฟฟ้า

ปีการศึกษา 2563

ลายมือชื่อนักศึกษา ______

ลายมือชื่ออาจารย์ที่ปรึกษา ______

KRITSADA MONGKOLDEE : DESIGN OF RAILWAY POWER CONDITIONER IN AUTOTRANSFORMER-FED TRACTION POWER SUPPLY SYSTEM. THESIS ADVISOR : ASSOC. PROF. DR.THANATCHAI KULWORAWANICHPONG, Ph.D., 312 PP.

RAILWAY POWER CONDITIONER/ CURRENT-BASED NEWTON-RAPHSON POWER FLOW METHOD/ AUTOTRANSFORMER-FED TRACTION POWER SUPPLY SYSTEM

Power quality problems such as voltage unbalance in AC traction power supply arises mostly when a traction system is fed from a weak power supply. Therefore, a railway power conditioner (RPC) is one of the best solutions, which is very necessary and more economical than building a new supply system. With the high cost of the RPC, selection of a suitable rating of the RPC will significantly help reduce its cost. Also, its computer simulation model is very essential for design and operation. This thesis studies and proposes an approach to optimally size the RPC, using Particle Swarm Optimisation (PSO) and the partial compensation principle. The Genetic Algorithm optimisation (GA) is also adopted in the study case for comparison. The mathematical models of traction equipment and the RPC are created for an autotransformer (AT)-fed power supply system, using the current-based Newton-Raphson power flow method. In addition, the incorporation of tap-changing ATs into the system is investigated. The East Corridor line in Denver, Colorado, USA, is adopted as a simulation case study.

The proposed optimal RPC sizing procedure could effectively find the RPC optimal sizes and the corresponding operation points in the case study, which adopted the traction power supply system and train operation of the East Corridor Line in Denver, Colorado, USA. The results show that the optimal RPC capacity in both V/V and Scott transformer cases, compared to the full compensation capacity, could be reduced by about 15 percent with targeted power factor of 0.95 and by up to 25 percent with targeted power factor of 0.90. Also, the voltage unbalance factor after compensation was improved, i.e. not exceeding 2 percent. Therefore, the obtained optimal sizes are a guideline for the selection of RPC's installed capacity.

Additionally, the investigation of tap-changing ATs in a traction substation reveals that the simultaneous tap change of all AT in traction feeders always caused greater power loss. Even though the optimal tap change could minimise power loss and voltage unbalance, and maximise power factor, the amounts were minimal. As a result, the concept of AT tap change might not be worth investing.

School of Electrical Engineering Student's Signature ______

Academic Year 2020 Advisor's Signature ______

Acknowledgements

I wish to express my sincere appreciation to my advisor, Associate Professor Dr. Thanatchai Kulworawanichpon, who gave helpful guidance and support throughout the period of study.

The grateful thanks are given to my international collaborators or oversea advisors, Assistant Professor Dr. Fulin ZHOU and Mr. Hiroaki MORIMOTO from Southwest Jiaotong University and Railway Technical Research Institute (RTRI), respectively, for their care and essential advice during my oversea research sessions as part of the scholarship.

The author is also indebted to the Royal Golden Jubilee Ph.D. programme (RGJ-Ph.D.) for financial support which comprehensively covered all expenses.

Finally, I would like to show my gratitude to Suranaree University of Technology (SUT) as it is my second home and a place for study with many memorable experiences happened there.

Kritsada Mongkoldee

TABLE OF CONTENTS

TABLE OF CONTENTS (CONTINUED)

Page

TABLE OF CONTENTS (CONTINUED)

Page

TABLE OF CONTENTS (CONTINUED)

Page

TABLE OF CONTENTS (CONTINUED)

Page

TABLE OF CONTENTS (CONTINUED)

Page

LIST OF TABLES

Table **Page**

LIST OF TABLES (CONTINUED)

Table **Page**

LIST OF TABLES (CONTINUED)

Table **Page**

LIST OF TABLES (CONTINUED)

Table **Page**

LIST OF FIGURES

Figure **Page**

LIST OF FIGURES (CONTINUED)

Figure **Page**

LIST OF FIGURES (CONTINUED)

Figure **Page**

LIST OF FIGURES (CONTINUED)

Figure **Page**

LIST OF FIGURES (CONTINUED)

Figure **Page**

LIST OF FIGURES (CONTINUED)

Figure **Page**

LIST OF FIGURES (CONTINUED)

Figure **Page**

LIST OF FIGURES (CONTINUED)

Figure **Page**

LIST OF FIGURES (CONTINUED)

Figure **Page**

LIST OF FIGURES (CONTINUED)

Figure **Page**

LIST OF ABBREVIATIONS AND SYMBOLS

AC	=	Alternating Current
AT	=	Autotransformer
BT	=	Booster Transformer
C	=	Catenary (in an AT-fed traction power supply system)
CBNR	=	Current-Based Newton Raphson
DC	=	Direct Current
DIA	=	Denver International Airport
D-STATCOM	=	Distribution Static Synchronous Compensator
D-SVC	=	Distribution Static VAR Compensator
DUS	=	Denver Union Station
DVR	=	Dynamic Voltage Regulator
ERPC	=	Enhanced Railway Power Conditioner
F	=	Feeder (in an AT-fed traction power supply system)
FACTS	=	Flexible Alternating Current Transmission System
FC	=	Fixed Capacitor
FRSC	=	Front Range Systems Consultants
GA	=	Genetic Algorithm
HBRPC	=	Half-Bridge Railway Power Conditioner
HRPC	=	Hybrid Railway Power Conditioner
IUF	=	Current Unbalance Factor

LIST OF ABBREVIATIONS AND SYMBOLS (CONTINUED)

KCL	=	Kirchhoff's current law
M	=	Main (Main phase of Scott transformer)
MCR	=	Magnetised-Controlled Reactor
MMC	=	Modular-Multilevel Converter
PCC	=	Point of Common Coupling
PF	=	Power Factor
PSO	=	Particle Swarm Optimisation
PWM	=	Pulse Width Modulation
R	=	Running Rail (in an AT-fed traction power supply system)
RMS	=	Root Mean Square
RPC	=	Railway Power Conditioner
RTD	=	Regional Transportation District
RTRI	=	Railway Technical Research Institute (Japan)
RUPQC	=	Railway Unified Power Quality Controller
SP	=	Sectioning Post
SPWM	=	Sinusoidal Pulse Width Modulation
SRT	=	State Railway of Thailand
STATCOM	=	Static Synchronous Compensator
SVC	=	Static VAR Compensator
T	=	Teaser (Teaser phase of Scott transformer)
TCHF	=	Thyristor-Controlled High Pass Filter

LIST OF ABBREVIATIONS AND SYMBOLS (CONTINUED)

TCR	=	Thyristor-Controlled Reactor
TSC	=	Thyristor-Switched Capacitor
UPFC	=	Unified Power Flow Controller
UPQC	=	Unified Power Quality Conditioner
VAR	=	Volt Ampere Reactive
VD	=	Voltage Deviation
VUF	=	Voltage Unbalance Factor
ZSRPC	=	Z-Source Railway Power Conditioner
a	=	Transformer's turns ratio (N_1/N_2) and Non-train load terms in G in CBNR power flow calculation
a_1	=	T-phase Scott transformer's turns ratio ($\sqrt{3}N_1/2N_2$)
a_2	=	M-phase Scott transformer's turns ratio (N_1/N_2)
a_{RPC}	=	RPC coupling transformer's turn ratio
d	=	Non-train load terms in H in CBNR power flow calculation
e_1	=	FR winding voltage (AT)
e_2	=	CR winding voltage (AT)
E_p	=	Primary winding excitation voltage
E_{p1}	=	T-phase primary winding voltage
E_{p2}	=	M-phase primary winding voltage
E_T	=	Secondary winding excitation voltage (across the centre tap and the other phases)

LIST OF ABBREVIATIONS AND SYMBOLS (CONTINUED)

E_φ	=	φ-phase secondary winding voltage, $\varphi \in \{T, M\}$
F	=	Current mismatch in CBNR power flow calculation
G	=	Real part of current mismatch in CBNR power flow calculation
H	=	Imaginary part of current mismatch in CBNR power flow calculation
i	=	Bus number in CBNR power flow calculation
I_-	=	Negative sequence current
I_+	=	Positive sequence current
I_1	=	Current flowing in FR winding (AT)
I_2	=	Current flowing in CR winding (AT)
I_C	=	Secondary current (catenary)
I_{com}	=	Compensating current in RPC model
I_F	=	Secondary current (feeder)
I_m	=	Current flowing in the magnitising branch (AT)
$I_{M\Omega}$	=	M-phase secondary current, $\Omega \in \{\mathrm{C, R, F}\}$
I_p	=	Primary current
I_R	=	Secondary current (running rail)
I_{RPC}	=	RPC converter's equivalent current in RPC model
I_T	=	Train load current
$I_{T\Omega}$	=	T-phase secondary current, $\Omega \in \{\mathrm{C, R, F}\}$

LIST OF ABBREVIATIONS AND SYMBOLS (CONTINUED)

I_{Δ}	=	Three-phase primary current, $\Delta \in \{A, B, C\}$
j	=	Iteration number in CBNR power flow calculation
J_{RPC}	=	RPC equivalent current matrix in RPC model
J_{SS}	=	Source current matrix
J_{TR}	=	Train load's current matrix in CBNR power flow calculation
m_{Δ}	=	Modulation index of RPC converters in RPC model, $\Delta \in \{\alpha, \beta\}$
N_B	=	The number of buses in a traction power supply system
P_{Δ}	=	Output active power of a converter in RPC model, $\Delta \in \{\alpha, \beta\}$
$P_{3\varphi}$	=	Substation's active power in three-phase side
P_C	=	RPC's transferred active power
PF*	=	Targeted power factor
$PF_{3\varphi}$	=	Three-phase side power factor
P_{Full}	=	Full compensating active power
P_L	=	Train load active power
P_{loss}	=	All power loss in a traction power supply system
P_T	=	Train load active power
q	=	Real part of train load current in CBNR power flow calculation

LIST OF ABBREVIATIONS AND SYMBOLS (CONTINUED)

Q_Δ	=	Output reactive power of a converter in RPC model, $\Delta \in \{\alpha, \beta\}$
Q_C	=	RPC's compensating reactive power
Q_T	=	Train load reactive power
r	=	Imaginary part of train load current in CBNR power flow calculation
$S_{converter}$	=	Compensating apparent power of an RPC's converter
S_{RPC}	=	RPC MVA size or compensating apparent power
S_{RPCo}	=	RPC MVA size before addition of penalty terms
S_{TR}	=	Train load apparent power
t	=	AT's tap position
U_Δ	=	Substation's secondary voltage in RPC model, $\Delta \in \{\alpha, \beta\}$
$U_{O\Delta}$	=	Voltage in high-voltage side of a coupling transformer in RPC model, $\Delta \in \{\alpha, \beta\}$
V_-	=	Negative sequence voltage
V_+	=	Positive sequence voltage
V_0	=	Primary input voltage
V_C	=	Secondary voltage (catenary)
V_{DC}	=	DC-link voltage in RPC model
V_F	=	Secondary voltage (feeder)

LIST OF ABBREVIATIONS AND SYMBOLS (CONTINUED)

$V_{M\Omega}$	=	M-phase secondary voltage, $\Omega \in \{C, R, F\}$
V_R	=	Secondary voltage (running rail)
$V_{T\Omega}$	=	T-phase secondary voltage, $\Omega \in \{C, R, F\}$
V_Δ	=	Three-phase primary voltage, $\Delta \in \{A, B, C\}$
$Y_{fixed\ centre\text{-}tapped\ AT}$	=	Admittance matrix of fixed centre-tapped AT
Y_{RE}	=	Rail-to-Earth admittance
Y_{RPC}	=	RPC admittance matrix in RPC model
Y_{SS}	=	Source admittance matrix
$Y_{tap\text{-}changing\ AT}$	=	Admittance matrix of tap-changing AT
Z_{C}	=	Catenary line impedance
$\mathrm{Z}_{\mathrm{Catenary}}$	=	Catenary system impedance matrix
z_e	=	Impedance connected between the centre tap and running rail
Z_{F}	=	Feeder line impedance
z_g	=	Winding leakage impedance (AT)
$Z_{L\Delta}$	=	A combination of coupling transformer's leakage impedance, reactor's reactance, and converter's impedance in RPC model, $\Delta \in \{\alpha, \beta\}$
z_m	=	Magnitising impedance (AT)
Z_p	=	Primary winding's leakage impedance
Z_{R}	=	Running rail impedance

LIST OF ABBREVIATIONS AND SYMBOLS (CONTINUED)

Z_{RE}	=	Rail-to-Earth impedance
Z_s	=	Secondary winding's leakage impedance
Z_{s1}	=	T-phase secondary winding leakage impedance
Z_{s2}	=	M-phase secondary winding leakage impedance
Z_Δ	=	Δ-phase primary winding leakage impedance, $\Delta \in \{A, B, C\}$
γ_1	=	Power-related penalty factor
γ_2	=	Power quality-related penalty factor
δ_Δ	=	Phase angle of converter's output AC voltage in RPC model, $\Delta \in \{\alpha, \beta\}$
$\delta_{C\Delta}$	=	Phase angle between U_Δ and $U_{O\Delta}$ in RPC model, $\Delta \in \{\alpha, \beta\}$
θ	=	Phase angle of bus voltage in CBNR power flow calculation
ϕ	=	Phase angle of admittance in CBNR power flow calculation

Chapter 1

Introduction

1.1 General introduction

Electrical energy demands have been increasing in the fast-growing world in that countries are modernised and industrialised. Also, each person consumes more electricity than ever before. Therefore, electrical utilities around the world have to generate and distribute adequate electrical power to customers with high quality, safety and reliability. With the growing demands, power quality issues have arisen in power transmission and distribution systems, mainly comprised of low power factor, harmonic distortion, voltage dip and swell, under- and over-voltage, voltage unbalance, voltage flicker, and transient disturbances. Major contributors to the impure power are power electronics converters, such as switch mode power supplies and rectifiers, arc furnaces, adjustable speed drives, switching and fault clearing, and other non-linear loads. When it comes to railway electrification currently booming in several countries including Thailand, traction systems are a single-phase load supplied from three-phase power systems and pose time-varying and intermittent electrical loads to a utility grid, particularly during acceleration. These loads predominantly causing voltage/current unbalance, voltage fluctuation, and voltage drops negatively affect other users' voltage-sensitive loads using the same power supply. In addition, the traditional electric locomotive using rectifiers or thyristor-based converters is the main cause of harmonics in traction power supplies. The PWM-based locomotive generates more high-order harmonics into feeding systems but less low-order harmonics. Mitigation measures are needed for railway operators to meet power quality requirements, maintain operational train performance in an acceptable level and also avoid penalties from a utility. The technological advance in power semiconductor devices has made the devices greater in voltage, current, and switching frequency ratings then a new generation of power semiconductor or static devices plays more important role than mechanically-controlled and fixed installation ones in compensator applications. For these reasons, flexible AC transmission systems (FACTS) and custom power devices for medium voltage applications, such as static VAR compensators (SVCs) and static synchronous compensators (STATCOMs) or distribution STATCOMs (DSTATCOMs), have been increasingly employed in railway traction power supplies connected to weak power systems, relatively low short circuit capacity, or the power system facing difficulties to extend or build a new transmission system. Recently, a new comprehensive compensator specifically designed for traction power supplies called "static railway power conditioner (RPC)" has been introduced by Railway Technical Research Institute (RTRI) and commercially used only in Shinkansen, Japan. Prior to the design and implementation of those compensators, mathematical modelling of them becomes unavoidable, the models of which are very important tools to study and estimate their effectiveness, efficiency, and other aspects, such as the optimal location of compensators in traction power systems, compensator rating determination, topology and control strategies for using with each type of traction transformers, etc.

This study focuses on using the RPC in the purpose of reducing voltage unbalance in a three-phase power supply system feeding an autotransformer (AT)-fed traction power supply system. With the expensive cost of the RPC, selection of RPC's ratings or sizes may be very useful; choosing the appropriate size of the RPC in a particular system significantly helps reduce the cost for a traction power supply operator. Accordingly, a need for design and sizing of the RPC, and a mathematical model for computer simulation arises.

1.2 Research objectives

(1) Apply the current-based Newton-Raphson power flow method in an autotransformer (AT)-fed power supply system.

(2) Develop an optimal sizing procedure of the railway power conditioner (RPC) in the AT-fed power supply system.

(3) Study the use of a tap-changing autotransformer in the AT-fed power supply system.

1.3 Scope of the study

(1) Study and create the steady-state model of the RPC, tap-changing autotransformer, and specially-connected transformer: V-connected and Scott transformer for the AT-fed power supply system using the current-based Newton-Raphson power flow method programmed in MATLAB.

(2) Study and develop an approach to optimally sizing the RPC in the AT-fed power supply system.

(3) Investigate the effect of using the tap-changing autotransformer on the AT-fed power supply system.

(4) Use the East Corridor Line in Denver as a test system and case study for simulation verification.

1.4 Limitation of the study

(1) Traction transformers used in this research are the V/V and Scott transformer.

(2) Only AT-fed traction power supply is applied in this research.

(3) The three-phase source is balanced and distortion-free in all simulation cases.

(4) Harmonics are not taken into consideration and analysis in this study.

(5) No regenerative power is generated by trains.

(6) The DC link voltage of the RPC is perfectly controlled and constant.

(7) Voltage unbalance in this study is only caused by traction load.

1.5 Expected benefits

The outcome of this study will be directly beneficial to an AC railway power supply designer in RPC size selection process. The proposed optimal sizing procedure can be used as a design guideline; additionally, the optimal selected size of RPC will more or less save the power supply cost.

1.6 Organisation of the thesis

The thesis is organised into 7 chapters. **Chapter 1** introduces the importance and objectives of the study as well as its scope and limitation. Basic AC railway electrification, power quality compensators for AC railway ranging from the traditional to modern ones, and mathematical models of those compensators studied in the past research are presented in **Chapter 2**. Then, modelling of the autotransformer-fed traction power supply components and the current-based Newton-Raphson power flow calculation method are described in **Chapter 3** and **Chapter 4**, respectively. **Chapter 5** contains the study of using tap-changing autotransformer in a railway power supply system. The optimal RPC sizing procedure including the review of RPC compensation principles is detailed in **Chapter 6**. Finally, the thesis is concluded in **Chapter 7**.

Chapter 2

General review

2.1 Introduction

This chapter presents a general review of AC railway electrification and power quality conditioning devices in railway applications. Firstly, means of AC railway electrification from the simplest to the most modern way of electrification are described, including a single-phase direct feeding system, booster transformer feeding system, autotransformer feeding system and co-phase system. Secondly, compensating and balancing devices in railway electrification are introduced. The most traditional way of balancing a three-phase power supply system at a traction substation is to use specially connected transformers such as V/V, Scott, and Le Blanc transformers. For more flexibility and better-compensating performance, power electronics devices are introduced and incorporated into AC traction substations alongside specially connected transformers. A static VAR compensator (SVC), a static synchronous compensator (STATCOM), a dynamic voltage regulator (DVR), a unified power quality conditioner (UPQC), and a static railway power conditioner (RPC) are described in this chapter. Finally, power flow models of those power electronics compensating devices are reviewed as a guide to develop the power flow model of an RPC in the later chapter.

2.2 AC railway electrification

A traction system of high-speed or intercity trains receives electrical power from a three-phase high-voltage power grid, which is stepped down to a single-phase traction drive level via a traction transformer at a traction substation. A 25 kV 50 Hz system is widely adopted and standardised. In some countries in Europe, such as Germany and Austria, the specific power supply system is used to supply the traction substation with a reduced frequency, 16.7 Hz, in order to prevent poor power quality power from entering the public grid and affecting other electrical power consumers, and also reduce losses in traction motors. A traction power plant is even built to isolate the traction power supply system in some circumstances. Fig. 2.1 shows the overall traction power supply system configuration. The high-speed train is generally powered through an overhead catenary system, as shown in Fig. 2.2. Several types of traction transformer, such as V/V, Scott, modified Woodbridge, and others, have been proposed and researched in the past studies to overcome grid unbalance issue. These transformers are discussed later in this chapter. Different AC traction power feeding systems have also been developed to perform better, namely, loss reduction, electromagnetic interference and stray/leakage currents (the current that does not flow in an intended path). The following are the brief descriptions of 4 different traction power feeding systems: a single-phase direct feeding system, a booster transformer (BT) feeding system, an autotransformer (AT) feeding system, and a co-phased traction feeding system.

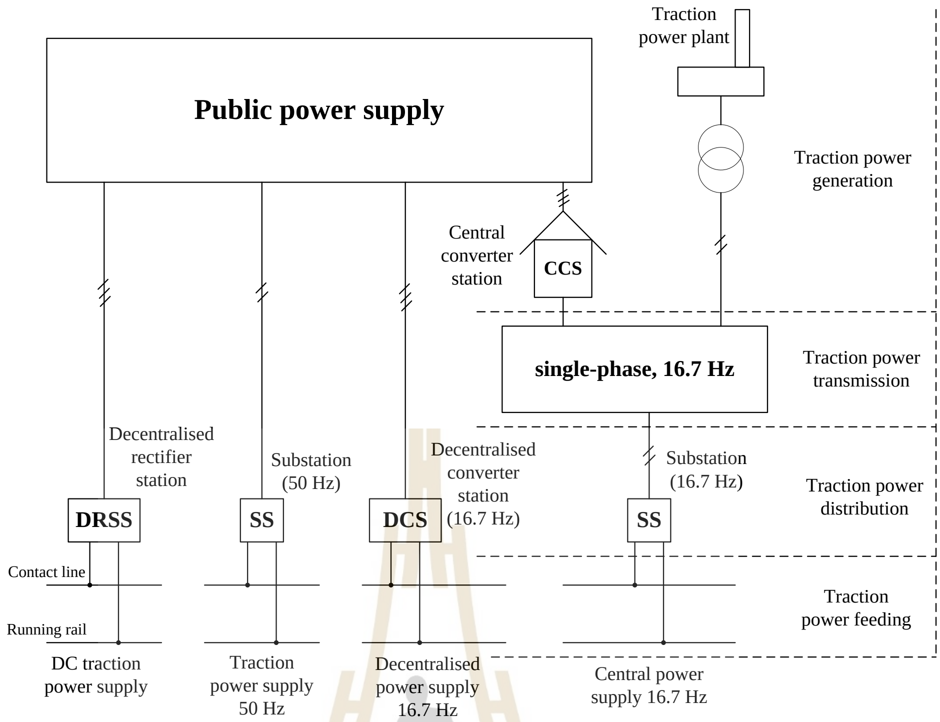

Fig. 2.1 Power supply structure for railway traction system (Friedrich et al., 2009)

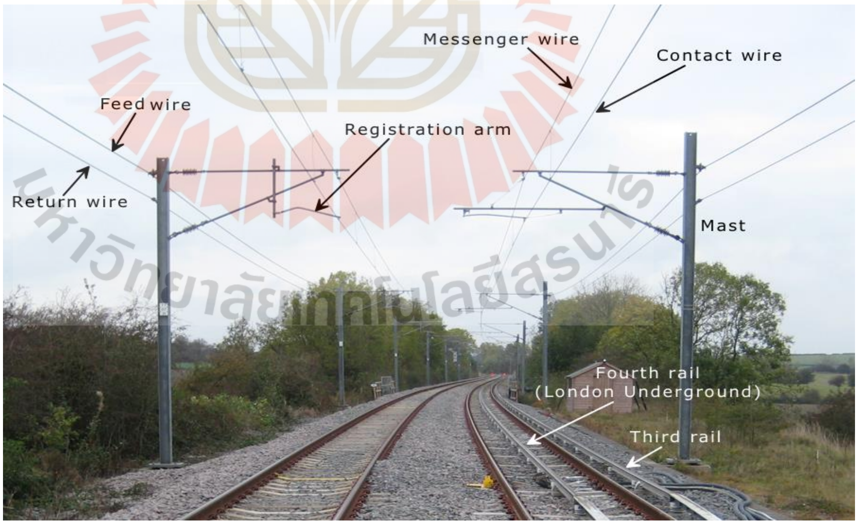

Fig. 2.2 Overhead catenary system

(http://www.railway-technical.com/infrastructure/electric-traction power.html, Retrieved 4th August 2020)

2.2.1 Single-phase direct feeding system

A single-phase direct feeding system is the simplest form of traction power supply because the structure is uncomplicated. The commonly used single-phase transformer is adopted, and no additional equipment is required. One pair of phases from the grid is fed to the traction transformer's primary side, which steps the input voltage down to a traction level, as shown in Fig. 2.3 (a). The traction current returns to the traction substation through the running rails; see Fig. 2.4 (a). Some portion of the return current leaks into the ground and flows through other metal structures before returning to the traction substation. The main drawback of this system is that the traction current in a catenary line causes inductive interference with the neighbouring signalling system. Additionally, the leakage current passing through metal structures causes corrosion on those structures. The magnitude of the leakage current depends on the traction current and the rail-to-earth conductance. The basic solution to reducing this leakage current is using an overhead return conductor connected to the running rails, installed parallel to the catenary conductor, as shown in Fig. 2.4 (b). Despite using this solution, a small leakage current still occurs. Another key problem of traction power supply is voltage unbalance at the grid side due to a heavy single-phase traction load. A phase rotation method is adopted as a simple solution, i.e., different pairs of phases connected to the adjacent traction substation; see Fig. 2.3 (b). With different phases, each feeding section is separated by a neutral section. Apart from the phase rotation method, a specially connected transformer and railway power conditioner are more effective tools for reducing the voltage unbalance. More details of these apparatuses are described later in this chapter.

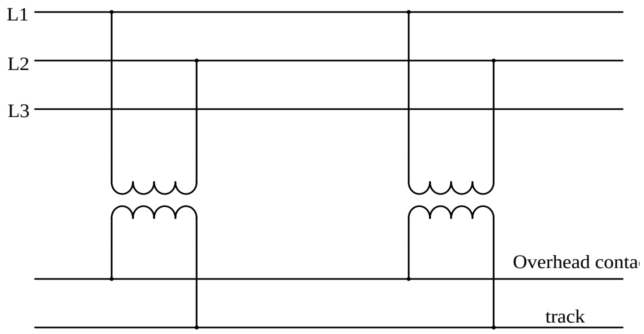

(a)

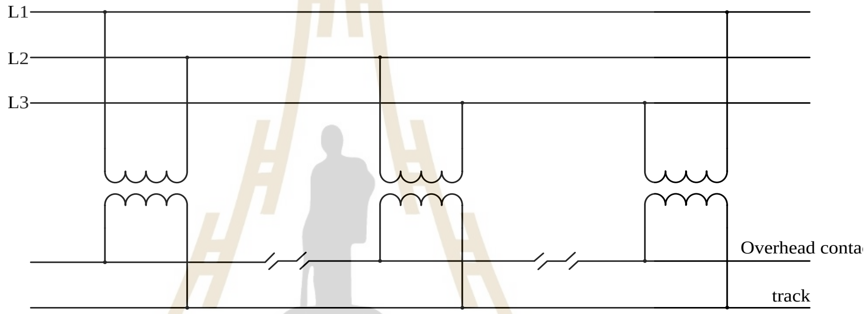

(b)

Fig. 2.3 Single-phase direct feeding system

(a) One phase supply, (b) Phase rotation

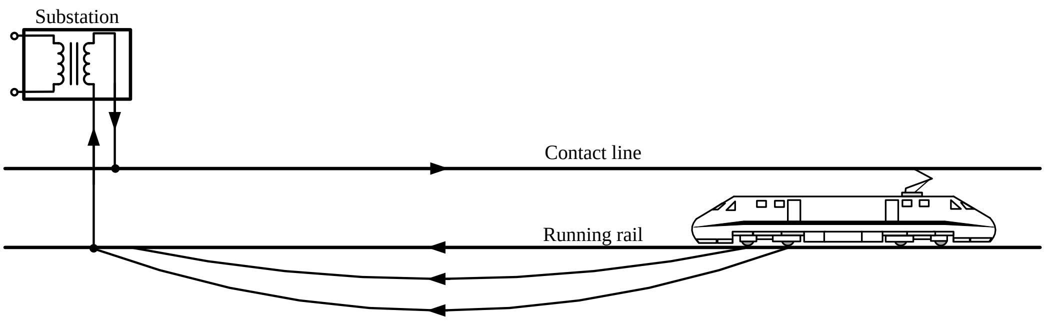

(a)

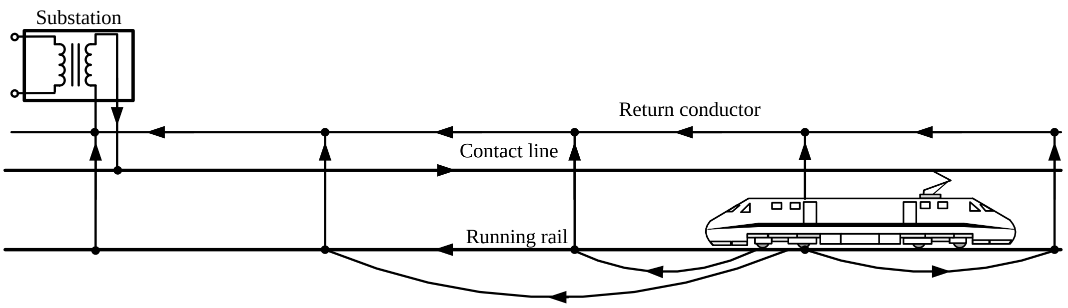

(b)

Fig. 2.4 Return current circuit (Friedrich et al., 2009)

(a) Without return conductor, (b) With return conductor

2.2.2 Booster transformer feeding system

Even though the single-phase traction feeding system with the return conductor can reduce the leakage current, the interference on the neighbouring signalling system remains unsolved. Accordingly, a booster transformer (BT) feeding system is put forward to mitigate the interference. The concept of using BT is that one can see BT as a current transformer with a 1:1 turn ratio. For this purpose, this BT is used to help force the return current to flow back in the return conductor with the same amount as the traction current, hence no leakage current theoretically. The distance between BTs is 4 km, an example figure when used in Japan in the past. The return conductor is bonded to the running rails at the half way between BTs, the contact line is connected to the primary winding of BT in series, and the return conductor is connected to the secondary winding of BT in series as illustrated in Fig. 2.5. The path of the traction current flow is also shown in Fig. 2.5. This scheme can not only reduce the leakage current and interference but also reduce the return current flowing through the running rails, i.e., the return current in the running rails only flow in the section with a train. When a train passes through BTs, a large amount of the traction current can bring about an electric arc at the BT section, which damages the overhead contact line and pantograph. A capacitor connected in series with BT can compensate for the reactance of BT, lowering the traction current and the corresponding arc mentioned and can also prevent voltage drops (Yasu, Yoshifumi, and Hiroki, 2001).

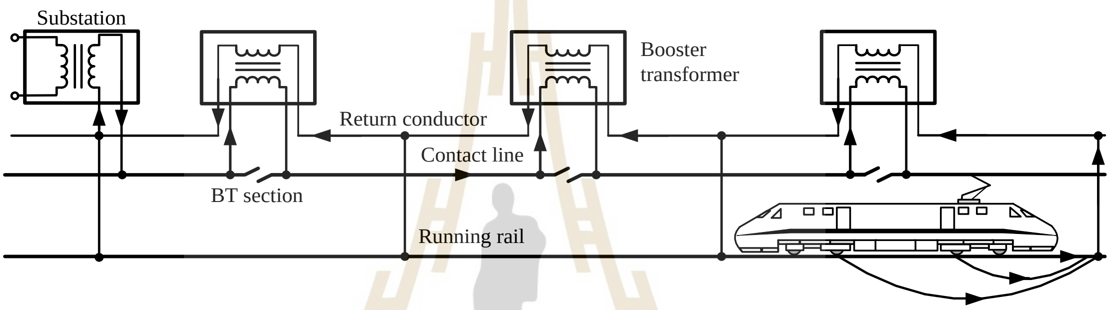

Fig. 2.5 Booster transformer feeding system (Friedrich et al., 2009)

2.2.3 Autotransformer feeding system

An autotransformer (AT) feeding system is further developed after the BT feeding system is not successful and is not in operation worldwide. The secondary winding of the traction transformer in this scheme has a mid-tap connected to the running rails, and the other two terminals are connected to a catenary feeder and a negative feeder. The output voltage of the traction substation becomes twice the voltage of the traction level, namely the catenary-to-rail voltage and the feeder-to-rail voltage are equal in magnitude but opposite in phase. The arrangement and connection of the traction transformer and AT is shown in Fig. 2.6. In theory, the current in the running rails exists only in the section having a train load. It is evident that the negative feeder is intended to be used as a return conductor and the magnitude of the catenary and negative feeder current is half of the traction current, as seen in Fig. 2.7. This lower supply current allows the AT feeding system to have more train load or higher capacity trains and less traction voltage drops. Also, a higher feeding voltage can transmit traction power over a longer distance. With almost no current flowing in the running rails between the traction substation and BT before the train position, the AT feeding system can eliminate electromagnetic interference with neighbouring circuits. Another obvious advantage of the AT system over the BT system is that there is no electric arc problem in the BT section. The AT system has now become a standard for a high-speed, long-distance railway power supply system; Shinkansen lines are an example of the systems adopting the 2×25 kV AT system. The AT installed in one of the Shinkansen lines is shown in Fig. 2.8.

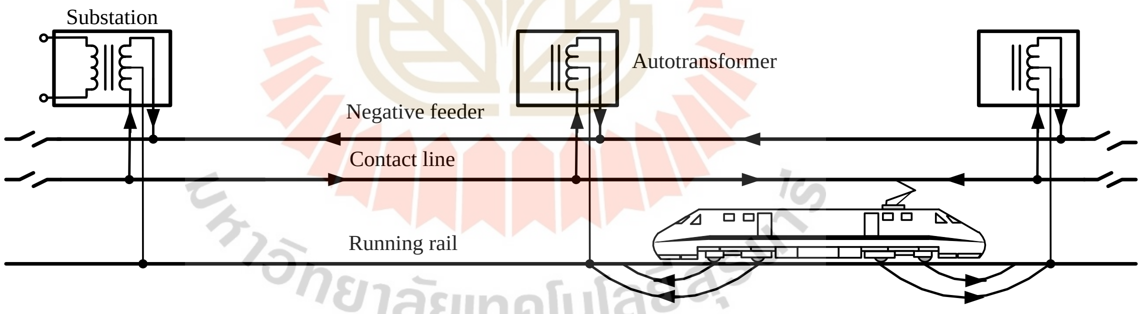

Fig. 2.6 Autotransformer transformer feeding system (Friedrich et al., 2009)

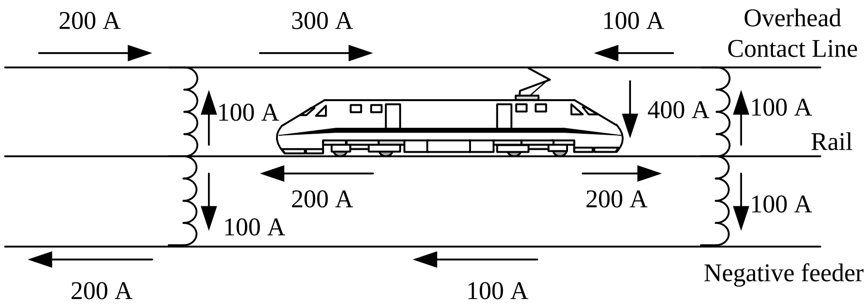

Fig. 2.7 Current path of the AT feeding system

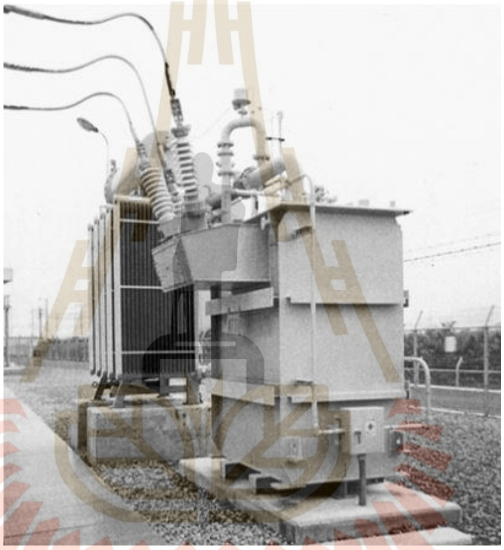

Fig. 2.8 Autotransformer in Shinkansen line (60/30 kV, 7500 kVA)

(Yasu et al., 2001)

2.2.4 Co-phase traction feeding system

Due to the introduction of a railway static power conditioner (RPC) in 1993, more power electronic devices have been adopted in railway applications. Heavy unbalanced three-phase, reactive power, and harmonics problems are solved simultaneously and effectively. Power quality problems not only hinder the operation of high-speed railway, but a neutral section can also cause arcs and prevent the development of high-speed operations. Hence, the reduction or elimination of the neutral section is essential for further improvement in the future. Based on this idea, a co-phase traction power supply system has been proposed in the late 20th century by a Chinese scholar (Li, Liu, Shu, Xie, and Zhou, 2014). The aims of the co-phase system are to eliminate the power quality problems mentioned above and reduce the neutral section. It can be noted that the co-phase system supplies traction loads with one phase using balancing transformers, as shown in Fig. 2.9. For instance, there is no phase splitting section at a traction substation, and another phase is only connected to the RPC or other types of power conditioners for compensation. The first proposed co-phase system can reduce half of the phase splitting section.

Nevertheless, the voltage magnitude, frequency and phase between each feeding section are still not exactly equal. Therefore, a sectioning post (SP) is still used in place of the neutral section to isolate the feeding section. It has been in trial operation at Meishan traction substation, the southwest of Chengdu, since 2010 (Li, Liu, Shu, Xie, and Zhou, 2014); currently, there are a few more traction substations in the planning of using the co-phase system in China.

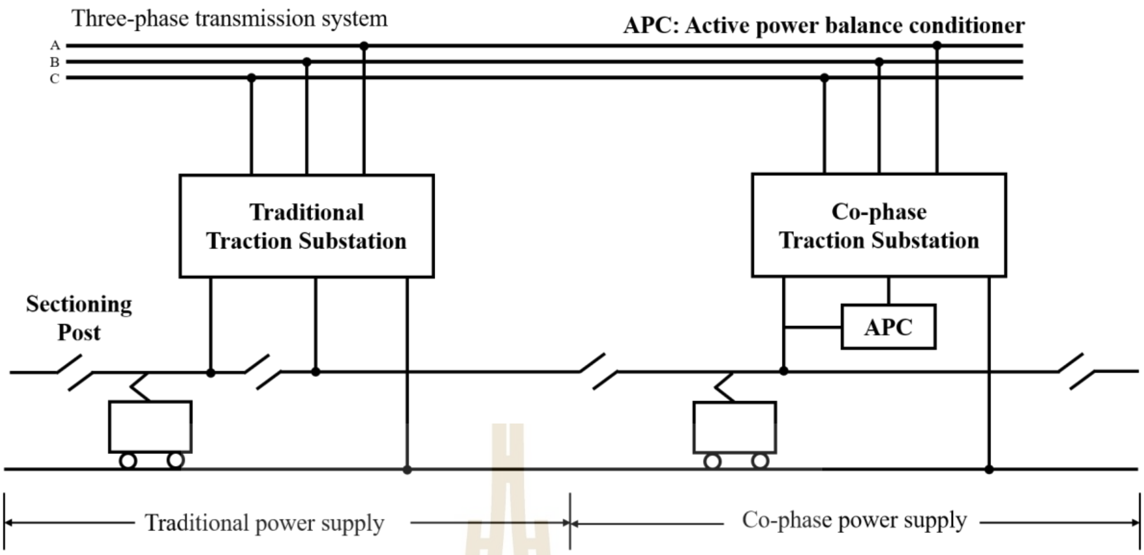

Fig. 2.9 Co-phase and traditional traction power supply system

(Li, Liu, Shu, Xie, and Zhou, 2014)

The major disadvantage of the co-phase system is its very high investment cost. Consequently, the research in this area has been continuously conducted to reduce the rating or capacity of the co-phase power supply device. For example, the co-phase power supply device is used in conjunction with a single-phase transformer and another back-up transformer, called a combined co-phase traction power supply system; see Fig. 2.10. This system can also operate as usual when the co-phase power supply device is not functional. However, the system has to tolerate the power quality problems until the co-phase device is fully restored. All phase splitting sections must be removed for a perfectly continuous power supply to reach higher operational speed. This concept leads to the development of an advanced co-phase power supply system. The whole substation is based on power electronic equipment, as shown in Fig 2.11. The three-phase converter and the single-phase inverter of the AC-DC-AC converter can operate separately and independently as long as the DC-link voltage is kept constant and stable.

The small-scale prototype has been built and tested to validate the system's configuration, control algorithm, and feasibility (He et al., 2014).

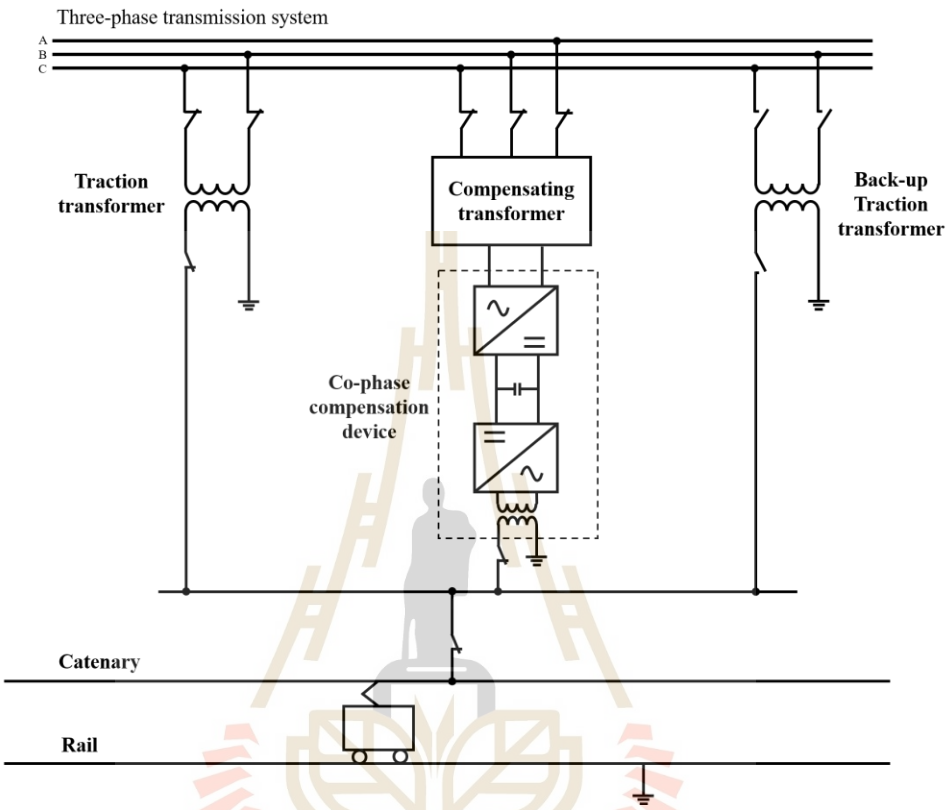

Fig. 2.10 Combined co-phase traction power supply system

(Li, Liu, Shu, Xie, and Zhou, 2014)

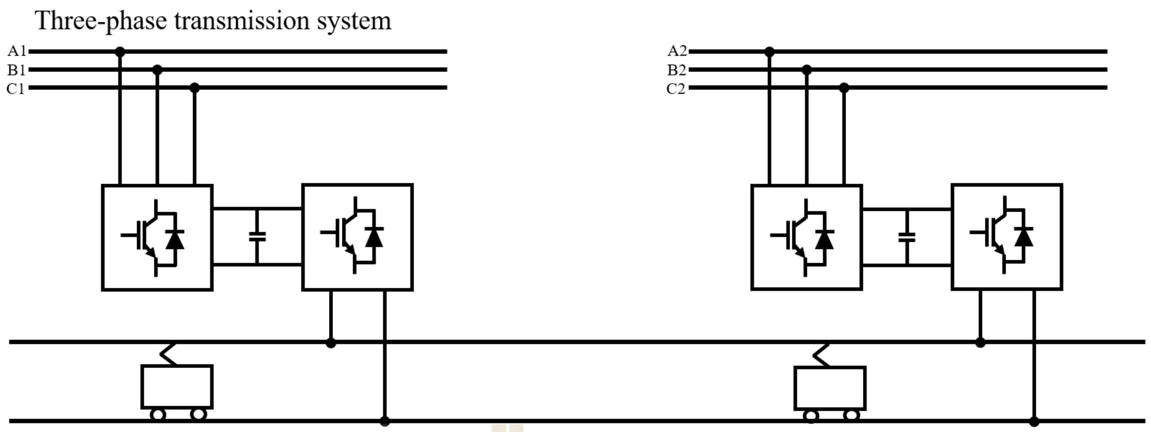

Fig. 2.11 Advanced co-phase traction power supply system (He et al., 2014)

2.3 Specially-connected transformers

A traction substation transformer has to transform three-phase voltages into a single-phase voltage to supply traction loads that are time-varying, fluctuating, and very heavy. A unbalance problem in the three-phase side has emerged since the early days of railway traction supply service. The simplest solution to this problem is using the phase rotation mentioned earlier. However, it is not very effective because of the uneven distribution of trains along a route. For this reason, several types of specially-connected transformers have been invented and researched. The specially connected transformers have their windings connected in a specific manner to re-distribute the loading of each phase. Generally, they have two output phases separately feeding traction load in two different directions. The following are a few examples of the specially-connected transformers in use: V/V transformer, Scott transformer, and Le Blanc transformer.

2.3.1 V/V transformer

A V/V transformer is the simplest type of specially connected transformer. It can be seen that it is built from two single-phase transformers with the input side connected in a three-phase manner and two separate output windings, as shown in Fig 2.12 (a). For example, the V/V transformer in the leftmost substation in Fig. 2.12 (b) has one primary winding connected to the AB phase and the other to the CB phase; this figure also shows that the phase rotation can be applied in this scheme. The phase angles of the corresponding output windings are the same as those of AB and CB phase; see the phasor diagram in Fig. 2.13. The magnitudes of the two output secondary windings are equal, and the phases are 60 degrees apart. Each section with different phases is isolated by a neutral section. Even though it is designed to balance the three-phase voltages/currents, it can eventually reduce the voltage unbalance to only half of the unbalance when using a single-phase transformer, and only if two secondary windings have the same amount of load. Another problem appears if one transformer is out of service and the other transformer or the other phase has to bear the full load, thus no unbalance is relieved (Ciccarelli, Fantauzzi, Lauria, and Rizzo, 2012). The V/V transformer is in operation in French TGV, British rail ECML, Finnish state railways, to name a few (Chen and Guo, 1996).

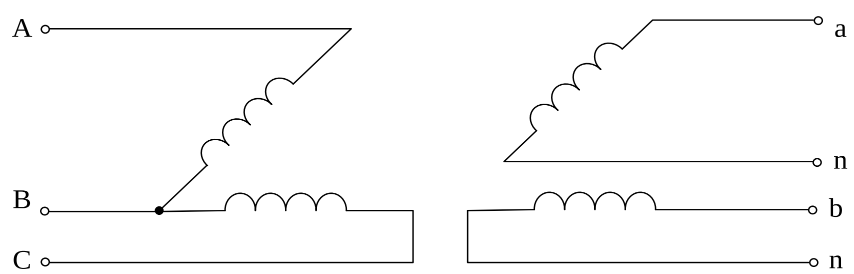

(a)

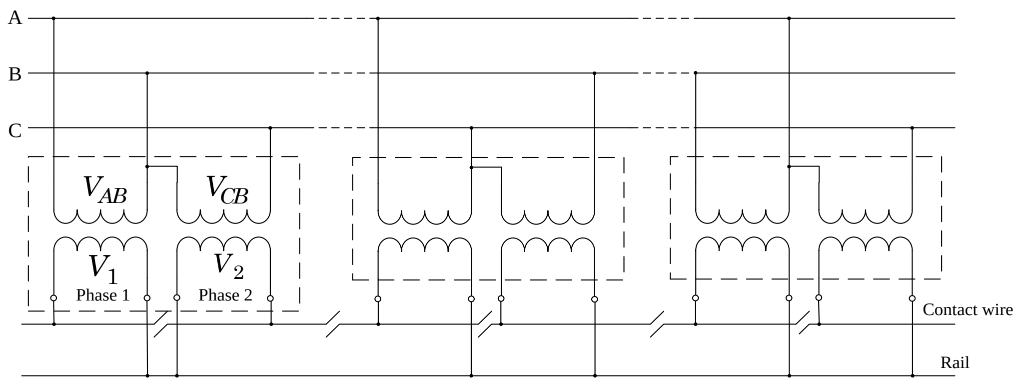

(b)

Fig. 2.12 V/V transformer connection

(a) Winding connection, (b) Traction power supply connection

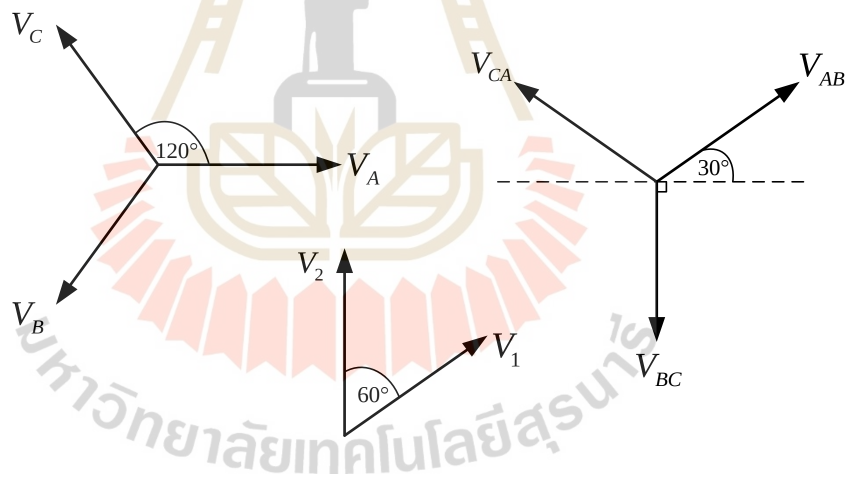

Fig. 2.13 Phasor diagram of V/V transformer

2.3.2 Scott transformer

A Westinghouse engineer, Charles Felton Scott, invented the Scott transformer in the late 1890s (Harold, 1953). The transformer has two primary and two secondary windings. Otherwise, it can be seen as two single-phase transformers with one transformer connected across one phase of the three-phase supply and the mid-tap of the other transformer's primary winding. The other transformer is connected across the remaining phases. The former is called a teaser (T) transformer or teaser phase, and the latter is a main (M) transformer or main phase, as seen in Fig. 2.14. Fig. 2.15 shows the phasor diagram and represents the winding connection of the leftmost substation in Fig. 2.14. The teaser voltage is in phase with C phase voltage, and the main voltage is in phase with phase AB; it can be noted that the teaser and main voltage are perpendicular to each other. Theoretically, the Scott transformer can completely reduce the voltage unbalance when both secondary winding loads are equal; this gives the Scott transformer an advantage over the V/V transformer (Aihara, Miyazawa, and Koizumi, 2012). Meanwhile, the Scott transformer is more expensive and more complicated in winding connection. Furthermore, the Scott transformer cannot be used in an extra-high-voltage transmission system that requires direct earthing. The Scott transformer has been seen in actual operation in the Tokaido Shinkansen line linking Tokyo and Osaka (Chen and Guo, 1996).

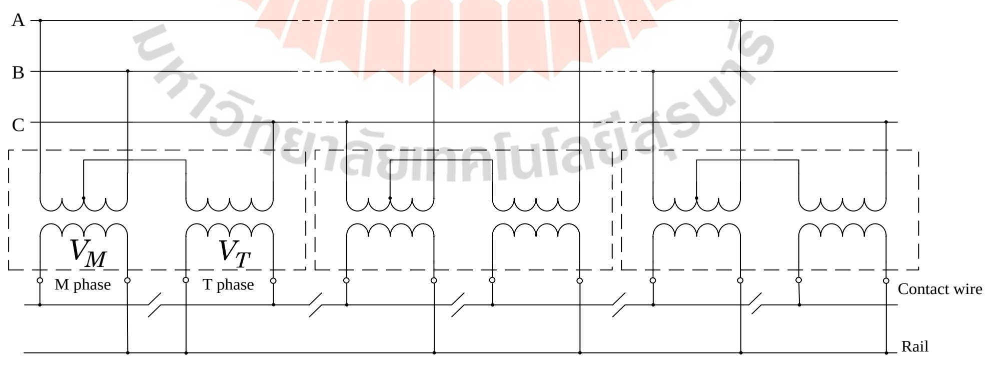

Fig. 2.14 Scott transformer connection in traction power supply

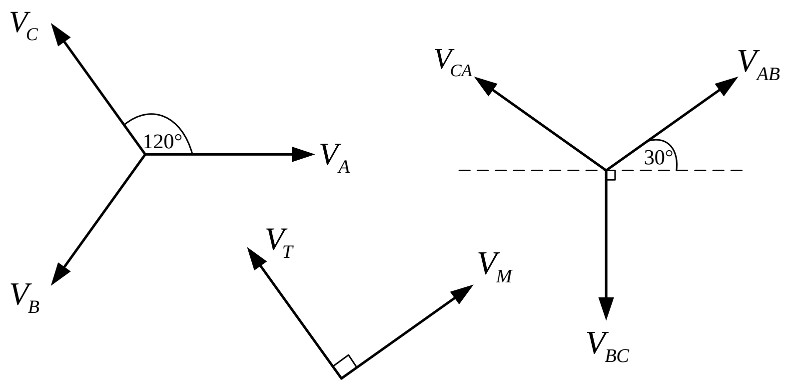

Fig. 2.15 Phasor diagram of Scott transformer

2.3.3 Le Blanc transformer

A Le Blanc transformer consists of two three-winding transformers and one two-winding transformer. The primary side of the Le Blanc transformer is connected in a delta connection to prevent the 3rd harmonic from flowing back to the three-phase power supply. All 5 secondary windings are interconnected to form two output circuits; two windings create one output, and three windings create the other (J. Martins, C. Martins, and Pires, 2015), as shown in Fig. 2.16. The output voltages of two circuits are the sum of the individual winding voltage. The phasor diagram of the primary and secondary voltages is illustrated in Fig. 2.17. Like the Scott transformer, the two output voltage phase angles are perpendicular to each other with the same magnitude. The Le Blanc transformer has slightly better performance in a voltage unbalance reduction than that of the Scott transformer. However, its winding arrangement is more complicated, and the investment cost higher. It is found to be used only in the Taiwan railway (Chen and Guo, 1996).

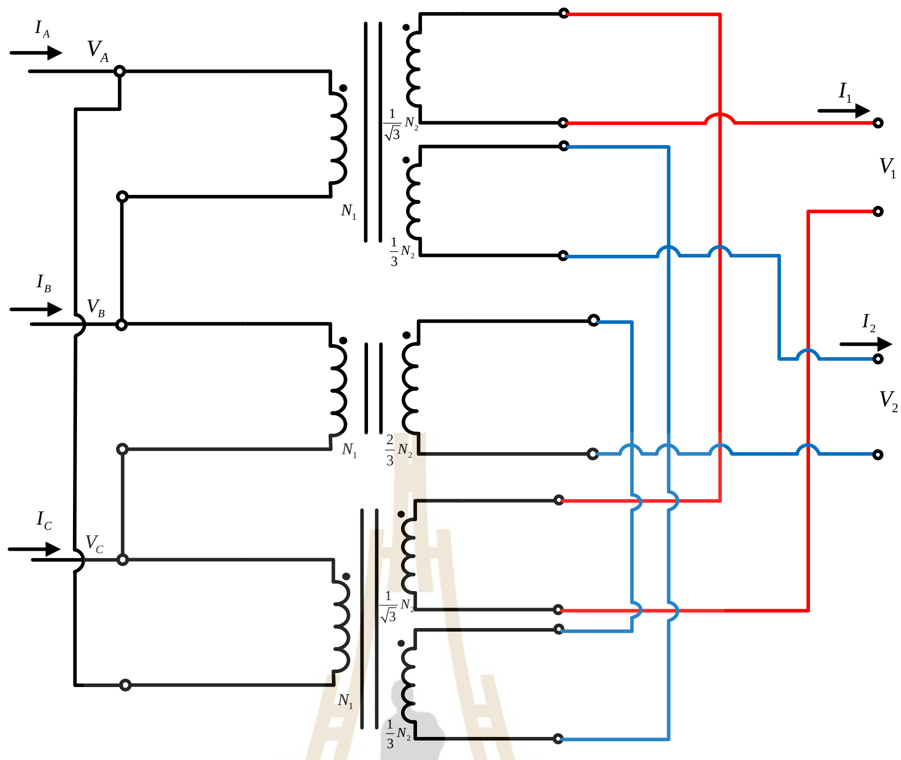

Fig. 2.16 Le Blanc transformer winding connection

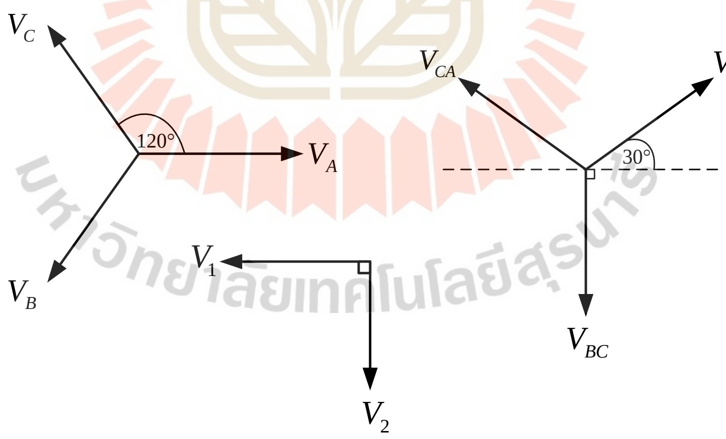

Fig. 2.17 Phasor diagram of Le Blanc transformer

It is noteworthy that the Scott and Le Blanc transformer have similar characteristics, i.e., two secondary voltages are equal in magnitude, and their phase angles are 90 degrees apart. The voltage unbalance is eliminated if two secondary windings are equally loaded. Transformers with these characteristics are also known or categorised as a balancing transformer. Other balancing transformers have been developed, such as a modified Woodbridge transformer, an impedance matching transformer, and a roof-delta or YNvd transformer. Their winding connection diagrams are shown in Fig. 2.18 - 2.20, respectively. Moreover, some of them are built in order for diminishing costs and complexity.

The voltage unbalance factors (VUFs) resulted from the use of the specially-connected transformers are plotted versus the load distribution between two secondary windings (k) in Fig. 2.21. The VUFs for a single-phase transformer, V/V transformer, and balancing transformers are approximated by (2.1) – (2.3), respectively, where $S_{1\phi}$ denotes the total traction substation load and $S_{3\phi}$ denotes the short-circuit capacity of the three-phase supply (Chen and Guo, 1996). It is shown that the single-phase transformer does not influence balancing voltages. The V/V transformer can merely reduce the voltage unbalance to 50% of that in the worst case (only one secondary winding is loaded). All balancing transformers can eliminate all voltage unbalance when the secondary loads are equally shared, $k = 0.5$ at the tip of the V-shaped curve. It is significant to notice that all traction transformers cannot reduce the voltage unbalance when only one secondary phase is loaded ($k = 0$ or $k = 1$). Apart from the mentioned balancing transformers, a common star-delta transformer is adopted due to its common use and common manufacture. Its voltage balancing behaviour is similar to that of the V/V transformer.

$$VUF = \frac{S_{1\phi}}{S_{3\phi}} \tag{2.1}$$

$$VUF = \left(3k^2 - 3k + 1\right)^{1/2} \frac{S_{1\phi}}{S_{3\phi}} \tag{2.2}$$

$$VUF = \left|1 - 2k\right| \frac{S_{1\phi}}{S_{3\phi}} \tag{2.3}$$

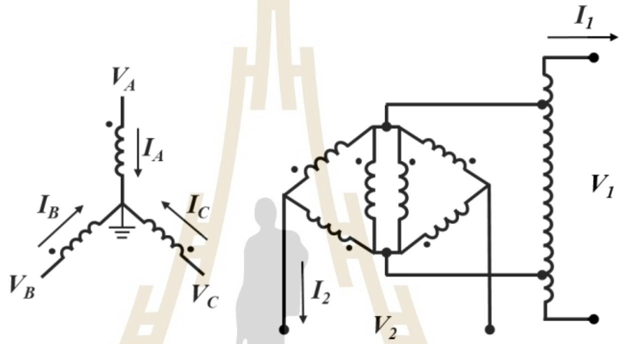

Fig. 2.18 Modified Woodbridge transformer winding connection

(Adapted from Chen and Guo, 1996)

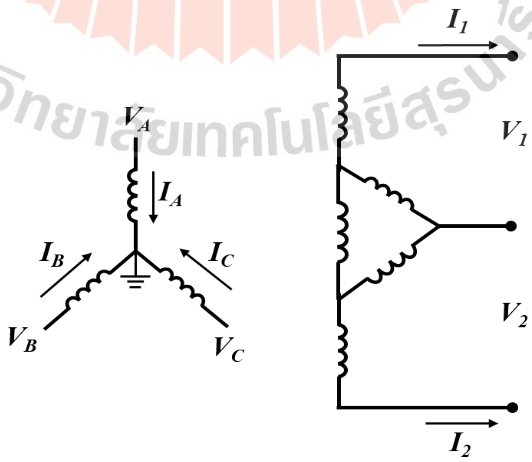

Fig. 2.19 Impedance matching transformer winding connection

(Adapted from Ciccarelli, Fantauzzi, Lauria, and Rizzo, 2012)

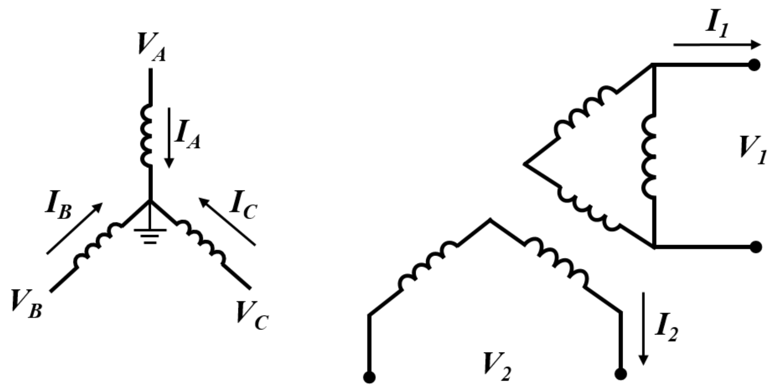

Fig. 2.20 Roof-delta transformer winding connection

(Adapted from Morimoto, Uzuka, Horiguchi, and Akita, 2009)

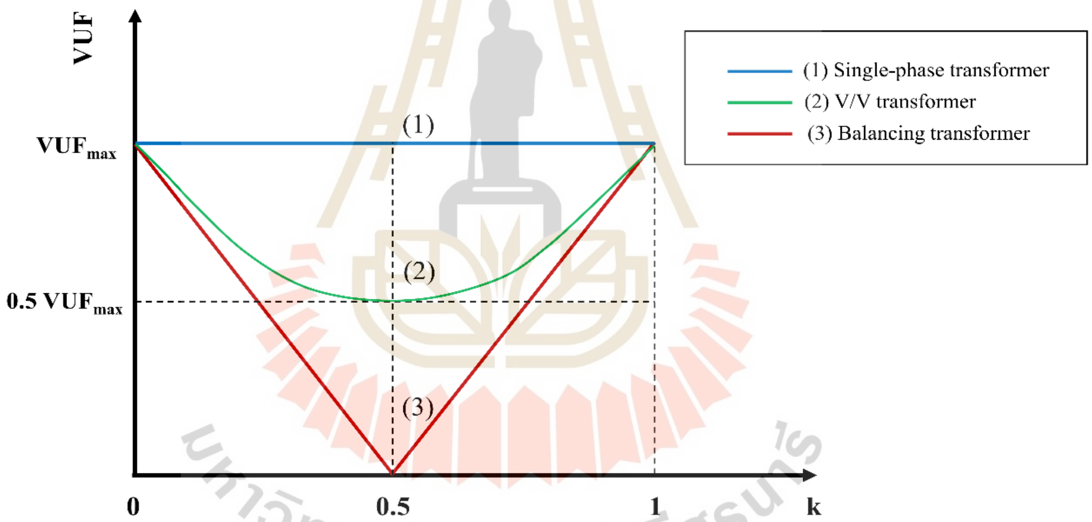

Fig. 2.21 VUFs versus load distribution curves for different transformer types

(Adapted from Chen and Guo, 1996)

2.4 Compensating devices in railway power supply systems

A heavy and single-phase traction load from electrified railway lines impose power quality problems into public grids feeding traction substations. Some of the predominant problems are negative-sequence currents/voltages, voltage drops both in a three-phase grid and along catenary feeders, harmonics currents, and low power factor. This section provides a brief review of the compensating devices or conditioners used and/or being researched in railway power supply.

2.4.1 Static VAR compensator (SVC)

A static VAR compensator (SVC) is a device used in transmission and distribution systems called distribution static VAR compensator (D-SVC) to provide dynamic and fast-acting reactive power control in a given bus and harmonic filtering. By controlling reactive power, the SVC can improve power factor, regulate bus voltages, suppress voltage fluctuation, and aid the balance of three-phase power systems. It has been extensively applied in many substations due to its low cost, simple control, and low maintenance. Typically, the SVC consists of a step-down transformer and other static equipment with reactors and capacitors; see Fig. 2.22. There are several types of the SVC: SVC using a thyristor-controlled reactor (TCR) and a fixed capacitor (FC), SVC using a TCR and a thyristor-switched capacitor (TSC), SVC using a saturable reactor, and before a static device was developed, mechanically switched shunt capacitors had been used for reactive power compensation (Noroozian, Petersson, Thorvaldson, Nilsson, and Taylor, 2003). Also, harmonic filters are included in the SVC to mitigate the harmonics produced by TCRs and by other loads in a system.

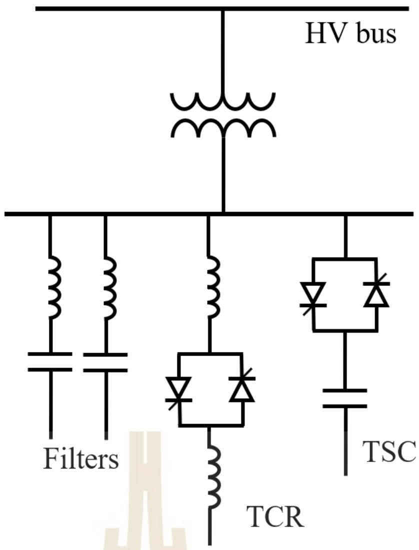

Fig. 2.22 SVC configurations

(Noroozian, Petersson, Thorvaldson, Nilsson, and Taylor, 2003)

The working principle of the SVC is to vary its susceptance to either absorb or feed reactive power from/to the point being compensated, or it can be said that the SVC can operate in both a capacitive and inductive range by adjusting the firing angle of a thyristor and switching on/off a capacitor in case of using the TCR and TSC, respectively. The steady-state characteristics of the SVC using a TCR and an FC are given here as an example of typical SVC characteristics. Fig. 2.23 shows the voltage-Mvar relationship of the SVC. The operational range is located between points A and B, or in some cases, the narrower range within the line AB in order to leave a little capacity as a reserve. In this range, the reactive power is continuously controlled by varying the firing angle (α) of the TCR, hence varying the susceptance of the SVC ($B_L(\alpha)$), and the voltage and reactive power are linearly related. The SVC functions as a normal inductor and capacitor outside the controlled region, i.e., the reactive power increases quadratically with the voltage.

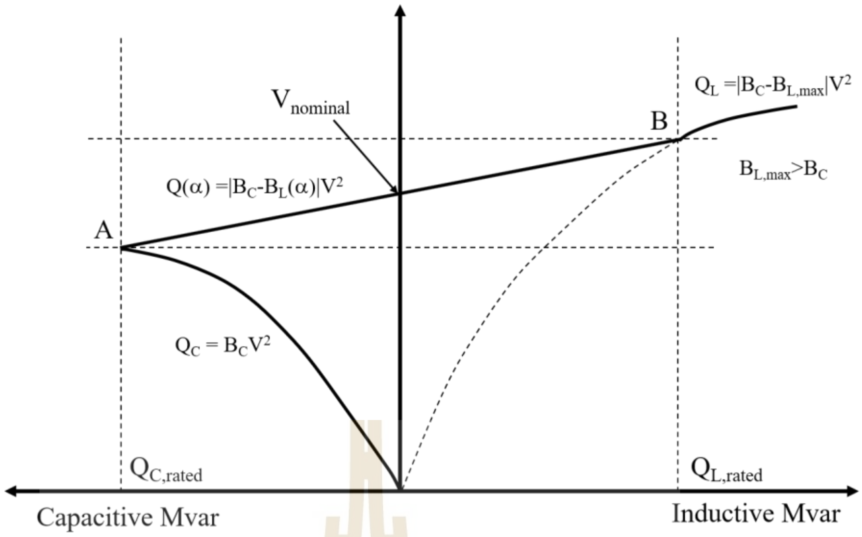

Fig. 2.23 Voltage-reactive power characteristic of the SVC

(Adapted from Vedam and Sarma, 2009)

In the light of the benefits of the SVCs use in transmission and distribution systems, AC railway power supply in many countries, such as France, UK, Australia, Japan, and China, has also adopted the technology of SVCs. Predominantly, to reduce negative-sequence currents/voltages and voltage support together with harmonic filtering and power factor improvement. The configurations and purposes vary with countries. For instance, Japan used an SVC to help balancing transformers to eliminate negative-sequence components. The Chinese Shenshuo railway and the Australian Queensland railway used an SVC to provide voltage support in the traction side and used another SVC installed in the system side to balance three-phase voltages of several traction substations using the same feeding substation. The Chunnel electric railway and An-ding traction substation in China also used a single-phase SVC to regulate traction side voltage, suppress harmonics and improve power factor (Wang, Liu, Yan, Fu, and Zhang, 2015). Various common configurations of SVCs in railway applications are as follows:

- *Configuration 1*: A three-phase SVC (both TCRs and FCs) is connected to the high-voltage side of a traction substation through a step-down transformer, as shown in Fig. 2.24 (a).
- *Configuration 2*: This configuration is similar to configuration 1 except that an FC is directly connected to the high-voltage side of a traction substation, as shown in Fig. 2.24 (b).
- *Configuration 3*: A three-phase SVC is connected to the secondary side of a traction substation transformer, as shown in Fig. 2.24 (c).
- *Configuration 4*: Two single-phase SVCs are separately connected to each secondary side of a traction substation transformer, as shown in Fig. 2.24 (d).
- *Configuration 5*: One single-phase SVC is connected to the secondary side of a traction transformer between the catenary (C) and rail (R) for an autotransformer (AT)-fed system; see Fig. 2.24 (e).
- *Configuration 6*: Two single-phase SVCs are connected to the secondary side of a traction transformer between the catenary (C) and rail (R), and between the feeder (F) and rail (R) for an AT-fed system; see Fig. 2.24 (f).

All SVC configurations in AC traction power supply mentioned above reduce the voltage unbalance and harmonics and improve power factor successfully, but each configuration has its advantage and drawback. The connection of SVCs with the high-voltage side of a traction substation like in Configuration 1 and 2 has a better balancing solution than other configurations. However, it requires greater insulation levels and higher costs. Unlike Configuration 1, the absence of a step-down transformer for an FC enables a better effect on harmonic filtering. Configuration 3 also employs a three-phase SVC but, instead, is connected to the traction side. Without a step-down transformer and lower-voltage rating, an individual SVC is less expensive. This configuration has a compensating coverage for only one traction substation compared to Configurations 1 and 2 that can operate covering several traction substations in the three-phase supply side. Configuration 4 has the advantages of independent reactive compensation or power factor improvement for each secondary phase, traction voltage

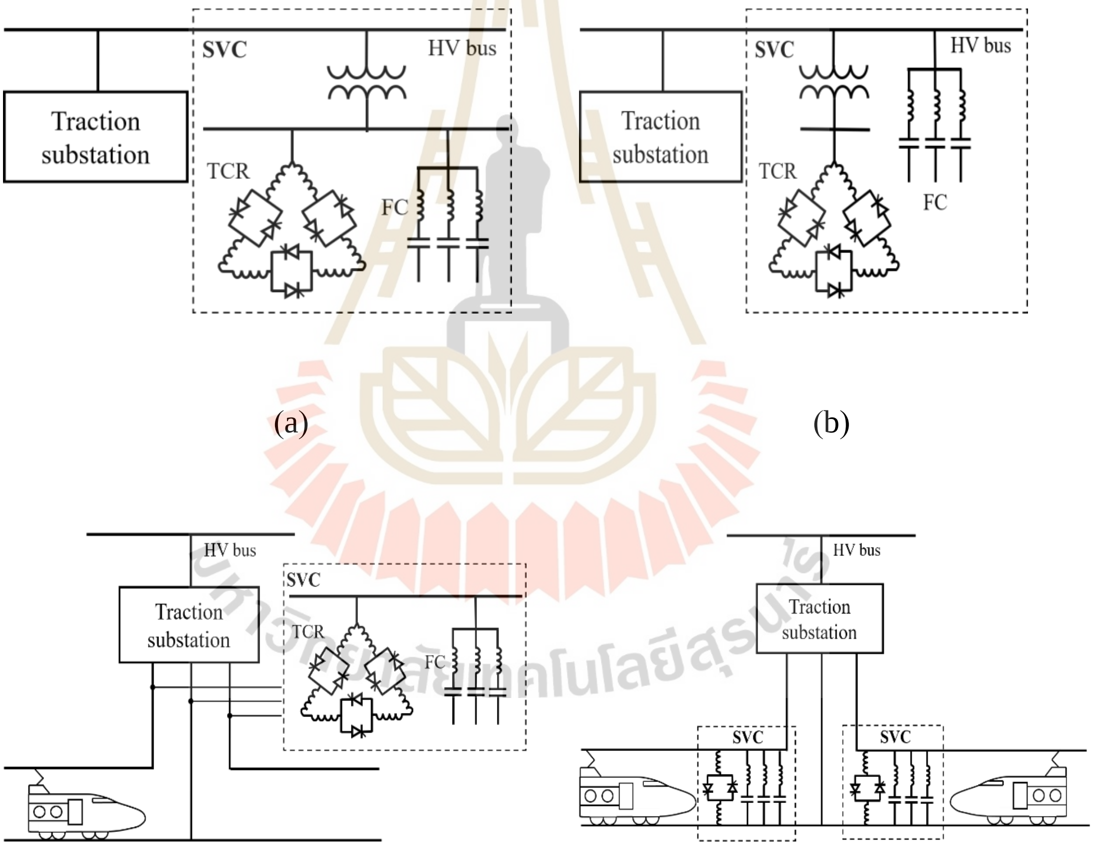

(a) (b)

(c) (d)

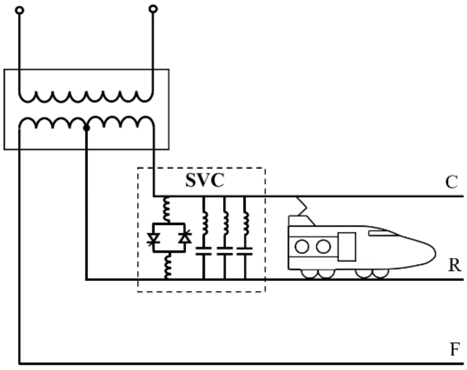

(e)

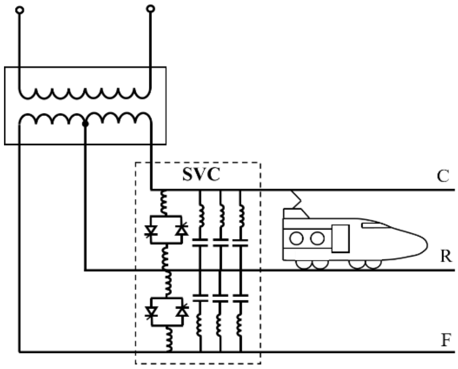

(f)

Fig. 2.24 SVC's common configurations in railway application (Adapted from Wang et al., 2015) (a) Configuration 1, (b) Configuration 2, (c) Configuration 3, (d) Configuration 4, (e) Configuration 5, and (f) Configuration 6

regulation, and traction voltage fluctuation suppression. Furthermore, the location of the SVC in this configuration varies according to its optimal operation. Kawahara, Hase, Mochinaga, Hidamizu, and Inoue (1997) revealed that it was preferable to place an SVC at the sectioning post (SP) rather than at the traction substation to reduce voltage drops. Also, this solution applies to Configuration 5. Placing an SVC at the SP effectively provides voltage support in the contingency case that one feeder has to supply the adjoining feeder that fails to operate. In the case of using SVCs in the AT-fed system, Configurations 5 and 6 are adopted. Configuration 6 has better performance and is costlier than Configuration 5, owing to using two SVCs for the C-R phase and F-R phase.

Apart from the common SVC configurations mentioned earlier, different control methods and configurations can be customised to meet specific objectives or requirements for different systems, e.g., different traction transformer types and the like. For instance, a phase-shifted Scott transformer type SVC and a new hybrid SVC have been proposed to be used specifically for the traction substation using the Scott transformer (Chu and Gu, 2006).

2.4.2 Static synchronous compensator (STATCOM)

A static synchronous compensator (STATCOM) is a converter-based compensating device and is one of the FACTS family. The term “static” refers to no moving components. In the most basic form, the STATCOM consists of a converter, i.e., either a voltage source converter or current source converter, a DC capacitor, and a step-down transformer, as shown in Fig. 2.25. It can outperform all the functions an SVC can do with faster response and more robustness. In addition, it takes up less installation area but is higher-priced. Besides, another energy storage could be fitted into the DC side of the STATCOM to provide the active power flow capability. With the development of high-power semiconductor devices, the STATCOM’s converter rating, especially the voltage source converter, can exceed 100 MVA at present.

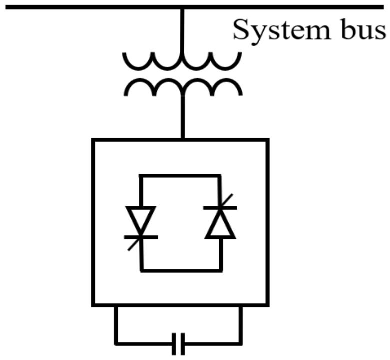

Fig. 2.25 The diagram of the STATCOM

From a power system viewpoint, the STATCOM is typically implemented in a transmission system. In contrast, in lower-voltage levels or a distribution system, a device called a “distribution STATCOM (DSTATCOM)” is employed. The latter is a member of the custom power devices. The distinctions between these two are their operation and systems for which they are used. The STATCOM generates symmetrical output voltages or injects symmetrical currents. On the contrary, the DSTATCOM can generate the unbalanced ones to compensate for unbalanced system voltages/currents.

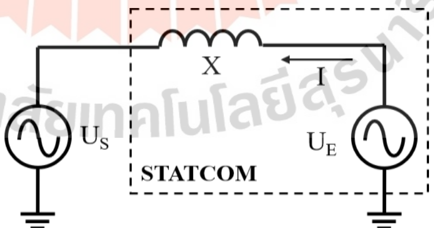

Fig. 2.26 The equivalent circuit of the STATCOM

The equivalent circuit of the STATCOM can be formed comprising of the AC source and reactance of the step-down transformer. The resistance is neglected due to its infinitesimal value relative to the reactance in Ohm. Fig. 2.26 shows the

STATCOM equivalent circuit connected to a system bus with the system bus voltage, converter voltage, and reactance denoted by U_S, U_E, and X, respectively. The flow of active and reactive power from the STATCOM to the system can be achieved and calculated by (2.4) and (2.5), where δ is the phase difference between U_S and U_E. Generally, the STATCOM only generates/absorbs reactive power to/from the system, so δ is completely zero. In actuality, δ has a small value due to the losses in the STATCOM.

$$P = \frac{U_E U_S}{X}\sin(\delta) \tag{2.4}$$

$$Q = \frac{U_E U_S}{X}\cos(\delta) - \frac{U_S^2}{X} \tag{2.5}$$

The major reasons for using the STATCOM in AC railway applications are to reduce voltage, current unbalances, compensate reactive power or regulate the traction voltage, and alleviate harmonics caused by train loads. It can be installed on the system side to solve the problems in grids supplying traction substations, as shown in Fig. 2.27. Furthermore, it can be installed on the lower-voltage traction side to compensate traction loads directly, provide voltage support, and reduce voltage fluctuation; see Fig. 2.28. The STATCOM can also operate with other devices, such as fixed capacitor banks and filters. Its control methods, simulation, and planning have been widely researched in literature. The practical applications in traction power supply systems, for example, are as follows:

- The adoption of the STATCOM and the fixed compensator for the traction substation using the Scott transformer in the Inner Mongolia region (Zhang, Liu, Pang, 2012).

- The use of the 16 MVA ABB STATCOM called SVC Light® and installed on the 90 kV three- phase traction power supply system as a balancer in the Evron substation, France. This case proved that using the SVC Light® was cheaper and had less construction time than building new transmission lines (Grunbaum, 2007).

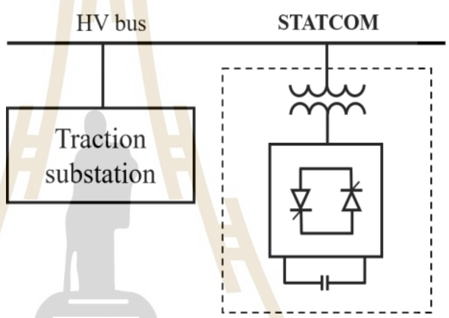

Fig. 2.27 The STATCOM in the high-voltage side

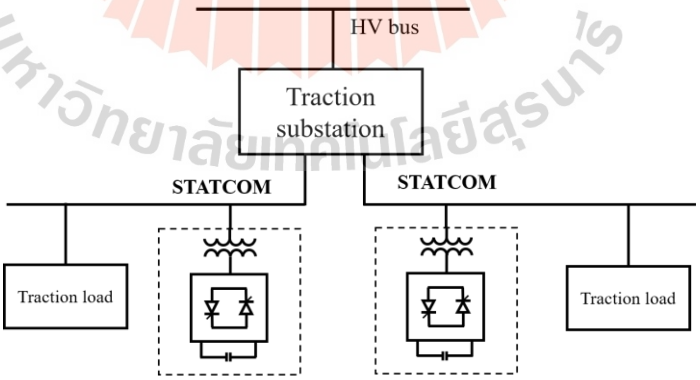

Fig. 2.28 The STATCOM in the traction side

2.4.3 Dynamic voltage regulator (DVR)

A dynamic voltage regulator or restorer (DVR) is a series-connected compensator for a power distribution system. It is one of the custom power devices whose FACTS counterpart is a static synchronous series compensator (SSSC). Its components are a converter, DC capacitor and/or DC storage system, and a series transformer, as shown in Fig. 2.29. In other words, the configuration is similar to the STATCOM, but the coupling transformer is interfaced with the system in series. Its primary duty is to detect and compensate voltage dips and swells dynamically and rapidly in the line where disturbances take place. It can also control active power flow in the line by injecting voltage in quadrature with the line voltage (Acha, Agelidis, Anaya-Lara, Miller, 2002). With its series compensation characteristics, the line reactance can be increased or decreased to regulate power transmission, i.e., decreasing the line reactance using capacitive compensation leads to more power transfer and vice versa. Fig. 2.30 demonstrates the basic series compensation principle and the transmitted power obtained by (2.6), which is consistent with the above explanation; where U_R is the receiving end voltage, U_S is the sending end voltage, X_C is the capacitive reactance generated by the DVR, and X_L is the line reactance, (Hingorani and Gyugyi, 2000).

$$P = \frac{U_R U_S}{(\mathrm{X}_L - \mathrm{X}_C)} \sin(\delta) \tag{2.6}$$

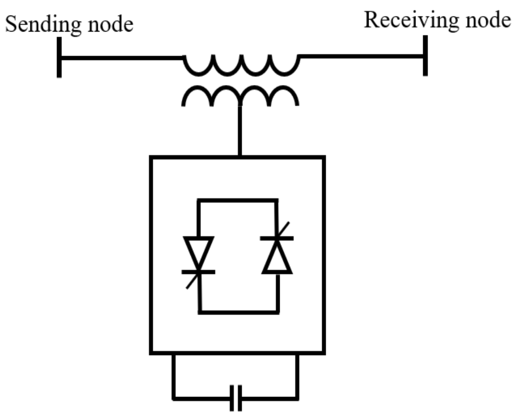

Fig. **2.29** The diagram of the DVR

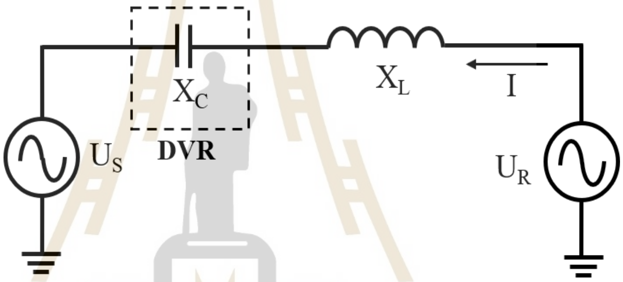

Fig. **2.30** The line compensation diagram of the DVR

The DVR and other kinds of series compensators have not been extensively mentioned in past literature on railway applications; because a series connection adds another bus in the system and it seems unlikely to install in an existing system compared to the shunt compensator. Instead, its computer simulation and modelling remain active, particularly in a distribution system with a high-maintenance and sensitive load. Sekhar, Kale, and Krishna (2014) presented the simulation and control of the DVR in the 25-kV traction power supply system to study its performance of the traction voltage regulation and compensation. See the schematic representation in Fig. 2.31.

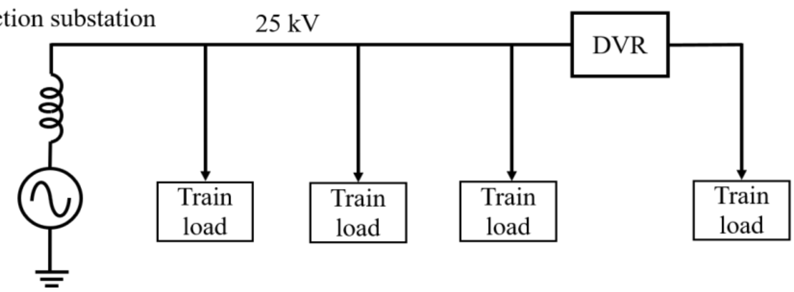

Fig. 2.31 The circuit representation of the DVR in the traction feeder

(Adapted from Sekhar, Kale, and Krishna, 2014)

2.4.4 Unified power quality conditioner (UPQC)

A unified power quality conditioner (UPQC) is a combined series-shunt compensator with the capabilities of a series and shunt active filter. It is a custom power device formed by a DVR as a series active filter and a DSTATCOM as a shunt active filter; both are connected to each other via a DC-link capacitor. The series part is responsible for load voltage-related problems, e.g., voltage unbalance, voltage harmonics, and voltage dips/swells. It generates the compensating voltage in series with

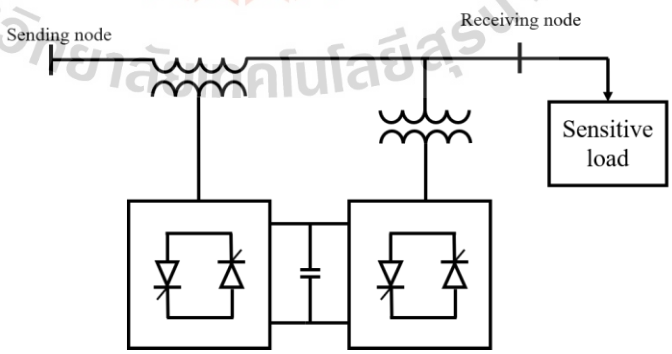

Fig. 2.32 The diagram of the conventional UPQC

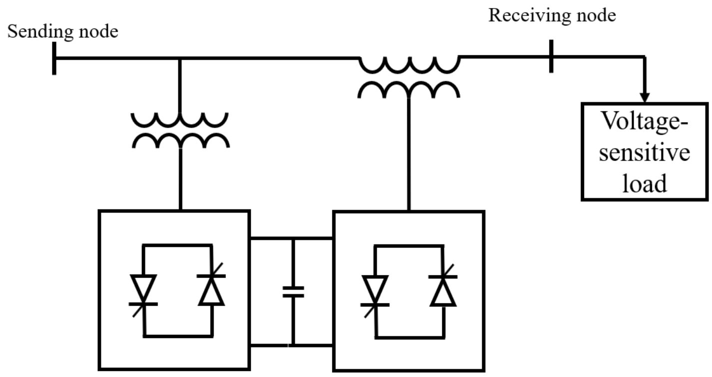

Fig. 2.33 The diagram of the left shunt UPQC

the system. The shunt part is responsible for current-related problems, e.g., negative-sequence currents, current distortion, power factor improvement, and injects the compensating current into the system. In addition to the original or conventional UPQC, as shown in Fig. 2.32, numerous UPQC topologies have been recently introduced for different specific purposes. The left shunt UPQC has been proposed for use with the specially voltage-sensitive load (Patnaik, Panda, and Mohanty, 2016); see Fig. 2.33. As opposed to the conventional one whose shunt converter is placed on the right side. Another new topology of the UPQC proposed a few years ago is an Open UPQC. As the name suggests, the shunt and series active filters of the Open UPQC are not linked together (Morris, Roberto, and Enrico, 2009). The Open UPQC is more advantageous and flexible in terms of use with multiple loads in which a few loads are sensitive, as illustrated in Fig. 2.34. The higher capacity of the series converter is installed on the upstream feeder and the small shunt converters on the downstream feeder to compensate for only the sensitive loads; this configuration helps reduce the overall size of the Open UPQC.

The UPQC is well-suited for a distribution system with critically sensitive loads. A FACTS device that performs the equivalent functions as the UPQC in a transmission system is a unified power flow controller (UPFC). According to past published researches, the UPQC has not been thoroughly studied and applied in railway traction power supply applications. As a result, the comprehensive compensative solution for the traction power supply system is created using the principle relatively similar to the UPQC, as presented in the following section.

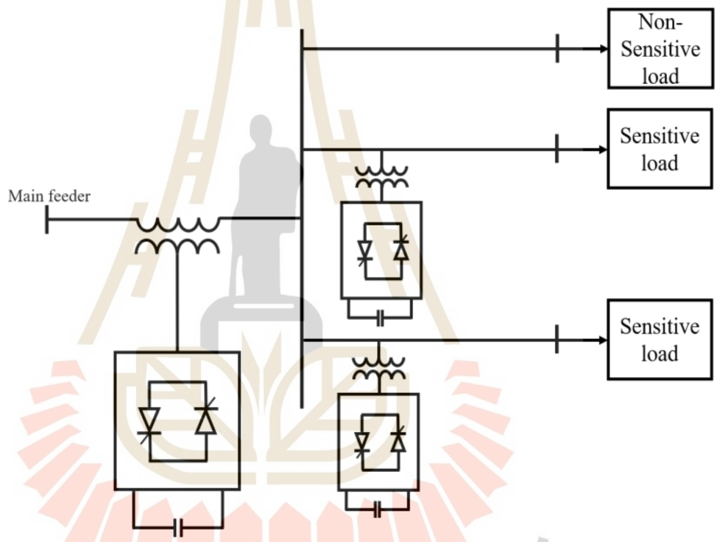

Fig. 2.34 The diagram of the Open UPQC

(Adapted from Tongzhen and Dongqiang, 2014)

2.4.5 Static railway power conditioner (RPC)

A static railway power conditioner (RPC) is a comprehensive compensator dedicated to railway power supply applications and originally pioneered by Mochinaga, Takeda, and Kasuike in 1993 from the Railway Technical Research Institute (RTRI), Japan. It was mainly intended to eliminate the voltage unbalance and fluctuation in a three-phase grid caused by a heavy single-phase traction load. Moreover, it was designed to boost the catenary voltage at the sectioning post and compensate harmonics. The RPC relies on the benefits of using balancing transformers, such as the Scott transformer, Modified Woodbridge transformer, Roof-delta transformer, and the like. It transfers half of the active power difference between both feeder loads from the lighter load side to the heavier load side to balance the power in the secondary side of traction transformers, which balances a three-phase grid at the point of common coupling. The RPC schematic representation and compensation diagram are shown in Fig. 2.35 and 2.36, respectively. The RPC structure consists of two converters with a back-to-back connection through the DC-link, enabling the RPC to transfer active power between two traction feeders with different phases and independently compensate reactive power and harmonics. Generally, there are two control modes of the RPC: SVC mode and RPC mode. The SVC mode achieves reactive compensation and voltage support like an SVC, especially when one of the traction substations is out of service, and the RPC has to support the extended feeder. The RPC mode transfers the active power between two secondary feeders of traction transformers, independently compensating the reactive power loads and harmonics currents.

The active power transfer is the top priority of this mode, and if the RPC capacity, left after performing the active power exchange, is sufficient to compensate the reactive power and harmonics. According to the published literature, the RPCs have been put into operation in two Shinkansen lines: Tohoku and Tokaido Shinkansen. In Tokaido Shinkansen, four traction substations were equipped with the RPC: Shimizu, Shin-Kikagawa, Shin-Biwajima, and Ritto substation (Horita et al., 2010). For Tohoku Shinkansen, the RPCs were installed at Shin-Numakunai and Shin-Hachinohe substations (Ohmi and Yoshii, 2010). Its high cost hinders it from widespread use; the RPC has been in actual operation only in Japan. Thus, the rigorous research in the RPC topologies and controls using computer simulation has been performed primarily to reduce its control and circuit complexity, capacity and cost, also to use with other types of traction transformers. Consequently, a hybrid RPC or RPC cooperated with other compensators has recently gained more attention from many researchers. The following RPCs are some of the modern compensators in AC railway power supply systems; all of them are in the research stage or developing process.

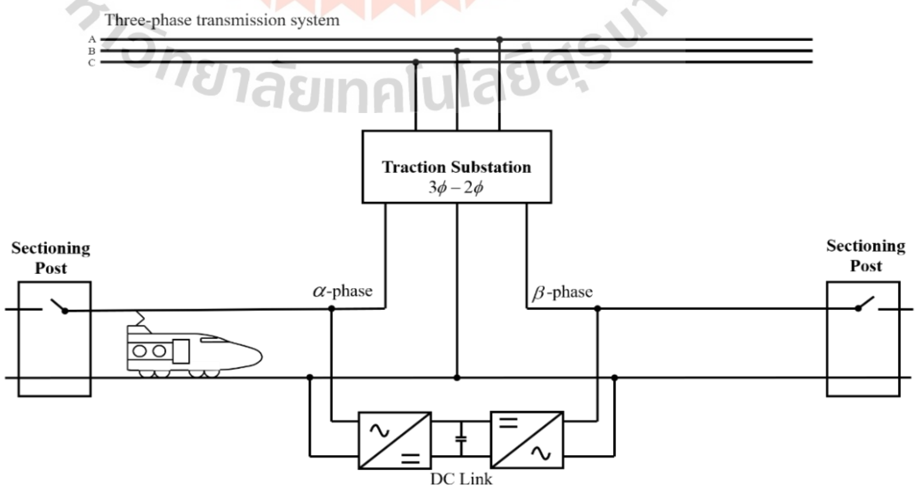

Fig. 2.35 The diagram of the RPC

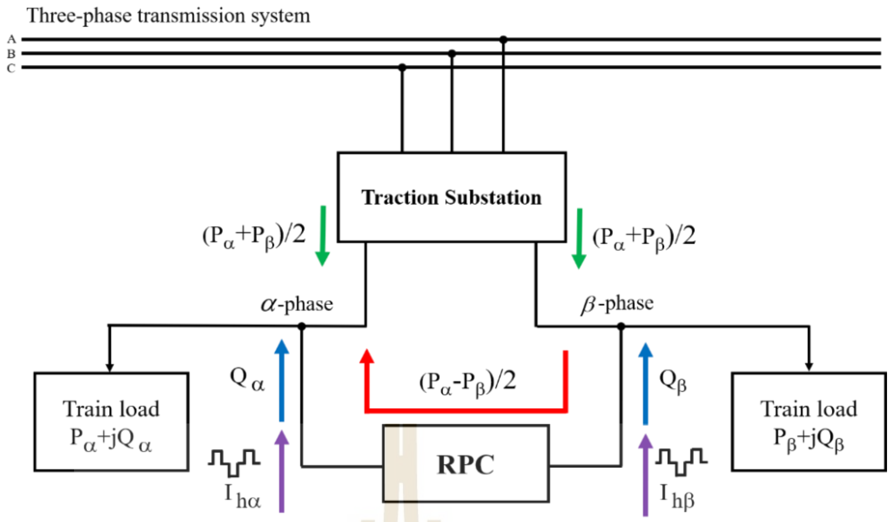

Fig. 2.36 The RPC compensation diagram

- *Enhanced railway power conditioner (ERPC)* – this RPC adopted closed-loop control by receiving three-phase currents/voltages on both the primary and secondary sides of the traction transformer and the DC-link voltage as input signals, then compensating until the optimal set point is reached. This direct control technique helps avoid a defect resulting from the slight differences in the transformer impedances and feeder lines (Chen et al., 2014).

- *Railway unified power quality controller (RUPQC)* – the RUPQC is introduced using the V/V transformer and consists of the traditional RPC, two TCRs installed on the lagging-phase secondary side, two thyristor-controlled high pass filter (TCHFs) installed on the leading-phase secondary side, and two single-phase three-winding transformers, as shown in Fig. 2.37. The TCRs and TCHFs compensate and shift the current phases while the RPC only transfers the active power between two secondary phases; therefore, the RPC's rating and cost are reduced (Zhang, Luo, Wu, and Ma, 2010).

- *Modular-multilevel-converter (MMC)-based RPC* – the MMC is another effective choice for the RPC. Shang, Dai, Wang, and Chen (2016) proposed the delta-connected MMC based RPC. This RPC controls the circulating current in the delta loop to compensate for the unbalance. There are other advantages concerning its control method, which can be found in the literature.

- *Half-bridge-converter-based RPC (HBRPC)* – this topology of the RPC uses a half-bridge converter; see Fig. 2.38, which has an advantage over the traditional RPC: reducing half the number of power switches, control complexity, and power losses while maintaining the same operation as the traditional RPC, e.g., reactive power, negative-sequence currents and harmonics compensation (Ma et al., 2013).

- *Hybrid railway power conditioner (HRPC)* – due to the high initial cost of the RPC, Liu and Dao (2016) developed the HRPC based on a half-bridge MMC as a low-cost option for traction substations with existing single-phase transformers. One side of the HRPC is connected to the traction feeder through an LC filter; the other side is coupled with the three-phase side via a step-down transformer, as illustrated in Fig. 2.39.

- *Z-source RPC (ZSRPC)* – a Z-source converter and impedance matching (IM) transformer are adopted to create a new topology of the RPC, as shown in Fig. 2.40. With the higher electrical efficiency and lower switching losses of the Z-source converter and proper control techniques, the ZSRPC can be designed to have lower rating and cost than those of the traditional RPC (Roudsari, Jalilian, and Jamali, 2016).

Besides, there are many other topologies and controls of the RPC under research and development. The above RPC topologies are some examples of the RPCs to demonstrate the research trend. The capabilities to improve power quality for each compensator mentioned above are summarised and compared in Table 2.1. All compensators can reduce the unbalance in the three-phase system. The DVR and UPQC are installed on the primary side of the traction transformer in this consideration. It is also noted that the RPC is capable of reducing all power quality problems in an AC railway power supply system despite its very high initial cost.

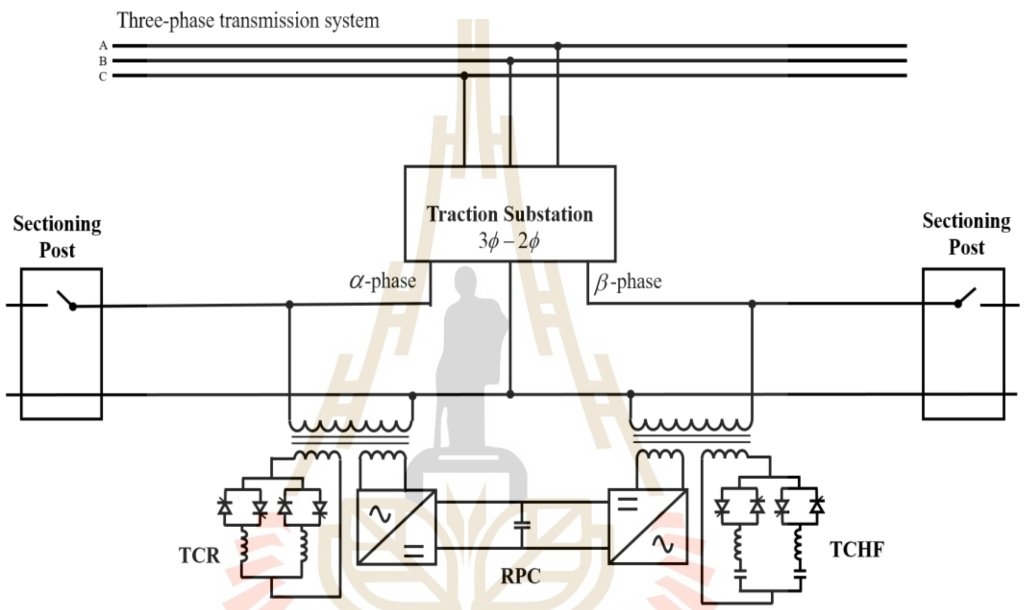

Fig. 2.37 The diagram of the RUPQC

(Adapted from Zhang, Luo, Wu, and Ma, 2010)

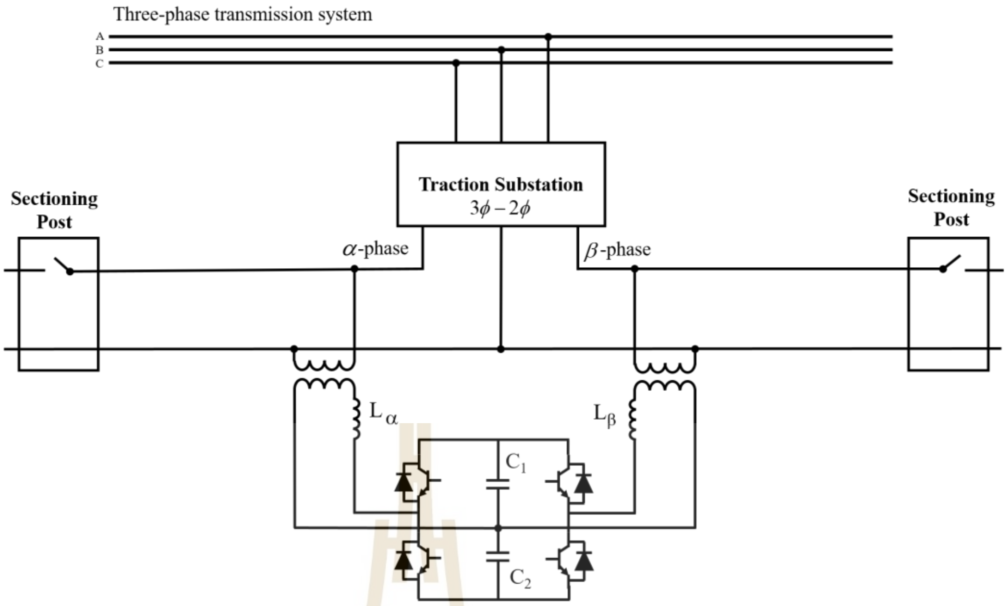

Fig. 2.38 The diagram of the HBRPC

(Adapted from Ma et al., 2013)

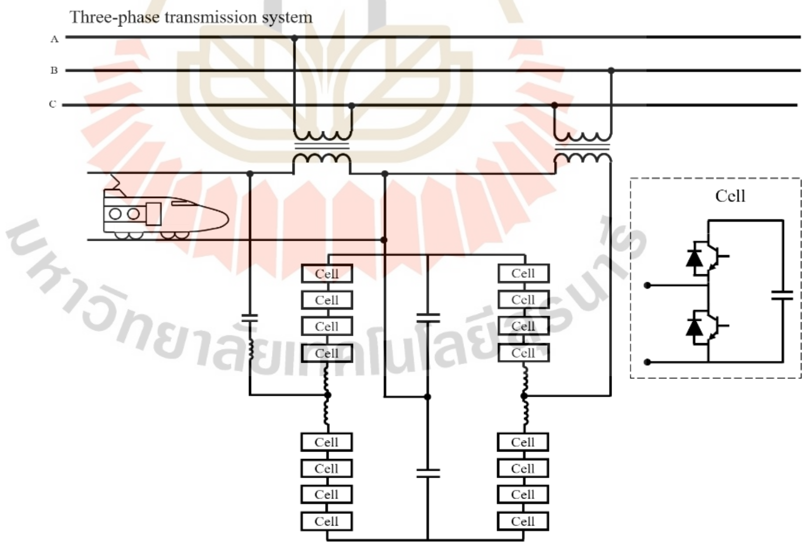

Fig. 2.39 The diagram of the HRPC

(Adapted from Liu and Dao, 2016)

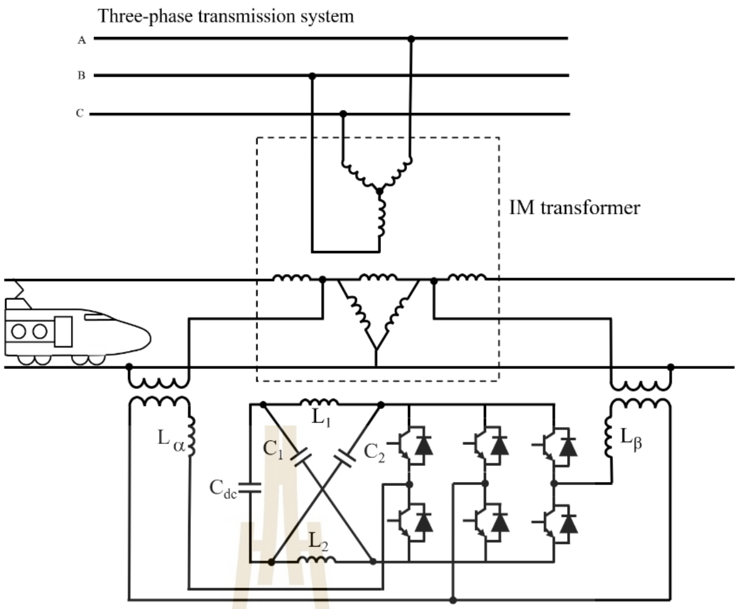

Fig. 2.40 The diagram of the ZSRPC

(Adapted from Roudsari, Jalilian, and Jamali, 2016)

Table 2.1 The compensators and their capabilities

Compensator	**Harmonic filtering**	**VAR compensation / Power factor improvement**	**Unbalance**	**Active power transfer**	**Voltage support**	**Cost**
SVC	-	✓	✓	-	✓	Low
STATCOM	✓	✓	✓	-	✓	High
DVR	✓	-	✓	-	✓	High
UPQC	✓	✓	✓	-	✓	Very high
RPC	✓	✓	✓	✓	✓	Very high

2.5 Power flow models of compensating devices

Given the compensators in section 2.4, the Newton-Raphson power flow models of them, as a tool to study steady-state operation, are briefly reviewed and described in this section.

2.5.1 SVC power flow model

The SVC can be modelled as a total variable reactance or susceptance by adjusting its TCR firing angle; see Fig. 2.41. The susceptance is taken as a state variable in the prevailing power flow system equations. During the iterative process, the susceptance is updated in such a way the voltage magnitude of the bus to which the SVC is connected is kept constant at the specified value. If the susceptance violates the upper and lower specified limits, the SVC is considered a normal reactance element, and the bus voltage is not regulated. The absorbed or consumed reactive power is not fixed at a limit value; nevertheless, it varies with the bus voltage.

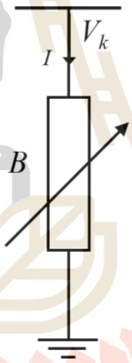

Fig. 2.41 The power flow model of the SVC
(Adapted from Ambriz-Perez, Acha, and Fuerte-Esquivel, 2000)

The current and reactive power of the SVC are expressed by (2.7) and (2.8), respectively. B is the total SVC susceptance, and V_k is the bus voltage.

$$I = jBV_k \tag{2.7}$$

$$Q_k = -BV_k^2 \tag{2.8}$$

The total susceptance becomes a state variable in the linearised equation; see (2.9), and the susceptance is updated using (2.10). Besides, the firing angle can be used as a state variable in place of the total susceptance by using the relation between the total equivalent susceptance (B_{eq}) and firing angle (α_{SVC}) as shown in (2.11), where X_C is the capacitive reactance of the SVC and X_L is the inductive reactance of the SVC.

$$\begin{bmatrix} \Delta P_k \\ \Delta Q_k \end{bmatrix}^i = \begin{bmatrix} 0 & 0 \\ 0 & Q_k \end{bmatrix}^i \begin{bmatrix} \Delta\theta_k \\ \Delta B_{SVC} / B_{SVC} \end{bmatrix} \tag{2.9}$$

$$B^{i+1}_{SVC} = B^{i}_{SVC} + \left(\frac{\Delta B_{SVC}}{B_{SVC}} \right)^i B^{i}_{SVC} \tag{2.10}$$

$$B_{eq} = -\frac{X_L - \frac{X_C}{\pi}\left(2(\pi - \alpha_{SVC}) + \sin(2\alpha_{SVC})\right)}{X_C X_L} \tag{2.11}$$

2.5.2 STATCOM power flow model

The STATCOM can be modelled as a variable fundamental voltage source coupled with a step-down transformer reactance (X_T); see Fig. 2.42. The converter bus is added into the system, and the converter voltage magnitude (V_{stat}) and phase angle (θ_{stat}) become state variables. The converter voltage magnitude and angle are adjusted within the limit range ($V_{stat,min} \le V_{stat} \le V_{stat,max}$ and $0 \le \theta_{stat} \le 2\pi$) so that the bus voltage is regulated at a specified value. In the case of converter voltage magnitude violation, the controlled bus will return to be a load bus and the converter voltage will be the limit value. The real and reactive powers of the converter bus and the regulated (kth) bus are calculated by (2.12) - (2.15).

$$P_{stat} = V_{stat}^2 G_T - V_{stat} V_k \left(G_T \cos(\theta_{stat} - \theta_k) + B_T \sin(\theta_{stat} - \theta_k) \right) \tag{2.12}$$

$$Q_{stat} = -V_{stat}^2 B_T - V_{stat} V_k \left(G_T \sin(\theta_{stat} - \theta_k) - B_T \cos(\theta_{stat} - \theta_k) \right) \tag{2.13}$$

$$P_k = V_k^2 G_T - V_k V_{stat} \left(G_T \cos(\theta_k - \theta_{stat}) + B_T \sin(\theta_k - \theta_{stat}) \right) \tag{2.14}$$

$$Q_k = -V_k^2 B_T - V_k V_{stat} \left(G_T \sin(\theta_k - \theta_{stat}) - B_T \cos(\theta_k - \theta_{stat}) \right) \tag{2.15}$$

The linearised matrix equation, as well as the Jacobian matrix, is obtained as the following equation.

$$\begin{bmatrix} \Delta P_k \\ \Delta Q_k \\ \Delta P_{stat} \\ \Delta Q_{stat} \end{bmatrix} = \begin{bmatrix} \frac{\partial P_k}{\partial \theta_k} & \frac{\partial P_k}{\partial V_k} V_k & \frac{\partial P_k}{\partial \theta_{stat}} & \frac{\partial P_k}{\partial V_{stat}} V_{stat} \\ \frac{\partial Q_k}{\partial \theta_k} & \frac{\partial Q_k}{\partial V_k} V_k & \frac{\partial Q_k}{\partial \theta_{stat}} & \frac{\partial Q_k}{\partial V_{stat}} V_{stat} \\ \frac{\partial P_{stat}}{\partial \theta_k} & \frac{\partial P_{stat}}{\partial V_k} V_k & \frac{\partial P_{stat}}{\partial \theta_{stat}} & \frac{\partial P_{stat}}{\partial V_{stat}} V_{stat} \\ \frac{\partial Q_{stat}}{\partial \theta_k} & \frac{\partial Q_{stat}}{\partial V_k} V_k & \frac{\partial Q_{stat}}{\partial \theta_{stat}} & \frac{\partial Q_{stat}}{\partial V_{stat}} V_{stat} \end{bmatrix} \begin{bmatrix} \Delta \theta_k \\ \frac{\Delta V_k}{V_k} \\ \Delta \theta_{stat} \\ \frac{\Delta V_{stat}}{V_{stat}} \end{bmatrix} \tag{2.16}$$

Additionally, the model can also work as a reactive power source or sink by setting the bus connected to the STATCOM as a load bus and specifying the reactive power generated at the converter bus.

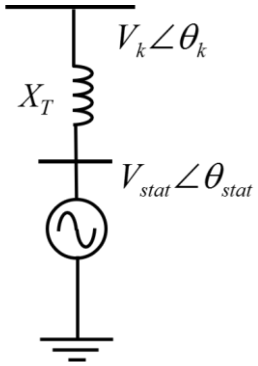

Fig. 2.42 The power flow model of the STATCOM (Adapted from Acha, Fuerte-Esquivel, Ambriz-Perez, and Angeles-Camacho, 2004)

2.5.3 DVR power flow model

In power flow calculation, the DVR is modelled similarly to the STATCOM. The distinction is that the DVR is a converter source (Thevenin equivalence) connected in series between two buses, as shown in Fig. 2.43 (a). The DVR power equations can be formed as in (2.17) and (2.18).

$$\begin{aligned} P_{DVR} = {} & V_{DVR}^2 G_T + V_{DVR} V_k \left(G_T \cos\left(\theta_{DVR} - \theta_k\right) + B_T \sin\left(\theta_{DVR} - \theta_k\right)\right) - \ldots \\ & V_{DVR} V_m \left(G_T \cos\left(\theta_{DVR} - \theta_m\right) + B_T \sin\left(\theta_{DVR} - \theta_m\right)\right) \end{aligned} \tag{2.17}$$

$$\begin{aligned} Q_{DVR} = {} & -V_{DVR}^2 B_T + V_{DVR} V_k \left(G_T \sin\left(\theta_{DVR} - \theta_k\right) - B_T \cos\left(\theta_{DVR} - \theta_k\right)\right) - \ldots \\ & V_{DVR} V_m \left(G_T \sin\left(\theta_{DVR} - \theta_m\right) - B_T \cos\left(\theta_{DVR} - \theta_m\right)\right) \end{aligned} \tag{2.18}$$

Apart from the common Thevenin equivalent model, Tosaphol Ratniyomchai and Thanatchai Kulworawanichpong (2006) proposed a three-phase DVR steady-state power flow current injection model. The model was expressed in the Norton equivalent form as depicted in Fig. 2.43 (b), and the Gauss-Seidel method was employed in the literature to solve the power flow problem with the DVR. The current mismatch equation at the buses across the DVR can be obtained as shown in (2.19) and (2.20), where Y_{ki} is the element of the bus admittance matrix, and I_C is the injected current.

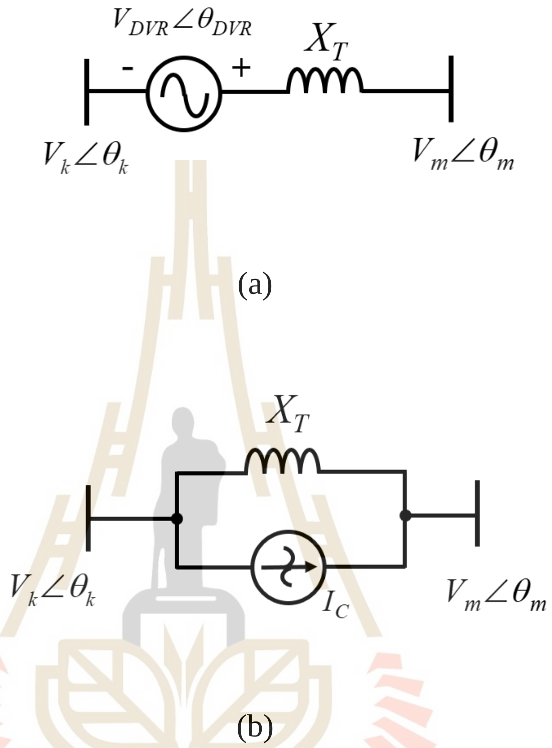

Fig. 2.43 The power flow model of the DVR

(a) Thevenin equivalent model, (b) Current injection model

$$\left(\frac{P_{sch,k}^{abc} - jQ_{sch,k}^{abc}}{V_k^{abc*}}\right) - I_{C,km}^{abc} = \sum_{i=1}^{n} Y_{ki}^{abc} V_i^{abc} \tag{2.19}$$

$$\left(\frac{P_{sch,m}^{abc} - jQ_{sch,m}^{abc}}{V_m^{abc*}}\right) + I_{C,km}^{abc} = \sum_{i=1}^{n} Y_{mi}^{abc} V_i^{abc} \tag{2.20}$$

2.5.4 UPQC power flow model

Based on steady-state analysis in the power flow calculation and from an equivalent circuit point of view, the UPQC power flow model resembles the UPFC one, irrespective of the control strategy and converter topology. Consequently, it is possible to create the UPQC model as a combination of the STATCOM and DVR model; see Fig. 2.44. The powers of the series and shunt converter are expressed in (2.21) and (2.22), respectively, where $Y_{cR} = G_{cR} + jB_{cR}$ is the admittance of the series converter and $Y_{vR} = G_{vR} + jB_{vR}$ is the admittance of the shunt converter. θ_{cR} and θ_{vR} is the phase angles of the series (V_{cR}) and shunt (V_{vR}) injected voltage, respectively. As the real power is exchanged between the shunt and series converter, i.e., the power entering one converter equals the power leaving the other, the constraint, as shown in (2.23), is included in power flow calculation. The Newton-Raphson Jacobian matrix formulation and further details can be found in the literature (Fuerte-Esquivel, Acha, and Ambriz-Perez, 2000).

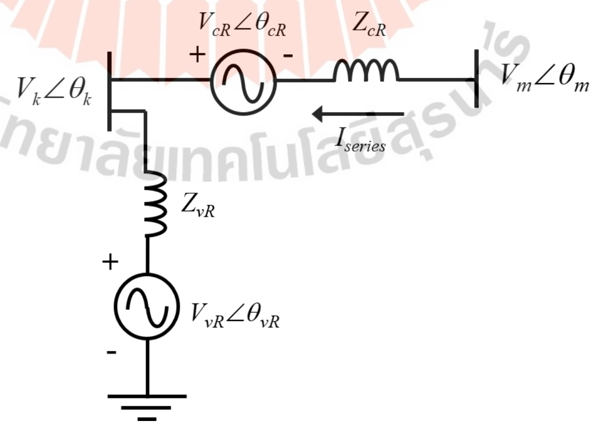

Fig. 2.44 The power flow model of the UPQC
(Adapted from Hosseini, Shayanfar, and Fotuhi-Firuzabad, 2009)

$$P_{cR} = V_{cR}^2 G_{cR} - V_{cR} V_k \left(G_{cR} \cos(\theta_{cR} - \theta_k) + B_{cR} \sin(\theta_{cR} - \theta_k) \right) + \ldots \\ V_{cR} V_m \left(G_{cR} \cos(\theta_{cR} - \theta_m) + B_{cR} \sin(\theta_{cR} - \theta_m) \right) \tag{2.21}$$

$$P_{vR} = -V_{vR}^2 G_{vR} + V_{vR} V_k \left(G_{vR} \cos(\theta_{vR} - \theta_k) + B_{vR} \sin(\theta_{vR} - \theta_k) \right) \tag{2.22}$$

$$P_{cR} + P_{vR} = 0 \tag{2.23}$$

In addition to the model mentioned above, the UPQC steady-state model for voltage compensation in a distribution system has been rigorously analysed and created by Hosseini, Shayanfar, and Fotuhi-Firuzabad (2009). The model was made so that the shunt converter only injected constant reactive power into the target bus. For example, no active power exchanged between the two converters (V_{cR} is orthogonal to the angle of the current flow in series branch) and the injected series voltage magnitude and its angle were both unknowns for the solution to regulating the target bus voltage magnitude at the specified value. Considering the series part in Fig. 2.44, the simple Kirchhoff's voltage law equation was derived, as shown in (2.24), by which V_{cR} and θ_{cR} are obtained. This equation was algebraically solved and used in the iterative process of the backward/forward sweep power flow method.

$$V_{cR} \angle \theta_{cR} = V_k \angle \theta_k + Z_{cR} I_{series} - V_m \angle \theta_m \tag{2.24}$$

Alternatively, other relevant power flow models of the UPFC can be adopted for the UPQC, such as the load injection method, decoupled method, π load injection method, indirect method, and ideal transformer method, and have been studied and reviewed in the literature (Zhang and et al., 2015).

Chapter 3

Modelling of traction power supply components

3.1 Introduction

This chapter describes the formulation of traction power supply components' steady-state models used in the current-based Newton Raphson power flow calculation method in Chapter 4. In the study, the traction power supply components introduced in this chapter are based on the autotransformer traction power supply system including traction transformers (single-phase transformer, V/V transformer, and Scott transformer) modelled as Norton equivalent current sources, autotransformers with and without tap-changing mechanism modelled as passive admittance elements, a catenary system modelled as an impedance per unit length, a train load modelled as a constant power load, and a railway power conditioner modelled as optimisation-integrated double Norton equivalent current sources.

3.2 Traction transformers

This section describes the modelling of traction transformers, which in turn are used in the current-based Newton-Raphson power flow calculation. The traction transformers considered in this thesis are a single-phase transformer, a V/V transformer and a Scott transformer, i.e. all transformers are designed for the autotransformer-fed traction power supply system. The modelling employs basic circuit analysis and aims to obtain a current injection or current source model with a current source matrix and an admittance matrix

3.2.1 Single phase transformer

An equivalent circuit of a single-phase transformer with a centre tap on a secondary winding is shown in Fig. 3.1. This model does not take a magnitising impedance into consideration. The relation between the primary and secondary voltages is expressed in equation (3.1). By using the Kirchhoff's voltage and current law, the voltage relation of both primary and secondary circuit and the current relation of the secondary circuit can be obtained as in equation (3.2) - (3.4) and equation (3.5), respectively. The primary current can be written as a function of the secondary currents shown in equation (3.6).

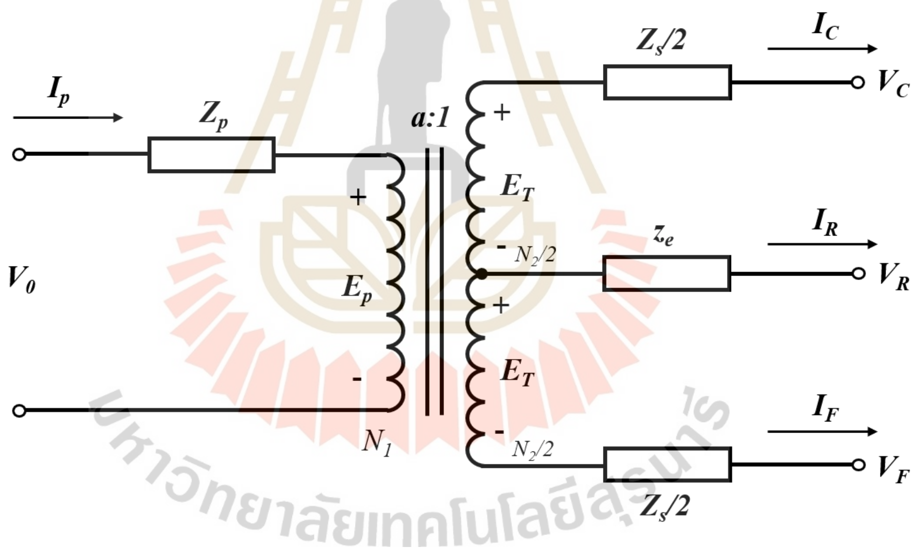

Fig. 3.1 Equivalent circuit of the single-phase transformer

$$\frac{E_p}{E_T} = 2a \tag{3.1}$$

$$V_0 = E_p + I_p Z_p \tag{3.2}$$

$$V_C - V_R = E_T + z_e I_R - \frac{Z_s}{2} I_C \tag{3.3}$$

$$V_R - V_F = E_T - z_e I_R + \frac{Z_s}{2} I_F \tag{3.4}$$

$$I_C + I_R + I_F = 0 \tag{3.5}$$

$$I_p = \frac{1}{2a}\left(I_C - I_F\right) \tag{3.6}$$

Substitute equation (3.6) into equation (3.2) and (3.1), then obtain equation (3.7) and (3.8).

$$E_p = V_0 - Z_p I_p = V_0 - \frac{1}{2a}\left(I_C - I_F\right) Z_p \tag{3.7}$$

$$E_T = \frac{1}{2a} E_p = \frac{1}{2a} V_0 - \frac{1}{4a^2}\left(I_C - I_F\right) Z_p \tag{3.8}$$

Substitute equation (3.8) into equation (3.3) and (3.4), then the following equations are obtained.

$$V_C - V_R = \frac{1}{2a} V_0 - A I_C + z_e I_R + B I_F \tag{3.9}$$

$$V_R - V_F = \frac{1}{2a} V_0 - B I_C - z_e I_R + A I_F \tag{3.10}$$

Equation (3.5), (3.9) and (3.10) can be written in a matrix form as in equation (3.11) and can be solved for the secondary currents in equation (3.12).

$$\begin{bmatrix} A & -z_e & -B \\ 1 & 1 & 1 \\ -B & -z_e & A \end{bmatrix} \begin{bmatrix} I_C \\ I_R \\ I_F \end{bmatrix} = \frac{V_0}{2a} \begin{bmatrix} 1 \\ 0 \\ -1 \end{bmatrix} + \begin{bmatrix} -1 & 1 & 0 \\ 0 & 0 & 0 \\ 0 & 1 & -1 \end{bmatrix} \begin{bmatrix} V_C \\ V_R \\ V_F \end{bmatrix} \tag{3.11}$$

$$\begin{bmatrix} I_C \\ I_R \\ I_F \end{bmatrix} = \frac{V_0}{2a(A+B)} \begin{bmatrix} 1 \\ 0 \\ -1 \end{bmatrix} - \frac{1}{(A+B)(2z_e + A - B)} \begin{bmatrix} A+z_e & -A-B & B-z_e \\ -A-B & 2(A+B) & -A-B \\ B-z_e & -A-B & A+z_e \end{bmatrix} \begin{bmatrix} V_C \\ V_R \\ V_F \end{bmatrix} \tag{3.12}$$

The current and admittance matrices are defined using equation (3.12) as follows. Finally, the current source or current injection model is illustrated in Fig. 3.2.

$$J_{SS} = \frac{V_0}{2a(A+B)} \begin{bmatrix} 1 \\ 0 \\ -1 \end{bmatrix}$$

$$Y_{SS} = \frac{1}{(A+B)(2z_e + A - B)} \begin{bmatrix} A+z_e & -A-B & B-z_e \\ -A-B & 2(A+B) & -A-B \\ B-z_e & -A-B & A+z_e \end{bmatrix}$$

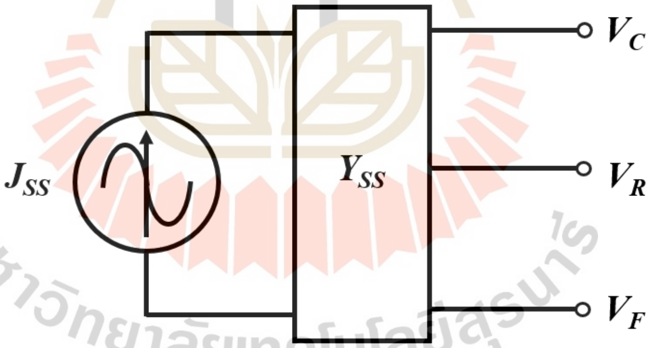

Fig. 3.2 The current injection model of the single-phase transformer

Note: variables' definitions

a transformer's turns ratio (N_1/N_2)

V_0 primary input voltage

E_p primary winding voltage

E_T secondary winding voltage (across the centre tap and the other phases)

I_p primary current

I_C secondary current (catenary)

I_R secondary current (running rail)

I_F secondary current (feeder)

V_C secondary voltage (catenary)

V_R secondary voltage (running rail)

V_F secondary voltage (feeder)

Z_p primary winding's leakage impedance

Z_s secondary winding's leakage impedance

z_e impedance connected between the centre tap and running rail

J_{SS} source current matrix

Y_{SS} source admittance matrix

$$A = \frac{Z_p}{4a^2} + \frac{Z_s}{2}, \quad B = \frac{Z_p}{4a^2}$$

3.2.2 V/V transformer

A V/V transformer can be simply considered as two single-phase transformers, α and β phase, as shown in Fig. 3.3. Therefore, the mathematical analysis of the model is similar to that of the single-phase transformer. The determination of the current source and admittance matrix is not required. The current injection model of the V/V transformer contains two single-phase transformer current injection models; see Fig. 3.4. The primary input voltage (V_0) is replaced by the line-to-line voltage according to the three-phase primary winding connection, e.g. V_{AB} and V_{CB} in Fig. 3.3.

Additionally, the relation between the three-phase primary currents and the primary currents of each winding is obtained by equation (3.13) where I_A, I_B and I_C represent the primary three-phase currents of phase A, B and C, respectively. $I_{C\alpha}$ and $I_{C\beta}$ represent the catenary current of α and β secondary winding, respectively. $I_{F\alpha}$ and $I_{F\beta}$ represent the feeder current of α and β secondary winding, respectively.

$$\begin{bmatrix} I_A \\ I_B \\ I_C \end{bmatrix} = \frac{1}{2a} \begin{bmatrix} 1 & 0 \\ -1 & -1 \\ 0 & 1 \end{bmatrix} \begin{bmatrix} I_{C\alpha} - I_{F\alpha} \\ I_{C\beta} - I_{F\beta} \end{bmatrix} \tag{3.13}$$

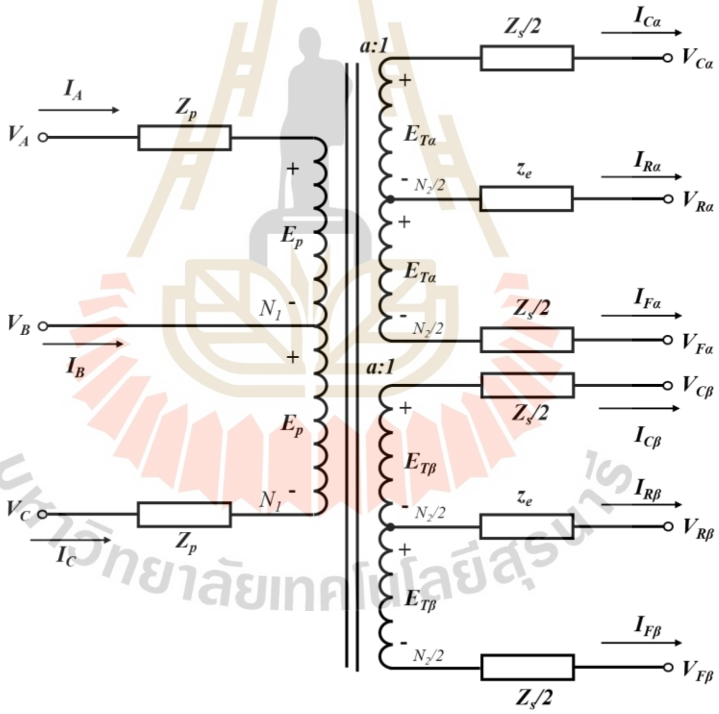

Fig. 3.3 Equivalent circuit of the V/V transformer

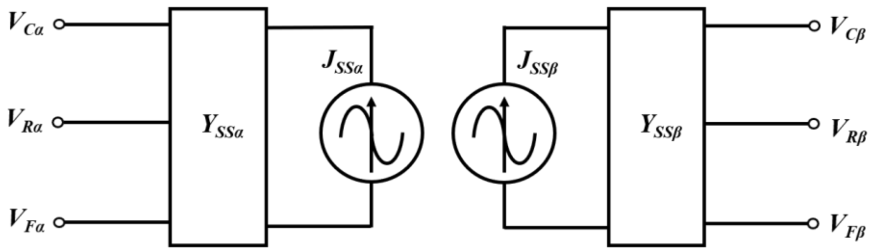

Fig. 3.4 The current injection model of the V/V transformer

3.2.3 Scott transformer

According to an equivalent circuit of the Scott transformer in Fig. 3.5, using the Kirchhoff's voltage law, the voltage equations for the primary circuit and the secondary circuit, Teaser phase (T) and Main phase (M), are obtained in equation (3.14) – (3.15) and equation (3.16) – (3.19), respectively.

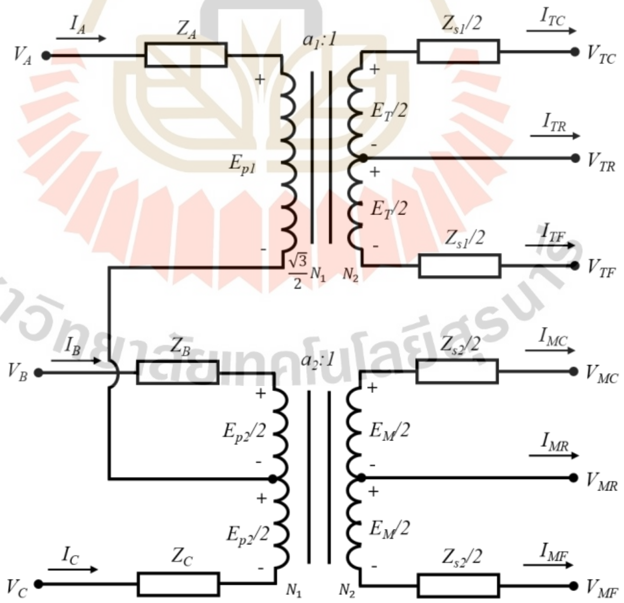

Fig. 3.5 Equivalent circuit of the Scott transformer

$$V_A - V_B = Z_A I_A - Z_B I_B + E_{p1} - \frac{E_{p2}}{2} \tag{3.14}$$

$$V_A - V_C = Z_A I_A - Z_C I_C + E_{p1} + \frac{E_{p2}}{2} \tag{3.15}$$

$$V_{TC} - V_{TR} = \frac{E_T}{2} - \frac{Z_{s1}}{2} I_{TC} \tag{3.16}$$

$$V_{TR} - V_{TF} = \frac{E_T}{2} + \frac{Z_{s1}}{2} I_{TF} \tag{3.17}$$

$$V_{MC} - V_{MR} = \frac{E_M}{2} - \frac{Z_{s2}}{2} I_{MC} \tag{3.18}$$

$$V_{MR} - V_{MF} = \frac{E_M}{2} + \frac{Z_{s2}}{2} I_{MF} \tag{3.19}$$

The relation between the primary and secondary currents is expressed in equation (3.20) – (3.22). And the sum of the primary currents is equal to zero according to the Kirchhoff's current law; see equation (3.23).

$$I_A = \frac{I_{TC}}{2a_1} - \frac{I_{TF}}{2a_1} \tag{3.20}$$

$$I_B = -\frac{I_{TC}}{4a_1} + \frac{I_{TF}}{4a_1} + \frac{I_{MC}}{2a_2} - \frac{I_{MF}}{2a_2} \tag{3.21}$$

$$I_C = -\frac{I_{TC}}{4a_1} + \frac{I_{TF}}{4a_1} - \frac{I_{MC}}{2a_2} + \frac{I_{MF}}{2a_2} \tag{3.22}$$

$$I_A + I_B + I_C = 0 \tag{3.23}$$

The relation between the primary and secondary winding's voltages is shown in equation (3.24). From equation (3.14) and (3.15), The T-phase and M-phase primary-side winding voltages can be derived as in equation (3.25) and (3.26), respectively.

$$E_{p1} = a_1 E_T , E_{p2} = a_2 E_M \tag{3.24}$$

$$E_{p1} = \frac{2V_A - V_B - V_C}{2} + \frac{Z_B}{2} I_B + \frac{Z_C}{2} I_C - Z_A I_A \tag{3.25}$$

$$E_{p2} = V_B - V_C + Z_C I_C - Z_B I_B \tag{3.26}$$

Substitute equation (3.20) - (3.22) into equation (3.25) and (3.26) to derive the T-phase and M-phase primary-side winding voltages shown in equation (3.27) and (3.28) which are substituted back into equation (3.16) – (3.19). Then, equation (3.29) – (3.32) are obtained.

$$\begin{aligned} E_{p1} = {} & \frac{2V_A - V_B - V_C}{2} + \frac{(Z_B - Z_C)}{4a_2} I_{MC} - \frac{(Z_B - Z_C)}{4a_2} I_{MF} \cdots \\ & - \frac{(4Z_A + Z_B + Z_C)}{8a_1} I_{TC} + \frac{(4Z_A + Z_B + Z_C)}{8a_1} I_{TF} \end{aligned} \tag{3.27}$$

$$\begin{aligned} E_{p2} = {} & (V_B - V_C) - \frac{(Z_B + Z_C)}{2a_2} I_{MC} + \frac{(Z_B + Z_C)}{2a_2} I_{MF} + \frac{(Z_B - Z_C)}{4a_1} I_{TC} \cdots \\ & - \frac{(Z_B - Z_C)}{4a_1} I_{TF} \end{aligned} \tag{3.28}$$

$$\begin{aligned} V_{TC} - V_{TR} = {} & \frac{(2V_A - V_B - V_C)}{4a_1} - \frac{(4Z_A + Z_B + Z_C + 8a_1^2 Z_{s1})}{16a_1^2} I_{TC} \cdots \\ & + \frac{(4Z_A + Z_B + Z_C)}{16a_1^2} I_{TF} + \frac{(Z_B - Z_C)}{8a_1 a_2} I_{MC} - \frac{(Z_B - Z_C)}{8a_1 a_2} I_{MF} \end{aligned} \tag{3.29}$$

$$\begin{aligned} V_{TR} - V_{TF} = {} & \frac{(2V_A - V_B - V_C)}{4a_1} - \frac{(4Z_A + Z_B + Z_C)}{16a_1^2} I_{TC} \cdots \\ & + \frac{(4Z_A + Z_B + Z_C + 8a_1^2 Z_{s1})}{16a_1^2} I_{TF} \cdots \\ & + \frac{(Z_B - Z_C)}{8a_1 a_2} I_{MC} - \frac{(Z_B - Z_C)}{8a_1 a_2} I_{MF} \end{aligned} \tag{3.30}$$

$$V_{MC}-V_{MR}=\frac{\left(V_B-V_C\right)}{2a_2}-\frac{\left(Z_B+Z_C+2a_2^2Z_{s2}\right)}{4a_2^2}I_{MC}+\frac{\left(Z_B+Z_C\right)}{4a_2^2}I_{MF}\cdots$$
$$+\frac{\left(Z_B-Z_C\right)}{8a_1a_2}I_{TC}-\frac{\left(Z_B-Z_C\right)}{8a_1a_2}I_{TF} \tag{3.31}$$

$$V_{MR}-V_{MF}=\frac{\left(V_B-V_C\right)}{2a_2}-\frac{\left(Z_B+Z_C\right)}{4a_2^2}I_{MC}+\frac{\left(Z_B+Z_C+2a_2^2Z_{s2}\right)}{4a_2^2}I_{MF}\cdots$$
$$+\frac{\left(Z_B-Z_C\right)}{8a_1a_2}I_{TC}-\frac{\left(Z_B-Z_C\right)}{8a_1a_2}I_{TF} \tag{3.32}$$

Equation (3.29) – (3.32) can be written in a matrix form as shown in equation (3.33) by which is solved for the secondary currents in equation (3.34).

$$\begin{bmatrix} V_{T,CR} \\ V_{T,RF} \\ V_{\mathrm{M},CR} \\ V_{\mathrm{M},RF} \end{bmatrix}=\begin{bmatrix} A/2 \\ A/2 \\ \mathrm{D}/2 \\ \mathrm{D}/2 \end{bmatrix}+\begin{bmatrix} -F & G & 0 & 0 \\ -G & F & 0 & 0 \\ 0 & 0 & -J & H \\ 0 & 0 & -H & J \end{bmatrix}\begin{bmatrix} I_{TC} \\ I_{TF} \\ I_{MC} \\ I_{MF} \end{bmatrix} \tag{3.33}$$

$$\begin{bmatrix} I_{TC} \\ I_{TF} \\ I_{MC} \\ I_{MF} \end{bmatrix}=\begin{bmatrix} \frac{F}{G^2-F^2} & \frac{-G}{G^2-F^2} & 0 & 0 \\ \frac{G}{G^2-F^2} & \frac{-F}{G^2-F^2} & 0 & 0 \\ 0 & 0 & \frac{J}{H^2-J^2} & \frac{-H}{H^2-J^2} \\ 0 & 0 & \frac{H}{H^2-J^2} & \frac{-J}{H^2-J^2} \end{bmatrix}\begin{bmatrix} V_{T,CR} \\ V_{T,RF} \\ V_{\mathrm{M},CR} \\ V_{\mathrm{M},RF} \end{bmatrix}-\begin{bmatrix} \frac{-1}{G+F}\frac{A}{2} \\ \frac{1}{G+F}\frac{A}{2} \\ \frac{-1}{J+H}\frac{D}{2} \\ \frac{1}{J+H}\frac{D}{2} \end{bmatrix} \tag{3.34}$$

As the sum of the secondary currents must be zero, the T-phase and M- phase running rail’s current can be determined. Finally, the matrix equations of the T-phase and M-phase equivalent current sources are derived as in equation (3.35) and (3.36), respectively. Subsequently, the source current and admittance matrices of the T-phase and M-phase equivalent current sources are obtained from equation (3.35) and (3.36). The current injection model of the Scott transformer is shown in Fig 3.6.

$$\begin{bmatrix} I_{TC} \\ I_{TR} \\ I_{TF} \end{bmatrix} = -\begin{bmatrix} \dfrac{F}{F^2-G^2} & \dfrac{-1}{F-G} & \dfrac{G}{F^2-G^2} \\ \dfrac{-1}{F-G} & \dfrac{2}{F-G} & \dfrac{-1}{F-G} \\ \dfrac{G}{F^2-G^2} & \dfrac{-1}{F-G} & \dfrac{F}{F^2-G^2} \end{bmatrix} \begin{bmatrix} V_{TC} \\ V_{TR} \\ V_{TF} \end{bmatrix} + \frac{1}{G+F}\frac{A}{2}\begin{bmatrix} 1 \\ 0 \\ -1 \end{bmatrix} \tag{3.35}$$

$$\begin{bmatrix} I_{MC} \\ I_{MR} \\ I_{MF} \end{bmatrix} = -\begin{bmatrix} \dfrac{J}{J^2-H^2} & \dfrac{-1}{J-H} & \dfrac{H}{J^2-H^2} \\ \dfrac{-1}{J-H} & \dfrac{2}{J-H} & \dfrac{-1}{J-H} \\ \dfrac{H}{J^2-H^2} & \dfrac{-1}{J-H} & \dfrac{F}{J^2-H^2} \end{bmatrix} \begin{bmatrix} V_{MC} \\ V_{MR} \\ V_{MF} \end{bmatrix} + \frac{1}{H+J}\frac{D}{2}\begin{bmatrix} 1 \\ 0 \\ -1 \end{bmatrix} \tag{3.36}$$

$$Y_{SS,T} = \begin{bmatrix} \dfrac{F}{F^2-G^2} & \dfrac{-1}{F-G} & \dfrac{G}{F^2-G^2} \\ \dfrac{-1}{F-G} & \dfrac{2}{F-G} & \dfrac{-1}{F-G} \\ \dfrac{G}{F^2-G^2} & \dfrac{-1}{F-G} & \dfrac{F}{F^2-G^2} \end{bmatrix}, \ J_{SS,T} = \frac{1}{G+F}\frac{A}{2}\begin{bmatrix} 1 \\ 0 \\ -1 \end{bmatrix}$$

$$Y_{SS,M} = \begin{bmatrix} \dfrac{J}{J^2-H^2} & \dfrac{-1}{J-H} & \dfrac{H}{J^2-H^2} \\ \dfrac{-1}{J-H} & \dfrac{2}{J-H} & \dfrac{-1}{J-H} \\ \dfrac{H}{J^2-H^2} & \dfrac{-1}{J-H} & \dfrac{F}{J^2-H^2} \end{bmatrix}, \ J_{SS,M} = \frac{1}{H+J}\frac{D}{2}\begin{bmatrix} 1 \\ 0 \\ -1 \end{bmatrix}$$

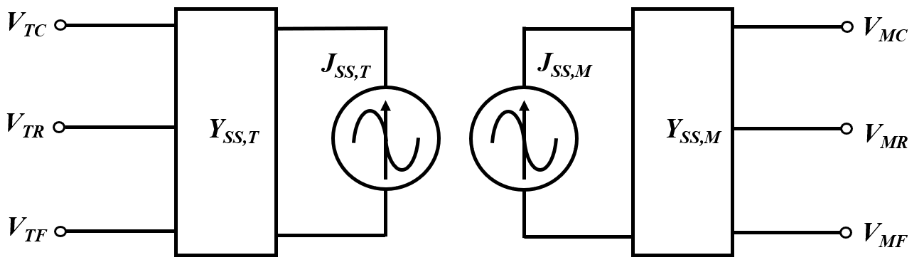

Fig. 3.6 The current injection model of the Scott transformer

Note: variables' definitions

a_1	T-phase transformer's turns ratio ($\sqrt{3}N_1 / 2N_2$)
a_2	M-phase transformer's turns ratio (N_1/N_2)
V_Δ	three-phase primary voltage, $\Delta \in \{A, B, C\}$
E_{p1}	T-phase primary winding voltage
E_{p2}	M-phase primary winding voltage
E_φ	φ-phase secondary winding voltage, $\varphi \in \{T, M\}$
$V_{T\Omega}$	T-phase secondary voltage, $\Omega \in \{C, R, F\}$
$V_{M\Omega}$	M-phase secondary voltage, $\Omega \in \{C, R, F\}$
I_Δ	three-phase primary current, $\Delta \in \{A, B, C\}$
$I_{T\Omega}$	T-phase secondary current, $\Omega \in \{C, R, F\}$
$I_{M\Omega}$	M-phase secondary current, $\Omega \in \{C, R, F\}$
Z_Δ	Δ-phase primary winding leakage impedance, $\Delta \in \{A, B, C\}$
Z_{s1}	T-phase secondary winding leakage impedance
Z_{s2}	M-phase secondary winding leakage impedance
$Y_{SS,\varphi}$	φ-phase admittance matrix, $\varphi \in \{T, M\}$
$J_{SS,\varphi}$	φ-phase source current matrix, $\varphi \in \{T, M\}$

$$A = \frac{(2V_A - V_B - V_C)}{2a_1},\ B = \frac{(4Z_A + Z_B + Z_C + 4a_1^2 Z_{s1})}{8a_1^2}$$

$$C = \frac{(Z_B - Z_C)}{4a_1 a_2},\ D = \frac{(V_B - V_C)}{a_2},\ E = \frac{(Z_B + Z_C + a_2^2 Z_{s2})}{2a_2^2}$$

$$F = \frac{(4Z_A + Z_B + Z_C + 8a_1^2 Z_{s1})}{16a_1^2},\ G = \frac{(4Z_A + Z_B + Z_C)}{16a_1^2}$$

$$H = \frac{(Z_B + Z_C)}{4a_2^2},\ J = \frac{(Z_B + Z_C + 2a_2^2 Z_{s2})}{4a_2^2}$$

3.3 Autotransformer and tap-changing autotransformer

The modelling of an autotransformer (AT) and a tap-changing AT is demonstrated in this section. The tap-changing AT's model is created first, then the normal AT (fixed centre-tapped AT) can be derived as the tap-changing AT's model with the tap setting of 1:1.

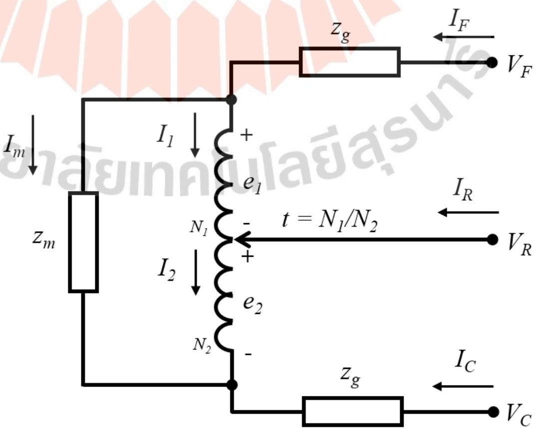

Fig. 3.7 Equivalent circuit of the tap-changing AT

(Thanatchai Kulworawanichpong, 2003)

An equivalent circuit with all specified variables is depicted in Fig. 3.7. The tap-changing AT's model is comprised of the winding between the tap and feeder terminal (F) with N_1 winding turns, referred to as FR winding; the winding between the tap and catenary terminal (C) with N_2 winding turns, referred to as CR winding; the tap connected to the rail terminal (R); the magnitising impedance across F and C. The tap setting parameter is t defined by the ratio of N_1:N_2. The relation between the FR winding and CR winding voltage and the relation between the FR winding and CR winding current are shown in equation (3.37) and (3.38), respectively.

$$\frac{e_1}{e_2} = \frac{N_1}{N_2} = t \tag{3.37}$$

$$I_1 = -\frac{1}{t} I_2 \tag{3.38}$$

According to the Kirchhoff's current law, the relation between the input currents (I_C, I_R and I_F) and winding currents (I_1, I_2 and I_m) is obtained as in equation (3.39) – (3.42).

$$I_2 = \frac{t}{t+1} I_R \tag{3.39}$$

$$I_m = \frac{1}{2}\left(I_F - I_C\right) - \frac{1}{2}\left(\frac{t-1}{t+1}\right) I_R \tag{3.40}$$

$$I_C = -I_m - \left(\frac{t}{t+1}\right) I_R \tag{3.41}$$

$$I_F = I_m - \left(\frac{1}{t+1}\right) I_R \tag{3.42}$$

Also, by using the Kirchhoff's voltage law, equation (3.43) and (3.44) are obtained as follows.

$$V_F - V_C = I_m\left(z_m + 2z_g\right) + \left(\frac{t-1}{t+1}\right) z_g I_R \tag{3.43}$$

$$V_F + V_C - 2V_R = -z_g I_R + \left(\frac{t-1}{t+1}\right) z_m I_m \tag{3.44}$$

Substitute equation (3.41) and (3.42) into equation (3.43) and (3.44), then the four equations expressing the relation between the currents and voltages of the tap-changing AT are shown in equation (3.45) – (3.48).

$$V_F - V_C = -\left(z_m + 2z_g\right) I_C - \left(z_g + \left(\frac{t}{t+1}\right) z_m\right) I_R \tag{3.45}$$

$$V_F - V_C = \left(z_m + 2z_g\right) I_F + \left(z_g + \left(\frac{1}{t+1}\right) z_m\right) I_R \tag{3.46}$$

$$V_F + V_C - 2V_R = -\left[z_g + \left(\frac{t-1}{t+1}\right)\left(\frac{t}{t+1}\right) z_m\right] I_R - \left(\frac{t-1}{t+1}\right) z_m I_C \tag{3.47}$$

$$V_F + V_C - 2V_R = \left[-z_g + \left(\frac{t-1}{t+1}\right)\left(\frac{1}{t+1}\right) z_m\right] I_R + \left(\frac{t-1}{t+1}\right) z_m I_F \tag{3.48}$$

Solve equation (3.45) – (3.48) to determine each of the currents as a function of V_C, V_R and V_F; see equation (3.49) – (3.51). Consequently, these equations can be written in a matrix form in equation (3.52) and the admittance matrix is subsequently derived. For the fixed centre-tapped AT, the admittance matrix can also be obtained by setting tap t as 1:1 or $t = 1$.

$$I_C = \left(\frac{\frac{1}{M}+\frac{1}{Q}}{\frac{P}{Q}-\frac{N}{M}}\right)V_C + \left(\frac{-\frac{2}{M}}{\frac{P}{Q}-\frac{N}{M}}\right)V_R + \left(\frac{\frac{1}{M}-\frac{1}{Q}}{\frac{P}{Q}-\frac{N}{M}}\right)V_F \tag{3.49}$$

$$I_R = \left(\frac{P+N}{NQ-MP}\right)V_C + \left(\frac{-2P}{NQ-MP}\right)V_R + \left(\frac{P-N}{NQ-MP}\right)V_F \tag{3.50}$$

$$I_F = \left(\frac{\frac{1}{R}+\frac{1}{S}}{\frac{N}{R}-\frac{P}{S}}\right)V_C + \left(\frac{-\frac{2}{R}}{\frac{N}{R}-\frac{P}{S}}\right)V_R + \left(\frac{\frac{1}{R}-\frac{1}{S}}{\frac{N}{R}-\frac{P}{S}}\right)V_F \tag{3.51}$$

$$\begin{bmatrix} I_C \\ I_R \\ I_F \end{bmatrix} = \begin{bmatrix} \left(\frac{\frac{1}{M}+\frac{1}{Q}}{\frac{P}{Q}-\frac{N}{M}}\right) & \left(\frac{-\frac{2}{M}}{\frac{P}{Q}-\frac{N}{M}}\right) & \left(\frac{\frac{1}{M}-\frac{1}{Q}}{\frac{P}{Q}-\frac{N}{M}}\right) \\ \left(\frac{P+N}{NQ-MP}\right) & \left(\frac{-2P}{NQ-MP}\right) & \left(\frac{P-N}{NQ-MP}\right) \\ \left(\frac{\frac{1}{R}+\frac{1}{S}}{\frac{N}{R}-\frac{P}{S}}\right) & \left(\frac{-\frac{2}{R}}{\frac{N}{R}-\frac{P}{S}}\right) & \left(\frac{\frac{1}{R}-\frac{1}{S}}{\frac{N}{R}-\frac{P}{S}}\right) \end{bmatrix} \begin{bmatrix} V_C \\ V_R \\ V_F \end{bmatrix} \tag{3.52}$$

$$Y_{tap-changing\ AT} = \begin{bmatrix} \left(\frac{\frac{1}{M}+\frac{1}{Q}}{\frac{P}{Q}-\frac{N}{M}}\right) & \left(\frac{-\frac{2}{M}}{\frac{P}{Q}-\frac{N}{M}}\right) & \left(\frac{\frac{1}{M}-\frac{1}{Q}}{\frac{P}{Q}-\frac{N}{M}}\right) \\ \left(\frac{P+N}{NQ-MP}\right) & \left(\frac{-2P}{NQ-MP}\right) & \left(\frac{P-N}{NQ-MP}\right) \\ \left(\frac{\frac{1}{R}+\frac{1}{S}}{\frac{N}{R}-\frac{P}{S}}\right) & \left(\frac{-\frac{2}{R}}{\frac{N}{R}-\frac{P}{S}}\right) & \left(\frac{\frac{1}{R}-\frac{1}{S}}{\frac{N}{R}-\frac{P}{S}}\right) \end{bmatrix}$$

$$Y_{fixed\ centre-tapped\ AT} = \begin{bmatrix} \dfrac{1}{2z_g} + \dfrac{1}{z_m + 2z_g} & -\dfrac{1}{z_g} & \dfrac{1}{2z_g} - \dfrac{1}{z_m + 2z_g} \\ -\dfrac{1}{z_g} & \dfrac{2}{z_g} & -\dfrac{1}{z_g} \\ \dfrac{1}{2z_g} - \dfrac{1}{z_m + 2z_g} & -\dfrac{1}{z_g} & \dfrac{1}{2z_g} + \dfrac{1}{z_m + 2z_g} \end{bmatrix}$$

Note: variables' definitions

V_Δ	Δ-phase voltage, $\Delta \in \{C, R, F\}$
I_Δ	Δ-phase current, $\Delta \in \{C, R, F\}$
I_1	current flowing in FR winding
I_2	current flowing in CR winding
I_m	current flowing in the magnitising branch
e_1	FR winding voltage
e_2	CR winding voltage
z_g	winding leakage impedance
z_m	magnitising impedance
$Y_{tap\text{-}changing\ AT}$	admittance matrix of tap-changing AT
$Y_{fixed\ centre\text{-}tapped\ AT}$	admittance matrix of fixed centre-tapped AT

$$M = z_g + \left(\frac{t-1}{t+1}\right)\left(\frac{t}{t+1}\right) z_m, \quad N = \left(\frac{t-1}{t+1}\right) z_m, \quad P = z_m + 2z_g$$

$$Q = z_g + \left(\frac{t}{t+1}\right) z_m, \quad R = -z_g + \left(\frac{t-1}{t+1}\right)\left(\frac{1}{t+1}\right) z_m, \quad S = z_g + \left(\frac{1}{t+1}\right) z_m$$

3.4 Catenary system

The power distribution or catenary system of the AT-fed railway power supply system consists of an overhead catenary line (C), a feeder line (F) as a current return path and running rails (R). In the power flow calculation, all those lines are represented by their impedances per unit length, i.e. catenary line impedance (Z_C), feeder line impedance (Z_F) and running rails impedance (Z_R). Furthermore, owing to the running rails placement on the ground or supports connected to the ground, a rail-to-earth impedance (Z_{RE}) is indispensable for modelling accuracy and ability to determine the rail potential.

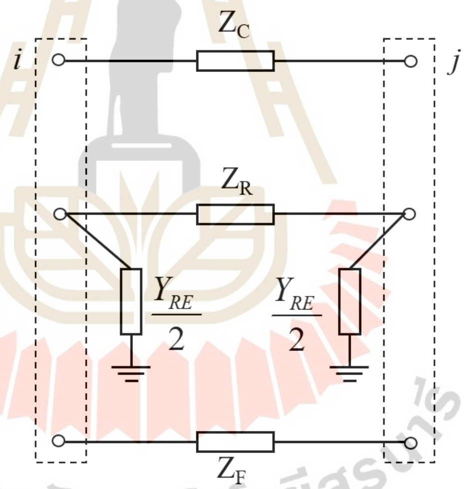

Fig. 3.8 Model of the catenary system in AT-fed power supply system

The incorporation of the catenary, feeder, rail impedance per length and rail-to-earth impedance forms the model of one section of the catenary system linking two nodes (*i* and *j* node) as shown in Fig. 3.8. The rail-to-earth impedance in the model is generally expressed as the rail-to-earth admittance (Y_{RE}), half of which is separately connected to each R sub-node; see Fig. 3.8 to further clarify the explanation. The 3×3 admittance impedance matrix of the model, equation (3.53), can be transformed into the admittance matrix to be included in the power flow calculation. For simplicity of calculation and data availability, the mutual impedances are not taken into account in this study. However, they can be incorporated into the impedance matrix if the values of the mutual impedances are provided or are calculated from the available geometric data of the overhead contact line structure.

$$Z_{catenary} = \begin{bmatrix} Z_{CC} & Z_{CR} & Z_{CF} \\ Z_{RC} & Z_{RR} & Z_{RF} \\ Z_{FC} & Z_{FR} & Z_{FF} \end{bmatrix} \tag{3.53}$$

3.5 Train load

There is a variety of ways to consider a train load. It can be modelled as a constant power load, a constant current load, or a constant impedance load. The train's power generally can be measured by on-board equipment and readily derived from the train movement simulation (Thanatchai Kulworawanichpong, 2003). Thus, the train load in this research is modelled as a constant power load. Nonetheless, in order to be incorporated into the current-based Newton-Raphson power flow calculation, the constant-power model of the train load is modified as a power-controlled current load connected between the catenary and rail sub-node of the train node, i.e. the current is altered to maintain the power during the power flow calculation. The controlled current, which can be added to the load-current term of the current-based power flow equation, is calculated by equation (3.54), where $S_{TR,i}$ is the train load apparent power, $V_{C,i}$ is the catenary voltage of the i-node, $V_{R,i}$ is the rail voltage of the i-node and $I_{T,i}$ is the train load current. Also, the presence of the train load model in the system is illustrated in Fig. 3.9.

$$I_{T,i} = \frac{S^{*}_{TR,i}}{\left(V_{C,i} - V_{R,i}\right)^{*}} \tag{3.54}$$

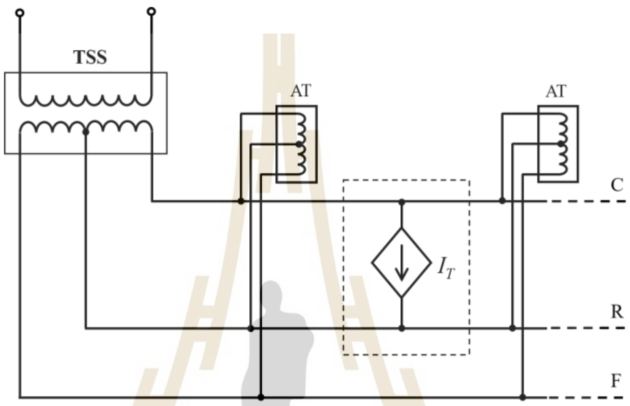

Fig. 3.9 Model of the train load in the AT-fed power supply system

3.6 Railway power conditioner

A railway power conditioner (RPC) has two converters joined by a capacitor or DC link in a back-to-back manner; accordingly, its steady-state model or current injection model in this study consists of two Norton's equivalent sources. It is assumed that the DC link voltage is perfectly controlled and constant. Fig. 3.10 shows the equivalent circuit of the RPC steady-state model. The output active and reactive powers of the converters are a function of the substation voltages (U_{Δ}), the converters' output voltages referred to the high-voltage side of the coupling transformers ($U_{O\Delta}$), and the phase angles between those voltages ($\delta_{C\Delta}$) as expressed in (3.55) and (3.56), respectively, where $\Delta \in \{\alpha, \beta\}$ and $Z_{L\Delta}$ is a combination of coupling transformer's leakage impedance, reactor's reactance, and converter's impedance. The output fundamental AC RMS voltages of the converters are dependent upon configuration of the converters and determined by the product of a modulation index (m) and a DC-link voltage (V_{DC}), and their phase angles are specified by δ_Δ. For example, equation (3.57) calculates the output voltage of a sinusoidal PWM (SPWM) converter (Dubey, 2005), which is used later in this study's simulation.

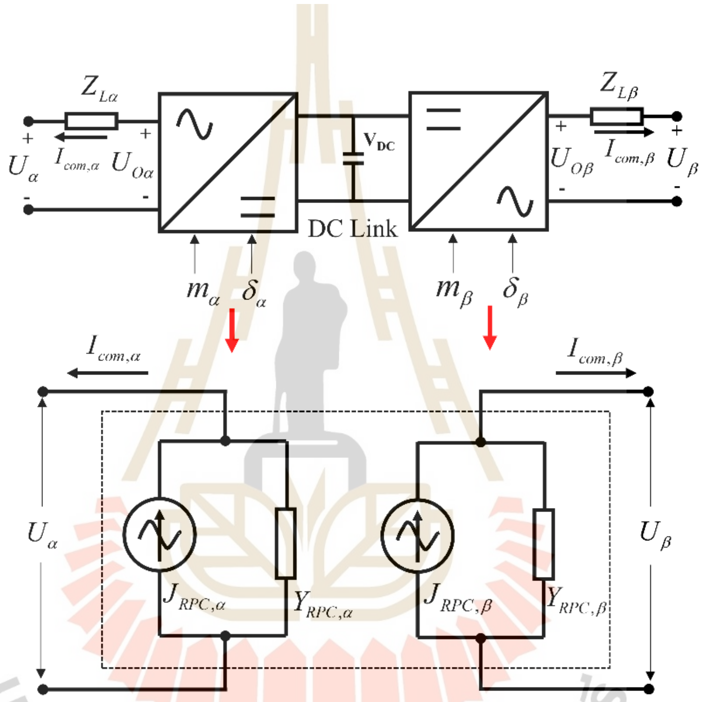

Fig. 3.10 RPC current injection model (Kritsada Mongkoldee and Thanatchai Kulworawanichpong, In press)

$$P_\Delta = \frac{U_\Delta U_{O\Delta}}{Z_{L\Delta}} \sin(\delta_{C\Delta}) \tag{3.55}$$

$$Q_\Delta = \frac{U_\Delta U_{O\Delta}}{Z_{L\Delta}} \cos(\delta_{C\Delta}) - \frac{U_{O\Delta}^2}{Z_{L\Delta}} \tag{3.56}$$

$$U_{O\Delta} = \frac{m_\Delta V_{DC}}{2\sqrt{2}} \angle \delta_\Delta \tag{3.57}$$

The RPC's current injection model is comprised of a current source and a source admittance/impedance for α and β phase, which are represented by a current matrix (J_{RPC}) and an admittance matrix (Y_{RPC}) shown in (3.58) and (3.59), respectively, when the RPC is connected to the catenary (C) and feeder (F) line of a traction substation. Both matrices are ultimately incorporated into the current-based power flow equation.

$$J_{RPC,\Delta} = \begin{array}{c} \begin{bmatrix} I_{RPC,\Delta} \\ 0 \\ -I_{RPC,\Delta} \end{bmatrix} \end{array} \begin{array}{c} C \\ R \\ F \end{array}, \; I_{RPC,\Delta} = \frac{a_{RPC} m_\Delta V_{DC}}{2\sqrt{2}\left|Z_{L\Delta}\right|} \angle \left(\delta_{C\Delta} - angle\left(Z_{L\Delta}\right)\right) \tag{3.58}$$

$$Y_{RPC,\Delta} = \begin{array}{c} \begin{array}{ccc} C & R & F \end{array} \\ \begin{bmatrix} 1/Z_{L\Delta} & 0 & -1/Z_{L\Delta} \\ 0 & 0 & 0 \\ -1/Z_{L\Delta} & 0 & 1/Z_{L\Delta} \end{bmatrix} \end{array} \begin{array}{c} C \\ R \\ F \end{array} \tag{3.59}$$

Since the two converters are placed on different feeding sections, certain constraints must be imposed to meet the following RPC operating conditions: (i) the active power flow in both converters must be equal in magnitude and opposite in direction and (ii) the reactive power generated by both converters must flow outwards in order to compensate the reactive load. However, the power flow calculation does not allow for this operating principle of RPC; accordingly, optimisation method is applied to complete this model by using the modulation indices and the phase angles as design variables and using the mentioned conditions as optimisation constraints.

Chapter 4

Power flow calculation

4.1 Introduction

This chapter describes a power flow calculation method used in the study called "Current-based Newton-Raphson (CBNR) power flow calculation method". This method was proposed in polar form and published in the article entitled Current-based Newton-Raphson power flow calculation for AT-fed railway power supply systems (Kritsada Mongkoldee and Thanatchai Kulworawanichpong, 2018); the rectangular form of the method was introduced earlier in the doctoral dissertation (Thanatchai Kulworawanichpong, 2003). Other power flow calculation methods, put forward in the above-mentioned article such as the Gauss-Seidel method and the Sequential Linear method, also offer the comparable outcome; however, the CBNR method is employed in this study thanks to its reasonable execution time and superior capability of handling higher train load, deeper analysis of the methods' performance can be referred to the article.

4.2 Current-based Newton-Raphson power flow calculation for the AT-fed traction power supply system

This CBNR method is formulated for the AT-fed traction power supply system, in which the multi-conductor system is applied: multiple sub-buses or sub-nodes constitute one main bus, three sub-buses in the AT-fed system (Catenary (C), Rail (R), and Feeder (F)); see Fig. 4.1. In each *i*th bus, the voltages and currents take the form of three-row matrices as shown in (4.1) – (4.2). Because this method is based on current, the traction load in (4.2) is the flow of current only between the catenary line and the rail: the amount of the traction current, derived from the train power ($S_{TR,i}$) and the train voltage, is calculated by (4.3). And the real and imaginary parts of the train current's complex values in (4.3) are shown in (4.4) – (4.9).

$$V_i = \begin{bmatrix} V_i^{\mathrm{C}} \\ V_i^{\mathrm{R}} \\ V_i^{\mathrm{F}} \end{bmatrix} = \begin{bmatrix} \left|V_i^{\mathrm{C}}\right| e^{j\theta_i^{\mathrm{C}}} \\ \left|V_i^{\mathrm{C}}\right| e^{j\theta_i^{\mathrm{R}}} \\ \left|V_i^{\mathrm{C}}\right| e^{j\theta_i^{\mathrm{F}}} \end{bmatrix} \tag{4.1}$$

$$J_{TR,i} = I_{T,i} \begin{bmatrix} 1 \\ -1 \\ 0 \end{bmatrix} = \begin{bmatrix} J_{TR,i}^{C} \\ J_{TR,i}^{\mathrm{R}} \\ J_{TR,i}^{\mathrm{F}} \end{bmatrix} = \begin{bmatrix} q_i^{C} + jr_i^{C} \\ q_i^{\mathrm{R}} + jr_i^{\mathrm{R}} \\ q_i^{\mathrm{F}} + jr_i^{\mathrm{F}} \end{bmatrix} \tag{4.2}$$

$$I_{T,i} = \frac{S_{TR,i}^{*}}{\left(V_i^{\mathrm{C}} - V_i^{\mathrm{R}}\right)^{*}} = \frac{\alpha P_{\mathrm{T},i} + \beta Q_{\mathrm{T},i}}{\tau} + j\frac{\beta P_{\mathrm{T},i} - \alpha Q_{\mathrm{T},i}}{\tau},\ S_{TR,i}^{*} = P_{\mathrm{T},i} - jQ_{\mathrm{T},i}$$
$$\alpha = \left|V_i^{C}\right|\cos\left(\theta_i^{C}\right) - \left|V_i^{\mathrm{R}}\right|\cos\left(\theta_i^{\mathrm{R}}\right),\ \beta = \left|V_i^{C}\right|\sin\left(\theta_i^{C}\right) - \left|V_i^{R}\right|\sin\left(\theta_i^{R}\right),\ \tau = \alpha^2 + \beta^2 \tag{4.3}$$

$$q_i^{C} = \frac{\alpha P_{\mathrm{T},i} + \beta Q_{\mathrm{T},i}}{\tau} \tag{4.4}$$

$$q_i^{\mathrm{R}} = -\frac{\alpha P_{\mathrm{T},i} + \beta Q_{\mathrm{T},i}}{\tau} \tag{4.5}$$

$$q_i^{F} = 0 \tag{4.6}$$

$$r_i^{C} = \frac{\beta P_{\mathrm{T},i} - \alpha Q_{\mathrm{T},i}}{\tau} \tag{4.7}$$

$$r_i^{\mathrm{R}} = -\frac{\beta P_{\mathrm{T},i} - \alpha Q_{\mathrm{T},i}}{\tau} \tag{4.8}$$

$$r_i^F = 0 \tag{4.9}$$

The current balance equation derived from KCL is the core equation of the method which is formed for every bus. The generalised equation of the ith bus and γth sub-bus is shown in (4.10) for a N_B-bus AT-fed railway power supply system, in which the first term represents the sum of every current flowing between the ith bus and other interconnected buses: each current is the product of the phasor voltage at bus h (V_h) and the ith-row-and-jth-column element of the system bus admittance matrix (Y_{ih}), the second term ($J_{SS,i}$) represents the source current of the bus, and the third term ($J_{TR,i}$) represents the load current of the bus.

$$\sum_{h=1}^{N_B}\sum_{m\in\psi} Y_{ih}^{(\gamma,\mathrm{m})} V_h^m - J_{SS,i}^{\gamma} + J_{TR,i}^{\gamma} = 0,\ \ \psi = \{\mathrm{C},\mathrm{R},\mathrm{F}\} \tag{4.10}$$

The current mismatch equation at bus i and sub-bus γ is formulated from the left side of equation (4.10) and denoted by F_i as shown in (4.11). F_i is decomposed into a real part (G_i) and imaginary part (H_i) in (4.12) and (4.13), respectively.

$$F_i^{\gamma} = \sum_{h=1}^{N_B}\sum_{m\in\psi} Y_{ih}^{(\gamma,\mathrm{m})} V_h^m - J_{SS,i}^{\gamma} + J_{TR,i}^{\gamma} = G_i^{\gamma} + jH_i^{\gamma} \tag{4.11}$$

$$G_i^{\gamma} = \sum_{h=1}^{N_B}\sum_{m\in\psi} \left| Y_{ih}^{(\gamma,\mathrm{m})} V_h^m \right| \cos\left(\phi_{ih}^{(\gamma,m)} + \theta_h^m\right) - \mathrm{Re}\left(J_{SS,i}^{\gamma}\right) + \mathrm{Re}\left(J_{TR,i}^{\gamma}\right) \tag{4.12}$$

$$H_i^{\gamma} = \sum_{h=1}^{N_B}\sum_{m\in\psi} \left| Y_{ih}^{(\gamma,\mathrm{m})} V_h^m \right| \sin\left(\phi_{ih}^{(\gamma,m)} + \theta_h^m\right) - \mathrm{Im}\left(J_{SS,i}^{\gamma}\right) + \mathrm{Im}\left(J_{TR,i}^{\gamma}\right) \tag{4.13}$$

G_i and H_i are further divided into non-train load terms (a_i and d_i) and train load terms (q_i and r_i); see (4.14) – (4.17).

$$G_i^{\gamma} = a_i^{\gamma} + q_i^{\gamma} \tag{4.14}$$

$$H_i^{\gamma} = d_i^{\gamma} + r_i^{\gamma} \tag{4.15}$$

$$a_i^{\gamma} = \sum_{h=1}^{N_B} \sum_{m \in \psi} \left| Y_{ih}^{(\gamma,\mathrm{m})} V_h^{\mathrm{m}} \right| \cos\left(\phi_{ih}^{(\gamma,\mathrm{m})} + \theta_h^{\mathrm{m}}\right) - \mathrm{Re}\left(J_{SS,i}^{\gamma}\right) \tag{4.16}$$

$$d_i^{\gamma} = \sum_{h=1}^{N_B} \sum_{m \in \psi} \left| Y_{ih}^{(\gamma,\mathrm{m})} V_h^{\mathrm{m}} \right| \sin\left(\phi_{ih}^{(\gamma,\mathrm{m})} + \theta_h^{\mathrm{m}}\right) - \mathrm{Im}\left(J_{SS,i}^{\gamma}\right) \tag{4.17}$$

Using the Taylor's theorem, G_i and H_i can be approximated by using the first derivative term of its Taylor series expansion shown in (4.18) and (4.19).

$$G_i^{\gamma} = \sum_{h=1}^{N_B} \sum_{m \in \psi} \frac{\partial G_i^{\gamma}}{\partial \left| V_h^{\mathrm{m}} \right|} \cdot \Delta \left| V_h^{\mathrm{m}} \right| + \sum_{h=1}^{N_B} \sum_{m \in \psi} \frac{\partial G_i^{\gamma}}{\partial \theta_h^{\mathrm{m}}} \cdot \Delta \theta_h^{\mathrm{m}} \tag{4.18}$$

$$H_i^{\gamma} = \sum_{h=1}^{N_B} \sum_{m \in \psi} \frac{\partial H_i^{\gamma}}{\partial \left| V_h^{\mathrm{m}} \right|} \cdot \Delta \left| V_h^{\mathrm{m}} \right| + \sum_{h=1}^{N_B} \sum_{m \in \psi} \frac{\partial H_i^{\gamma}}{\partial \theta_h^{\mathrm{m}}} \cdot \Delta \theta_h^{\mathrm{m}} \tag{4.19}$$

For a N_B-bus system, all buses' equation (4.18) and (4.19) form a matrix equation (4.20) with the $6N_B \times 6N_B$ Jacobian matrix (J). The elements of the Jacobian matrix are the derivatives with respect to bus voltage magnitudes and angles of equation (4.4) – (4.9) and (4.16) – (4.17), shown in the end of this section.

$$\begin{bmatrix} G \\ H \end{bmatrix} = \begin{bmatrix} \dfrac{\partial a}{\partial |V|} + \dfrac{\partial q}{\partial |V|} & \dfrac{\partial a}{\partial \theta} + \dfrac{\partial q}{\partial \theta} \\ \dfrac{\partial d}{\partial |V|} + \dfrac{\partial r}{\partial |V|} & \dfrac{\partial d}{\partial \theta} + \dfrac{\partial r}{\partial \theta} \end{bmatrix} \begin{bmatrix} \Delta |V| \\ \Delta \theta \end{bmatrix} = \begin{bmatrix} M_1 + L_1 & M_2 + L_2 \\ M_3 + L_3 & M_4 + L_4 \end{bmatrix} \begin{bmatrix} \Delta |V| \\ \Delta \theta \end{bmatrix} = J \begin{bmatrix} \Delta |V| \\ \Delta \theta \end{bmatrix} \tag{4.20}$$

The small changes of bus voltage magnitudes and angles can be obtained from (4.20) and are used to update the next iteration's bus voltage magnitudes and angles shown in (4.21). The mentioned calculation is repeated until the current mismatch is below the specified tolerance. The flowchart of the CBNR power flow calculation method is depicted in Fig. (4.1).

$$\begin{bmatrix} |V| \\ \theta \end{bmatrix}^{j+1} = \begin{bmatrix} |V| \\ \theta \end{bmatrix}^{j} - \begin{bmatrix} \Delta|V| \\ \Delta\theta \end{bmatrix}^{j} \tag{4.21}$$

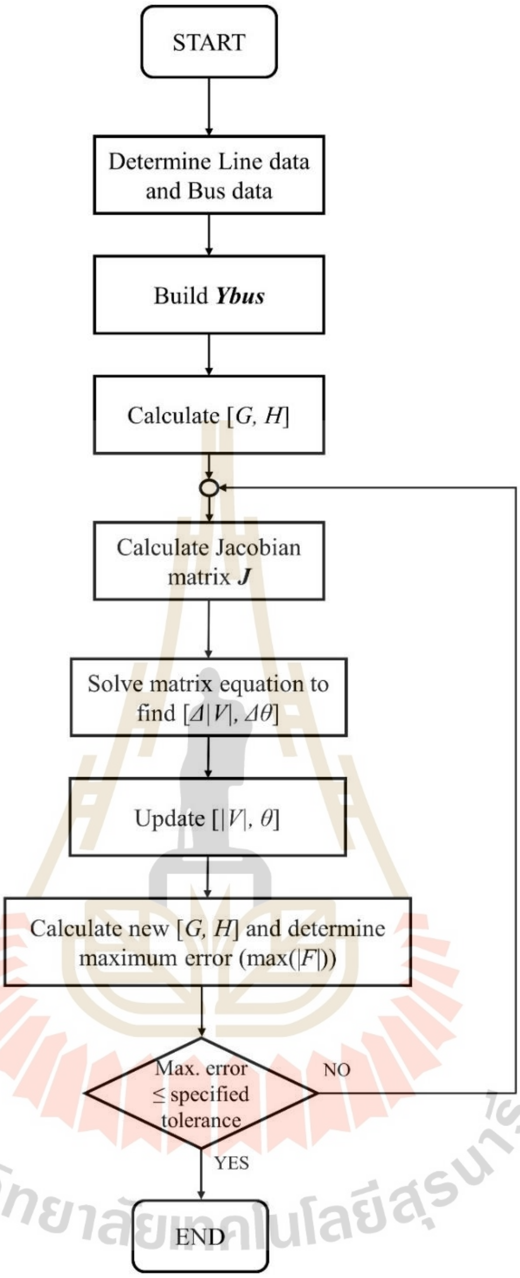

Fig. 4.1 CBNR power flow method flowchart

4.3 Jacobian matrix elements

The following are calculation of the elements of the Jacobian matrix in (4.20), i.e. M1 – M4 and L1 – L4. For other conditions apart from the following, the elements are zero.

- [M1] to [M4];

$$\left[M_1\right]:\frac{\partial a_i^{\gamma}}{\partial\left|V_h^{\mathrm{m}}\right|}=\left|Y_{ih}^{(\gamma,\mathrm{m})}\right|\cos(\phi_{ih}^{(\gamma,\mathrm{m})}+\theta_h^{\mathrm{m}})$$

$$\left[M_2\right]:\frac{\partial a_i^{\gamma}}{\partial\theta_h^{\mathrm{m}}}=-\left|Y_{ih}^{(\gamma,\mathrm{m})}\ \mathrm{V}_h^{\mathrm{m}}\right|\sin(\phi_{ih}^{(\gamma,\mathrm{m})}+\theta_h^{\mathrm{m}})$$

$$\left[M_3\right]:\frac{\partial d_i^{\gamma}}{\partial\left|V_h^{\mathrm{m}}\right|}=\left|Y_{ih}^{(\gamma,\mathrm{m})}\right|\sin(\phi_{ih}^{(\gamma,\mathrm{m})}+\theta_h^{\mathrm{m}})$$

$$\left[M_4\right]:\frac{\partial d_i^{\gamma}}{\partial\theta_h^{\mathrm{m}}}=\left|Y_{ih}^{(\gamma,\mathrm{m})}\ \mathrm{V}_h^{\mathrm{m}}\right|\cos(\phi_{ih}^{(\gamma,\mathrm{m})}+\theta_h^{\mathrm{m}})$$

- [L1] to [L4] (For i = h);

  - [L1]:

(a) γ = C, m = C

$$\frac{\partial q_i^{\mathrm{C}}}{\partial\left|V_h^{\mathrm{C}}\right|}=\frac{\tau\left(P_{\mathrm{T},i}\cos\left(\theta_i^{\mathrm{C}}\right)+Q_{\mathrm{T},i}\sin\left(\theta_i^{\mathrm{C}}\right)\right)-\rho\left(2\left|V_i^{\mathrm{C}}\right|-2\left|V_i^{\mathrm{R}}\right|\cos\left(\theta_i^{\mathrm{C}}-\theta_i^{\mathrm{R}}\right)\right)}{\tau^2}$$

(b) γ = C, m = R

$$\frac{\partial q_i^{\mathrm{C}}}{\partial\left|V_h^{\mathrm{R}}\right|}=\frac{-\tau\left(P_{\mathrm{T},i}\cos\left(\theta_i^{R}\right)+Q_{\mathrm{T},i}\sin\left(\theta_i^{R}\right)\right)-\rho\left(2\left|V_i^{R}\right|-2\left|V_i^{C}\right|\cos\left(\theta_i^{\mathrm{C}}-\theta_i^{\mathrm{R}}\right)\right)}{\tau^2}$$

(c) γ = R, m = C

$$\frac{\partial q_i^{\mathrm{R}}}{\partial \left|V_h^{\mathrm{C}}\right|} = -\frac{\tau\left(P_{\mathrm{T},i}\cos\left(\theta_i^{\mathrm{C}}\right)+Q_{\mathrm{T},i}\sin\left(\theta_i^{\mathrm{C}}\right)\right)-\rho\left(2\left|V_i^{\mathrm{C}}\right|-2\left|V_i^{\mathrm{R}}\right|\cos\left(\theta_i^{\mathrm{C}}-\theta_i^{\mathrm{R}}\right)\right)}{\tau^2}$$

(d) γ = R, m = R

$$\frac{\partial q_i^{\mathrm{R}}}{\partial \left|V_h^{\mathrm{R}}\right|} = -\frac{-\tau\left(P_{\mathrm{T},i}\cos\left(\theta_i^{R}\right)+Q_{\mathrm{T},i}\sin\left(\theta_i^{R}\right)\right)-\rho\left(2\left|V_i^{R}\right|-2\left|V_i^{C}\right|\cos\left(\theta_i^{\mathrm{C}}-\theta_i^{\mathrm{R}}\right)\right)}{\tau^2}$$

- [L2]:

(a) γ = C, m = C

$$\frac{\partial q_i^{\mathrm{C}}}{\partial \theta_h^{\mathrm{C}}} = \frac{\tau\left|V_i^{\mathrm{C}}\right|\left(-P_{\mathrm{T},i}\sin\left(\theta_i^{\mathrm{C}}\right)+Q_{\mathrm{T},i}\cos\left(\theta_i^{\mathrm{C}}\right)\right)-\rho\left(2\left|V_i^{\mathrm{C}}\right|\left|V_i^{\mathrm{R}}\right|\sin\left(\theta_i^{\mathrm{C}}-\theta_i^{\mathrm{R}}\right)\right)}{\tau^2}$$

(b) γ = C, m = R

$$\frac{\partial q_i^{\mathrm{C}}}{\partial \theta_h^{\mathrm{R}}} = \frac{-\tau\left|V_i^{\mathrm{R}}\right|\left(-P_{\mathrm{T},i}\sin\left(\theta_i^{\mathrm{R}}\right)+Q_{\mathrm{T},i}\cos\left(\theta_i^{\mathrm{R}}\right)\right)+\rho\left(2\left|V_i^{\mathrm{C}}\right|\left|V_i^{\mathrm{R}}\right|\sin\left(\theta_i^{\mathrm{C}}-\theta_i^{\mathrm{R}}\right)\right)}{\tau^2}$$

(c) γ = R, m = C

$$\frac{\partial q_i^{\mathrm{R}}}{\partial \theta_h^{\mathrm{C}}} = -\frac{\tau\left|V_i^{\mathrm{C}}\right|\left(-P_{\mathrm{T},i}\sin\left(\theta_i^{\mathrm{C}}\right)+Q_{\mathrm{T},i}\cos\left(\theta_i^{\mathrm{C}}\right)\right)-\rho\left(2\left|V_i^{\mathrm{C}}\right|\left|V_i^{\mathrm{R}}\right|\sin\left(\theta_i^{\mathrm{C}}-\theta_i^{\mathrm{R}}\right)\right)}{\tau^2}$$

(d) γ = R, m = R

$$\frac{\partial q_i^{\mathrm{R}}}{\partial \theta_h^{\mathrm{R}}} = -\frac{-\tau\left|V_i^{\mathrm{R}}\right|\left(-P_{\mathrm{T},i}\sin\left(\theta_i^{\mathrm{R}}\right)+Q_{\mathrm{T},i}\cos\left(\theta_i^{\mathrm{R}}\right)\right)+\rho\left(2\left|V_i^{\mathrm{C}}\right|\left|V_i^{\mathrm{R}}\right|\sin\left(\theta_i^{\mathrm{C}}-\theta_i^{\mathrm{R}}\right)\right)}{\tau^2}$$

- [L3]:

(a) γ = C, m = C

$$\frac{\partial r_i^{\mathrm{C}}}{\partial \left|V_h^{\mathrm{C}}\right|} = \frac{\tau\left(P_{\mathrm{T},i}\sin\left(\theta_i^{\mathrm{C}}\right) - Q_{\mathrm{T},i}\cos\left(\theta_i^{\mathrm{C}}\right)\right) - \sigma\left(2\left|V_i^{\mathrm{C}}\right| - 2\left|V_i^{\mathrm{R}}\right|\cos\left(\theta_i^{\mathrm{C}} - \theta_i^{\mathrm{R}}\right)\right)}{\tau^2}$$

(b) γ = C, m = R

$$\frac{\partial r_i^{\mathrm{C}}}{\partial \left|V_h^{R}\right|} = \frac{-\tau\left(P_{\mathrm{T},i}\sin\left(\theta_i^{\mathrm{R}}\right) - Q_{\mathrm{T},i}\cos\left(\theta_i^{\mathrm{R}}\right)\right) - \sigma\left(2\left|V_i^{\mathrm{R}}\right| - 2\left|V_i^{\mathrm{C}}\right|\cos\left(\theta_i^{\mathrm{C}} - \theta_i^{\mathrm{R}}\right)\right)}{\tau^2}$$

(c) γ = R, m = C

$$\frac{\partial r_i^{\mathrm{R}}}{\partial \left|V_h^{\mathrm{C}}\right|} = -\frac{\tau\left(P_{\mathrm{T},i}\sin\left(\theta_i^{\mathrm{C}}\right) - Q_{\mathrm{T},i}\cos\left(\theta_i^{\mathrm{C}}\right)\right) - \sigma\left(2\left|V_i^{\mathrm{C}}\right| - 2\left|V_i^{\mathrm{R}}\right|\cos\left(\theta_i^{\mathrm{C}} - \theta_i^{\mathrm{R}}\right)\right)}{\tau^2}$$

(d) γ = R, m = R

$$\frac{\partial r_i^{\mathrm{R}}}{\partial \left|V_h^{R}\right|} = -\frac{-\tau\left(P_{\mathrm{T},i}\sin\left(\theta_i^{\mathrm{R}}\right) - Q_{\mathrm{T},i}\cos\left(\theta_i^{\mathrm{R}}\right)\right) - \sigma\left(2\left|V_i^{\mathrm{R}}\right| - 2\left|V_i^{\mathrm{C}}\right|\cos\left(\theta_i^{\mathrm{C}} - \theta_i^{\mathrm{R}}\right)\right)}{\tau^2}$$

- [L4]:

(a) γ = C, m = C

$$\frac{\partial r_i^{\mathrm{C}}}{\partial \theta_h^{\mathrm{C}}} = \frac{\tau\left|V_i^{\mathrm{C}}\right|\left(P_{\mathrm{T},i}\cos\left(\theta_i^{\mathrm{C}}\right) + Q_{\mathrm{T},i}\sin\left(\theta_i^{\mathrm{C}}\right)\right) - \sigma\left(2\left|V_i^{\mathrm{C}}\right|\left|V_i^{\mathrm{R}}\right|\sin\left(\theta_i^{\mathrm{C}} - \theta_i^{\mathrm{R}}\right)\right)}{\tau^2}$$

(b) γ = C, m = R

$$\frac{\partial r_i^{\mathrm{C}}}{\partial \theta_h^{\mathrm{R}}} = \frac{-\tau\left|V_i^{\mathrm{R}}\right|\left(P_{\mathrm{T},i}\cos\left(\theta_i^{\mathrm{R}}\right) + Q_{\mathrm{T},i}\sin\left(\theta_i^{\mathrm{R}}\right)\right) + \sigma\left(2\left|V_i^{\mathrm{C}}\right|\left|V_i^{\mathrm{R}}\right|\sin\left(\theta_i^{\mathrm{C}} - \theta_i^{\mathrm{R}}\right)\right)}{\tau^2}$$

(c) γ = R, m = C

$$\frac{\partial r_i^{\mathrm{R}}}{\partial \theta_h^{\mathrm{C}}} = -\frac{\tau\left|V_i^{\mathrm{C}}\right|\left(P_{\mathrm{T},i}\cos\left(\theta_i^{\mathrm{C}}\right) + Q_{\mathrm{T},i}\sin\left(\theta_i^{\mathrm{C}}\right)\right) - \sigma\left(2\left|V_i^{\mathrm{C}}\right|\left|V_i^{\mathrm{R}}\right|\sin\left(\theta_i^{\mathrm{C}} - \theta_i^{\mathrm{R}}\right)\right)}{\tau^2}$$

(d) γ = R, m = R

$$\frac{\partial r_i^{\mathrm{R}}}{\partial \theta_h^{\mathrm{R}}} = -\frac{-\tau\left|V_i^{\mathrm{R}}\right|\left(P_{\mathrm{T},i}\cos\left(\theta_i^{\mathrm{R}}\right)+Q_{\mathrm{T},i}\sin\left(\theta_i^{\mathrm{R}}\right)\right)+\sigma\left(2\left|V_i^{\mathrm{C}}\right|\left|V_i^{\mathrm{R}}\right|\sin\left(\theta_i^{\mathrm{C}}-\theta_i^{\mathrm{R}}\right)\right)}{\tau^2}$$

where $\rho=\left|V_i^{C}\right|\left(P_{\mathrm{T},i}\cos\left(\theta_i^{C}\right)+Q_{\mathrm{T},i}\sin\left(\theta_i^{C}\right)\right)-\left|V_i^{\mathrm{R}}\right|\left(P_{\mathrm{T},i}\cos\left(\theta_i^{\mathrm{R}}\right)+Q_{\mathrm{T},i}\sin\left(\theta_i^{\mathrm{R}}\right)\right)$

$$\sigma=\left|V_i^{C}\right|\left(P_{\mathrm{T},i}\sin\left(\theta_i^{C}\right)-Q_{\mathrm{T},i}\cos\left(\theta_i^{C}\right)\right)-\left|V_i^{\mathrm{R}}\right|\left(P_{\mathrm{T},i}\sin\left(\theta_i^{\mathrm{R}}\right)-Q_{\mathrm{T},i}\cos\left(\theta_i^{\mathrm{R}}\right)\right)$$

Chapter 5

Tap-changing autotransformer investigation

5.1 Introduction

This chapter investigates the autotransformer (AT) tap change in the AT traction power supply system using tap changing ATs. It is expected and hypothesised that the AT tap setting, using tap changing ATs alone, more or less improves some aspects of traction supply power quality such as voltage unbalance, power factor at the point of common coupling (PCC), and power losses. The details of the study procedure and results are as follows.

5.2 Test procedure

A 2×25 traction power feeding system with two feeder sections and one traction transformer depicted as a diagram in Fig. 5.1 is established for the tap-changing AT investigation. The traction system supplies left and right feeder arms (referenced to the traction substation), each of which has three ATs with an equal distance from each other, 10 km in this study, and has one train load located X_T from the traction substation.

The test procedure can be divided into two main parts: Part 1 all equally fixed taps (varying tap range of 0.7 – 1.4) and Part 2 optimally searched taps. In each part, the test is composed of 4 loading conditions: (1) the worst case or the most unbalanced condition, (2) the balanced condition, (3) the light-loaded and slightly unbalanced condition and (4) the heavy-loaded and slightly unbalanced condition. These loading conditions are quantitatively summarised in Table 5.1. Traction loads with all kinds of locomotives or a combination of traditional rectifier locomotives and modern PWM-based locomotives generally have the power factor in the range of 0.8 – 0.9 (Roudsari, Jalilian, and Jamali, 2018); as a result, the average power factor of 0.85 is adopted for all the loading conditions. Moreover, all these 4 cases are performed separately for the V/V and Scott traction transformer and for two different train positions, i.e. X_T = 25 km (Position 1) and X_T = 5 km (Position 2). The whole test procedure is hierarchically illustrated in Fig. 5.2 and the simulation parameters are shown in Table 5.2.

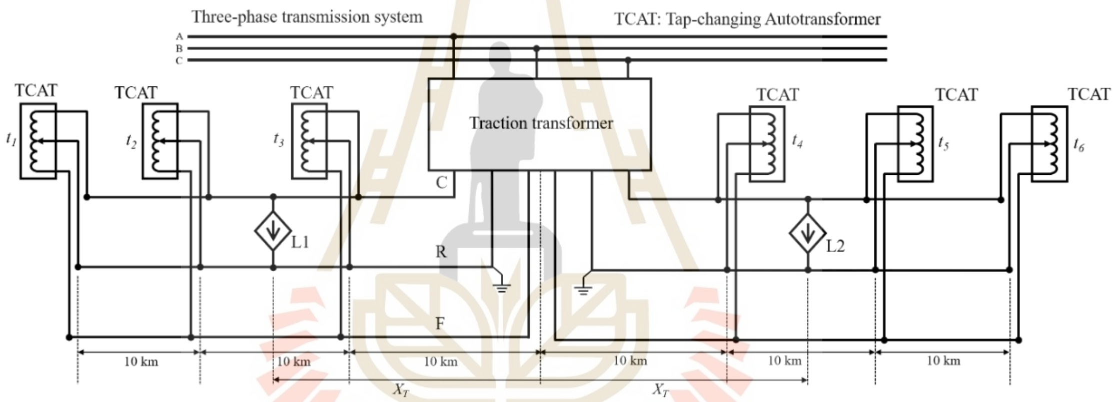

Fig. 5.1 Diagram of traction power system for tap-changing AT investigation

Table 5.1 Loading conditions in test cases

Case	Left arm load (MW)	Right arm load (MW)	Power factor
Case 1	10	0	0.85
Case 2	5	5	0.85
Case 3	2	3	0.85
Case 4	7	8	0.85

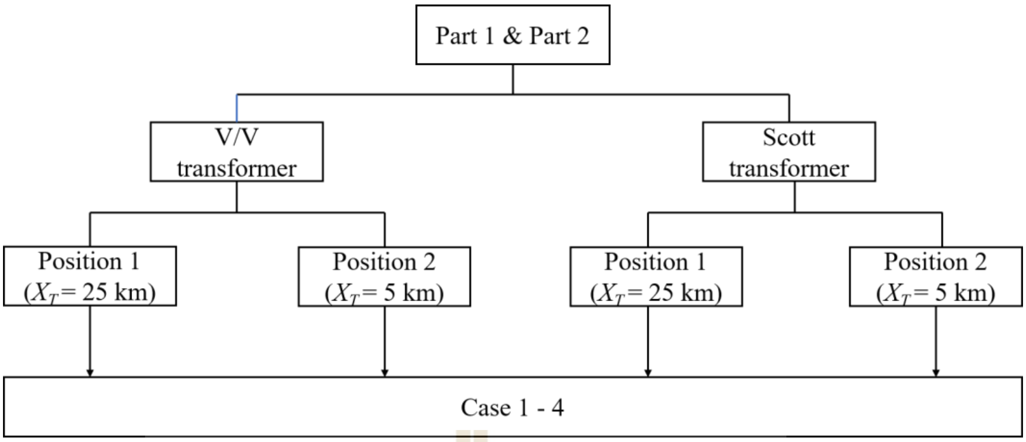

Fig. 5.2 Diagram of test procedure

Given the results of the test, the following variables are the outputs of the simulation and are taken into consideration and analysis.

- Voltage unbalance factor ($VUF = |V_-|/|V_+|$: a ratio of negative sequence voltage magnitude to positive sequence one)
- Current unbalance factor ($IUF = |I_-|/|I_+|$: a ratio of negative sequence current magnitude to positive sequence one)
- Three-phase side power factor ($PF_{3\varphi} = (P_A + P_B + P_C) / (S_A + S_B + S_C)$)
- Three-phase side active and reactive power consumption
- Single-phase active and reactive power consumption at each supply arm
- Traction substation voltages (CF, CR, FR)
- Train voltages
- Power loss ($P_{loss} = P_{3\varphi} - \Sigma\, P_{load}$)
- Rail potentials at both traction substations and trains

- Voltage deviation (VD = $\Sigma|V_{nominal}-V_i|$, the sum of all nodes' voltages in kV, $V_{nominal}$ = 25 kV)

In order to investigate how changing taps affects the traction power supply system, the simulation results of different cases will be compared to one another by considering the above-mentioned variables as described in the following sections.

Table 5.2 System parameters in the AT tap changing test

Parameters	Values
Grid short circuit capacity (MVA)	2700
Grid voltage (kV)	230
Catenary impedance (Ω/km)	0.1192 + j0.752
Feeder impedance (Ω/km)	0.2036 + j0.884
Running rail resistance (Ω/km)	0.1648 + j0.6709
Rail-to-earth resistance (Ω·km)	0.5
Substation earthing resistance (Ω)	0.25
Scott transformer primary winding leakage impedance (Ω)	0.01 + j0.833
Scott transformer secondary winding leakage impedance (Ω)	0.2 + j0.8333
AT half-winding leakage impedance (Ω)	0.1564 + j0.09997
AT magnetising impedance (kΩ)	101.4 + j279.1

5.3 Simulation results and discussions

All the descriptive and graphical results of the test procedure described in 5.2 are demonstrated in this section, which are mainly broken down into Part 1 and Part 2. The detailed raw data of the results such as the graphical results of Part 1 and the optimal tap position in Part 2 are all shown in Appendix A.

5.3.1 Part 1: All equally fixed tap

The simulation results of all test cases in Part 1 can be described and discussed in 5 different aspects: (1) unbalance, (2) three-phases power consumption and loss, (3) traction substation voltages, (4) rail potentials, and (5) train voltages as follows. Table 5.3 and 5.4 show the optimal points of each variables for the Scott transformer and V/V transformer system, respectively. All the graphs associated with the following results and discussion are shown in Fig. A.1 – A.38 in Appendix A: voltage & current unbalance, three-phase power factor, active & reactive power consumption in a three-phases side and in an individual supply arm, power losses, voltage deviation, traction substation voltages, train voltages, rail voltages, and currents at a traction substation.

- **Unbalance**

The variations of the voltage unbalance in every case have the same trend in which the VUFs increase as the taps are further adjusted in either direction. The increasing rate of the VUFs is proportional to the difference of train loads in two supply arms. Nevertheless, in the tap range of 0.7 – 1.4, the VUFs in percentage are insignificantly affected by tap changing, particularly resulting in a negative way. The V/V transformer system is more heavily influenced by changing taps. The optimum tap setting in most cases for the V/V transformer system is 1:1 or centre-tapped while the tap setting in the range of 0.7 – 0.9 leads to the minimum VUFs for the Scott transformer system.

Compared to the voltage unbalance, the variations of the current unbalance give opposite results. The taps of 1:1 appears to be the points at which the IUFs are maximum due to the maximum difference of the secondary currents in two supply arms. As the taps are adjusted away from 1:1 in either direction, the secondary currents, both catenary and feeder current, are increased in a relatively similar rate. In spite of a small difference between two arm supply currents, it suffices to reduce the IUFs. A degree of the IUF decreasing rate is dependent on the amount of the loads themselves and also the amount of the load difference between two supply arms.

- **Three-phase power consumption and loss**

The amount of the three-phase real and reactive power depends obviously on the amount of the train loads. The three-phase power consumption becomes greater as the taps are adjusted away from the tap position 1:1 in either direction due to the fact that the catenary current and feeder current become greatly unequal, one of which is greater than the other one, then the greater current is the main contributor to an increase of active and reactive power consumption as well as power loss. An increase in reactive power also worsens the power factor. In summary, the minimised power & reactive power, power loss, and the maximised power factor are found at the taps of 1:1 or centre taps. Even though a few points are not caused by the taps of 1:1, they are considered sufficiently close to centre taps. These results are applicable to both the Scott and V/V transformer system.

- **Traction substation voltages**

The original primary aim of changing transformer taps is to regulate voltages. Accordingly, the results show that if the taps are adjusted below 1:1 (<1), the CR voltages are increased. On the other hands, if the taps are adjusted above 1:1 (>1), the FR voltages are increased. Ones expect that the voltage level is close to the nominal value as much as possible. The maximum CR and FR voltages are around [0.73-0.76] and [1.25-1.37] for the Scott transformer system, respectively, and are around [0.90-0.91] and [1.06-1.11] for the V/V transformer system, respectively. It is clear that both CR and FR voltages cannot be boosted simultaneously. Another noteworthy point is that the taps at which both CR and FR voltages are equal are in the range of 0.8 – 1.0. In this circumstance, the taps are set in favour of stepping up the CR voltages because the only CR phase is loaded and the CR voltages are always dropped.

For the CF voltages, it is shown that tap changing makes the voltages drop. The maximum CF voltages in most cases occur at the centre tap despite a few cases occurring at the tap positions of 0.98 and 0.99. The reason for this result is that the further the taps are adjusted away from the centre tap, the more either of the catenary or feeder currents rises, hence leading to greater voltage drops. Apart from the variations of the voltage magnitudes, voltage deviation is another key factor used in consideration of tap changing. As shown by the results in this test, the lowest VD of the system in case 1 of the Scott transformer system is at the centre tap; for the other cases with the V/V transformer system the minimum VDs are in the tap range of 1.01-1.06. This indicates that the slight tap changing does not considerably improve an overall voltage drop for both the Scott and V/V transformer system in every case.

- **Rail potentials**

Rail potentials or rail voltages (potential difference between rails and the remote earth) are not the main objective regarding AT tap changing; however, they are also influenced by tap changing as seen in the results. The rail voltages in this explanation are classified as a rail voltage at a traction substation and a rail voltage at a train. For the rail voltages at the traction substation, adjusting the taps in either direction highly raises the rail voltages. In addition, the results show that the minimum rail voltages lie in the tap range of 0.93 – 1.00. The trend and variation of the rail voltage at the traction substation in each case is nearly similar to one another. For the rail voltages at the trains, it is found that the rail voltages increase with the tap setting and the magnitudes of the rail voltages directly depend on the amount of the train loads. The minimum and maximum rail voltages in all cases are at the margins of the varying tap range, 0.7 and 1.4, respectively. The above descriptions of the results are applicable to both the Scott and V/V transformer system.

- **Train voltages**

The train loads are fed by the CR phase of the traction power supply arms; therefore, the sole approach to increasing the train voltages by tap changing is adjusting the tap towards the position of less than 1:1. This assumption is consistent with the test results which demonstrate that the train voltages are escalated as the tap setting is declined. The maximum train voltages in this test are achieved when the taps are set at the lowest margin, 0.7. It is likely that the train voltages will become greater in amount if the taps are adjusted beyond the lowest margin. All the cases of the Scott and V/V transformer system produce the same trends of the mentioned results.

Table 5.3 Test case results in the system using the Scott transformer

Variables \ Train position		Position 1				Position 2			
		Case 1	**Case 2**	**Case 3**	**Case 4**	**Case 1**	**Case 2**	**Case 3**	**Case 4**
VUF (%)	Min.	0.56	1.86×10^{-6}	0.05	0.06	0.46	1.23×10^{-6}	0.04	0.05
	tap	0.82	0.70	0.86	0.81	0.90	0.70	0.94	0.88
IUF (%)	Max.	99.70	4.12×10^{-4}	20.76	8.22	99.67	3.34×10^{-4}	20.11	6.94
	tap	1.00	1.02	1.00	1.01	1.00	1.00	1.00	1.00
3φ *PF*	Max.	0.72	0.80	0.82	0.77	0.82	0.84	0.84	0.83
	tap	0.99	0.99	1.00	0.99	1.00	1.00	1.00	1.00
$P_{3\varphi}$ (MW)	Min.	10.84	10.32	5.09	15.80	10.20	10.10	5.04	15.22
	tap	1.00	1.00	1.00	1.00	1.00	1.00	1.00	1.00
$Q_{3\varphi}$ (Mvar)	Min.	10.34	7.75	3.50	13.23	7.03	6.62	3.24	10.21
	tap	0.99	1.00	1.00	0.99	1.00	1.00	1.00	1.00
P_T (MW)	Min.	10.82	5.16	2.03	7.33	10.17	5.05	2.01	7.09
	tap	0.99	1.00	1.00	1.00	1.00	1.00	1.00	1.00
Q_T (Mvar)	Min.	10.23	3.86	1.37	5.96	6.94	3.29	1.29	4.70
	tap	0.98	1.00	1.00	0.99	1.00	1.00	1.00	1.00
P_M (MW)	Min.	0.01	5.16	3.06	8.45	0.01	5.05	3.02	8.11
	tap	1.00	1.00	1.00	1.00	1.00	1.00	1.00	1.00
Q_M (Mvar)	Min.	0.02	3.86	2.13	7.19	0.02	3.29	1.94	5.43
	tap	1.00	1.00	1.00	0.99	1.00	1.00	1.00	1.00
P_{loss} (MW)	Min.	0.84	0.32	0.09	0.80	0.20	0.10	0.04	0.22
	tap	1.00	1.00	1.00	1.00	1.00	1.00	1.00	1.00
VD (kV)	Min.	33.82	26.63	12.30	44.45	8.11	7.40	3.71	11.34
	tap	1.00	1.06	1.02	1.04	1.00	1.03	1.01	1.05

Table 5.3 Test case results in the system using the Scott transformer (Continued)

Variables \ Train position		Position 1				Position 2			
		Case 1	**Case 2**	**Case 1**	**Case 2**	**Case 1**	**Case 2**	**Case 1**	**Case 2**
$V_{CF,T}$ (kV)	Max.	49.38	49.76	49.91	49.63	49.56	49.79	49.92	49.70
	tap	0.98	1.00	1.00	0.99	1.00	1.00	1.00	1.00
$V_{CR,T}$ (kV)	Max.	24.76	24.96	25.04	24.89	24.82	24.96	25.04	24.91
	tap	0.76	0.74	0.74	0.75	0.74	0.74	0.73	0.74
$V_{FR,T}$ (kV)	Max.	24.76	24.97	25.05	24.90	24.91	25.01	25.06	24.97
	tap	1.25	1.34	1.36	1.32	1.36	1.37	1.37	1.37
$V_{CF,M}$ (kV)	Max.	50.00	49.76	49.87	49.56	50.00	49.79	49.88	49.66
	tap	1.00	1.00	1.00	0.99	1.00	1.00	1.00	1.00
$V_{CR,M}$ (kV)	Max.	25.09	24.96	25.02	24.85	25.09	24.96	25.02	24.88
	tap	0.73	0.74	0.74	0.75	0.73	0.74	0.73	0.74
$V_{FR,M}$ (kV)	Max.	25.09	24.97	25.03	24.86	25.09	25.01	25.04	24.95
	tap	1.37	1.34	1.36	1.30	1.37	1.37	1.37	1.37
$V_{rail,T,\ at\ TSS}$ (V)	Min.	1.39	0.92	0.85	1.19	32.96	16.26	6.57	22.96
	tap	0.98	0.99	1.00	0.99	0.93	0.97	0.99	0.95
$V_{rail,M,\ at\ TSS}$ (V)	Min.	0.01	0.92	1.29	1.66	0.02	16.26	9.70	26.21
	tap	1.00	0.99	1.00	0.99	1.00	0.97	0.98	0.95
$V_{rail,T,\ at\ train}$ (V)	Min.	52.02	22.43	8.51	32.93	44.11	20.82	7.74	29.95
	tap	0.70	0.70	0.70	0.70	0.70	0.70	0.70	0.70
$V_{rail,M,\ at\ train}$ (V)	Min.	0.00	22.43	12.95	38.73	0.00	20.82	11.97	34.61
	tap	1.00	0.70	0.70	0.70	1.00	0.70	0.70	0.70
$V_{train,T}$ (kV)	Max.	22.06	25.63	27.16	24.41	25.20	25.92	26.32	25.64
	tap	0.70	0.70	0.70	0.70	0.70	0.70	0.70	0.70
$V_{train,M}$ (kV)	Max.	28.05	25.63	26.68	23.72	26.57	25.92	26.18	25.50
	tap	0.70	0.70	0.70	0.70	0.70	0.70	0.70	0.70

Table 5.4 Test case results in the system using the V/V transformer

Variables \ Train position		Position 1				Position 2			
		Case 1	**Case 2**	**Case 3**	**Case 4**	**Case 1**	**Case 2**	**Case 3**	**Case 4**
VUF (%)	Min.	2.00	0.83	0.42	1.40	1.60	0.77	0.40	1.20
	tap	0.98	1.00	1.00	0.99	1.00	1.00	1.00	1.00
IUF (%)	Max.	99.84	49.70	53.76	51.44	99.85	49.69	53.05	50.29
	tap	1.00	1.00	1.00	1.01	1.00	1.00	1.00	1.00
3φ *PF*	Max.	0.71	0.80	0.82	0.76	0.82	0.84	0.84	0.83
	tap	0.98	0.99	1.00	0.99	1.00	1.00	1.00	1.00
$P_{3\varphi}$ (MW)	Min.	10.91	10.33	5.09	15.85	10.20	10.10	5.04	15.22
	tap	0.99	1.00	1.00	1.00	1.00	1.00	1.00	1.00
$Q_{3\varphi}$ (Mvar)	Min.	10.69	7.79	3.51	13.45	7.06	6.62	3.24	10.24
	tap	0.99	1.00	1.00	0.99	1.00	1.00	1.00	1.00
P_L (MW)	Min.	10.89	5.16	2.03	7.34	10.18	5.05	2.01	7.09
	tap	0.99	1.00	1.00	1.00	1.00	1.00	1.00	1.00
Q_L (Mvar)	Min.	10.57	3.87	1.37	5.99	6.97	3.29	1.29	4.71
	tap	0.97	1.00	1.00	0.99	1.00	1.00	1.00	1.00
$\mathrm{P_R}$ (MW)	Min.	0.01	5.16	3.06	8.49	0.01	5.05	3.02	8.12
	tap	1.00	1.00	1.00	1.00	1.00	1.00	1.00	1.00
Q_R (Mvar)	Min.	0.02	3.89	2.13	7.38	0.02	3.30	1.94	5.45
	tap	1.00	1.00	1.00	0.99	1.00	1.00	1.00	1.00
P_{loss} (MW)	Min.	0.91	0.33	0.09	0.85	0.20	0.10	0.04	0.22
	tap	0.99	1.00	1.00	1.00	1.00	1.00	1.00	1.00
VD (kV)	Min.	45.33	32.19	14.39	54.47	15.36	11.82	5.58	18.16
	tap	1.02	1.04	1.03	1.02	1.03	1.04	1.01	1.05

Table 5.4 Test case results in the system using the V/V transformer (Continued)

Variables \ Train position		Position 1				Position 2			
		Case 1	**Case 2**	**Case 1**	**Case 2**	**Case 1**	**Case 2**	**Case 1**	**Case 2**
$V_{CF,L}$ (kV)	Max.	48.31	49.52	49.87	49.24	48.86	49.62	49.89	49.48
	tap	0.98	0.99	1.00	0.99	1.00	1.00	1.00	1.00
$V_{CR,L}$ (kV)	Max.	24.17	24.79	24.97	24.65	24.42	24.82	24.97	24.74
	tap	0.90	0.90	0.90	0.90	0.90	0.90	0.90	0.90
$V_{FR,L}$ (kV)	Max.	24.17	24.79	24.97	24.65	24.50	24.86	24.98	24.80
	tap	1.06	1.10	1.11	1.09	1.10	1.11	1.11	1.11
$V_{CF,R}$ (kV)	Max.	49.06	48.98	49.51	48.22	49.21	49.09	49.54	48.57
	tap	0.99	1.00	1.00	0.99	1.00	1.00	1.00	1.00
$V_{CR,R}$ (kV)	Max.	24.56	24.51	24.78	24.13	24.63	24.55	24.78	24.28
	tap	0.91	0.91	0.91	0.91	0.91	0.91	0.91	0.91
$V_{FR,R}$ (kV)	Max.	24.56	24.51	24.78	24.13	24.63	24.59	24.81	24.34
	tap	1.09	1.09	1.09	1.07	1.10	1.10	1.10	1.09
$V_{rail,L,\ at\ TSS}$ (V)	Min.	1.50	0.93	0.87	1.25	35.04	17.11	6.90	24.16
	tap	0.98	0.99	1.00	0.99	0.93	0.97	0.99	0.95
$V_{rail,R,\ at\ TSS}$ (V)	Min.	0.01	0.91	1.34	1.63	0.02	17.33	10.23	28.21
	tap	1.00	0.99	1.00	0.98	1.00	0.97	0.98	0.95
$V_{rail,L,\ at\ train}$ (V)	Min.	55.12	22.79	8.59	33.69	45.20	21.03	7.81	30.31
	tap	0.70	0.70	0.70	0.70	0.70	0.70	0.70	0.70
$V_{rail,R,\ at\ train}$ (V)	Min.	0.00	23.16	13.21	41.00	0.00	21.34	12.17	35.85
	tap	1.00	0.70	0.70	0.70	1.00	0.70	0.70	0.70
$V_{train,L}$ (kV)	Max.	20.82	25.22	26.89	23.86	24.57	25.60	26.08	25.28
	tap	0.70	0.70	0.70	0.70	0.70	0.70	0.70	0.70
$V_{train,R}$ (kV)	Max.	27.24	24.82	26.17	22.40	25.89	25.25	25.73	24.61
	tap	0.70	0.70	0.70	0.70	0.70	0.70	0.70	0.70

Moreover, another point for discussion is a comparison of two different train positions (Position 1 and Position 2) in the traction power supply system. The train in Position 1 is located further away from the traction substation, hence more transmission losses in the catenary & feeder line and running rails. Therefore, the active & reactive power consumption is greater than that of Position 2 in all cases as shown by the simulation results. This further train position also leads to poorer power factors and more unbalance in the three-phase supply side due to the fact that the more amount of power consumption has more possibility of increase in reactive power and secondary load unbalance, respectively. Considering the voltage deviation, the results clearly show that the voltage deviation for Position 1 is higher than that of Position 2 because of the higher level of voltage drops along the track including the train voltage. For the rail voltages at the traction substation, the rail voltage in the case of Position 2 is greater than that of Position 1. This circumstance occurs because the train in Position 2 is located next to the substation, hence causing the higher amount of current flowing in the rails. On the contrary, the rail current normally becomes nearly zero if the train position is beyond the first AT from the substation; therefore, the rail voltage in this case is lower. Above all, the tap changing is not highly influential in the train positions.

This paragraph summarises Part 1 simulation results. The tap changing can hardly improve the voltage unbalance even though it helps reduce the current unbalance when adjusting the taps away from the centre tap. Other traction supply system characteristics are worsened; the active & reactive power consumption, power loss, voltage deviation, and rail voltages at the substation are significantly increased. The power factors in the three-phase side are also greatly dropped. While the train voltages are able to be regulated via the tap changing, changing the taps to the positions at which are adjusted away from the centre point in either direction is more likely to deteriorate the system such as the increase in losses and lower power factors. As a result, the simultaneous tap changing of all ATs in the system does not produce a positive outcome for traction power supply performance.

5.3.2 Part 2: Optimally searched tap

In this part, the taps are optimally searched by using the Particle Swarm Optimisation method (PSO) based on loss minimisation, VUF minimisation, and three-phase power factor maximisation. The optimisation process has been performed three times in each case. The raw data of the results are presented in Appendix A. The following are the result descriptions on each optimisation target.

- Loss minimisation

From Fig. 5.3 - 5.4, the optimisation is able to find the optimal tap positions that lead to the minimised power losses, i.e. the reduction of the power losses is expressed by a power loss difference relative to a power loss in the base case. The maximum loss reduction percentage that the optimisation can attain is approximately 0.6%, representing only 523.5 W in case 3 (P1) for both Scott and V/V transformer system. On the other hand, the maximum loss reduction in watts is 1,670 W in case 4 (P1) of the Scott transformer system. One can deduce from these figures that the amounts of loss reduction are relatively small when compared to the amounts of the train loads. According to the loss minimisation results, the power loss could not be more diminished; any tap position patterns differing from the obtained optimal-searched ones definitely result in loss increments. Therefore, the tap changing does not significantly influence the loss redution capability. The systems with different traction transformer types, in addition, do not show much difference in each case's loss reduction. Likewise, other characteristics of the system such as voltage deviation, rail voltages, train voltages, traction power consumptions, etc. almost resemble those in the base cases; see Appexdix A for the detailed result data.

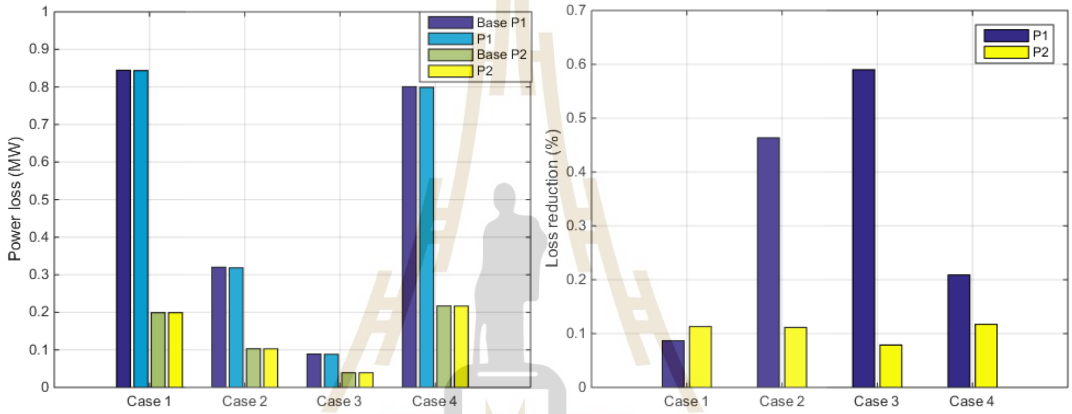

(a) (b)

Fig. 5.3 Power loss results in Scott transformer system

(a) Power loss in MW, (b) Power loss reduction percentage

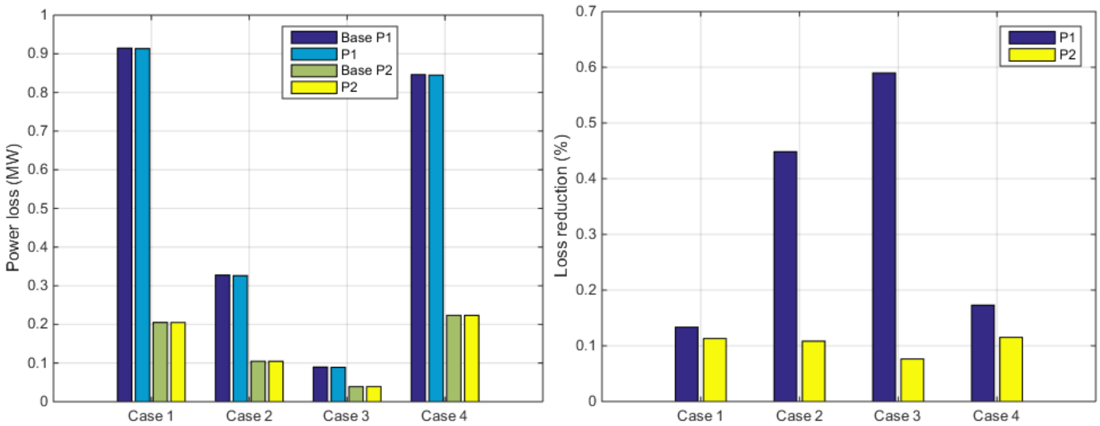

(a) (b)

Fig. 5.4 Power loss results in V/V transformer system

(a) Power loss in MW, (b) Power loss reduction percentage

- VUF minimisation

The reduced VUFs at the point of common coupling (PCC) are also able to be attained through tap change. Fig. 5.5 and 5.6 show the VUFs and the amounts of VUF reduction in Scott and V/V transformer system, respectively. The VUFs can be reduced to 50% of the base cases in the Scott transformer system. The amounts of VUF reduction percentage in case 2 of the Scott transformer system appear to be extinctly high because balanced loading of the Scott transformer makes three-phase side voltages completely balanced in theory. For this reason, this large amount of VUF reduction percentage corresponds to the VUF reduction (the difference between the VUF in the base case and in the optimised case) in the extent of only one in ten million percent. The Scott transformer system with the assistance of optimal tap change has better performance in VUF reduction than that of the V/V transformer system owing to the intrinsic balancing capability of balancing transformers.

In the condition of VUF minimisation, other aspects of the traction power supply system are worsened even though the results are seemingly positive. For example, the power loss in case 3 (P1) of the Scott transformer system increases up to 4.16 MW, amounting to 45 times greater than the base case value. Furthermoure, the three-phase power factor drops to less than 0.5 in the same case. This indicates that searching for optimal tap positions subject to only VUF minimisation leads to adverse effects on a traction power supply system, particularly elevated loss, and reflects that the tap change is very unlikely to be a proper solution to three-phase unbalance reduction.

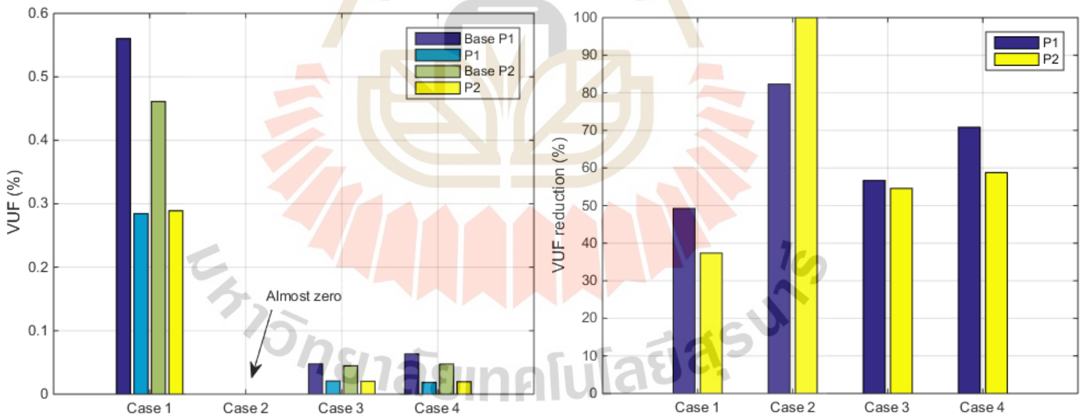

(a) (b)

Fig. 5.5 VUF results in Scott transformer system

(a) VUF, (b) VUF reduction percentage

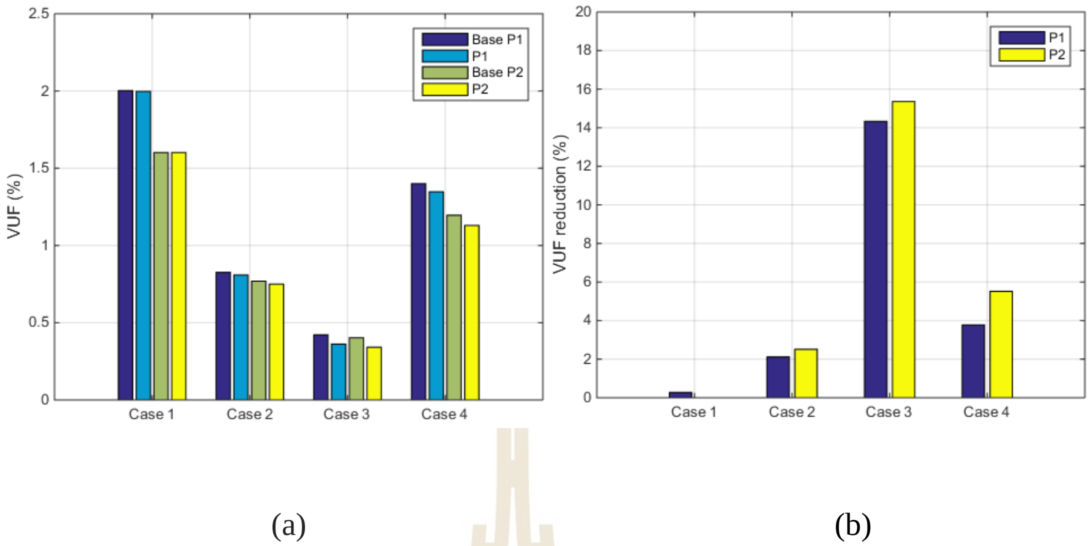

Fig. 5.6 VUF results in V/V transformer system

(a) VUF, (b) VUF reduction percentage

- Three-phase power factor maximisation

The power factor on the three-phase side is another essential key factor in power quality of power systems. Improving the power factor corresponds to a decrease in reactive power, hence improving traction power system equipment utilisation capability. Fig. 5.7 and 5.8 depict the power factors and the percentages of power factor improvement at the PCC in Scott and V/V transformer system, respectively. It is obvious that the optimal tap positions can be found in order to minimise the three-phase power factor; however, the reduced power factors are insignificant and/or meaningless, the maximum amount of the power factor reduction is less than 0.3 percent compared to the base case. The train voltages are slightly elevated due to this small reactive power reduction. Other relevant quantities resulted from the optimisation do not considerably deviate from the values of the base cases. From the point of view of the Scott and V/V transformer system, the amounts of power factor improvement are not much different from each other.

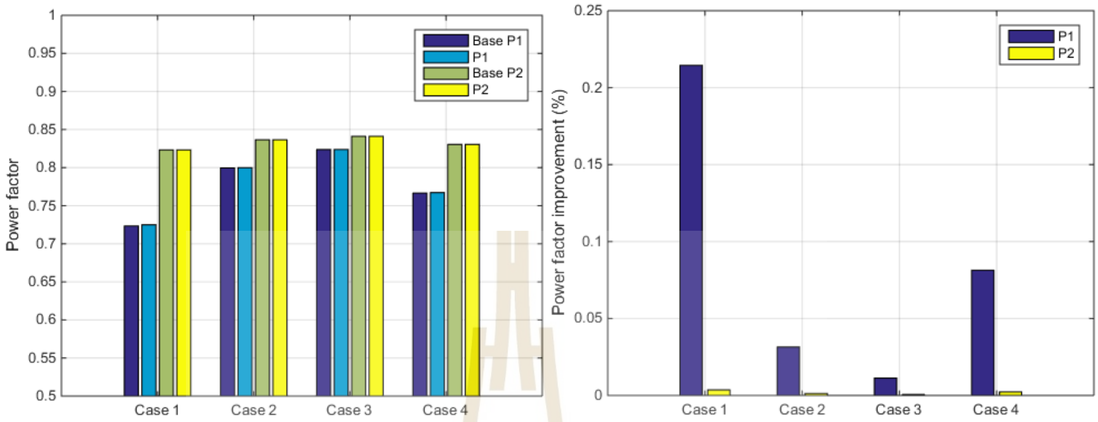

(a) (b)

Fig. 5.7 3-phase power factor results in Scott transformer system

(a) 3-phase power factor, (b) 3-phase power factor improvement as a percentage

From a tap position viewpoint, the tap positions in position 2 of the power factor and power loss optimisation are only changed in the level of less than 0.6 percent. This implies that the lower the traction load and the closer to the traction substation, the smaller the tap position is changed. For instance, in the power loss minimisation the maximum tap position changes occur at case 2 and 4 in which have relatively high loads on both power supply arms among all cases. For the VUF minimisation, at least one of the optimal tap positions reaches the lower (0.8) or upper (1.2) boundary. It can be deduced from this result that the optimisation process can possibly search other solutions outside the boundary. This boundary is set to prevent over-imbalance between the catenary-to-rail and feeder-to-rail voltage and current. In addition, the tap position which is further located away from the centre position causes more loss in the system due to current unbalance in an AT's winding as well as catenary-feeder current unbalance.

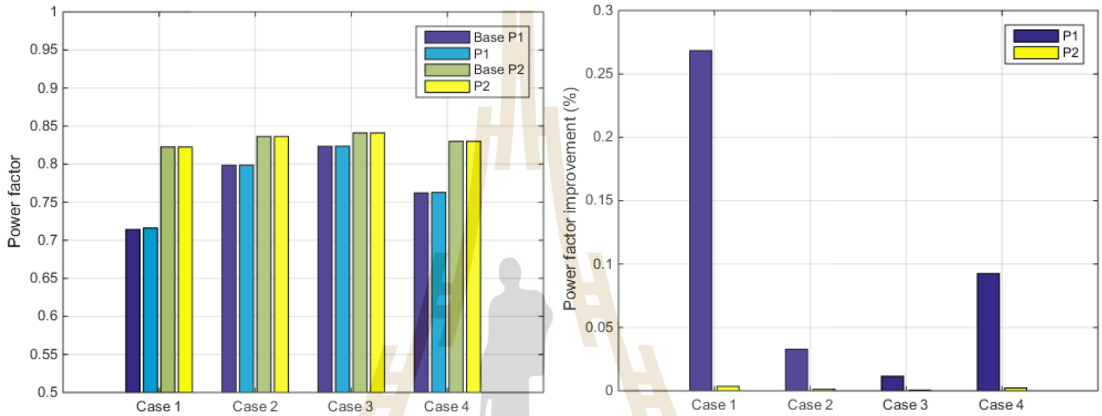

(a)

(b)

Fig. 5.8 3-phase power factor results in V/V transformer system

(a) 3-phase power factor, (b) 3-phase power factor improvement as a percentage

Chapter 6

Optimal sizing of railway power conditioner

6.1 Introduction

This chapter presents a basic review of the RPC compensation principle, composed mainly of full and partial-compensation in the V/V and Scott transformer. Then, the proposed optimal RPC sizing procedure is introduced. In the following section, the test system used in the simulation of the proposed procedure and simulation study cases is described. The simulation results are shown and discussed at the end of the chapter.

6.2 Basic RPC compensation principle

An RPC has three main functions: active power transfer, reactive power compensation, harmonics suppression. Each function can be operated independently. The original purpose of using the RPC is to completely eliminate the negative-sequence current, reactive power, and harmonics caused by single-phase traction load. However, according to a national standard, all those power quality features are not necessarily perfectly compensated. This notion leads to various compensation strategies: full compensation, partial compensation, and other approaches, as described in the following sub-items. For all compensation methods, Fig. 6.1 shows the diagram of a traction power supply system with the flow direction of feeding, load, and compensating currents.

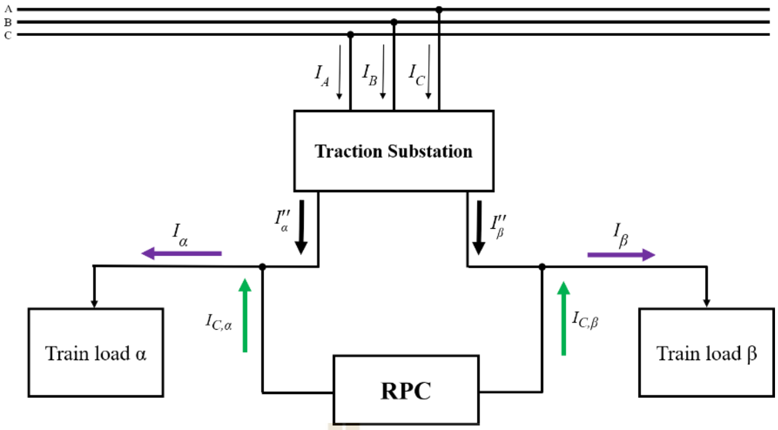

Fig. 6.1 Diagram of the traction power supply system with an RPC

6.2.1 Full compensation

- Scott transformer

Assume that the train load currents of both supply arms of the traction power supply with the Scott transformer are unequal, namely the α-phase load (I_α) is greater than the β-phase load (I_β), the power factors of the train loads are $\cos(\varphi_\alpha)$ and $\cos(\varphi_\beta)$, respectively. The compensation has two stages, including reactive compensation and active compensation. The reactive power compensation is both reactive power elimination and a reduction of reactive power unbalance; the active compensation is to make active power balanced. The phasor diagram of the compensation in the Scott transformer system is illustrated in Fig. 6.2. Each converter of the RPC independently compensates its reactive power; the α-phase and β-phase reactive compensating currents are $I_{qC,\alpha}$ and $I_{qC,\beta}$, respectively. The load currents are purely active after the reactive power compensation. The other stage is to equalise the remaining active power by transferring the excessive power from the heavy-side feeder arm to the other side; the amount of the transferred active power is equal to half of the difference between the α-phase and β-phase active powers. All compensating currents are shown in (6.1) – (6.4).

$$I_{qC,\alpha} = I_\alpha \cos\left(\varphi_\alpha\right) \tag{6.1}$$

$$I_{qC,\beta} = I_\beta \cos\left(\varphi_\beta\right) \tag{6.2}$$

$$I_{pC,\alpha} = -\frac{I'_\alpha - I'_\beta}{2} \tag{6.3}$$

$$I_{pC,\beta} = \frac{I'_\alpha - I'_\beta}{2} \tag{6.4}$$

Equation (6.1) – (6.4) can be multiplied by the nominal traction voltage (assume that $V_\alpha = V_\beta$) to obtain the required reactive and active compensating powers in (6.5) – (6.7).

$$Q_{C,\alpha} = V_\alpha I_\alpha \cos\left(\varphi_\alpha\right) = Q_{Load,\alpha} \tag{6.5}$$

$$Q_{C,\beta} = V_\beta I_\beta \cos\left(\varphi_\beta\right) = Q_{Load,\beta} \tag{6.6}$$

$$P_C = \frac{P_{Load,\alpha} - P_{Load,\beta}}{2} \tag{6.7}$$

The above compensating powers directly determine the size or capacity of the RPC converters. Due to the RPC consisting of two converters connected in a back-to-back manner, the capacity of the RPC is theoretically determined by the sum of the two converters' capacities. In reality, the converter capacities are different because of different reactive power loads in two supply arms, which are expressed in (6.8) and (6.9). Thus, only the converter with higher capacity is selected to calculate the size of the RPC; see (6.10).

$$S_{conv,\alpha} = \sqrt{P_C^2 + Q_{C,\alpha}^2} \tag{6.8}$$

$$S_{conv,\beta} = \sqrt{P_C^2 + Q_{C,\beta}^2} \tag{6.9}$$

$$S_{RPC} = 2 \times \max\left(S_{conv,\alpha}, S_{conv,\beta}\right) \tag{6.10}$$

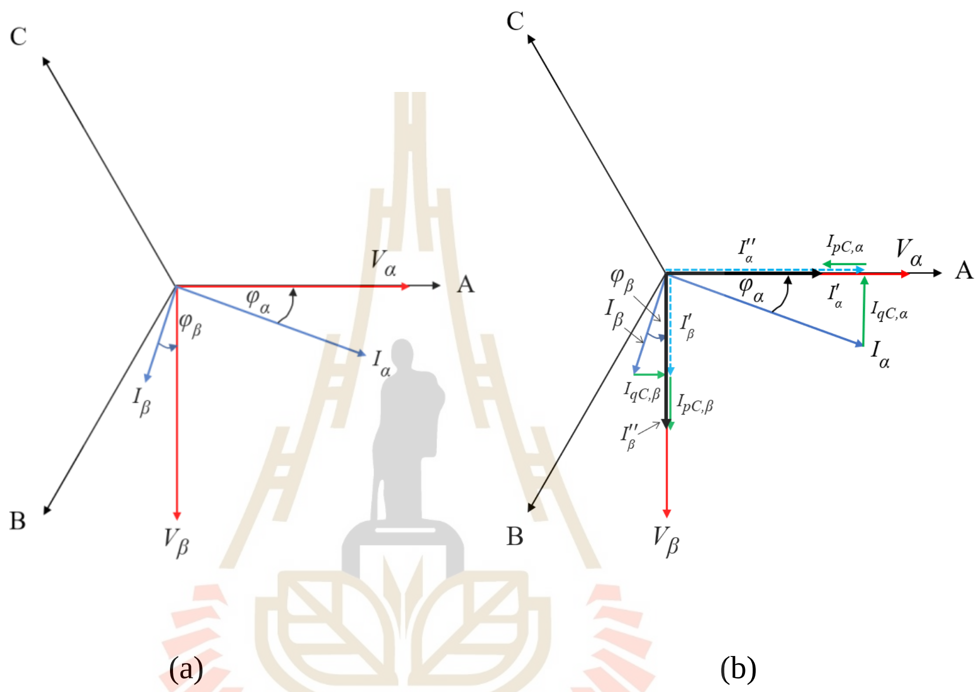

Fig. 6.2 Phasor diagram of RPC compensation in the Scott transformer system (a) Before compensation, (b) After compensation

- V/V transformer

Unlike the compensation principle for the Scott transformer system, the compensation process of the V/V transformer system has three stages; there is additional reactive compensation. The first two stages are the same as that of the Scott transformer system: the first reactive power compensation (traction load power factor improvement) and active power balancing. After the first two stages of compensation are accomplished, the compensated load currents (I'_{α} and I'_{β}) are equal in magnitude and in phase with their corresponding supply voltages (V_{α} and V_{β}). At this point, the three-phase currents are not balanced since the secondary-side currents are not in phase with the primary-side phase voltages. Therefore, the above-introduced additional reactive power compensation is required to shift the phase angles of the previous-stage-compensated currents. The compensating currents of the first two stages are the same as (6.1) – (6.4), and the additional reactive compensating currents are shown in (6.11) and (6.12). The total compensating apparent powers are written in (6.13) and (6.14). The size of the RPC with the V/V transformer can be calculated by (6.10) in a similar way to that of the Scott transformer system. The phasor diagram in Fig. 6.3 shows the phasors of the mentioned currents and voltages.

$$I'_{qC,\alpha} = I'_{\alpha} \tan\left(30^{\circ}\right) \tag{6.11}$$

$$I'_{qC,\beta} = I'_{\beta} \tan\left(30^{\circ}\right) \tag{6.12}$$

$$S_{com,\alpha} = -P_C - j\left(Q_{Load,\alpha} + Q_{add,\alpha}\right),\ Q_{add,\alpha} = I'_{qC,\alpha} V_{\alpha} \tag{6.13}$$

$$S_{com,\beta} = P_C + j\left(-Q_{Load,\beta} + Q_{add,\beta}\right),\ Q_{add,\beta} = I'_{qC,\beta} V_{\beta} \tag{6.14}$$

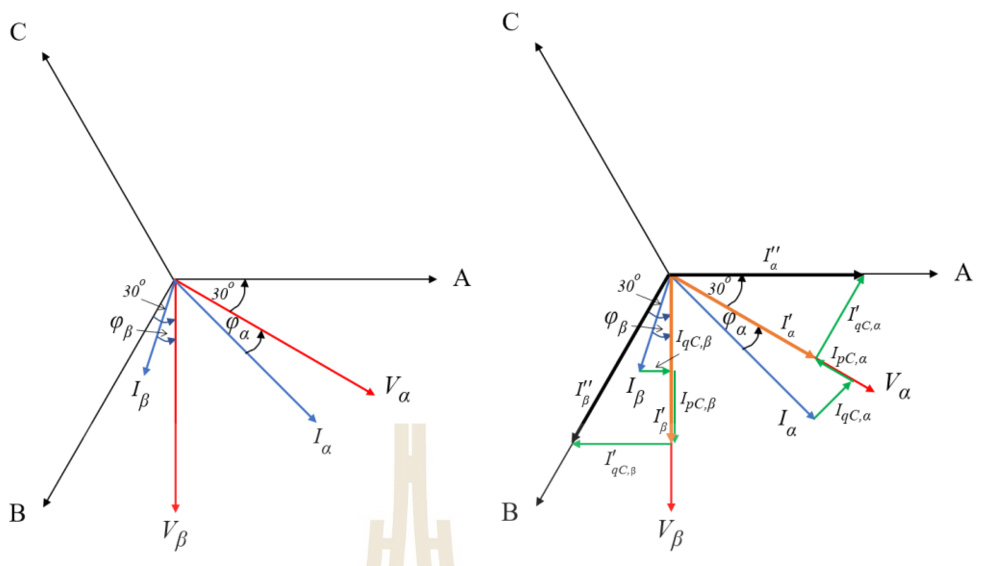

(a) (b)

Fig. 6.3 Phasor diagram of RPC compensation in the V/V transformer system

(a) Before compensation, (b) After compensation

6.2.2 Partial compensation

- Scott transformer

Compared to the full compensation principle of the RPC with the Scott transformer, the compensating currents or powers in partial compensation are less than the values in (6.1) – (6.7). The factors k_p, $k_{q\alpha}$, and $k_{q\beta}$ are used to adjust the compensating active and reactive powers, i.e., k_p, $k_{q\alpha}$, and $k_{q\beta} \in [0,1]$. These factors can be found to satisfy the required/standardised power quality indices, such as voltage unbalance factor, power factor, and the like. Therefore, the compensating reactive and active powers are expressed in (6.15) – (6.17).

$$Q_{C,\alpha} = k_{q\alpha} V_\alpha I_\alpha \cos\left(\varphi_\alpha\right) = k_{q\alpha} Q_{Load,\alpha} \tag{6.15}$$

$$Q_{C,\beta} = k_{q\beta} V_\beta I_\beta \cos\left(\varphi_\beta\right) = k_{q\beta} Q_{Load,\beta} \tag{6.16}$$

$$P_C = k_p \left(\frac{P_{Load,\alpha} - P_{Load,\beta}}{2} \right) \tag{6.17}$$

- V/V transformer

The concept of the partial compensation for the V/V transformer system is similar to that of the Scott transformer system. In addition to the principle described in the Scott transformer part, the $k_{q\alpha}$ and $k_{q\beta}$ are separated into the traction compensating reactive power part and the additional compensating reactive power part as ($k_{q\alpha 1}$, $k_{q\alpha 2}$) and ($k_{q\beta 1}$, $k_{q\beta 2}$) respectively, shown in (6.18) and (6.19). Regardless of compensation control strategies, as a result, these factors can be independently configured to obtain the standard power quality indices.

$$S_{com,\alpha} = -k_p P_C - j\left(k_{q\alpha 1} Q_{Load,\alpha} + k_{q\alpha 2} Q_{add,\alpha}\right) \tag{6.18}$$

$$S_{com,\beta} = k_p P_C + j\left(-k_{q\beta 1} Q_{Load,\beta} + k_{q\beta 2} Q_{add,\beta}\right) \tag{6.19}$$

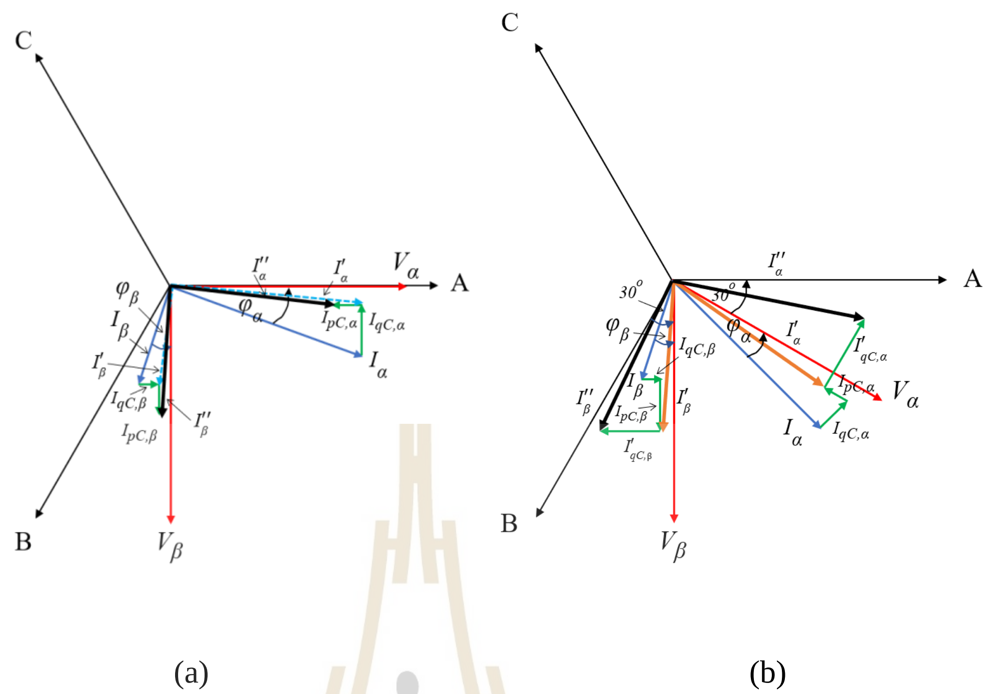

Fig. 6.4 Phasor diagram of RPC partial compensation

(a) Scott transformer system, (b) V/V transformer system

- Partial compensation in the past literature

Several researchers have extensively studied the partial compensation concept in the countries where the high-speed railway is greatly developed, or the strict policy on high-speed railway is imposed, such as China. It has been adopted in the conventional RPC, the hybrid RPC, and the RPC used in the co-phase traction power supply system. Wei, Jiang, and Zhang (2008) proposed the decoupling compensation of negative-sequence current and reactive power. The negative-sequence current is caused by both active and reactive power differences—the excessive reactive power results from the inductive load and the reactive power loss in the catenary system. The compensation capacities can be independently and flexibly controlled by the coefficients k_{pN}, k_{qN}, and k_{qR} as shown in (6.20) - (6.22), where k_{pN}, k_{qN}, and $k_{qR} \in [0,1]$.

The first priority of compensation can be set as reactive power or negative-sequence compensation depending on the loading condition and the required compensating capacity. In the case of the negative-sequence priority compensation mode, k_{pN} and k_{qN} are determined first. The remaining capacity compensates for reactive power. In the other case, k_{qR} is determined first, and the remaining capacity compensates for the negative-sequence power. If the negative-sequence or reactive power demands exceed the RPC capacity, only the negative-sequence ($k_{qR} = 0$) or reactive power (k_{pN} and $k_{qN} = 0$) is compensated at a full capacity of RPC.

$$P_C = k_{pN} \frac{P_{Load,\alpha} - P_{Load,\beta}}{2} \tag{6.20}$$

$$Q_{C\alpha} = k_{qN} \left(\frac{Q_{Load,\alpha} - Q_{Load,\beta}}{2} \right) + k_{qR} \left(\frac{Q_{Load,\alpha} + Q_{Load,\beta}}{2} \right) \tag{6.21}$$

$$Q_{C\beta} = -k_{qN} \left(\frac{Q_{Load,\alpha} - Q_{Load,\beta}}{2} \right) + k_{qR} \left(\frac{Q_{Load,\alpha} + Q_{Load,\beta}}{2} \right) \tag{6.22}$$

As the required compensating current depends on compensation targets, such as the three-phase power factor at the point of common coupling, the power factor target variation was studied to determine the best condition. Babu and Sreejaya (2015) discovered that setting the power factor target in phases A, B, and C as inductive, inductive, and capacitive, respectively, resulted in minimum RPC capacity when the power factor was varied between 0.9 and 1 in both co-phased and traditional RPC systems. After that, in 2017, Hu and et al. found that the previously mentioned power factor target did not provide minimum RPC capacity in every loading condition. Accordingly, every condition of the power factor target was tested in the whole traction load range (both sides of the traction power supply arms). Then the optimal conditions were selected in accordance with the current load point. This optimal control strategy maintained the power quality indices under a nation's standard, reducing RPC capacity.

The research on applications of the partial compensation principle has been continuously conducted. Recently, a group of researchers proposed another concept of the control strategy called "flexible fractional compensating mode," which was mainly intended to fully utilise the RPC's unused capacity for approaching the full compensation. This approach not only reduced RPC capacity but also maximised the capacity utilisation and kept the power quality indices at a specified standard level (Roudsari, Jalilian, and Jamali, 2018).

6.2.3 Others

In addition to the full and partial compensation, other measures have been studied to reduce RPC capacity and cost while satisfying the power quality standard, e.g., a hybrid system (RPC working in tandem with other compensators) and the Steinmetz theory. The additional compensators used in the hybrid RPC (HRPC) are generally passive, such as static var compensators (SVCs), thyristor switched capacitors (Ghassemi, Fazel, Maghsoud, and Farshad, 2014) and so on, due to their simple structures and lower costs. Therefore, they are more suitable to cooperate with the RPC, which is intrinsically costly.

The SVC-based RPC compensation configuration has been widespread in recent research. In general, instead of utilising RPC, SVCs were installed on both secondary windings of traction transformers and used to supply reactive loads and compensate low-order harmonics. The RPC's only burden was active power transfer (active power balance) and/or high-order harmonics suppression; hence the RPC's capacity could be significantly reduced. Various types of SVCs have been adopted in the past research, such as a magnetic-controlled reactor (MCR)-based SVC (Chen and et al., 2016) and a thyristor-controlled reactor (TCR)-based SVC (Arabahmadi, Banejad, and Dastfan, 2018); they worked in combination with harmonic filters as shown in Fig. 2.24 (d). The SVCs and harmonic filters could also be installed on the secondary-side additional winding of the coupling transformer (An and et al., 2018); see Fig. 2.37.

Another compensation principle uses the Steinmetz theory, where inductive and capacitive elements are basically connected to the single-phase-loaded three-phase power supply to equalise the load of each phase, as shown in Fig. 6.5. In traction power supply with RPCs, the inductive and capacitive elements are replaced by RPCs in every consecutive traction substation. According to Steinmetz's balancing theory, the approach with RPCs in every traction substation working together can considerably lessen the transferred power or capacity of the RPCs. Jafarikaleybar, Kazemzadeh, and Farshad (2015) put forward the idea of using Yd11 and Yd5 with an RPC. Moreover, two types of transformers were alternately installed at the consecutive traction substation, so the voltages of the adjoining feeders were equal in both magnitude and phase or as equal as possible ($V_1 – V_5$). This configuration could help reduce the insulation level at the sectioning post; see Fig. 6.6. The paper found that each RPC's power capacity could be reduced to more than 80% compared with the conventional RPC's capacity when purely resistive load and no harmonics were considered.

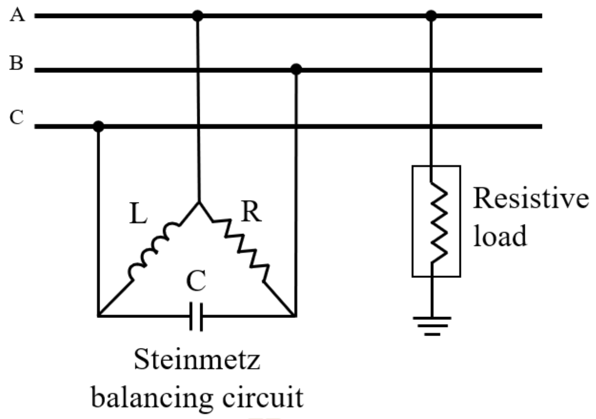

Fig. 6.5 Steinmetz RLC balancing circuit

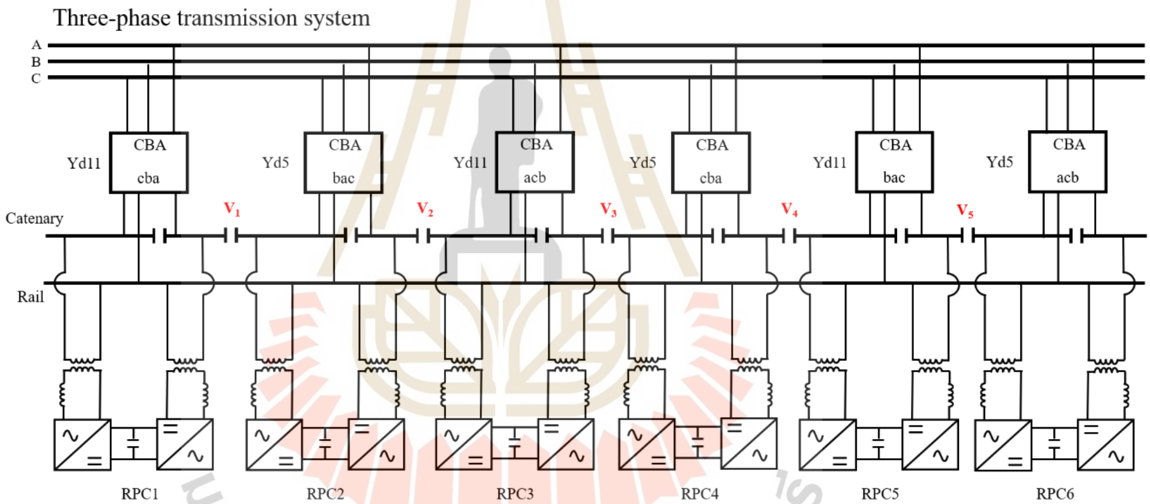

Fig. 6.6 Traction power supply configuration using Steinmetz balancing theory

(Jafarikaleybar, Kazemzadeh, and Farshad, 2015)

6.3 Optimal sizing procedure

The proposed RPC optimal sizing procedure is a method to determine the RPC's minimised design capacity, based on the AT power supply system components' steady-state models in Chapter 3, the power flow calculation in Chapter 4, the partial compensation principle, and an optimisation method. Firstly, the optimisation's objective function is introduced. Using modulation indices (*m*) and phase angles (δ) - the converters' control variables - in both converters as inputs, the objective function is the calculation of the RPC capacity using the CBNR power flow method and the power supply models proposed in this study under RPC's operation constraints and power quality constraints. The objective function's equation and constraints are shown in (6.23) and (6.24), respectively. The RPC operation constraints consist of equal transfer active power (a tolerance, ΔP, is applied to ease the optimal searching process), amount of active power transfer not exceeding half of the difference between two secondary feeder's loads or full-compensating active power, ranges of reactive power compensation within limits, and suitable condition of α- and β-phase reactive power at a substation (leading or lagging). The power quality constraints are the maximum allowable voltage unbalance factor (VUF) and minimum allowable three-phase power factor. As this objective function is unlikely to be used with constrained optimisation methods, the penalty method is employed to represent the constraints in unconstrained optimisation. The penalty terms are added to the RPC capacity derived from the power flow calculation (S_{RPCo}); see the flow chart describing the objective function in Fig. 6.7.

$$\text{Minimise } [S_{RPC} = f(m_\alpha, m_\beta, \delta_\alpha, \delta_\beta)] \tag{6.23}$$

$$
\begin{aligned}
&\left|P_{C\alpha} - P_{C\beta}\right| \le \Delta P_{tolerance} \\
&P_C \le P_{Full} = (P_{L\alpha} - P_{L\beta})/2 \\
&Q_{min,\alpha} \le |Q_{C\alpha}| \le Q_{max,\alpha} \\
&Q_{min,\beta} \le |Q_{C\beta}| \le Q_{max,\beta} \\
&\left.\begin{matrix} Q_\alpha \le 0 \\ Q_\beta \ge 0 \end{matrix}\right\} \rightarrow \text{V/V}, \left.\begin{matrix} Q_\alpha \ge 0 \\ Q_\beta \ge 0 \end{matrix}\right\} \rightarrow \text{Scott} \\
&VUF \le VUF_{target} \\
&PF \ge PF_{target}
\end{aligned}
$$

$$
\text{For V/V}: \begin{cases} Q_{C\alpha,full} = Q_{L\alpha} - (P_{L\alpha} - \operatorname{sign}(P_{L\alpha} - P_{L\beta})P_{Full})\tan\left(\dfrac{\pi}{6}\right): & \begin{matrix} Q_{C\alpha,full} > 0 \rightarrow \begin{cases} Q_{\max,\alpha} = Q_{C\alpha,full} \\ Q_{\min,\alpha} = 0 \end{cases} \\ Q_{C\alpha,full} < 0 \rightarrow \begin{cases} Q_{\max,\alpha} = 0 \\ Q_{\min,\alpha} = Q_{C\alpha,full} \end{cases} \end{matrix} \\ Q_{\max,\beta} = Q_{C\beta,full} = Q_{L\beta} + (P_{L\beta} - \operatorname{sign}(P_{L\beta} - P_{L\alpha})P_{Full})\tan\left(\dfrac{\pi}{6}\right), Q_{\min,\beta} = 0 & \end{cases} \tag{6.24}
$$

$$
\text{For Scott}: \begin{cases} Q_{\max,\alpha} = Q_{C\alpha,full} = Q_{L\alpha}, Q_{\min,\alpha} = 0 \\ Q_{\max,\beta} = Q_{C\beta,full} = Q_{L\beta}, Q_{\min,\beta} = 0 \end{cases}
$$

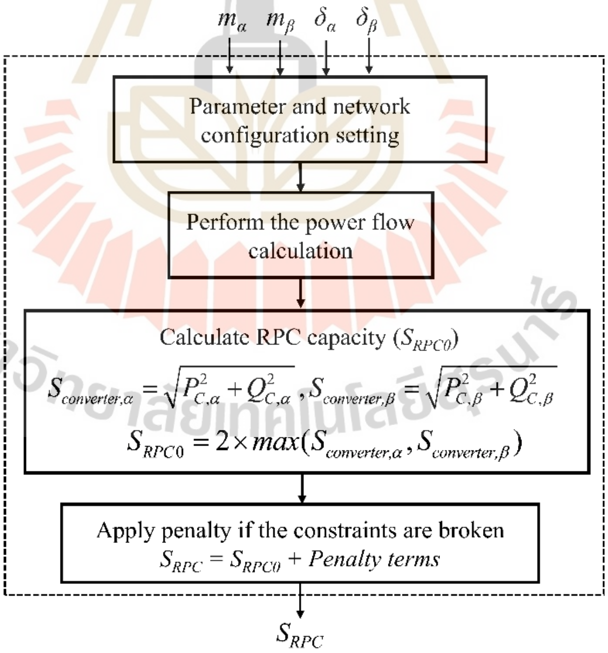

Fig. 6.7 Objective function flow chart

(Kritsada Mongkoldee and Thanatchai Kulworawanichpong, In press)

There are two main penalty terms, including a power-related term and a power quality-related term, which are further divided into 8 terms: (1) the square of the transferred active power difference between α-phase and β-phase load, (2) the square of the difference between the current transferred active power and the full-compensating active power, (3) the square of the difference between the current α-phase compensating reactive power and the full-compensating reactive power, (4) the square of the difference between the current β-phase compensating reactive power and the full-compensating reactive power, (5) the square of a magnitude of the α-phase reactive power, (6) the square of a magnitude of the β-phase reactive power, (7) the square of VUF, and (8) the sum of the inverse squares of each phase's power factor. In addition, each term of the power-related terms and the power quality-related terms is multiplied by the factor γ_1 and γ_2, respectively, to adjust the penalty values. The selection of γ_1 and γ_2 is fully described in Appendix D. Each of the penalty terms is added to S_{RPCo} only if the constraint of that penalty term is not satisfied, i.e., if all constraints are satisfied, no penalty is added. Equation 6.25 shows all penalty terms added to the S_{RPCo}. The optimisation method used in this study is the Particle Swarm Optimisation (PSO) because the objective function is highly non-linear and discontinuous. Accordingly, a heuristic-based method is a better solution regarding convergence and global minimum search in a large space. The Genetic Algorithm (GA) is also performed in the same case study to confirm superior convergence, and the results are compared to those of the PSO - see Appendix D. Both PSO and GA are run by built-in functions in MATLAB.

$$\begin{aligned} S_{RPC} = \; & S_{RPCo} + \gamma_1(|P_{C\alpha} - P_{C\beta}|^2 + |P_C - P_{Full}|^2 + |Q_{Full,\alpha} - Q_{C\alpha}|^2 + |Q_{Full,\beta} - Q_{C\beta}|^2 + \ldots \\ & + |Q_\alpha|^2 + |Q_\beta|^2) + \gamma_2(VUF^2 + (PF_A^{-2} + PF_B^{-2} + PF_C^{-2})) \end{aligned} \tag{6.25}$$

In order to find the optimal RPC size, the optimisation, as mentioned above, is conducted in 6 critical load points: (1) the maximum substation active power (P_{max}), (2) the maximum substation reactive power (Q_{max}), (3) the maximum substation apparent power (S_{max}), (4) the maximum difference between α- and β-phase active power (ΔP_{max}), (5) the maximum difference between α- and β-phase reactive power (ΔQ_{max}), and (6) the maximum difference between α- and β-phase apparent power (ΔS_{max}). The maximum load points cover high reactive compensation scenarios; the maximum difference load points cover high unbalance load scenarios. The traction load versus time is obtained by the train movement calculation shown in Appendix C. The maximum capacity is then selected to be the optimal RPC capacity covering all loading conditions (100% rating). The constraints are set to follow the principle of partial compensation; therefore, the optimal size is automatically based on partial compensation. The size is kept as small as possible but still maintains the standard power quality. The whole optimal sizing process is shown in Fig. 6.8.

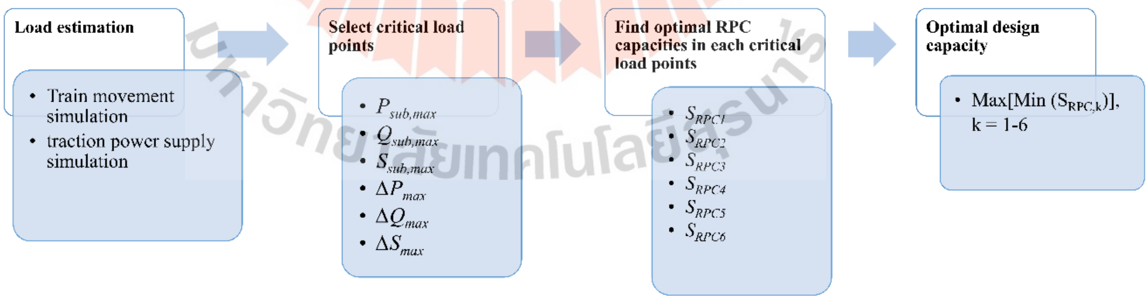

Fig. 6.8 RPC optimal sizing procedure flow diagram

(Kritsada Mongkoldee and Thanatchai Kulworawanichpong, In press)

6.4 Simulation test system

To validate the RPC optimal sizing procedure, the East Corridor line in Denver, Colorado, is adopted as a case study. The East Corridor line, currently called A line, is a commuter rail line linking Denver International Airport (DIA) and Denver Union Station (DUS). It is one of the electrified rail routes in the Regional Transportation District (RTD) transportation expansion plan under the FasTracks programme. The AC load-flow study was conducted, and the report was issued in 2009. Finally, the line was officially opened for operation in April 2016. Unlike the current rail line data after construction completion, this study follows the data in the load-flow simulation report in 2009. The map of the East Corridor line and the power supply diagram are shown in Fig. 6.9 and 6.10, respectively.

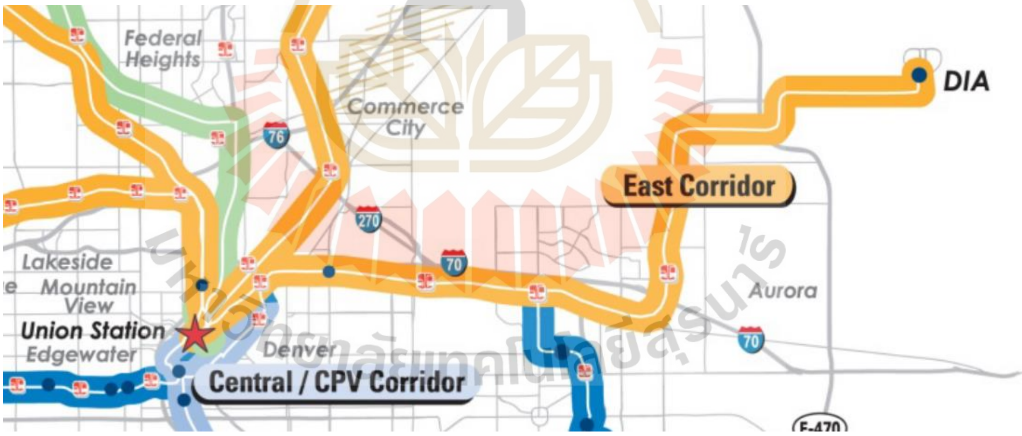

Fig. 6.9 The map of the East Corridor line (Front Range Systems Consultants FRSC, LTK and Parsons joint venture, 2009)

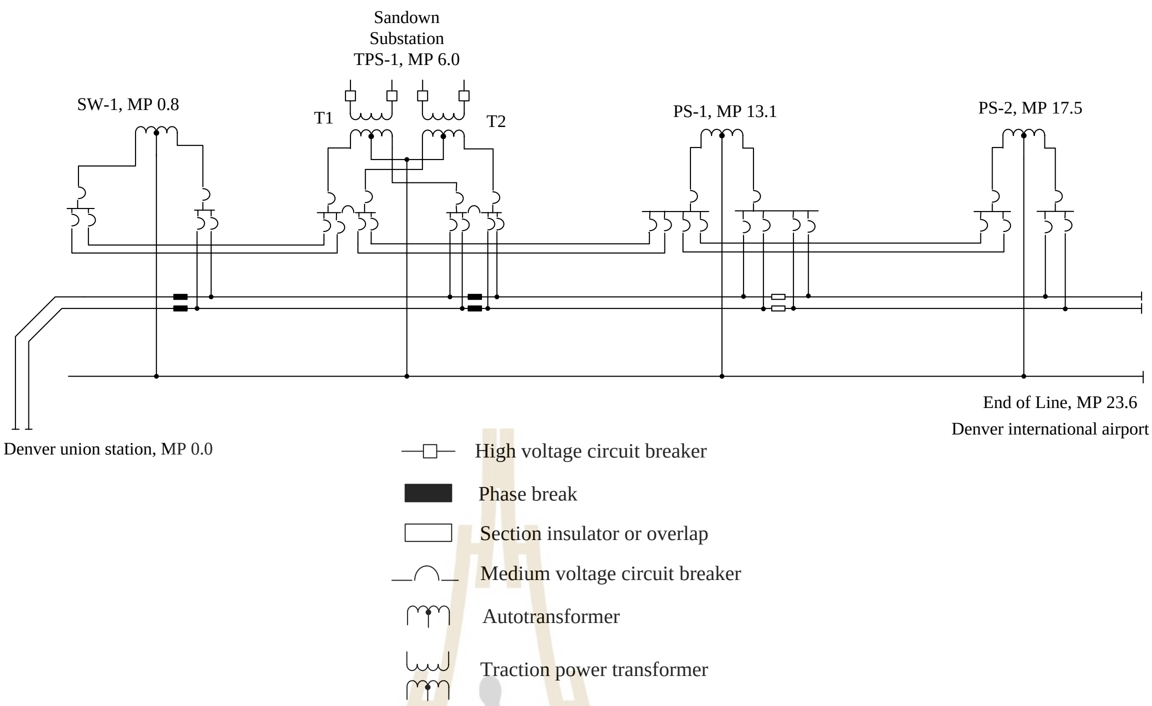

Fig. 6.10 The power supply diagram of the East Corridor line

(Front Range Systems Consultants FRSC, LTK and Parsons joint venture, 2009)

The traction power supply system of the East Corridor line is a 2×25 kV AT-fed system with one traction substation (Sandown) located at MilePost 6.0 (MP 0.0 at DUS). At the traction substation, there are two single-phase transformers connecting in a V/V configuration. One transformer (T1), connected to AB phase in the primary-side and referred to as α phase, supplies the line towards the west and the other transformer (T2), connected to CB in the primary-side and referred to as β phase, supplies the line towards the east. In addition, the west side has a shorter distance with only one AT, and the east side to DIA has two ATs. The traction substation is connected to the 115-kV grid with a short circuit capacity of 6910 MVA. The train operation information and power supply data are given by the commuter rail AC electrification load-flow simulation report (27th February 2009). The general and power supply data of the East Corridor line are tabulated in Table 6.1 – 6.3; the RPC's parameters are shown in Table 6.4. The train and catenary specifications are summarised as follows:

Train specification

Design weight:	176000 lb.
Rotating weight:	14750 lb.
Design Acceleration:	2.50 mph/s
Design Deceleration:	-2.50 mph/s
Mechanical Efficiency:	0.93
Electrical Efficiency:	0.87
Auxiliary Power:	35 kW/car
Drive Power Factor:	1.00
Auxiliary Power Factor:	0.80

Catenary specification

Feeder Impedance:	0.311+j1.356 Ω/mile
Catenary Impedance:	0.248+j1.024 Ω/mile
Rail Impedance:	0.1648+j0.6709 Ω/mile
Rail-to-earth Resistance:	0.5 Ω·m

Table 6.1 East Corridor line general information (Front Range Systems Consultants FRSC, LTK and Parsons joint venture, 2009)

Route length (mile)	The number of passenger stations	Station dwelling time (s)	Maximum speed (mph)	Maximum acceleration rate (mph/s)	Headway (minutes)
23.6	9	35	79	2.5	15

Table 6.2 Traction power supply parameters (Front Range Systems Consultants FRSC, LTK and Parsons joint venture, 2009)

Substations	Paralleling stations	Switching stations	The number of traction power transformers	The number of ATs	Transformer rating (MVA)	Transformer impedance (p.u.)
		SW-1 (MP 0.8)		2	2	j0.015
TPS-1 (MP 6.0)			2		10	j0.07
	PS-1 (MP 13.1)			1	2	j0.015
	PS-2 (MP 17.5)			1	2	j0.015

Table 6.3 Passenger stations and locations (Front Range Systems Consultants FRSC, LTK and Parsons joint venture, 2009)

Station name	Location (mile)
Denver Union Station (DUS)	0
40th and 40th	1.846
Colorado Boulevard	3.593
Central Park Boulevard	6.383
Peoria	8.879
40th and Airport	12.731
64th Avenue Station Option 1	15.555
72nd and Himalaya (Highpoint) Option 2	18.002
Denver International Airport (DIA)	22.995

Table 6.4 RPC's parameters in the simulation (Kritsada Mongkoldee and Thanatchai Kulworawanichpong, In press)

Coupling transformers' turns ratio	50/3
Inductor's inductance (mH)*	0.5
DC voltage (V)	11,000

*(Ma and et al., 2013)

6.5 Simulation case study

This simulation is to test the proposed optimal RPC sizing method with the mentioned case study. The power supply parameters and train load are modified for the system to have adverse power quality problems: (1) the short circuit capacity of the three-phase grid is reduced to 500 MVA from 6910 MVA, slightly less than the Bangkok SRT Red line's short circuit capacity of about 760 MVA as a reference value (final traction power supply study no. EM3-PS-DS-1018 rev. 04), (2) the power factor of the tractive load is 0.80, considering the worst-case with AC-DC traditional locomotives dominating the line, and (3) the tractive effort and train weight are increased. The RPC is added to the only one traction substation of the East Corridor line, as shown in Fig 6.11. The simulation has 2 cases with different rating tractive force (Fig. 6.12) and train weight. Each case is simulated with two different traction transformers, i.e., V/V and Scott transformer. Table 6.5 shows the details of each case. The train weight and tractive effort in case 1 double those of the base case, equivalent to a two-fold carrying load or more train service with a headway of 5 minutes. In case 2, the train weight and tractive effort triple those of the base case; this scenario represents even more carrying load and heavier train traffic. Therefore, case 1 and case 2 are the scenarios that accommodate an extension of the East Corridor line's rail traffic and more passengers for the next 20-30 years. Table 6.6 shows the influence of train service frequency or headway on electrical loads at the traction substation in the base case. By performing the train movement simulation and power flow calculation, the voltage unbalance factor (VUF) and the substation power consumption of each case without RPC operation are obtained in Fig. 6.13 – 6.18. The power quality indexes of critical load points in the base case (VUF and three-phase power factor) are summarised in Table 6.7 for the V/V transformer and Table 6.8 for the Scott transformer. The maximum active power, reactive power, and apparent power occur at the same load point. Likewise, the load points with maximum active power difference, reactive power difference, and apparent power difference coincide with one another. It is evident that the maximum VUF is greater than 2% in case 1 and 3% at the maximum power difference load point in case 2, which clearly exceeds the standard.

Further, the three-phase power factors are heavily affected by traction load, especially in the common return phase (phase C). This study follows the standard proposed by Hu S. and et al. (2017), the Chinese national standard. The VUF must be kept under 2%, and the power factor must be greater or equal to 0.90 to avoid penalty. This simulation is done with power factor targets of both 0.90 and 0.95. The electrical parameters used for RPC in the simulation are as follows: the coupling transformer's turns ratio is 50/3, the inductor's inductance in mH is 0.5 (Ma and et al., 2013), and DC-link voltage is 11 kV. It is assumed that the coupling transformer and the converters are lossless.

Table 6.5 Different parameters in case studies

Case	Short circuit capacity (MVA)	Tractive load power factor	Train weight (tonne)	Maximum tractive force (kN)
Base case	500	0.80	86.61	85.87
Case 1	500	0.80	173.23	171.74
Case 2	500	0.80	259.84	257.61

Table 6.6 East Corridor line's electrical loads at the substation with different headways

Headway (min.)	Max. 3ϕ apparent power (MVA)	Max. 3ϕ reactive power (MVar)	Max. VUF (%)	Min. 3ϕ power factor
5	13.2169	8.3972	1.8670	0.7673
10	8.2242	5.1406	1.2213	0.7731
15 (base)	6.1309	3.7865	1.1914	0.7779

Table 6.7 Critical load points without RPC (V/V transformer)

Case		S_α (MVA)	S_β (MVA)	*VUF*/*IUF* (%)	$\cos(\varphi_A)$	$\cos(\varphi_B)$	$\cos(\varphi_C)$
1	Max. ΔP, ΔQ, ΔS	0	8.0985 + j6.4584	2.2377/100	0.7521	0.9830	0.3083
	Max. P, Q, S	3.5783 + j2.7592	4.9614 + j3.9207	1.1986/52.6219	0.9869	0.8387	0.3387
2	Max. ΔP, ΔQ, ΔS	0	11.775 + j9.7578	3.4685/100	0.7443	0.9758	0.2580
	Max. P, Q, S	5.2027 + j4.0692	7.2628 + j5.9073	1.8336/53.1740	0.9832	0.8326	0.3090

Table 6.8 Critical load points without RPC (Scott transformer)

Case		S_α (MVA)	S_β (MVA)	*VUF*/*IUF* (%)	$\cos(\varphi_A)$	$\cos(\varphi_B)$	$\cos(\varphi_C)$
1	Max. ΔP, ΔQ, ΔS	0	8.0985 + j6.4584	2.2796/100	0.3415	0.9793	0.2887
	Max. P, Q, S	3.5783 + j2.7592	4.9614 + j3.9207	0.3780/16.4855	0.7669	0.8440	0.6729
2	Max. ΔP, ΔQ, ΔS	0	11.775 + j9.7578	3.6037/100	0.3415	0.9680	0.2227
	Max. P, Q, S	5.2027 + j4.0692	7.2628 + j5.9073	0.5938/17.0335	0.7491	0.8307	0.6466

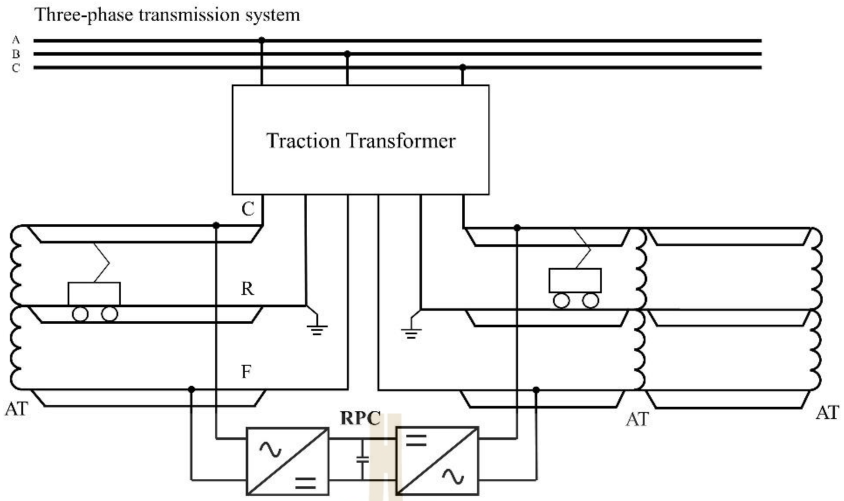

Fig. 6.11 Power supply system diagram with RPC

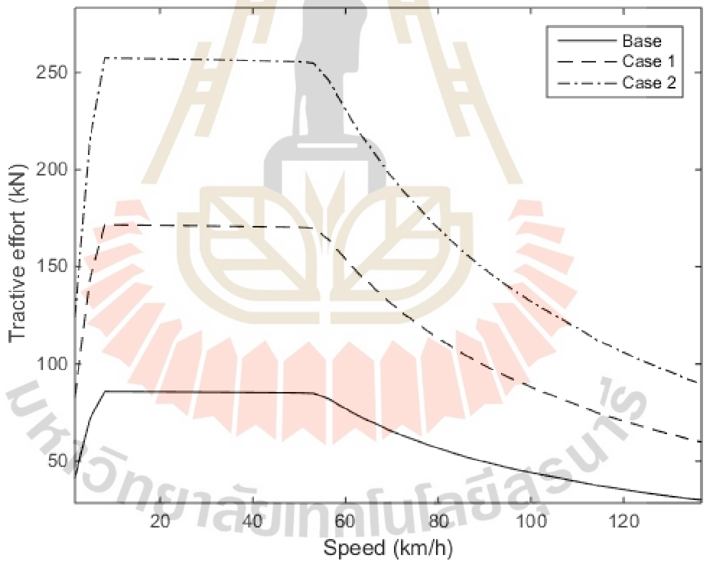

Fig. 6.12 Tractive effort versus speed curves

(Kritsada Mongkoldee and Thanatchai Kulworawanichpong, In press)

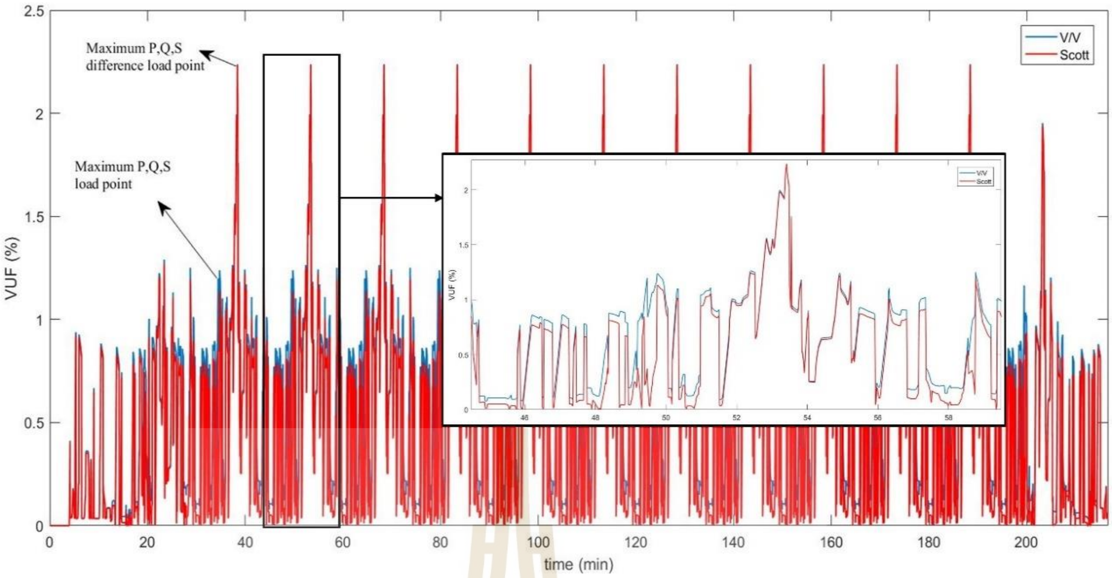

Fig. 6.13 VUF in case 1

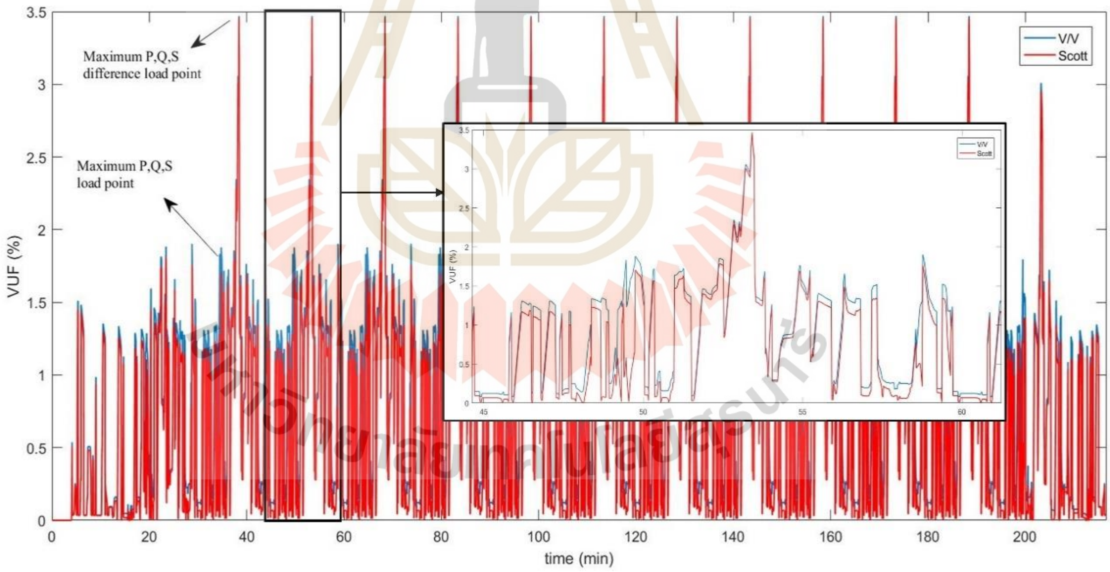

Fig. 6.14 VUF in case 2

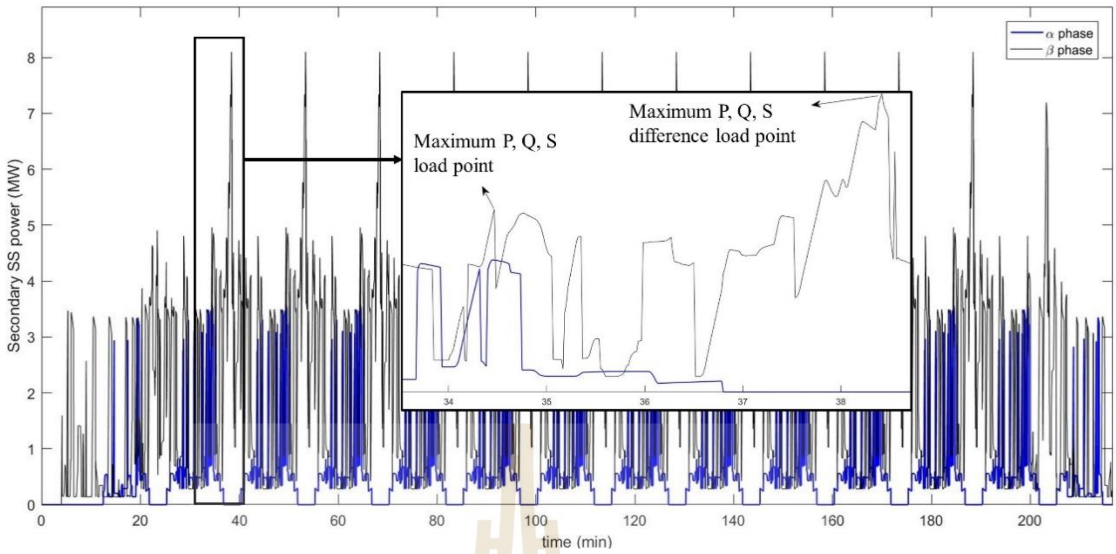

Fig. 6.15 Substation active power consumption in case 1

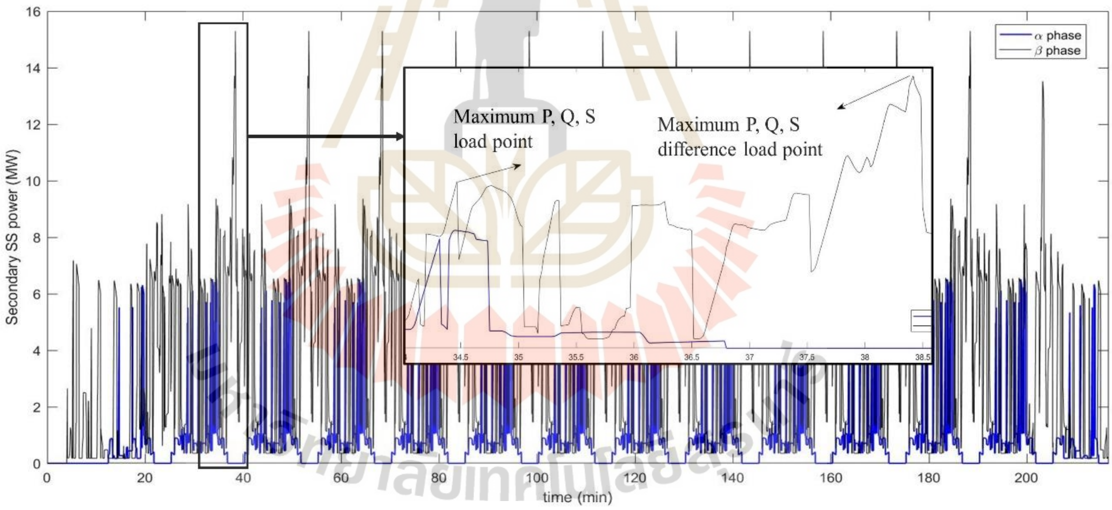

Fig. 6.16 Substation active power consumption in case 2

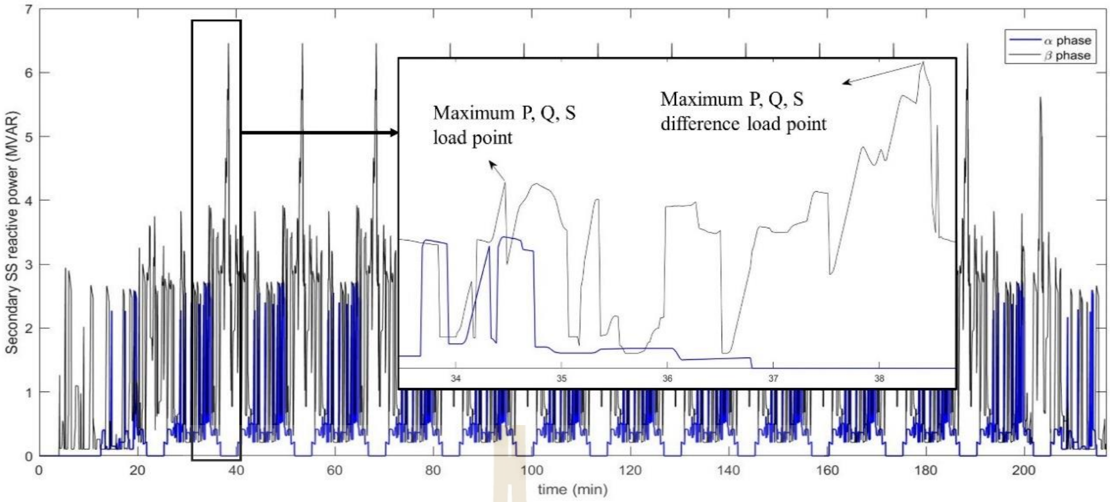

Fig. 6.17 Substation reactive power consumption in case 1

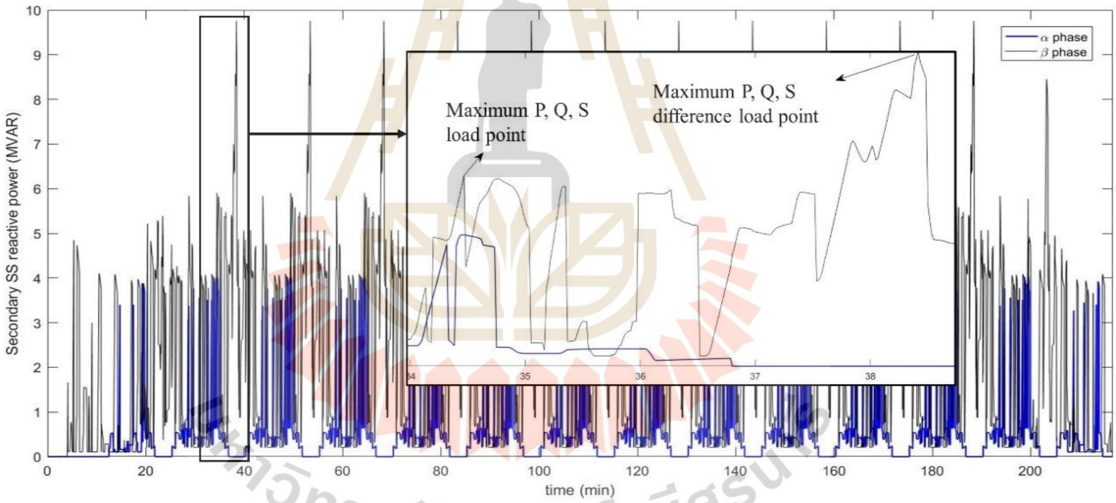

Fig. 6.18 Substation reactive power consumption in case 2

6.6 Simulation results and discussion

The following describes the results of the simulation detailed in the previous section and the PSO results. When using the V/V transformer, the optimal RPC operation points, after-compensated power factors and VUFs under power factor targets PF* ≥ 0.95 and PF* ≥ 0.90 are presented in Table 6.9 and 6.10, respectively. Those of Scott transformer are shown in Table 6.11 and 6.12, respectively. In the V/V transformer case, Fig. 6.19 summarises the optimal sizes of RPC in MVA, including full compensation capacities, partial-compensation capacities with PF* ≥ 0.95, and partial-compensation capacities with PF* ≥ 0.90. Fig. 6.20 and 6.21 show the optimal values of transferred power and compensating reactive power. Those of Scott transformer case are shown in Fig. 6.22 – 6.24, respectively.

After compensation, the VUFs are less than 2.0% in all cases. Also, the VUFs in the Scott transformer case are less than the V/V transformer case, both before and after compensation, due to a balancing feature of Scott transformer. The power factors are also improved to exceed the specified targets. As the β phase load (receiving from CB phase from a three-phase transmission system) in the critical load points of this case study is greater than that of α phase, reactive compensation of β phase determines a reactive compensation capacity of a converter in RPC. For this reason, the C-phase power factors are exactly equal to the target values i.e., the largest amount of compensating reactive power occurs in this phase. In contrast, the power factors of the rest are more than the target values, except in the maximum power difference case of the V/V transformer.

The optimal sizes of RPC are shown in Table 6.13. They can be chosen between a capacity with $PF^* = 0.90$ and $PF^* = 0.95$, i.e., for V/V transformer, 14.41 – 16.11

MVA (case 1) and 21.55 – 23.97 MVA (case 2); for Scott transformer, 11.99 – 12.88 MVA (case 1) and 18.08 – 19.57 (case 2). The lower boundary capacity is adequate to avoid a low power factor penalty. However, the upper boundary capacity can be chosen for a wider margin in case of contingencies. Capacity higher than the upper boundary is not deemed optimal; the one lower than the lower boundary is insufficient to maintain standard power quality requirements. Compared with the full compensation capacity, the upper boundary values account for about 83% and 85% of the full compensation capacity in the V/V and Scott transformer cases, respectively. Likewise, the lower boundary values account for about 74% and 79% of the full compensation capacity in the V/V and Scott transformer cases, respectively. So, a reduction of up to 25% in capacity can be achieved by the proposed procedure. Another important aspect of this simulation is that reactive power load is significantly high compared to current PWM traction technologies, which produce the power factor close to unity. Therefore, reactive power constitutes the majority of the RPC capacity.

On the contrary, an active power proportion of RPC capacity is only 9% – 13% for V/V transformer case and 22% – 25% for the Scott transformer case. This implies that the RPC size is significantly reduced if only unity power factor locomotives are in service. An amount of compensating reactive power is optimised to compensate so that the power factor is improved to the targeted value, β phase, in this case study. In addition, it is evident that the compensating reactive power of the Scott transformer is always less than that of the V/V transformer, which is consistent with the explanation in section 6.2. From the results, the size of RPC used with the Scott transformer is approximately 16% – 19%, less than with the V/V transformer.

Voltage unbalance and low power factor is likely to impact other electricity consumers in the same transmission feeder at any instance. Accordingly, the proposed optimal RPC sizing procedure considers every load point, i.e., power quality must always be kept according to the standard at all times. All in all, the RPC's size selection is heavily influenced and dependent upon the traction substation load and the law and regulations of power companies or electric utilities.

Table 6.9 Optimal operating points with corresponding unbalances and power factors (V/V, PF* ≥ 0.95)

Case		m_α	m_β	δ_α (degree)	δ_β (degree)	VUF/IUF (%)	cos(φ_A)	cos(φ_B)	cos(φ_C)
1	Max. ΔP, ΔQ, ΔS	0.732	0.900	26.308	89.602	0.628/38.424	0.95	-0.978	0.95
	Max. P, Q, S	0.765	0.850	27.8	88.353	0.222/12.698	0.996	0.983	0.95
2	Max. ΔP, ΔQ, ΔS	0.710	0.962	24.18	89.503	0.818/34.359	0.951	-0.987	0.95
	Max. P, Q, S	0.756	0.884	25.779	88.463	0.403/15.624	0.997	0.953	0.95

Table 6.10 Optimal operating points with corresponding unbalances and power factors (V/V, PF* ≥ 0.90)

Case		m_α	m_β	δ_α (degree)	δ_β (degree)	VUF/IUF (%)	cos(φ_A)	cos(φ_B)	cos(φ_C)
1	Max. ΔP, ΔQ, ΔS	0.734	0.885	27.180	88.805	0.817/49.209	0.90	-0.980	0.90
	Max. P, Q, S	0.762	0.835	27.604	88.483	0.333/18.556	0.99	0.954	0.90
2	Max. ΔP, ΔQ, ΔS	0.726	0.943	26.280	87.774	1.320/55.137	0.90	-0.967	0.90
	Max. P, Q, S	0.755	0.867	26.108	88.102	0.510/19/354	0.995	0.943	0.90

Table 6.11 Optimal operating points with corresponding unbalances and power factors (Scott, PF* ≥ 0.95)

Case		m_α	m_β	δ_α (degree)	δ_β (degree)	*VUF/IUF* (%)	cos(φ_A)	cos(φ_B)	cos(φ_C)
1	Max. ΔP, ΔQ, ΔS	0.773	0.846	-8.258	91.646	0.241/14.577	0.999	0.980	0.9504
	Max. P, Q, S	0.809	0.801	-4.499	87.888	0.219/12.451	0.996	0.975	0.95
2	Max. ΔP, ΔQ, ΔS	0.773	0.908	-9.522	90	0.570/24.061	0.998	-0.999	0.95
	Max. P, Q, S	0.798	0.822	-6.698	86.871	0.078/2.966	0.963	0.963	0.95

Table 6.12 Optimal operating points with corresponding unbalances and power factors (Scott, PF* ≥ 0.90)

Case		m_α	m_β	δ_α (degree)	δ_β (degree)	*VUF/IUF* (%)	cos(φ_A)	cos(φ_B)	cos(φ_C)
1	Max. ΔP, ΔQ, ΔS	0.772	0.840	-7.215	90.807	0.392/23.574	0.999	0.999	0.90
	Max. P, Q, S	0.793	0.786	-4.571	87.899	0.221/12.068	0.974	0.943	0.90
2	Max. ΔP, ΔQ, ΔS	0.772	0.893	-8.560	89.301	0.799/33.394	0.999	-0.999	0.90
	Max. P, Q, S	0.807	0.797	-6.819	87.012	0.332/12.375	0.975	0.941	0.90

Table 6.13 Optimal RPC sizes

Transformer	Case	Target power factor (*PF**)	Full compensation capacity (MVA)	$S_{optimal}$ (MVA)
V/V	1	0.95	19.37	16.11
		0.90		14.40
	2	0.95	28.83	23.97
		0.90		21.55
Scott	1	0.95	15.25	12.88
		0.90		11.94
	2	0.95	22.79	19.57
		0.90		18.08

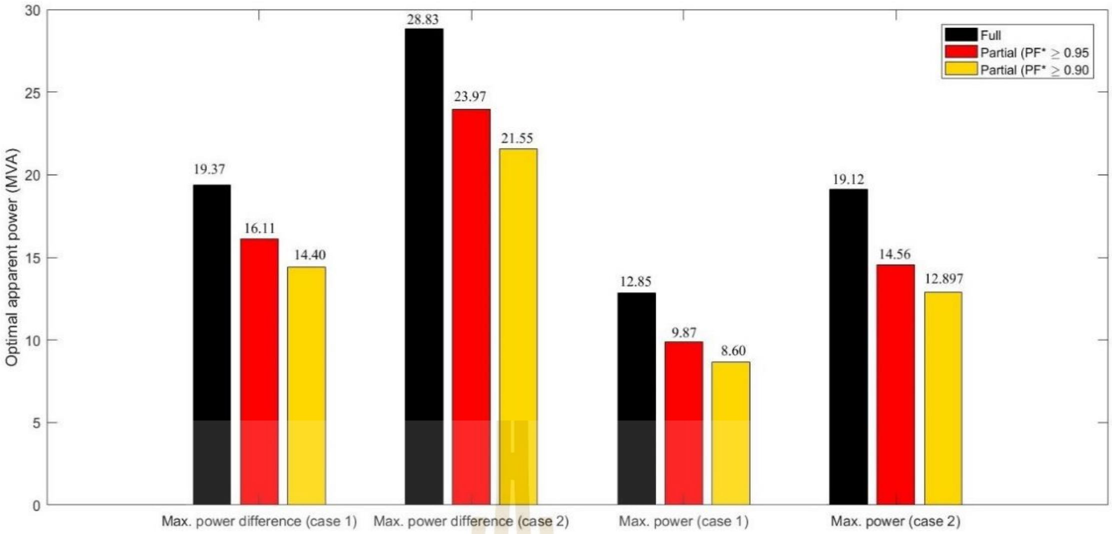

Fig. 6.19 Optimal RPC compensating apparent power (V/V transformer)

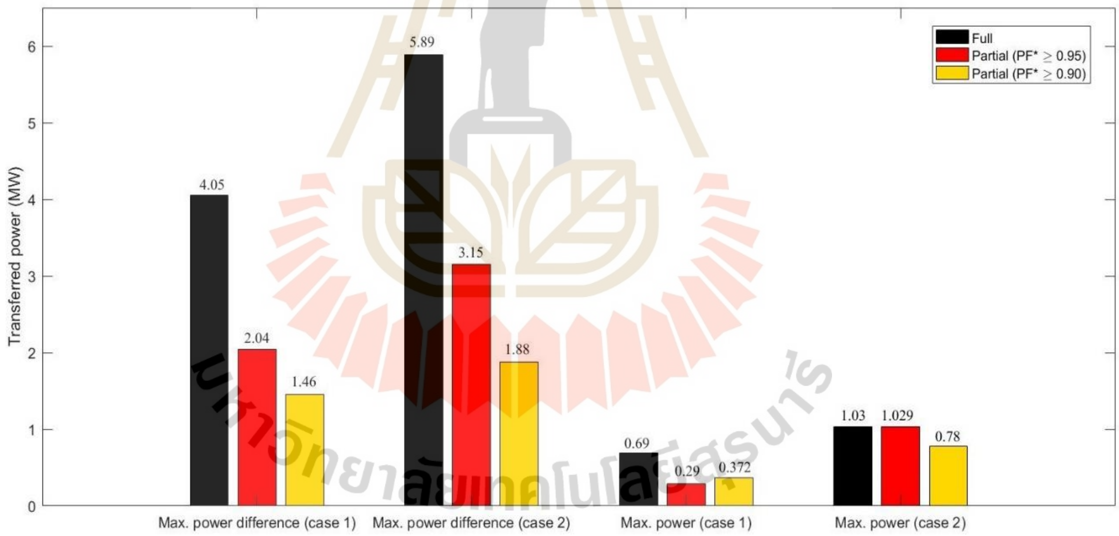

Fig. 6.20 Optimal RPC transferred active power (V/V transformer)

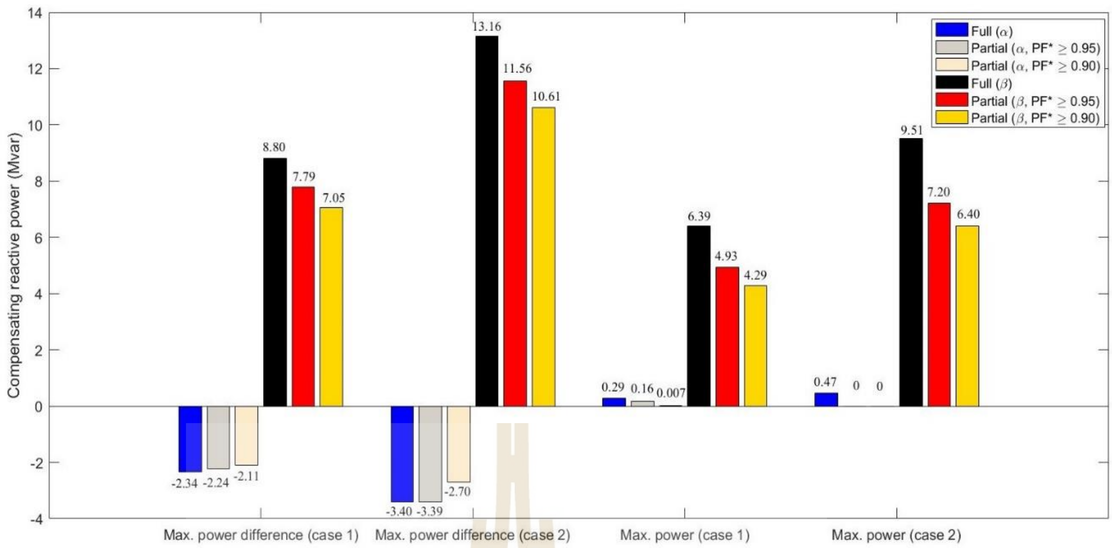

Fig. 6.21 Optimal RPC compensating reactive power (V/V transformer)

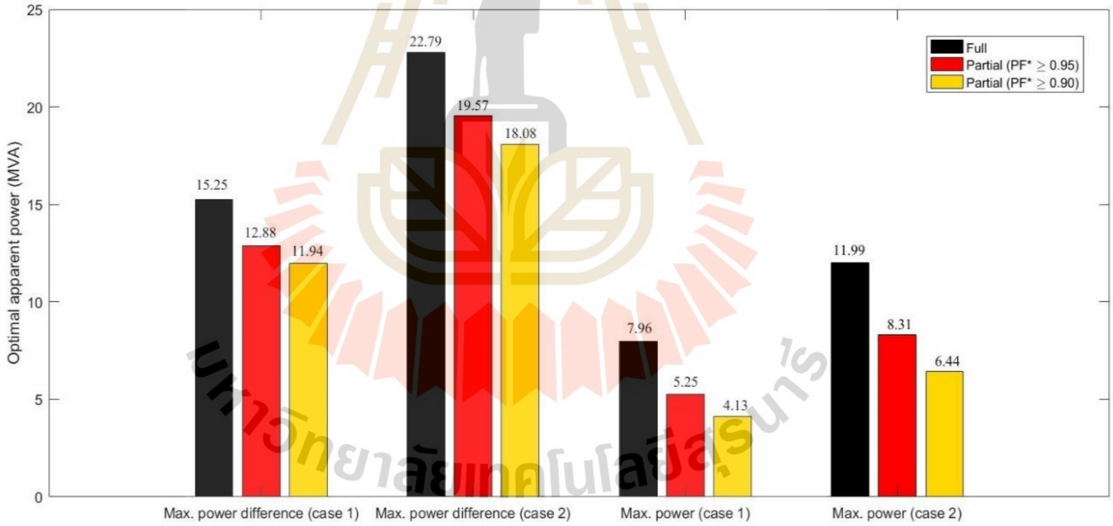

Fig. 6.22 Optimal RPC compensating apparent power (Scott transformer)

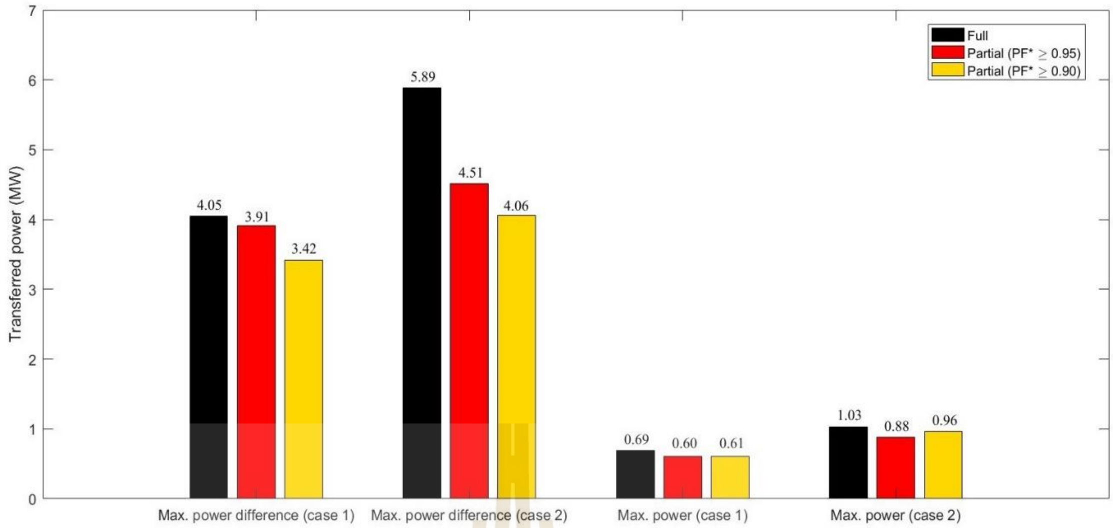

Fig. 6.23 Optimal RPC transferred active power (Scott transformer)

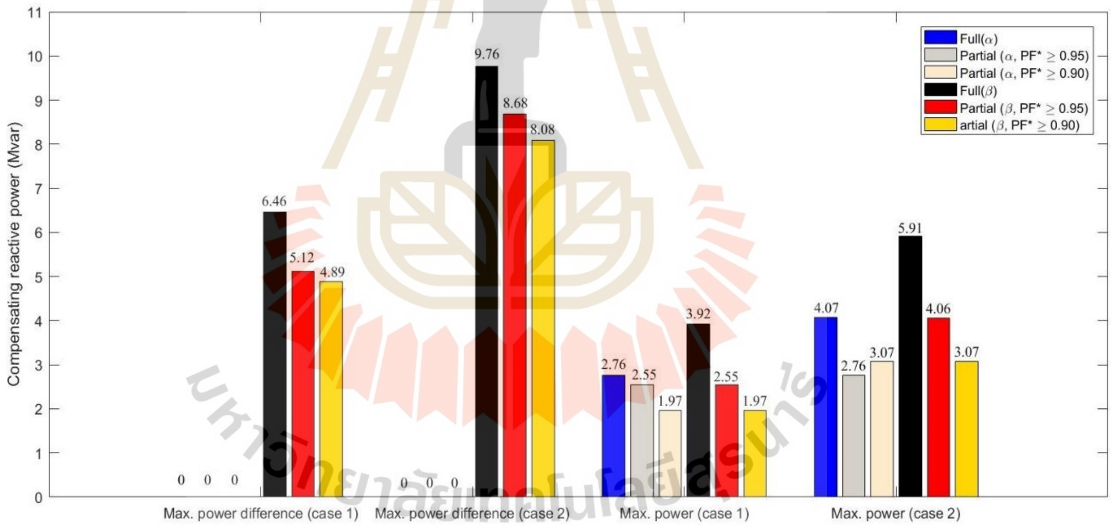

Fig. 6.24 Optimal RPC compensating reactive power (Scott transformer)

Chapter 7

Conclusion and recommendations

7.1 Conclusion

The following are the conclusion of this research, which is divided into 3 parts according to the research objectives.

1. The current-based Newton-Raphson (CBNR) power flow calculation method was successfully developed for an AT-fed railway power supply system in Chapter 4 with its traction power supply component models described in Chapter 3. The CBNR method and mathematical models are the core of simulation in this research. The correctness of the proposed calculation and models was verified in Appendix B.

2. Chapter 5 studied the AT tap change in the AT-fed traction power supply system. The tap setting was divided into 2 parts: the simultaneous tap change and optimally-searched tap change. The results of Part 1 (simultaneous tap change) could be briefly summarised that the tap change caused a larger amount of power loss in every case no matter the direction of the tap change was adjusted. Therefore, this concept of the tap change was not recommended and unlikely to be put into actual operation. The results of Part 2 (optimal tap setting) showed some signs of improvement; the optimal tap setting achieves the power loss minimisation, the three-phase power factor maximisation, and VUF minimisation. Nevertheless, the improvements of those values (the minimised power loss, the maximised power

factor, and the minimised VUF) were not significant, namely they were not considerably different from the values in the case without tap changing. For instance, the power loss reduction was less than 1% compared with no tap-changing case. In particular, the power loss was very high under the condition of VUF minimisation. This indicated that the idea of the optimal AT tap change undeniably gained some improvement; however, it did not seem worthwhile to implement in actual power supply system, i.e. it might not be worth investing on modifying the normal system into the tap-changing AT system which includes the tap changing mechanism, control and communication system. As a result, it needs the further study of investment costs in the future.

3. The optimal RPC sizing procedure and its case study were introduced in Chapter 6. The results confirmed that the proposed sizing procedure could find RPC optimal sizes as well as RPC's operation points in the case study under the principle of partial compensation, VUF $\leq$ 2% and power factor $\in$ [0.90, 0.95]. The optimal sizes contained the lower value (targeted power factor = 0.90) and the upper value (targeted power factor = 0.95). These boundaries are a guideline when selecting an RPC's installation capacity. Designers can either select the lower boundary in order to attain the minimum required compensation capacity or select the capacity in between to have a wider and safer margin for a contingency case that may cause a substandard power factor with being penalised. In addition, the size selection depends on traction substation loads and, national standards and regulations or power grid requirements.

7.2 Recommendations for future work

1. Recent RPC research has investigated several new types of converters and their control strategies. The proposed RPC optimal sizing procedure can possibly be adopted for those new converters as well as other existing converters with slight model modification in an AC-DC transformation equation.

2. The execution time or calculation time of the proposed procedure is highly dependent upon optimisation methods. In the future, there is possibility to enhance the calculation of this procedure when more heuristic optimisation methods are introduced. Then, it is worth an attempt to use alternative methods in this procedure.

3. This research focuses on an RPC installed at a traction substation. In future research, an installation and use of RPC at a sectioning point together with the function of regenerative power transfer between two different phase sections may be considered.

4. Economic breakeven points and expected return from investment in RPC can be thoroughly studied in the future when sufficiently detailed prices of RPC and its components, as well as installation and inspection costs, are available.

7.3 Research publication

7.3.1 Journals

Mongkoldee, K. and Kulworawanichpong, T. (2018). Current-based Newton-Raphson power flow calculation for AT-fed railway power supply systems. International Journal of Electrical Power and Energy Systems. 98 (June): 11-22.

Mongkoldee, K., Ratniyomchai T., and Kulworawanichpong, T. (2018). Scott Transformer Power Flow Model in Autotransformer Traction Feeding System. International Journal of Industrial Electronics and Electrical Engineering. 6 (6): 23-27.

Mongkoldee, K. and Kulworawanichpong, T. (2022). Comparative Study of Compensation Capacities using Railway Power Conditioner and Steinmetz Compensator in Traction Substation with V/V Transformer. Rajamangala University of Technology Srivijaya Research Journal. 14 (1). (In press).

Mongkoldee, K. and Kulworawanichpong, T. (In press). Optimal Sizing of AC Railway Power Conditioner in Autotransformer-Fed Railway Power Supply System. International Journal of Electrical Power and Energy Systems.

7.3.2 Conference papers

Mongkoldee, K., Leeton, U., and Kulworawanichpong, T. (2016). Single train movement modelling and simulation with rail potential consideration. In Proceeding of the IEEE/SICE International Symposium on System Integration (SII) (pp. 7-12). (n.p.) IEEE.

Mongkoldee, K. and Kulworawanichpong, T. (2018). AC railway power flow modelling integrated with RPC. In Proceeding of the Technical Meeting on Transportation and Electric Railway (pp. 77-80). (n.p.) IEEJapan.

Mongkoldee, K. and Kulworawanichpong, T. “Train movement simulation with rail potential consideration”, The 3rd Thailand Rail Academic Symposium: (TRAS2016), Bangkok, Thailand, September 1-2, 2016.

Mongkoldee, K. and Kulworawanichpong, T. “Models of special transformers for railway power supply systems”, The 4rd Thailand Rail Academic Symposium: (TRAS2017), Nakhon Ratchasima, Thailand, August 31- September 1, 2017.

Mongkoldee, K., Zhou F. and Kulworawanichpong, T. “Effect of autotransformer tap-changing on traction power supply performances”, The IEEJ PES – IEEE PES Thailand Joint Symposium, Bangkok, Thailand, March 18, 2019.

Reference

Acha, E., Agelidis, V. G., Anaya-Lara, O., and Miller, T. J. E. (2002). **Power Electronic Control in Electrical Systems**. Oxford: Newnes.

Acha, E., Fuerte-Esquivel, C. R., Ambriz-Perez, H., and Angeles-Camacho, C. (2004). **FACTS Modelling and Simulation in Power Networks**. Chichester, West Sussex: John Wiley & Sons.

Aihara, Y., Miyazawa, R., and Koizumi, H. (2012). A study on the effect of the Scott transformer on the three-phase unbalance in distribution network with single-phase generators. In **Proceeding of the 3rd IEEE International Symposium on Power Electronics for Distributed Generation Systems** (pp. 283-290). (n.p.) IEEE.

Ambriz-Perez, H., Acha, E., and Fuerte-Esquivel, C. R. (2000). Advanced SVC models for Newton-Raphson load flow and Newton optimal power flow studies. **IEEE Transactions on Power Systems**. 15 (1): 129-136.

An, B. and et al. (2016). An Asymmetrical Connection Balance Transformer-Based Hybrid Railway Power Conditioning System with Cost-Function Optimization. **IEEE Transactions on transportation electrification**. 4 (2): 577-590.

Arabahmadi, M., Banejad, M., and Dastfan, A. (2018). Hybrid Railway Traction Power Quality Compensator for power rating reduction of converters. In **Proceeding of the 9th Annual Power Electronics, Drives Systems and Technologies Conference (PEDSTC)** (pp. 306-311). (n.p.) IEEE.

Babu, A. and Sreejaya, P. (2015). Reduced Rating Railway Power Conditioners in Co-phase Traction and Traditional Traction System. In **Proceeding of the 2015 International Conference on Control, Communication & Computing India (ICCC)** (pp. 291-296). (n.p.) IEEE.

Chen, B. and et al. (2016). Electrical magnetic hybrid power quality compensation system for V/V traction power supply system. **IET Power Electronics**. 9 (1): 62-70.

Chen, B-K. and Guo, B-S. (1996). Three phase models of specially connected transformers. **IEEE Transactions on Power Delivery**. 11 (1): 323-330.

Chen, Q. and et al. (2014). Operation and control of enhanced railway power conditioner. In **Proceeding of the International Conference on Power System Technology (POWERCON2014)** (pp. 2375-2381). (n.p.) IEEE.

Chu, W-S. and Gu, J-C. (2006). A new hybrid SVC scheme with Scott transformer for balance improvement. In **Proceeding of the 2006 IEEE/ASME Joint Rail Conference** (pp. 217-224). (n.p.) IEEE.

Ciccarelli, F., Fantauzzi, M., Lauria, D., and Rizzo, R. (2012). Special transformers arrangement for AC railway systems. In **Electrical Systems for Aircraft, Railway and Ship Propulsion (ESARS), 2012**. (n.p.) IEEE.

Dai, Y., Liu, L., and Li, Y. (2011). An Intelligent Parameter Selection Method for Particle Swarm Optimization Algorithm. In **Proceeding of the 2011 International Joint Conference on Computational Sciences and Optimization** (pp. 960-964). (n.p.) IEEE.

Dubey, G. K. (2005). **Fundamentals of Electrical Drives** (2nd ed.). Harrow, U.K.: Alpha Science International.

Friedrich, K., Rainer, P., Axel, S., and Egid, S. (2009). **Contact lines for electric railways** (2nd ed.). Erlangen: Publicis Publishing.

Front Range Systems Consultants FRSC, LTK and Parsons joint venture. (2009). Commuter Rail AC Electrification Load-Flow Simulation Report (Revision 1).

Fuerte-Esquivel, C. R., Acha, E., and Ambriz-Perez, H. (2000). A comprehensive Newton-Raphson UPFC model for the quadratic power flow solution of practical power networks. **IEEE Transactions on Power Systems**. 15 (1): 102-109.

Ghassemi, A., Fazel, S. S., Maghsoud, I., and Farshad S. (2014). Comprehensive study on the power rating of a railway power conditioner using thyristor switched capacitor. **IET Electrical Systems in Transportation**. 4 (4): 97-106.

Grunbaum, R. (2007). FACTS for dynamic load balancing and voltage support in rail traction. In **Proceeding of the European Conference on Power Electronics and Applications** (pp. 1-10). (n.p.) IEEE.

Hagh, M. T. and Sabahi, M. (2016). A single phase unified power quality conditioner (UPQC). In **Proceeding of the IEEE international conference on Power System Technology (POWERCON2007)** (pp. 1-4). (n.p.) IEEE.

Harold, P. C. (1953). **The electrical manufacturers, 1875-1900: A study in competition, entrepreneurship, technical change, and economic growth**. (n.p.) Harvard University Press.

He, X. and et al. (2014). Advanced Cophase Traction Power Supply System Based on Three-Phase to Single-Phase Converter. **IEEE Transactions on Power Electronics**. 29 (10): 5323-5333.

He, Z., Zheng, Z., and Hu, H. (2016). Power quality in high-speed railway systems. **International Journal of Rail Transportation**. 4 (2): 71-97.

Hingorani, N. G. and Gyugyi, L. (2000). **Understanding FACTS concepts and technology of flexible AC transmission**. Piscataway, NJ: IEEE Press.

Horita, Y. and et al. (2010). Single-phase STATCOM for feeding system of Tokaido Shinkansen. In **Proceeding of the International Power Electronics Conference** (pp. 2165-2170). (n.p.) IEEE.

Hosseini, M., Shayanfar, H. A., and Fotuhi-Firuzabad, M. (2009). Modeling of unified quality conditioner (UPQC) in distribution system load flow. **Energy Conversion and Management**. 50 (6): 1578-1585.

Hosseini, S. H., Sarhangzadeh, M., and Shahnia, F. (2012). A novel control scheme of the statcom for power quality improvement in electrified railways. In **Proceeding of the 37th IEEE Power Electronics Specialists Conference** (pp. 1-5). (n.p.) IEEE.

Hu, S. and et al. (2017). A Power Factor-Oriented Railway Power Flow Controller for Power Quality Improvement in Electrical Railway Power System. **IEEE Transactions on Industrial Electronics**. 64 (2): 1167-1177.

Jafarikaleybar, H., Kazemzadeh, R., and Farshad, S. (2015). Power rating reduction of Railway Power Quality compensator using Steinmetz theory. In **Proceeding of the 6th Power Electronics, Drive systems & Technologies Conference (PEDSTC2015)** (pp. 442-447). (n.p.) IEEE.

Kawahara, K., Hase, S-I., Mochinaga, Y., Hisamizu, Y., and Inoue, T. (1997). Compensation of voltage drop using static Var compensator at sectioning post in AC railway system. **The Power Conversion Conference – Nagaoka 1997.** 2: 955-960.

Kazibwe, W. E., and Sendaula, M. H. (1993). **Electrical power quality control techniques**. New York: Van Nostrand Reinhold.

Kotturu, J. and Agarwal, P. (2015). Comparative performance analysis of UPQC and Open UPQC. In **Proceeding of the Annual IEEE India Conference (INDICON2015)** (pp. 1-6). (n.p.) IEEE.

Kusko, A., and Thompson, M. T. (2007). **Power quality in electrical systems**. New York: McGraw-Hill.

Lee, S. H., Base, I. S., Jung, C. H., and Kim J.-O. (2003). A study on system stability improvement of distribution system with high speed electric railway using STATCOM. **The IEEE PES Transmission and Distribution Conference and Exposition.** 1: 61-67.

Li, Q., Liu, W., Shu, Z., Xie, S., and Zhou, F. (2014). Co-phase power supply system for HSR. In **International Power Electronics Conference (IPEC-Hiroshima 2014 – ECCE ASIA)**. (n.p.) IEEE

Liu, L. and Dai, N. Y. (2016). Hybrid railway power conditioner based on half-bridge modular multilevel converter. In **Proceeding of the IEEE Energy Conversion Congress and Exposition (ECCE)** (pp. 1-7). (n.p.) IEEE.

Ma, F. and et al. (2013). A simplified power conditioner based on half-bridge converter for high-speed railway system. **IEEE Transactions on Industrial Electronics**. 60 (2): 728-738.

Martins, J., Martins, C., and Pires, V. F. (2015). A modelling scheme for the Le Blanc transformer. In **9th International Conference on Compatibility and Power Electronics (CPE), 2015**. (n.p.) IEEE

Mitsubishi-Hitachi-Sumitomo Consortium (MHSC). (2018). Final Traction Power Supply Study (Revision 4).

Mochinaga, Y., Takeda, M., Hisamizu, Y., Miyashita, T. and Hasuike, K. (1993). Static power conditioner using GTO converters for AC electric railway. In **Proceeding of the Power Conversion Conference - Yokohama 1993** (pp. 641-646). (n.p.) IEEE.

Mongkoldee, K. and Kulworawanichpong, T. (2018). AC railway power flow modelling integrated with RPC. In **Proceeding of the Technical Meeting on Transportation and Electric Railway** (pp. 77-80). (n.p.) IEEJapan.

Mongkoldee, K. and Kulworawanichpong, T. (2018). Current-based Newton-Raphson power flow calculation for AT-fed railway power supply systems. **International Journal of Electrical Power & Energy Systems**. 98 (June): 11-22.

Mongkoldee, K. and Kulworawanichpong, T. (In press). Optimal Sizing of AC Railway Power Conditioner in Autotransformer-Fed Railway Power Supply System. **International Journal of Electrical Power & Energy Systems**.

Mongkoldee, K., Leeton, U., and Kulworawanichpong, T. (2016). Single Train Movement Modelling and Simulation with Rail Potential Consideration. In **Proceeding of the 2016 IEEE/SICE International Symposium on System Integration Power** (pp. 7-12). (n.p.) IEEE.

Morimoto, H., Uzuka, T., Horiguchi, A., and Akita, T. (2009). New type of feeding transformer for AC railway traction system. In **International Conference on Power Electronics and Drive Systems (PEDS)**. (n.p.) IEEE

Morris, B., Roberto, F., and Enrico, T. (2009). A new proposal for power quality and custom power improvement: OPEN UPQC. **IEEE Transactions on Power Delivery**. 24 (4): 2107-2116.

Noroozian, M., Petersson, A. N., Thorvaldson, B., Nilsson, B. A., and Taylor, C. W. (2003). Benefits of SVC and STATCOM for electric utility application. **The Transmission and Distribution Conference and Exposition (IEEE PES).** 3: 1192-1199.

Ohmi, M. and Yoshii, Y. (2010). Validation of railway static power conditioner in Tohoku Shinkansen on actual operation. In **Proceeding of the International Power Electronics Conference** (pp. 2160-2164). (n.p.) IEEE.

Patnaik, N., Panda, A. K., and Mohanty, P. R. (2016). Performance and comparative rating evaluation of single phase left shunt UPQC. In **Proceeding of the IEEE international conference on Power Electronics, Drives and Energy Systems (PEDES2016)** (pp. 1-6). (n.p.) IEEE.

Ratniyomchai, T. and Kulworawanichpong, T. (2006). Steady-state power flow modeling for a dynamic voltage restorer. In **Proceeding of the 5th WSEAS International Conference on Applications of Electrical Engineering** (pp. 6-11). Stevens Points, Wisconsin: World Scientific and Engineering Academy and Society.

Roudsari, H. M., Jalilian, A., and Jamali, S. (2018). Flexible Fractional Compensating Mode for Railway Static Power Conditioner in a V/v Traction Power Supply System. **IEEE Transactions on Industrial Electronics**. 65 (10): 7963-7974.

Roudsari, H. M., Jalilian, A., and Jamalli, S. (2016). A Z-source railway static power conditioner for power quality improvement. In **Proceeding of the 7th Power Electronics and Drive Systems Technologies Conference (PEDSTC)** (pp. 261-267). (n.p.) IEEE.

Sekhar, G. C., Kale, V. S., and Krishna, G. V. (2014). Application of DVR to improve voltage profile of Indian Railway traction system. In **Proceeding of the 6th IEEE Power India International Conference (PIICON)** (pp. 1-4). (n.p.) IEEE.

Shang, J., Dai, N. Y., Wang, B., and Chen, H. (2016). Railway power conditioner based on delta-connected modular multilevel converter. In **Proceeding of the IEEE Energy Conversion Congress and Exposition (ECCE)** (pp. 1-7). (n.p.) IEEE.

Thanatchai Kulworawanichpong. (2003). **Optimising AC Electric Railway Power Flows with Power Electronic Control.** Ph.D. Dissertation, University of Birmingham, United Kingdom.

Tongzhen, W. and Dongqiang, J. (2014). A new topology of OPEN UPQC. In **Proceeding of the 9th IEEE Conference on Industrial Electronics and Applications (ICIEA)** (pp. 1313-1318). (n.p.) IEEE.

Vedam, R. S., and Sarma, M. S. (2009). **Power quality VAR compensation in power systems**. Boca Raton, FL: CRC Press.

Wang, H., Liu, Y., Yan, K., Fu, Y., and Zhang, C. (2015). Analysis of static Var compensators installed in different positions in electric railways. **IET Electrical Systems in Transportation**. 5 (3): 129-134.

Wei, Y., Jiang, Q., and Zhang, X. (2008). A novel control strategy for optimization of power capacity based on railway power static conditioner. In **Proceeding of the 2018 Twenty-Third Annual IEEE Applied Power Electronics Conference and Exposition** (pp. 1669-1674). (n.p.) IEEE.

Xiaqing, L. and Li, Z. (2007). Research on balance compensation of STATCOM. In **Proceeding of the second IEEE conference on Industrial Electronics and Applications (ICIEA2007)** (pp. 563-568). (n.p.) IEEE.

Yasu, O., Yoshifumi, M., and Hiroki, N. (2001). Railway electric power feeding systems. In Railway technical research institute and East Japan railway culture foundation (eds.). **Japanese railway technology today** (pp. 48-58). (n.p.) East Japan railway culture foundation.

Zhang, N. and et al. (2015). A review of different UPFC steady models in power flow algorithm. In **Proceeding of the 5th international conference on Electric Utility Deregulation and Restructuring and Power Technologies** (pp. 2420-2424). (n.p.) IEEE.

Zhang, Q. Liu, G., and Pang, Y. (2012). Control method of STATCOM for electric railway. In **Proceeding of the World Automation Congress (WAC)** (pp. 1-4). (n.p.) IEEE.

Zhang, Y., Luo, A., Wu, C., and Ma, F. (2010). The electrical model and parameter design of hybrid railway unified power quality controller (RUPQC). In **Proceeding of China International Conference on Electricity Distribution (CICED2010)** (pp. 1-8). (n.p.) IEEE.

Appendix A

Raw data results of autotransformer tap changing investigation

A.1 Introduction

The graphical and tabulated results of the AT tap changing investigation in Chapter 5, consisting of the results of every cases in Part 1 and Part 2 for both Scott and V/V transformer systems, are collected and displayed in this Appendix.

A.2 Part 1

A.2.1 Scott transformer system

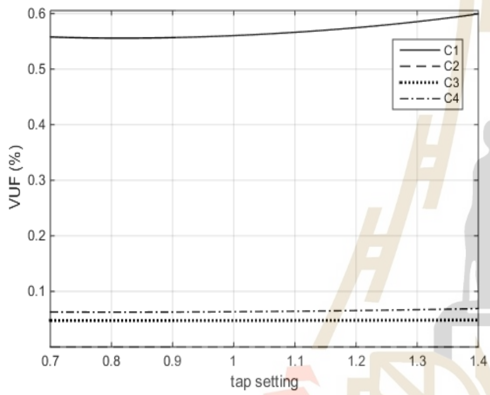

(a)

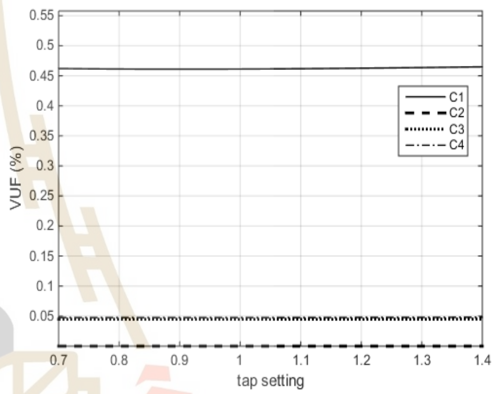

(b)

Fig. A.1 VUF in the Scott transformer system

(a) Position 1, (b) Position 2

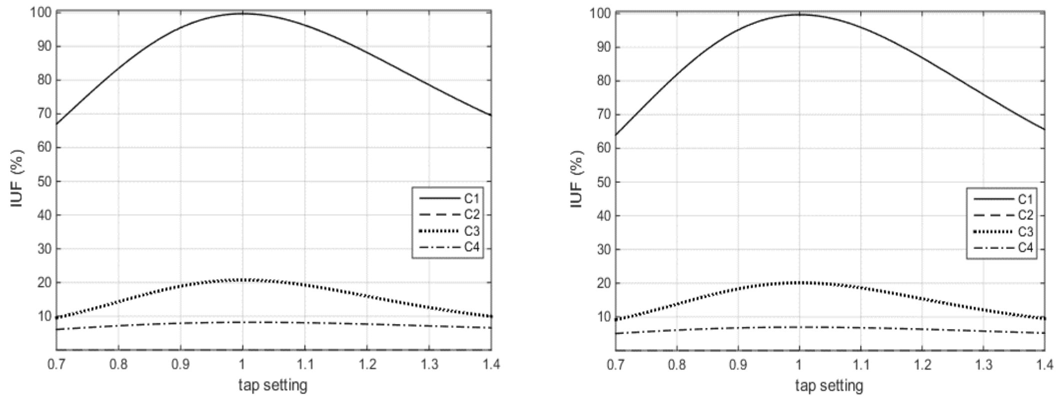

(a) (b)

Fig. A.2 IUF in the Scott transformer system

(a) Position 1, (b) Position 2

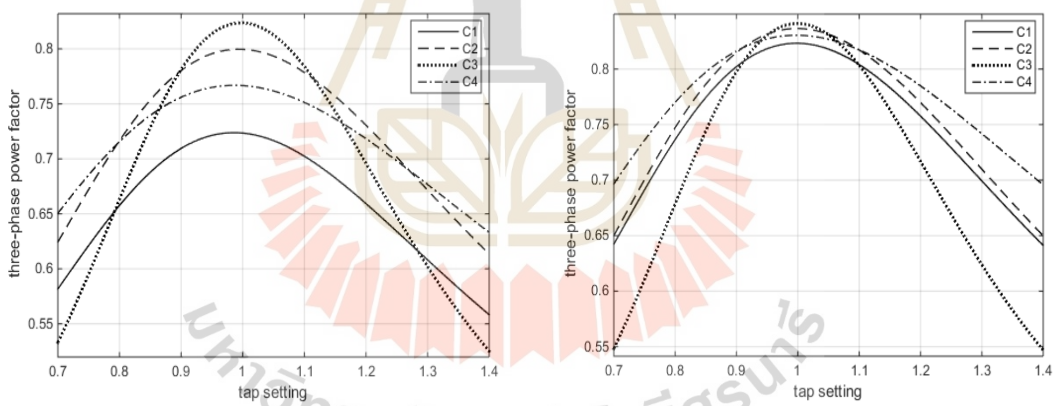

(a) (b)

Fig. A.3 Three-phase power factors in the Scott transformer system

(a) Position 1, (b) Position 2

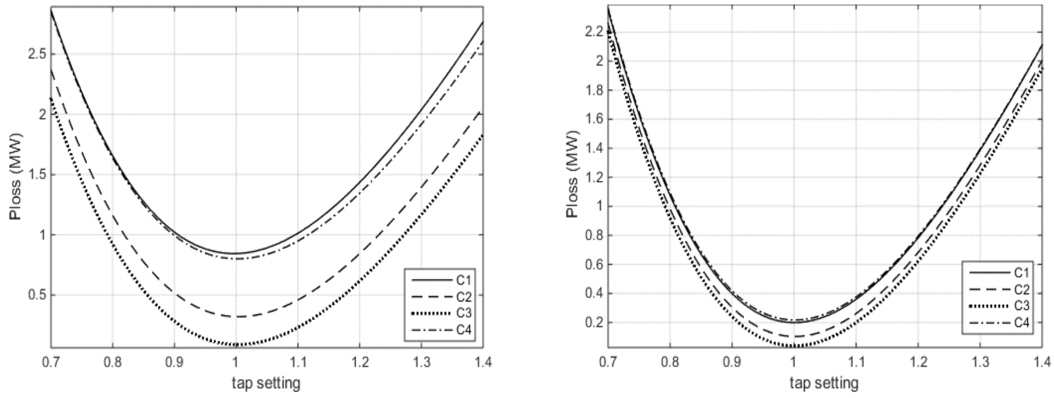

(a) (b)

Fig. A.4 Power losses in the Scott transformer system

(a) Position 1, (b) Position 2

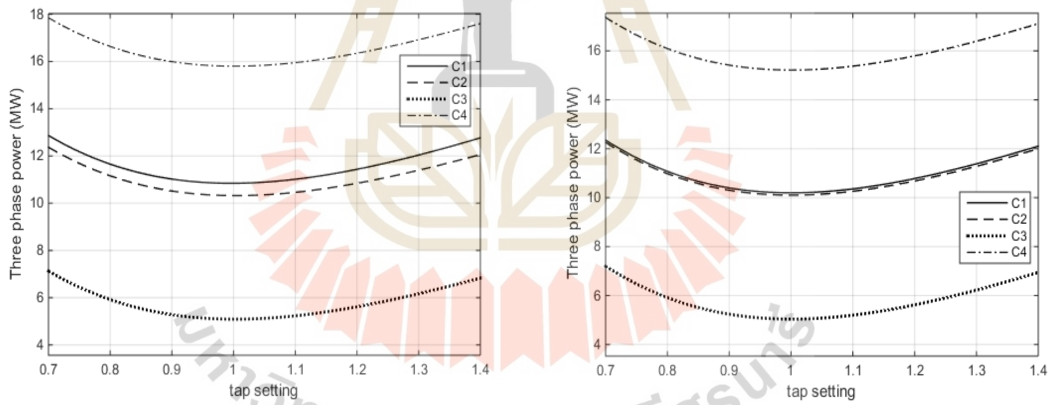

(a) (b)

Fig. A.5 Three-phase active power in the Scott transformer system

(a) Position 1, (b) Position 2

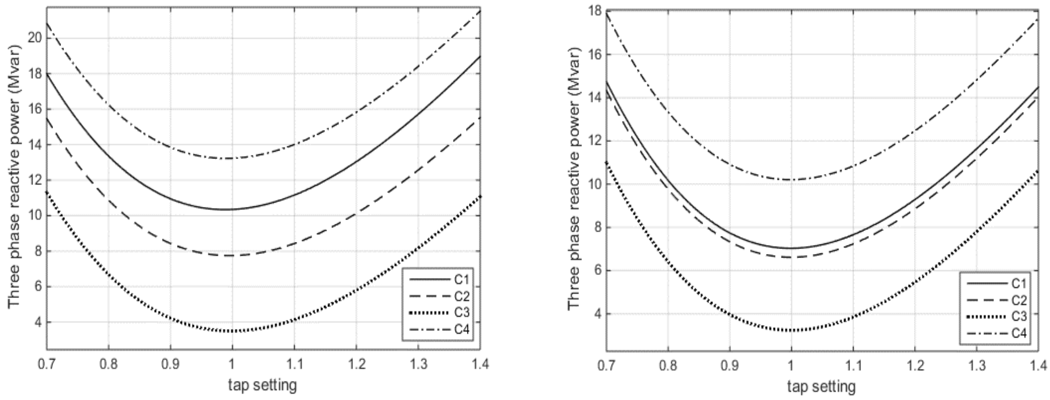

(a) (b)

Fig. A.6 Three-phase reactive power in the Scott transformer system

(a) Position 1, (b) Position 2

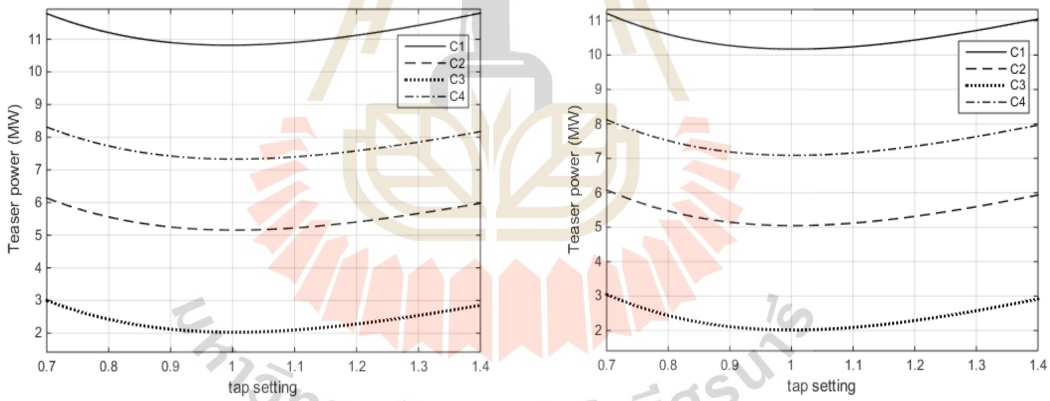

(a) (b)

Fig. A.7 Teaser phase active power in the Scott transformer system

(a) Position 1, (b) Position 2

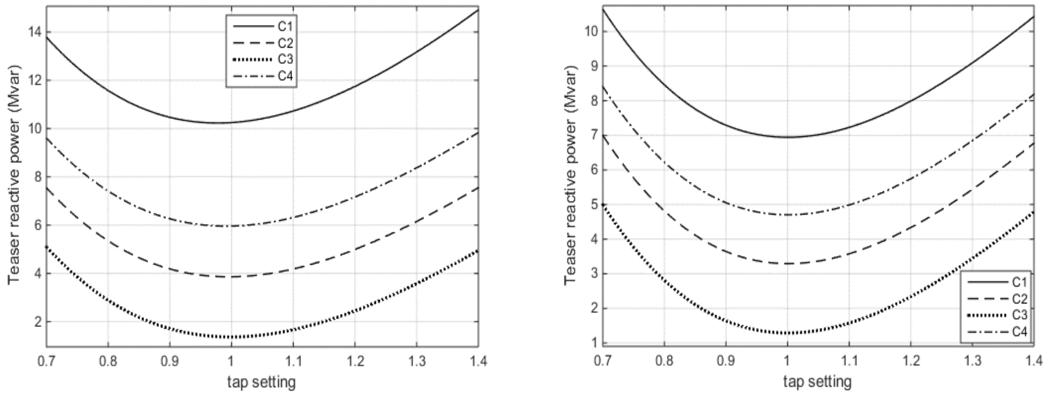

(a) (b)

Fig. A.8 Teaser phase reactive power in the Scott transformer system

(a) Position 1, (b) Position 2

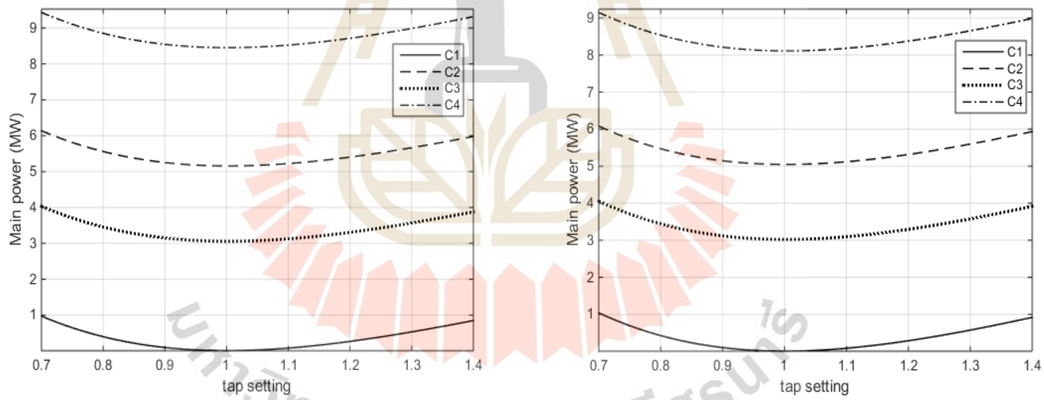

(a) (b)

Fig. A.9 Main phase active power in the Scott transformer system

(a) Position 1, (b) Position 2

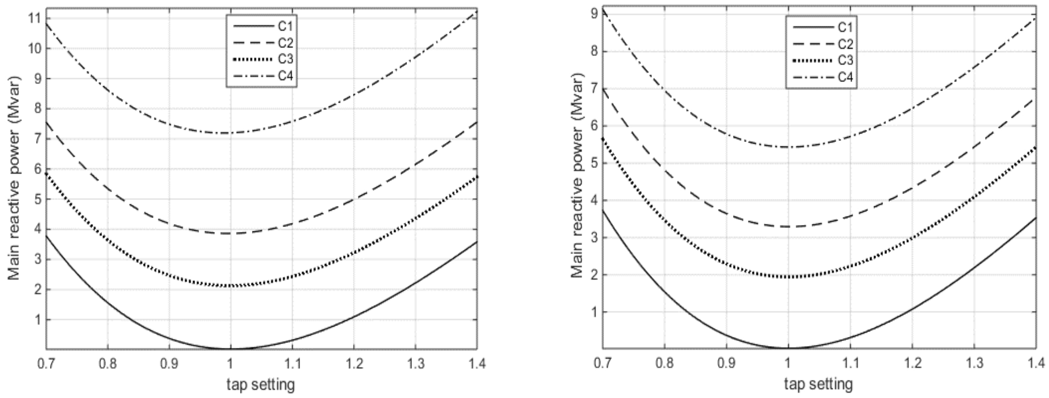

(a) (b)

Fig. A.10 Main phase reactive power in the Scott transformer system

(a) Position 1, (b) Position 2

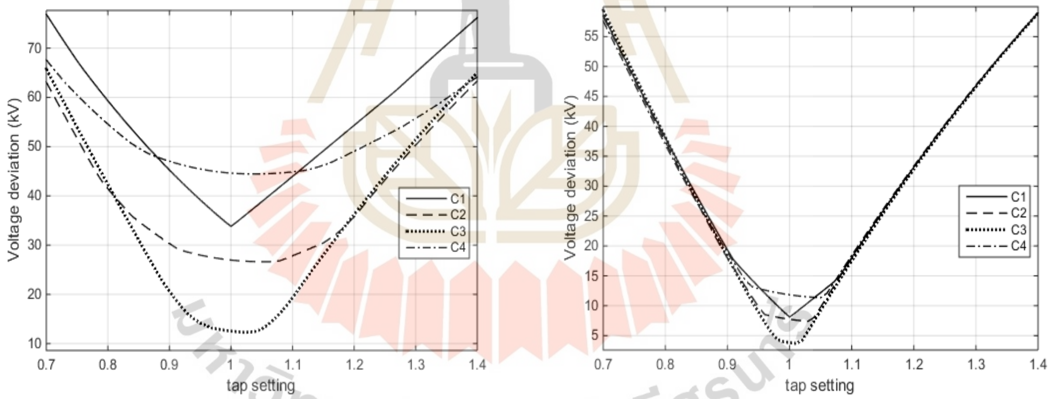

(a) (b)

Fig. A.11 Voltage deviation in the Scott transformer system

(a) Position 1, (b) Position 2

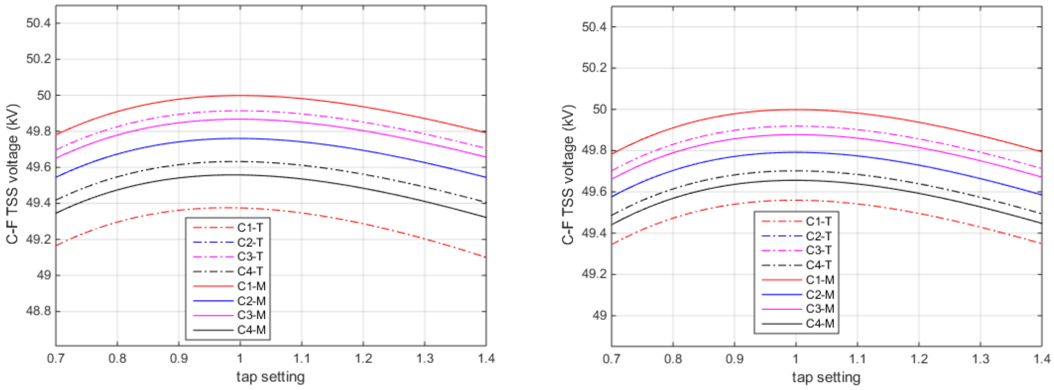

(a) (b)

Fig. A.12 CF traction substation voltages in the Scott transformer system

(a) Position 1, (b) Position 2

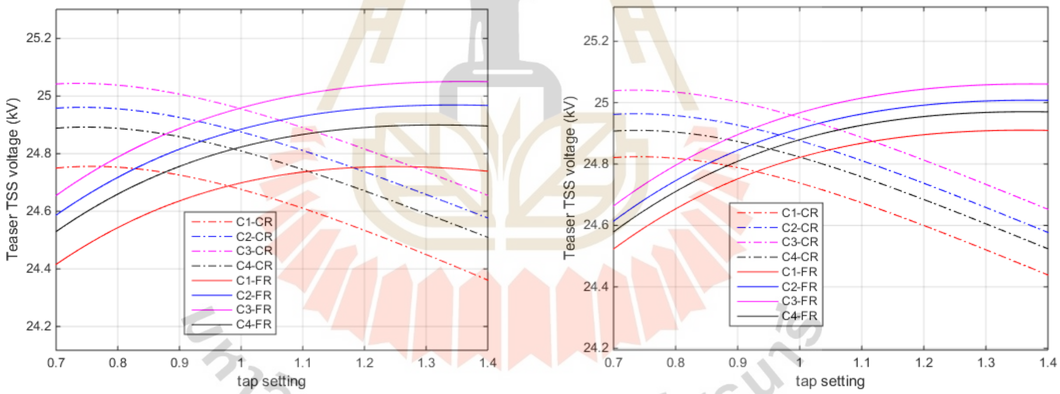

(a) (b)

Fig. A.13 CR and FR traction substation voltages in the Scott transformer system

(Teaser phase) (a) Position 1, (b) Position 2

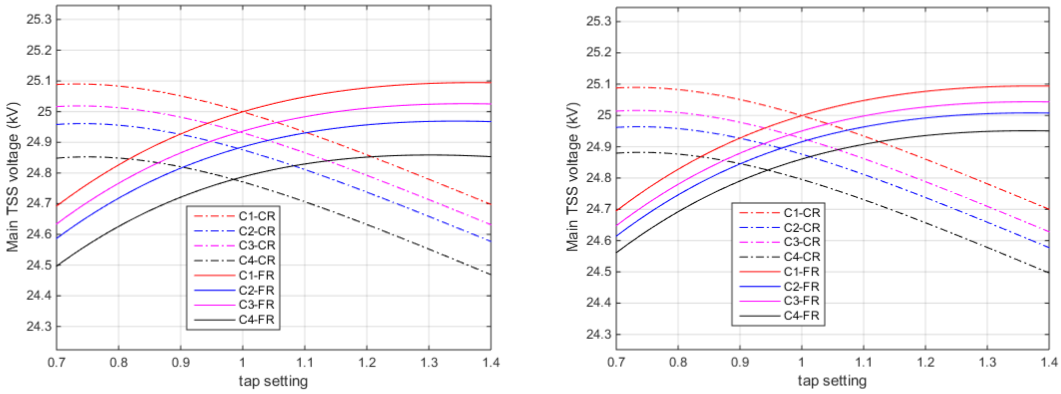

(a) (b)

Fig. A.14 CR and FR traction substation voltages in the Scott transformer system (Main phase) (a) Position 1, (b) Position 2

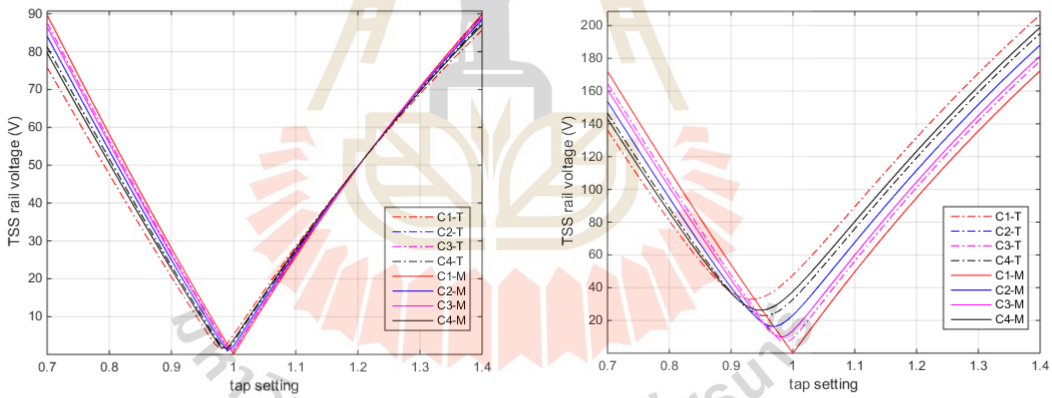

(a) (b)

Fig. A.15 Rail voltages at the traction substation in the Scott transformer system (a) Position 1, (b) Position 2

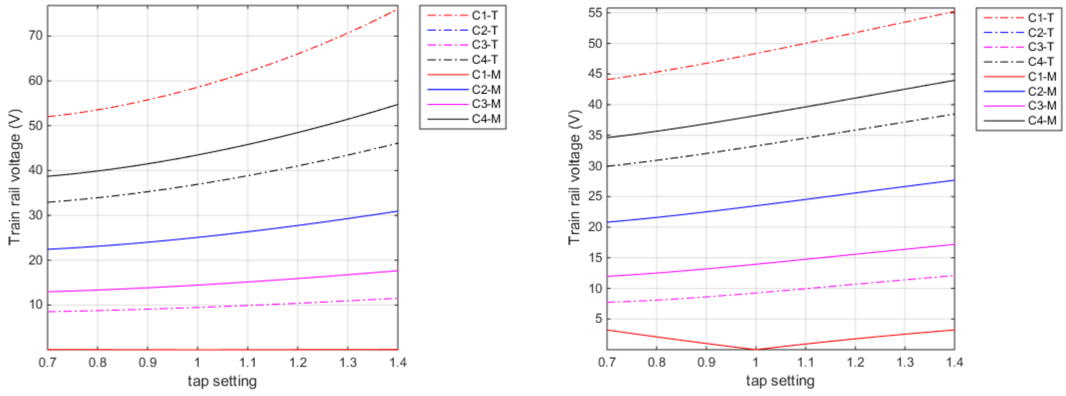

(a) (b)

Fig. A.16 Rail voltages at the trains in the Scott transformer system

(a) Position 1, (b) Position 2

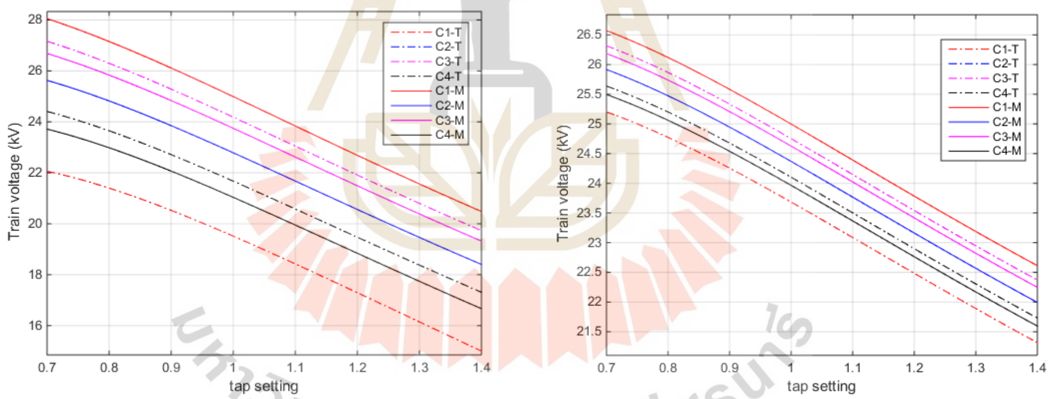

(a) (b)

Fig. A.17 Train voltages in the Scott transformer system

(a) Position 1, (b) Position 2

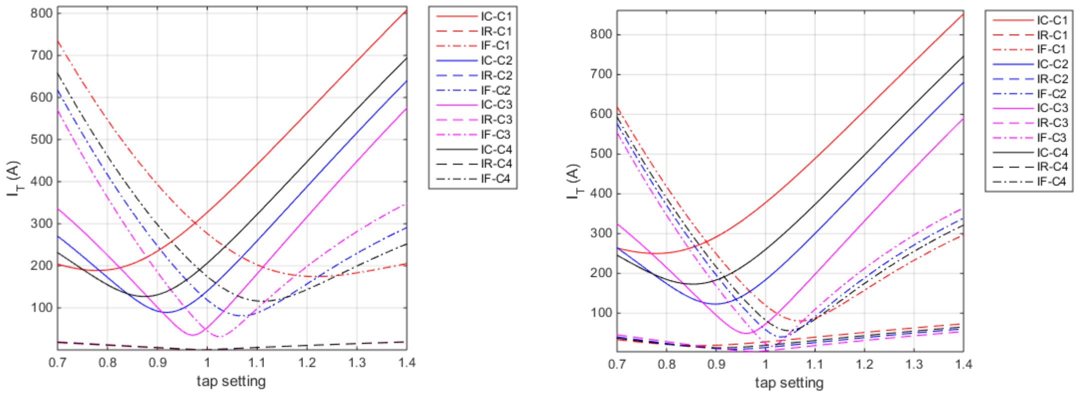

(a) (b)

Fig. A.18 Teaser phase currents at the traction substation in the Scott transformer system (a) Position 1, (b) Position 2

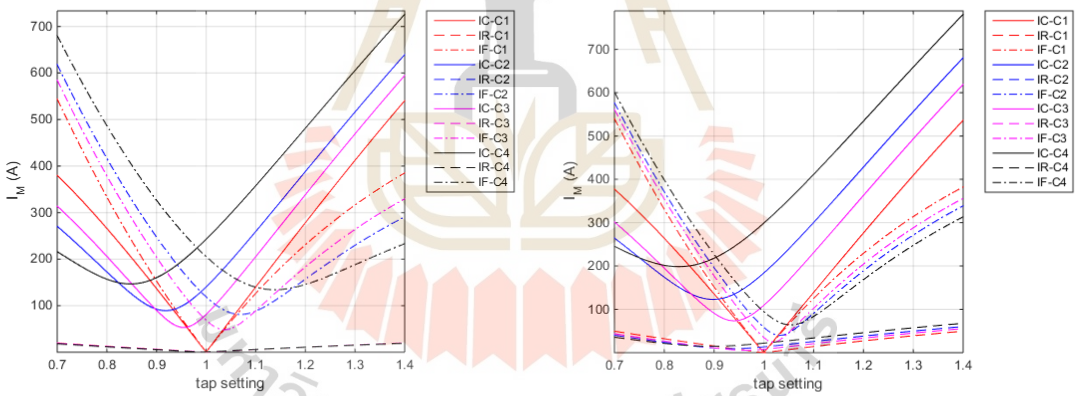

(a) (b)

Fig. A.19 Main phase currents at the traction substation in the Scott transformer system (a) Position 1, (b) Position 2

A.2.2 V/V transformer system

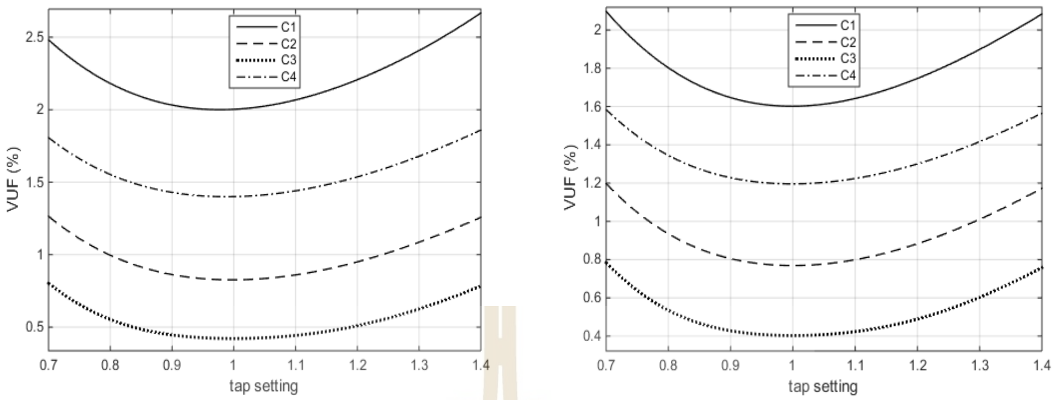

(a) (b)

Fig. A.20 VUF in the V/V transformer system

(a) Position 1, (b) Position 2

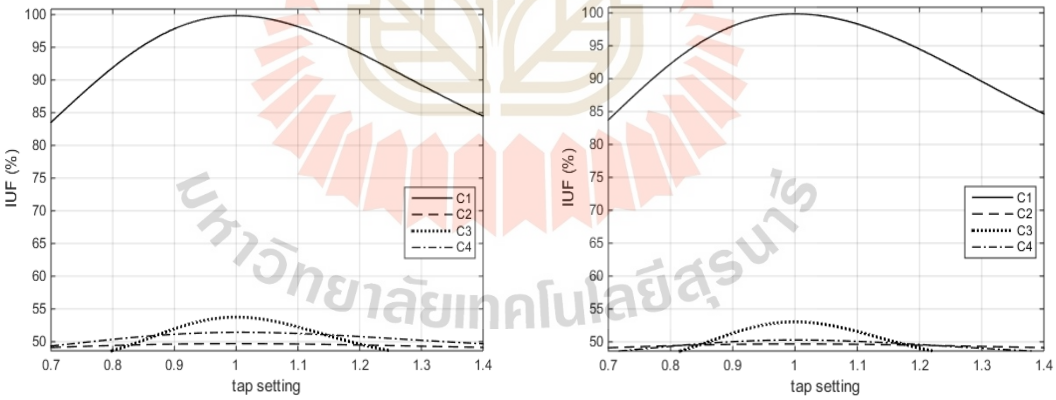

(a) (b)

Fig. A.21 IUF in the V/V transformer system

(a) Position 1, (b) Position 2

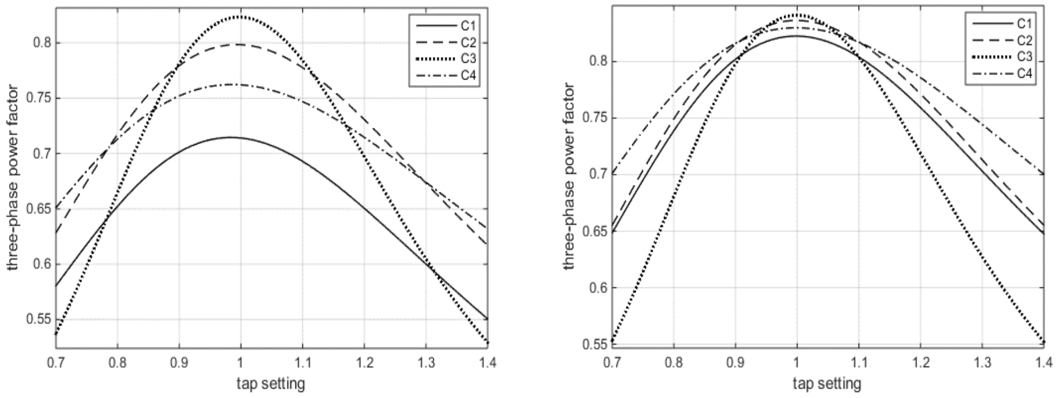

(a) (b)

Fig. A.22 Three-phase power factors in the V/V transformer system

(a) Position 1, (b) Position 2

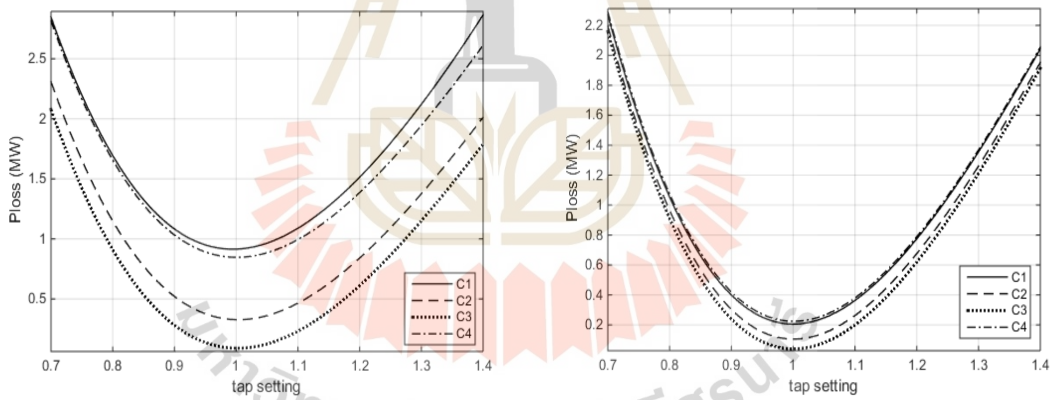

(a) (b)

Fig. A.23 Power losses in the V/V transformer system

(a) Position 1, (b) Position 2

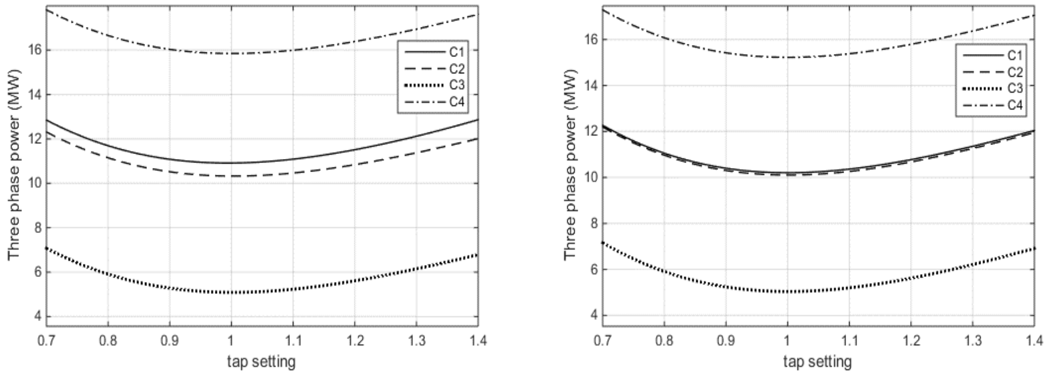

(a) (b)

Fig. A.24 Three-phase active power in the V/V transformer system

(a) Position 1, (b) Position 2

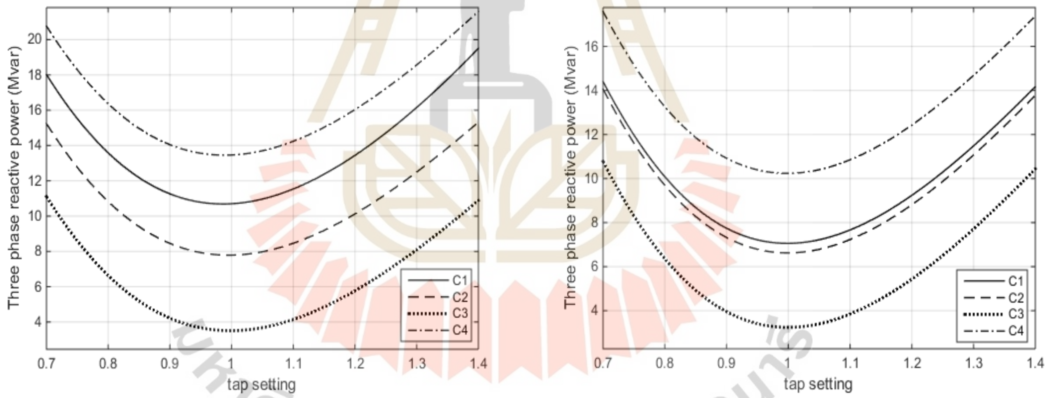

(a) (b)

Fig. A.25 Three-phase reactive power in the V/V transformer system

(a) Position 1, (b) Position 2

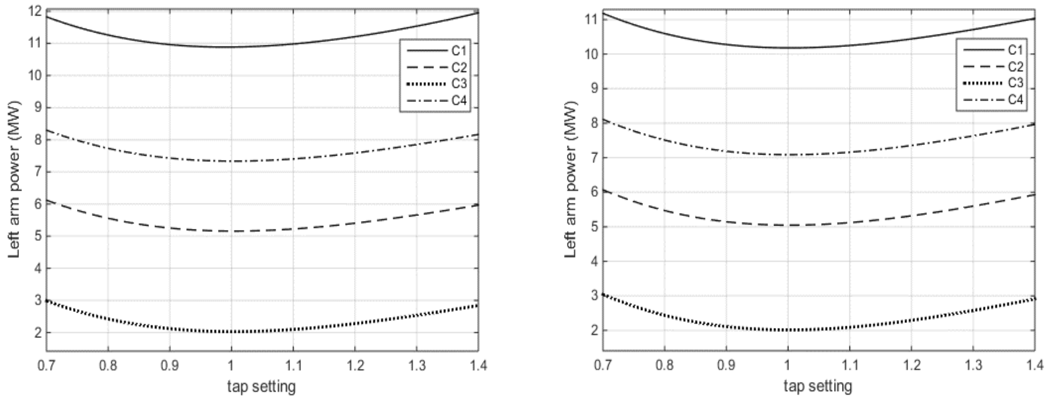

(a) (b)

Fig. A.26 Left arm active power in the V/V transformer system

(a) Position 1, (b) Position 2

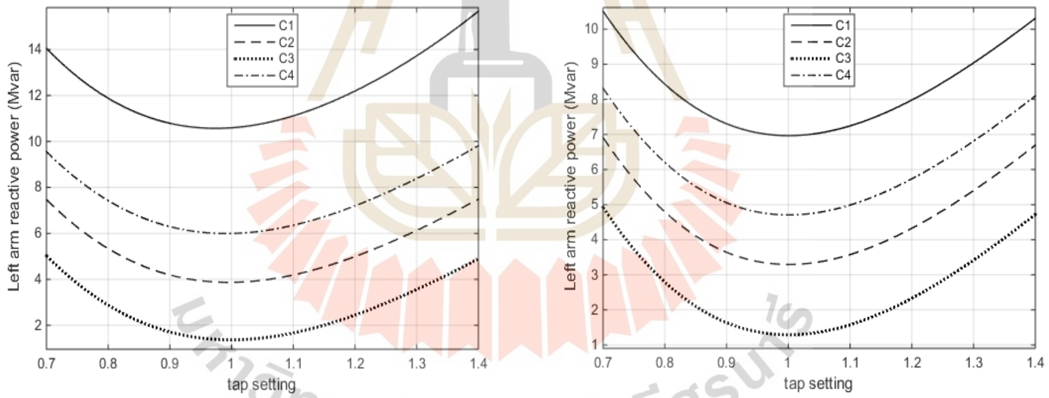

(a) (b)

Fig. A.27 Left arm reactive power in the V/V transformer system

(a) Position 1, (b) Position 2

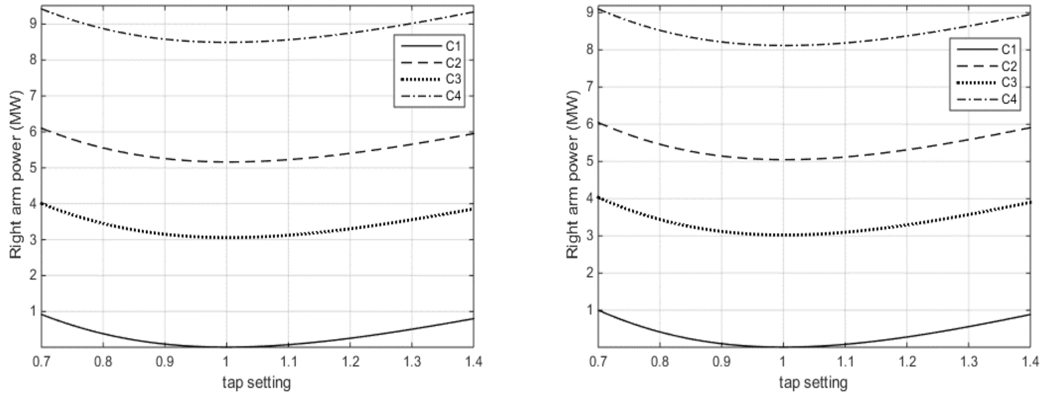

(a) (b)

Fig. A.28 Right arm active power in the V/V transformer system

(a) Position 1, (b) Position 2

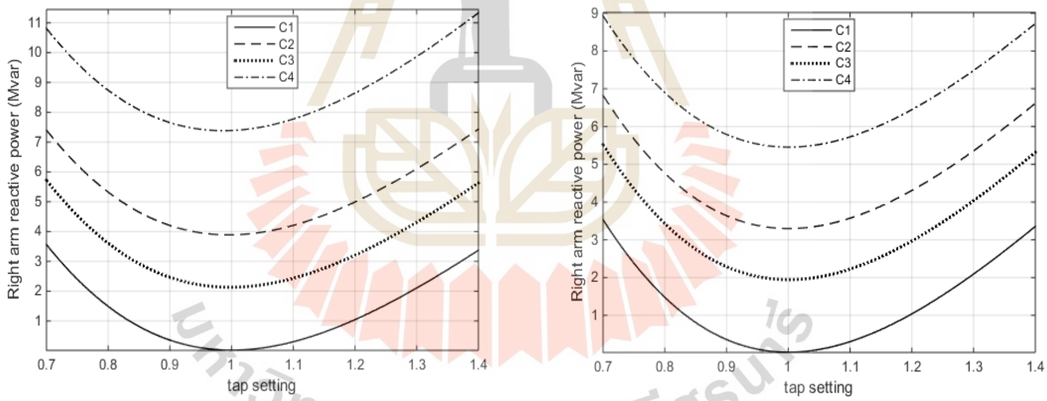

(a) (b)

Fig. A.29 Right arm reactive power in the V/V transformer system

(a) Position 1, (b) Position 2

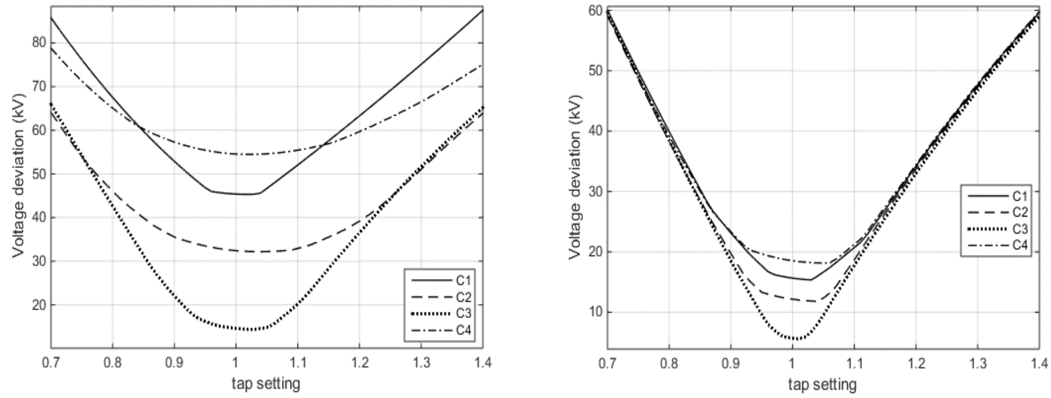

(a) (b)

Fig. A.30 Voltage deviation in the V/V transformer system

(a) Position 1, (b) Position 2

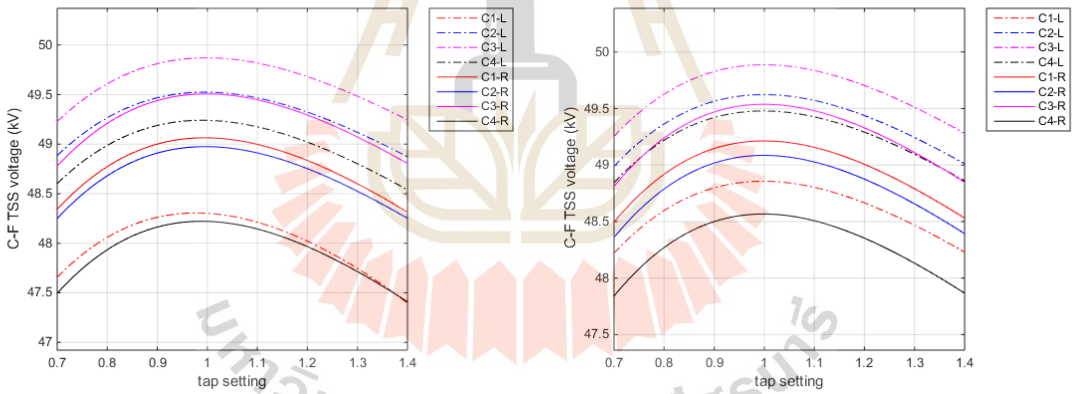

(a) (b)

Fig. A.31 CF traction substation voltages in the V/V transformer system

(a) Position 1, (b) Position 2

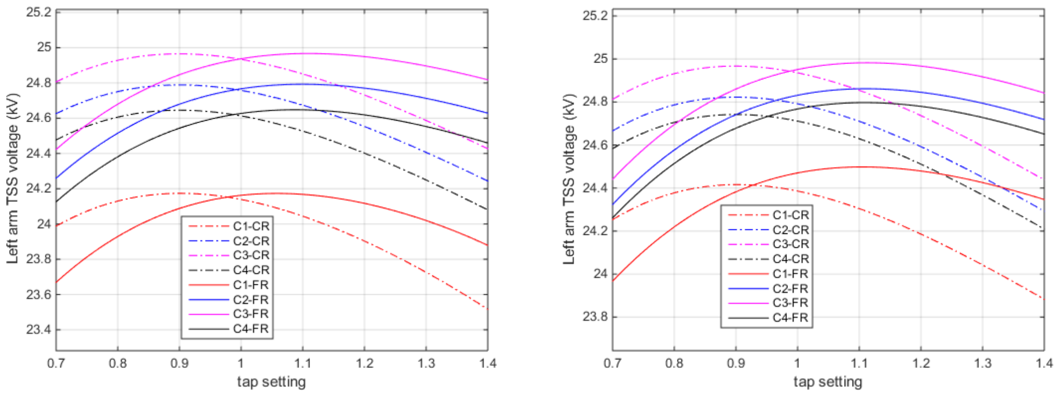

(a) (b)

Fig. A.32 CR and FR traction substation voltages in the V/V transformer system (Left arm) (a) Position 1, (b) Position 2

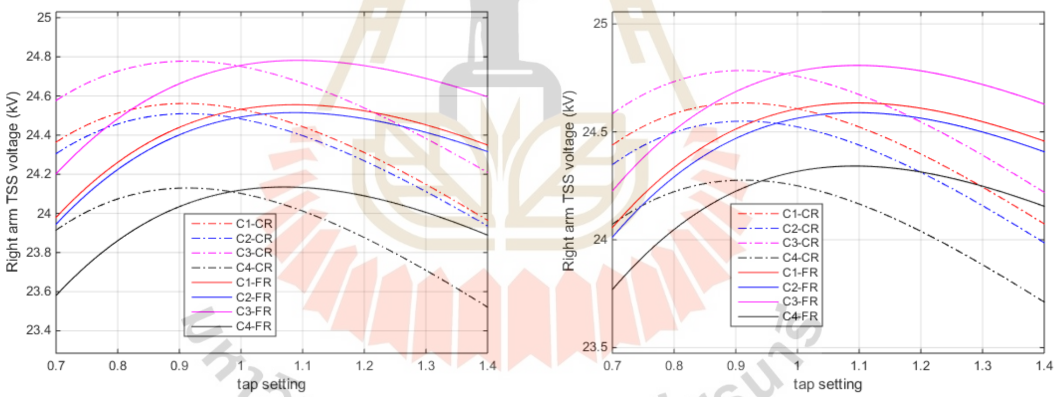

(a) (b)

Fig. A.33 CR and FR traction substation voltages in the V/V transformer system (Right arm) (a) Position 1, (b) Position 2

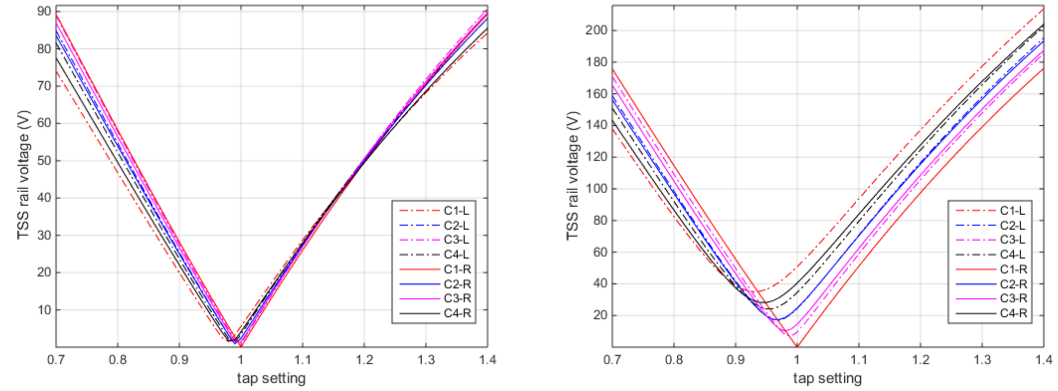

(a) (b)

Fig. A.34 Rail voltages at the traction substation in the V/V transformer system

(a) Position 1, (b) Position 2

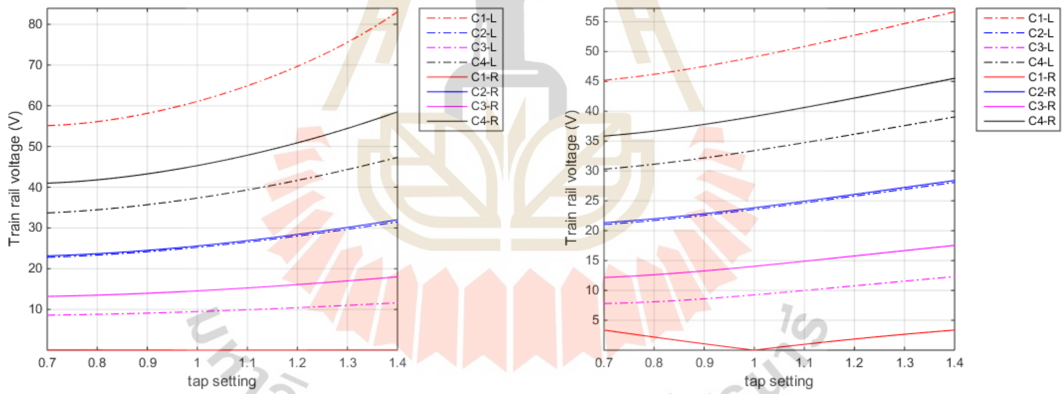

(a) (b)

Fig. A.35 Rail voltages at the trains in the V/V transformer system

(a) Position 1, (b) Position 2

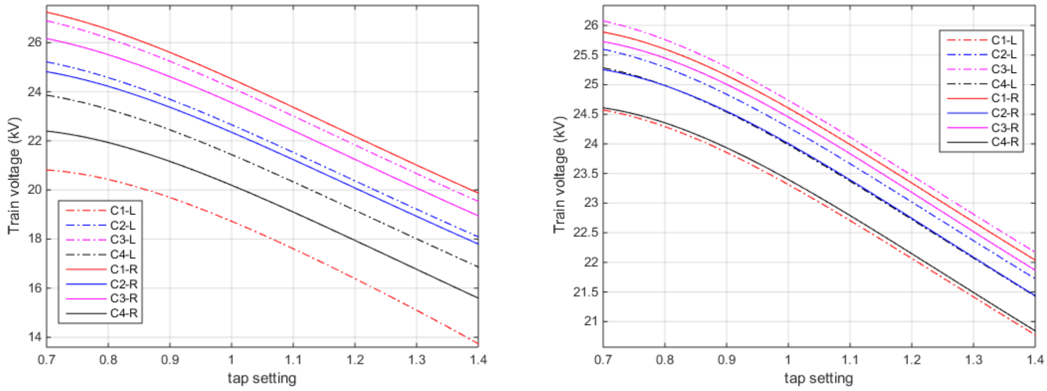

(a) (b)

Fig. A.36 Train voltages in the V/V transformer system

(a) Position 1, (b) Position 2

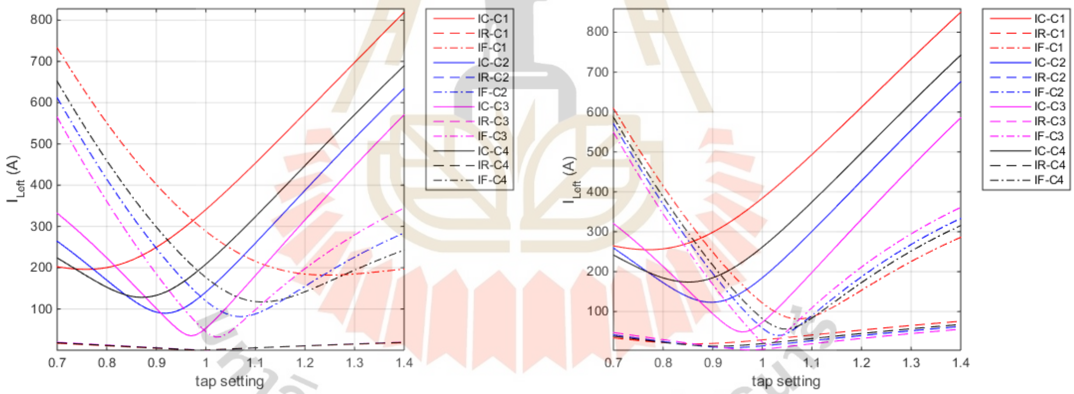

(a) (b)

Fig. A.37 Left arm currents at the traction substation in the V/V transformer system

(a) Position 1, (b) Position 2

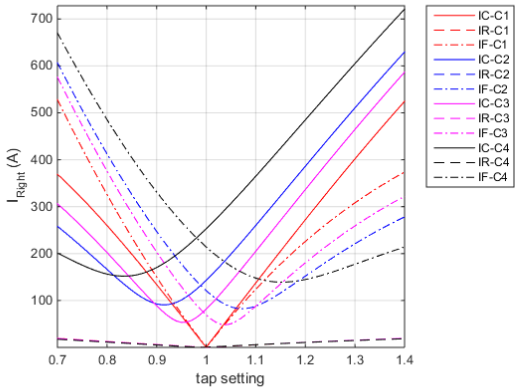

(a)

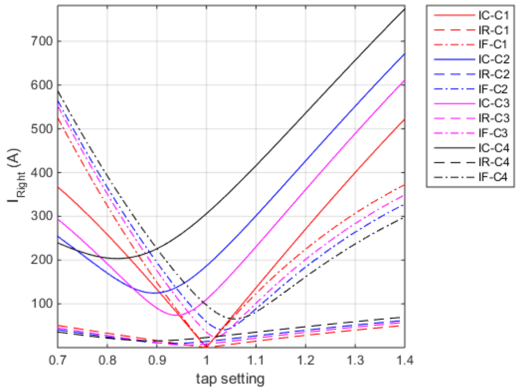

(b)

Fig. A.38 Right arm currents at the traction substation in the V/V transformer system (a) Position 1, (b) Position 2

A.3 Part 2

A.3.1 Scott transformer system

Table A.1 Loss minimisation results (Scott 1)

Train position	Case	No.	VUF (%)	IUF (%)	3φ PF	3φ Power (MW)	3φ Reactive (Mvar)
P1	Base	-	0.560344649	99.69960935	0.72342411	10.84417502	10.34920002
	1	1	0.560257182	99.69957439	0.723485885	10.84344387	10.3466484
		2	0.560246854	99.69957341	0.723498867	10.84344344	10.34625842
		3	0.560249171	99.69956093	0.723495885	10.84344387	10.34634831
	Base	-	1.98×10^{-06}	4.12×10^{-04}	0.799613588	10.32002954	7.750407566
	2	1	1.64206×10^{-06}	0.000341169	0.798941459	10.31854599	7.76735805
		2	1.13173×10^{-06}	0.000235137	0.798941462	10.31854602	7.767357972
		3	6.30314×10^{-06}	0.001309576	0.79892902	10.31854649	7.767692783
	Base	-	0.047625414	20.75552506	0.823718094	5.088736672	3.502789941
	3	1	0.047659421	20.76228846	0.823316969	5.088213168	3.507734699
		2	0.047673617	20.76750235	0.823279248	5.08821577	3.508235356
		3	0.047651461	20.75975692	0.823353924	5.088214035	3.507246554
	Base	-	0.063391031	8.217173648	0.766616393	15.80069116	13.23440084
	4	1	0.063389907	8.210352219	0.765928281	15.79901959	13.26181713
		2	0.063411379	8.213179904	0.765932469	15.79901821	13.26164055
		3	0.063503153	8.228213666	0.766241376	15.79949208	13.24909987
P2	Base	1	0.461207131	99.66836302	0.823256407	10.19908103	7.032692633
	1	1	0.461235722	99.66835464	0.823188659	10.19885611	7.034333443
		2	0.461235481	99.66835524	0.82318908	10.19885607	7.034322253
		3	0.461235491	99.66835054	0.823189033	10.19885619	7.034323576
	Base	-	1.50×10^{-06}	0.000334142	0.836545802	10.10298453	6.616965739

Table A.1 Loss minimisation results (Scott 1) (Continued)

Train position	Case	No.	VUF (%)	IUF (%)	3φ PF	3φ Power (MW)	3φ Reactive (Mvar)
P2	2	1	1.71685×10^{-06}	0.000381787	0.836511004	10.10286989	6.61780752
		2	1.41558×10^{-06}	0.000314791	0.836510748	10.10286987	6.617814262
		3	1.547×10^{-06}	0.000344015	0.83651083	10.10286994	6.617812144
	Base	-	0.044741511	20.11054599	0.841079791	5.038938584	3.240617219
	3	1	0.044742831	20.1108188	0.841061414	5.038907932	3.240839515
		2	0.044743002	20.11092888	0.841062848	5.038908286	3.24082085
		3	0.044742873	20.11084353	0.841061665	5.038907927	3.240836203
	Base	-	0.047485192	6.939583576	0.830430838	15.21682535	10.20870576
	4	1	0.047489017	6.939806507	0.830377977	15.21657194	10.21062934
		2	0.047488897	6.939790451	0.830378187	15.2165725	10.21062141
		3	0.047489281	6.93985689	0.830379336	15.21657135	10.21057512

Table A.2 Loss minimisation results (Scott 2)

Train position	Case	No.	P_T (MW)	Q_T (Mvar)	P_M (MW)	Q_M (Mvar)	P_{loss} (MW)	VD (kV)
P1	Base	-	10.81711356	10.24836163	0.008620878	0.023731669	0.844175021	33.81922053
	1	1	10.81646623	10.24614471	0.008620926	0.023731797	0.843443866	33.82834252
		2	10.81646824	10.2457645	0.00862088	0.023731658	0.843443444	33.82850923
		3	10.81646706	10.24584756	0.008621081	0.023732862	0.84344387	33.82683361
	Base	-	5.156625119	3.861042137	5.156623472	3.861033762	0.320029539	26.96343488
	2	1	5.155847348	3.869368563	5.155845682	3.869369388	0.318545993	26.83433149
		2	5.155847288	3.86933177	5.155845481	3.869404957	0.31854602	26.83421514
		3	5.155845621	3.869589966	5.15584508	3.869471413	0.318546495	26.83221821

Table A.2 Loss minimisation results (Scott 2) (Continued)

Train position	Case	No.	P_T (MW)	Q_T (Mvar)	P_M (MW)	Q_M (Mvar)	P_{loss} (MW)	VD (kV)
P1	Base	-	2.029545474	1.368197399	3.05757638	2.127847701	0.088736672	12.54426616
	3	1	2.029364818	1.369748223	3.057206295	2.131133019	0.088213168	12.44103089
		2	2.029364859	1.369693004	3.057207783	2.131684587	0.08821577	12.43766894
		3	2.02936506	1.369694233	3.0572127	2.13072189	0.088214035	12.44954603
	Base	-	7.329556173	5.961858671	8.453650015	7.199496845	0.800691164	44.61540036
	4	1	7.328623915	5.975480273	8.452839674	7.213003397	0.799019587	44.5437585
		2	7.328624741	5.975019563	8.452837651	7.213288257	0.799018213	44.54424387
		3	7.328936332	5.967119952	8.453002258	7.208659022	0.79949208	44.56252001
P2	Base	1	10.17411935	6.943044604	0.008620878	0.023731669	0.199081029	8.109603547
	1	1	10.17387791	6.944625897	0.008620889	0.023731754	0.198856114	8.133930346
		2	10.17387527	6.944605425	0.00862088	0.023731701	0.198856073	8.133356338
		3	10.17387257	6.944596589	0.008620963	0.023732096	0.198856192	8.132642503
	Base	-	5.047625511	3.29289367	5.04762524	3.292892379	0.102984531	7.738186834
	2	1	5.047546829	3.293241103	5.047546218	3.293232759	0.102869886	7.751410024
		2	5.047547212	3.29324178	5.047546604	3.293241629	0.102869872	7.75182745
		3	5.047546466	3.293239785	5.047545471	3.293234542	0.102869939	7.750945965
	Base	-	2.014633314	1.289637472	3.022333321	1.943030329	0.038938584	3.837631675
	3	1	2.014618667	1.289689155	3.022302982	1.943149709	0.038907932	3.842353933
		2	2.01461924	1.289677293	3.022305704	1.943153425	0.038908286	3.842926231
		3	2.014618805	1.289686997	3.022302632	1.943147815	0.038907927	3.842119403
	Base	-	7.086859947	4.703471194	8.11201621	5.432880625	0.21682535	11.83032113
	4	1	7.086725825	4.704239616	8.111851786	5.433874202	0.216571937	11.86189227
		2	7.086720693	4.704220509	8.111833071	5.433798067	0.216572501	11.85563389
		3	7.0867244	4.70420245	8.111845961	5.433833343	0.216571347	11.85948986

Table A.3 Loss minimisation results (Scott 3)

Train position	Case	No.	$V_{CF,T}$ (kV)	$V_{CR,T}$ (kV)	$V_{FR,T}$ (kV)	$V_{CF,M}$ (kV)	$V_{CR,M}$ (kV)	$V_{FR,M}$ (kV)
P1	Base	-	49.37469649	24.67609686	24.69859988	49.9986742	24.99931842	24.99935578
	1	1	49.37484059	24.67986625	24.69497464	49.99867419	24.99930803	24.99936616
		2	49.37486192	24.67997958	24.69488263	49.9986742	24.99932662	24.99934758
		3	49.37485707	24.67990289	24.69495448	49.99867413	24.99928657	24.99938757
	Base	-	49.76026619	24.87546363	24.88480266	49.76050545	24.87558329	24.88492226
	2	1	49.7598121	24.8728538	24.88695839	49.76005131	24.8729727	24.88707869
		2	49.75981408	24.87284839	24.88696577	49.76004934	24.87296019	24.88708923
		3	49.75979965	24.87272408	24.88707566	49.76004564	24.87293064	24.88711508
	Base	-	49.9142519	24.95539	24.95886192	49.86715672	24.93091826	24.9362385
	3	1	49.91416718	24.95369004	24.96047716	49.86697793	24.92884087	24.93813709
		2	49.91417061	24.95396462	24.960206	49.86694748	24.92855613	24.93839139
		3	49.91417057	24.95398299	24.9601876	49.86700086	24.92919326	24.93780764
	Base	-	49.6323107	24.80919851	24.82311237	49.55795552	24.77073515	24.78722058
	4	1	49.63156652	24.80702228	24.82454439	49.55721983	24.76972274	24.78749728
		2	49.631592	24.80711687	24.82447528	49.55720393	24.76963869	24.78756543
		3	49.63202268	24.80775111	24.82427174	49.55745185	24.76891888	24.78853316
P2	Base	1	49.55962584	24.73823793	24.82144202	49.9986742	24.99931847	24.99935573
	1	1	49.55953792	24.73812774	24.82146455	49.9986742	24.99931109	24.9993631
		2	49.55953853	24.73810295	24.82148995	49.9986742	24.9993109	24.9993633
		3	49.55953848	24.73807722	24.82151563	49.99867418	24.99931527	24.99935891
	Base	-	49.79158296	24.87597739	24.91561894	49.7917909	24.87608145	24.91572282
	2	1	49.79156038	24.87559413	24.91597969	49.79176866	24.87569099	24.91609111
		2	49.79156042	24.8756015	24.91597235	49.79176825	24.87569913	24.91608257
		3	49.79156038	24.87558688	24.91598694	49.79176841	24.87567603	24.91610582

Table A.3 Loss minimisation results (Scott 3) (Continued)

Train position	Case	No.	$V_{CF,T}$ (kV)	$V_{CR,T}$ (kV)	$V_{FR,T}$ (kV)	$V_{CF,M}$ (kV)	$V_{CR,M}$ (kV)	$V_{FR,M}$ (kV)
P2	Base	-	49.91855262	24.95155323	24.96700151	49.87728659	24.9269636	24.95032777
	3	1	49.9185489	24.95131476	24.96723628	49.87727851	24.92668357	24.95059976
		2	49.91854962	24.95133453	24.96721723	49.87727879	24.9267647	24.9505189
		3	49.91854904	24.95132138	24.9672298	49.87727854	24.92667208	24.95061128
	Base	-	49.70203935	24.82275812	24.87930756	49.65603478	24.79540734	24.8606619
	4	1	49.7019937	24.82246868	24.87955148	49.65597767	24.79519761	24.86081469
		2	49.70199374	24.82239884	24.87962136	49.65597805	24.79496729	24.86104539
		3	49.70199549	24.82245218	24.87956977	49.65597881	24.79513121	24.86088224

Table A.4 Loss minimisation results (Scott 4)

Train position	Case	No.	TSS $V_{rail,T}$ (V)	TSS $V_{rail,M}$ (V)	Train $V_{rail,T}$ (V)	Train $V_{rail,M}$ (V)	$V_{T,train}$ (kV)	$V_{M,train}$ (kV)
P1	Base	-	5.228255243	0.00869568	58.60518401	0.000236219	19.51354776	24.99176273
	1	1	3.634767573	0.013270738	58.49174989	0.000611915	19.54482353	24.9921977
		2	3.591873606	0.00518074	58.48355485	0.000328046	19.54770184	24.99184655
		3	3.623174622	0.023067266	58.48643376	0.002001903	19.54670406	24.98955052
	Base	-	2.242731124	2.242718134	25.09448983	25.09434366	22.78569413	22.78582685
	2	1	3.266699741	3.267000182	25.21758932	25.21753209	22.63512351	22.63514398
		2	3.269583153	3.272068684	25.21734151	25.2179912	22.63549633	22.63464266
		3	3.321209825	3.284312242	25.22111054	25.21868663	22.63159679	22.63372112
	Base	-	0.849541772	1.294122416	9.457090341	14.44713989	24.18457081	23.74695386
	3	1	1.566934003	2.150827661	9.468630183	14.4840413	24.10399787	23.63769817
		2	1.445551439	2.269964215	9.466130089	14.48878106	24.10770172	23.62528805
		3	1.437396555	2.000248254	9.4658282	14.47890198	24.10787031	23.64867148

Table A.4 Loss minimisation results (Scott 4) (Continued)

Train position	Case	No.	TSS $V_{rail,T}$ (V)	TSS $V_{rail,M}$ (V)	Train $V_{rail,T}$ (V)	Train $V_{rail,M}$ (V)	$V_{T,train}$ (kV)	$V_{M,train}$ (kV)
P1	Base	-	3.297785464	3.881565236	36.93670698	43.48926705	21.67261977	21.03680292
	4	1	4.068026761	4.148019015	37.15031144	43.69269564	21.51988833	20.91748481
		2	4.032525632	4.181192832	37.14282539	43.69717661	21.52444009	20.91499293
		3	3.856191907	4.555029299	37.0419486	43.65796219	21.59957626	20.9431676
P2	Base	1	47.73759513	0.016664353	48.35331777	0.000426671	23.68332705	24.99726111
	1	1	47.83204867	0.022993218	48.34111341	0.000533292	23.68253373	24.99718637
		2	47.8475445	0.023165884	48.34193	0.000544452	23.68228027	24.99718438
		3	47.86368186	0.019642034	48.3426994	0.000939444	23.68201956	24.99722856
	Base	-	23.20279415	23.202693	23.49771921	23.4976167	24.36778337	24.36788968
	2	1	23.46240703	23.46660867	23.49723066	23.49734597	24.36398586	24.36401798
		2	23.45778507	23.46176285	23.49709599	23.49709022	24.36406047	24.36410192
		3	23.46693141	23.47609914	23.49737095	23.49757668	24.36391248	24.36386733
	Base	-	9.142503168	13.77940416	9.25358441	13.95111598	24.75140947	24.6256488
	3	1	9.301047701	13.96784002	9.253517935	13.95063788	24.74900943	24.62284405
		2	9.287339499	13.91724008	9.253694357	13.949481	24.74920688	24.62366497
		3	9.296668501	13.97492286	9.253510827	13.95083418	24.74907597	24.62272751
	Base	-	32.8395974	37.74362357	33.26052528	38.22867249	24.10122421	23.96461449
	4	1	33.04544329	37.9004537	33.25608764	38.22155497	24.09846096	23.96270066
		2	33.08915667	38.04431972	33.25772439	38.22755751	24.09775306	23.96036472
		3	33.05535104	37.94170143	33.25675774	38.22342592	24.09828742	23.96202356

Table A.5 VUF minimisation results (Scott 1)

Train position	Case	No.	VUF (%)	IUF (%)	3φ PF	3φ Power (MW)	3φ Reactive (Mvar)
P1	Base	-	0.560344649	99.69960935	0.72342411	10.84417502	10.34920002
	1	1	0.28442454	29.63166691	0.552411174	14.07241282	21.23484571
		2	0.288734103	30.64616073	0.557337568	13.94045257	20.76759798
		3	0.284424541	29.63160488	0.552410176	14.07241626	21.23490611
	Base	-	1.98×10^{-06}	4.12×10^{-04}	0.799613588	10.32002954	7.750407566
	2	1	8.04507×10^{-07}	0.000138287	0.716534011	11.15964327	10.86401081
		2	3.50497×10^{-07}	6.0247E-05	0.716537805	11.15966301	10.86391179
		3	5.2601×10^{-07}	9.04158E-05	0.716534317	11.15965186	10.86400961
	Base	-	0.047625414	20.75552506	0.823718094	5.088736672	3.502789941
	3	1	0.020665409	2.739443531	0.454529166	9.131528692	17.89487694
		2	0.022375799	3.148310758	0.468029517	8.866584547	16.74149658
		3	0.02063976	2.718813813	0.453409327	9.165891706	18.01811489
	Base	-	0.063391031	8.217173648	0.766616393	15.80069116	13.23440084
	4	1	0.018482476	1.370856549	0.562794185	20.02256287	29.40789391
		2	0.023265683	2.562863867	0.698143969	16.88062116	17.31133718
		3	0.033219949	2.512810779	0.568125638	19.82961761	28.72361455
P2	Base	1	0.461207131	99.66836302	0.823256407	10.19908103	7.032692633
	1	1	0.289956674	31.76731142	0.571046709	13.84637646	19.90508573
		2	0.289689912	34.00903601	0.590447892	13.37688627	18.2846968
		3	0.288970024	31.71059754	0.570575543	13.81285688	19.88122599
	Base	-	1.50×10^{-06}	0.000334142	0.836545802	10.10298453	6.616965739
	2	1	2.28812×10^{-08}	4.17177×10^{-06}	0.747301658	10.98190522	9.76487944
		2	9.13446×10^{-07}	0.0001002	0.571394844	13.84887487	19.89067546
		3	5.25356×10^{-11}	9.57991×10^{-09}	0.74730973	10.98202249	9.764744825

Table A.5 VUF minimisation results (Scott 1) (Continued)

Train position	Case	No.	VUF (%)	IUF (%)	3φ PF	3φ Power (MW)	3φ Reactive (Mvar)
P2	Base	-	0.044741511	20.11054599	0.841079791	5.038938584	3.240617219
	3	1	0.022151709	3.18840033	0.46765597	8.662972943	16.37377437
		2	0.020328516	2.923429648	0.469857727	8.711390681	16.36646875
		3	0.020347688	2.929725536	0.470106029	8.705612196	16.34452539
	Base	-	0.047485192	6.939583576	0.830430838	15.21682535	10.20870576
	4	1	0.019579436	1.723401919	0.627546537	18.899786	23.44842439
		2	0.019597987	1.728048663	0.628133186	18.88525004	23.3942796
		3	0.020473888	1.754226477	0.619408526	19.15188998	24.27404753

Table A.6 VUF minimisation results (Scott 2)

Train position	Case	No.	P_T (MW)	Q_T (Mvar)	P_M (MW)	Q_M (Mvar)	P_{loss} (MW)	VD (kV)
P1	Base	-	10.81711356	10.24836163	0.008620878	0.023731669	0.844175021	33.81922053
	1	1	10.8174119	10.27735823	3.212803606	10.78374775	4.072412823	61.21221919
		2	10.81646667	10.24637113	3.083624197	10.35496423	3.94045257	60.16027083
		3	10.81741513	10.27741779	3.212803593	10.78374771	4.072416258	61.21225809
	Base	-	5.156625119	3.861042137	5.156623472	3.861033762	0.320029539	26.96343488
	2	1	5.558762421	5.347161262	5.558749161	5.347218752	1.159643272	41.44169396
		2	5.558766644	5.347113509	5.558765314	5.347170051	1.159663006	41.44211294
		3	5.558762421	5.347161262	5.558757893	5.347218107	1.159651864	41.44003164
	Base	-	2.029545474	1.368197399	3.05757638	2.127847701	0.088736672	12.54426616
	3	1	4.284245645	8.962866366	4.811317536	8.78557486	4.131528692	46.63072662
		2	4.123560486	8.36811507	4.700610692	8.201664672	3.866584547	49.24648377
		3	4.302508007	9.026896131	4.82690873	8.842713856	4.165891706	46.89934579

Table A.6 VUF minimisation results (Scott 2) (Continued)

Train position	Case	No.	P_T (MW)	Q_T (Mvar)	P_M (MW)	Q_M (Mvar)	P_{loss} (MW)	VD (kV)
P1	Base	-	7.329556173	5.961858671	8.453650015	7.199496845	0.800691164	44.61540036
	4	1	9.73392334	14.60882771	10.21307974	14.48794715	5.022562869	81.75978735
		2	8.121756686	8.667446512	8.714936691	8.464311493	1.88062116	54.45368074
		3	9.549232181	13.95778829	10.21298928	14.48759632	4.82961761	81.60090634
P2	Base	1	10.17411935	6.943044604	0.008620878	0.023731669	0.199081029	8.109603547
	1	1	10.64092745	8.799065854	3.134724591	10.83813709	3.846376461	38.22410967
		2	10.43043096	8.080395196	2.904025792	10.03899944	3.376886269	34.15785306
		3	10.62554095	8.839974957	3.133810443	10.83467128	3.812856881	36.63483868
	Base	-	5.047625511	3.29289367	5.04762524	3.292892379	0.102984531	7.738186834
	2	1	5.471858011	4.812179165	5.471864735	4.812235308	0.981905218	37.45500466
		2	6.901472317	9.856527895	6.901513969	9.856675386	3.848874873	32.86547661
		3	5.47191736	4.812114125	5.471923802	4.8121698	0.982022488	37.43599392
	Base	-	2.014633314	1.289637472	3.022333321	1.943030329	0.038938584	3.837631675
	3	1	4.025078077	8.191471912	4.591432461	8.008606275	3.662972943	34.23085316
		2	4.071764932	8.177566413	4.593030452	8.014862278	3.711390681	35.62938257
		3	4.068223581	8.165231993	4.59093383	8.005772872	3.705612196	35.69411624
	Base	-	7.086859947	4.703471194	8.11201621	5.432880625	0.21682535	11.83032113
	4	1	9.169904553	11.68681046	9.657555712	11.48161237	3.899785999	40.46390724
		2	9.162202335	11.65916304	9.650857639	11.45567724	3.885250039	40.31002688
		3	9.2838971	12.10006725	9.810198331	11.944815	4.151889983	42.30665585

Table A.7 VUF minimisation results (Scott 3)

Train position	Case	No.	$V_{CF,T}$ (kV)	$V_{CR,T}$ (kV)	$V_{FR,T}$ (kV)	$V_{CF,M}$ (kV)	$V_{CR,M}$ (kV)	$V_{FR,M}$ (kV)
P1	Base	-	49.37469649	24.67609686	24.69859988	49.9986742	24.99931842	24.99935578
	1	1	49.37310112	24.67610035	24.697001	49.39125771	24.80302093	24.58823933
		2	49.37482826	24.67989807	24.69493048	49.41584754	24.60395449	24.81189333
		3	49.37309779	24.67609411	24.69700392	49.39125771	24.80302093	24.58823933
	Base	-	49.76026619	24.87546363	24.88480266	49.76050545	24.87558329	24.88492226
	2	1	49.67336759	24.95564828	24.71771991	49.67368942	24.95581011	24.71787991
		2	49.67337029	24.95564755	24.71772334	49.67369197	24.95581138	24.71788119
		3	49.67336759	24.95564828	24.71771991	49.67368943	24.9558096	24.71788043
	Base	-	49.9142519	24.95539	24.95886192	49.86715672	24.93091826	24.9362385
	3	1	49.48585212	24.67071282	24.81513958	49.49110687	24.85458424	24.63652356
		2	49.51760398	24.87065062	24.64695402	49.52379989	24.65300577	24.87079427
		3	49.48219769	24.66818279	24.81401518	49.48783523	24.85369312	24.63414305
	Base	-	49.6323107	24.80919851	24.82311237	49.55795552	24.77073515	24.78722058
	4	1	49.13748409	24.46312787	24.67435624	49.14233993	24.66878047	24.47355946
		2	49.47778961	24.81356003	24.6642299	49.48397262	24.63215196	24.85182093
		3	49.17631849	24.51260629	24.6637123	49.14236024	24.66878653	24.47357371
P2	Base	1	49.55962584	24.73823793	24.82144202	49.9986742	24.99931847	24.99935573
	1	1	49.44961882	24.57688956	24.87278697	49.38878886	24.80044646	24.58834744
		2	49.49534111	24.69504854	24.80035482	49.43436538	24.61438242	24.81998432
		3	49.45093189	24.63440799	24.81658845	49.38898495	24.80055152	24.58843846
	Base	-	49.79158296	24.87597739	24.91561894	49.7917909	24.87608145	24.91572282
	2	1	49.70371111	24.95779164	24.74592881	49.7040028	24.95793905	24.74607309
		2	49.41946628	24.80166784	24.61780156	49.42003634	24.80195444	24.61808502
		3	49.70371439	24.95779156	24.74593217	49.70400611	24.95793892	24.74607652

Table A.7 VUF minimisation results (Scott 3) (Continued)

Train position	Case	No.	$V_{CF,T}$ (kV)	$V_{CR,T}$ (kV)	$V_{FR,T}$ (kV)	$V_{CF,M}$ (kV)	$V_{CR,M}$ (kV)	$V_{FR,M}$ (kV)
P2	Base	-	49.91855262	24.95155323	24.96700151	49.87728659	24.9269636	24.95032777
	3	1	49.52824764	24.65960649	24.86864853	49.53440726	24.64819789	24.8862153
		2	49.52871024	24.8699458	24.65876451	49.53405207	24.64797276	24.88608525
		3	49.52940277	24.87039007	24.65901278	49.53458922	24.64867733	24.88591781
	Base	-	49.70203935	24.82275812	24.87930756	49.65603478	24.79540734	24.8606619
	4	1	49.30427808	24.73477601	24.56951601	49.30970824	24.51534805	24.79439698
		2	49.30585562	24.73559368	24.57027582	49.31118631	24.51612512	24.79509802
		3	49.28072533	24.72200098	24.55873787	49.2864642	24.72557223	24.56092048

Table A.8 VUF minimisation results (Scott 4)

Train position	Case	No.	TSS $V_{rail,T}$ (V)	TSS $V_{rail,M}$ (V)	Train $V_{rail,T}$ (V)	Train $V_{rail,M}$ (V)	$V_{T,train}$ (kV)	$V_{M,train}$ (kV)
P1	Base	-	5.228255243	0.00869568	58.60518401	0.000236219	19.51354776	24.99176273
	1	1	4.862234129	48.61521013	58.95278837	1.624895209	19.37870924	21.59876974
		2	3.618534063	46.91250434	58.49376557	1.797890488	19.54395692	21.62333536
		3	4.864227759	48.61521015	58.95345689	1.624895206	19.37845151	21.59876977
	Base	-	2.242731124	2.242718134	25.09448983	25.09434366	22.78569413	22.78582685
	2	1	53.87742939	53.87785572	23.11131171	23.11113339	24.82083323	24.81968417
		2	53.87644396	53.87784155	23.11169061	23.11113055	24.82053668	24.82102846
		3	53.87742939	53.8775887	23.11131171	23.11144249	24.82083323	24.81919687
	Base	-	0.849541772	1.294122416	9.457090341	14.44713989	24.18457081	23.74695386
	3	1	32.58706256	49.28108912	9.939634221	16.11067903	21.92983955	20.10921095
		2	50.54808081	49.33714854	10.61617414	17.86184284	22.66273559	21.49618808
		3	32.90418524	49.61784176	9.949886448	16.11851976	21.90897036	20.09694038

Table A.8 VUF minimisation results (Scott 4) (Continued)

Train position	Case	No.	TSS $V_{rail,T}$ (V)	TSS $V_{rail,M}$ (V)	Train $V_{rail,T}$ (V)	Train $V_{rail,M}$ (V)	$V_{T,train}$ (kV)	$V_{M,train}$ (kV)
P1	Base	-	3.297785464	3.881565236	36.93670698	43.48926705	21.67261977	21.03680292
	4	1	47.71074698	44.06813227	40.97484658	52.37319996	19.46012075	17.19085133
		2	33.74454526	49.74634239	37.01797698	48.47754764	21.92152883	18.84120766
		3	34.12677967	44.06628123	41.29233819	52.37296718	19.15455436	17.19092943
P2	Base	1	47.73759513	0.016664353	48.35331777	0.000426671	23.68332705	24.99726111
	1	1	131.7061606	93.4550335	51.91853648	0.273369051	22.39571838	24.9004728
		2	56.53737571	90.23478343	48.47217494	0.191395939	23.45007887	22.87519418
		3	85.54994554	93.46099179	49.70648517	0.272980623	22.97602677	24.90091982
	Base	-	23.20279415	23.202693	23.49771921	23.4976167	24.36778337	24.36788968
	2	1	94.85215419	94.8535175	21.59993649	21.59983159	25.47330934	25.47346924
		2	82.10571743	82.10704104	23.37703629	23.37676107	24.78541119	24.78571002
		3	94.8503812	94.85168996	21.60035536	21.60024115	25.47329721	25.47345654
	Base	-	9.142503168	13.77940416	9.25358441	13.95111598	24.75140947	24.6256488
	3	1	91.91715271	104.059682	9.791191471	15.86373672	23.02471853	22.88192951
		2	92.96213818	104.1007322	9.057561424	15.865386	25.15079294	22.88076713
		3	93.04557797	103.7193417	9.039741141	15.86043421	25.15313176	22.88620767
	Base	-	32.8395974	37.74362357	33.26052528	38.22867249	24.10122421	23.96461449
	4	1	75.91887722	123.3036682	32.75246333	42.00795297	24.46205103	22.21929855
		2	75.93616871	123.2746465	32.75483756	41.99956148	24.46534283	22.22251638
		3	75.0177997	77.73675761	32.8850793	36.81711382	24.40678792	24.42216044

Table A.9 Three-phase power factor maximisation results (Scott 1)

Train position	Case	No.	VUF (%)	IUF (%)	3φ PF	3φ Power (MW)	3φ Reactive (Mvar)
P1	Base	-	0.560344649	99.69960935	0.72342411	10.84417502	10.34920002
	1	1	0.559679913	99.6995844	0.72497565	10.85498146	10.31294553
		2	0.559677769	99.69957873	0.724975636	10.85494077	10.3129073
		3	0.559680715	99.69958679	0.724975648	10.85499653	10.3129599
	Base	-	1.98×10^{-06}	4.12×10^{-04}	0.799613588	10.32002954	7.750407566
	2	1	1.72613×10^{-06}	0.000358836	0.799865369	10.32486932	7.74727196
		2	1.42623×10^{-06}	0.000296491	0.799865366	10.32486919	7.747271963
		3	5.37525×10^{-06}	0.001117436	0.799865267	10.32484224	7.747254401
	Base	-	0.047625414	20.75552506	0.823718094	5.088736672	3.502789941
	3	1	0.047633774	20.75690867	0.823810688	5.089864146	3.502340988
		2	0.047634395	20.75719543	0.823810664	5.089860103	3.502338518
		3	0.047633914	20.75703842	0.823810675	5.089847277	3.502329549
	Base	-	0.063391031	8.217173648	0.766616393	15.80069116	13.23440084
	4	1	0.063298798	8.205580733	0.767239941	15.81302534	13.21860885
		2	0.06329644	8.205329328	0.767239888	15.81292074	13.21852367
		3	0.063298215	8.205525003	0.76723994	15.8129874	13.21857721
P2	Base	1	0.461207131	99.66836302	0.823256407	10.19908103	7.032692633
	1	1	0.461219748	99.66838282	0.823285901	10.19972682	7.032356036
		2	0.461219738	99.66837942	0.823285839	10.19972617	7.03235722
		3	0.461219638	99.668376	0.823285886	10.19972493	7.03235512
	Base	-	1.50×10^{-06}	0.000334142	0.836545802	10.10298453	6.616965739
	2	1	1.45792×10^{-06}	0.000324212	0.836556436	10.10327795	6.616877698
		2	2.51346×10^{-06}	0.000558941	0.836555514	10.10326141	6.616891151
		3	1.24178×10^{-06}	0.000276144	0.83655638	10.10328765	6.616885526

Table A.9 Three-phase power factor maximisation results (Scott 1) (Continued)

Train position	Case	No.	VUF (%)	IUF (%)	3φ PF	3φ Power (MW)	3φ Reactive (Mvar)
P2	Base	-	0.044741511	20.11054599	0.841079791	5.038938584	3.240617219
	3	1	0.04474226	20.11070859	0.841084612	5.03901111	3.240600377
		2	0.044742214	20.11067915	0.841084644	5.039013526	3.240601508
		3	0.044742282	20.11071674	0.841084647	5.039011779	3.240600356
	Base	-	0.047485192	6.939583576	0.830430838	15.21682535	10.20870576
	4	1	0.047487497	6.939763261	0.830449649	15.2175174	10.20842497
		2	0.047487171	6.93970881	0.830449657	15.21753253	10.20843481
		3	0.047486781	6.939654863	0.830449683	15.21752626	10.20842958

Table A.10 Three-phase power factor maximisation results (Scott 2)

Train position	Case	No.	P_T (MW)	Q_T (Mvar)	P_M (MW)	Q_M (Mvar)	P_{loss} (MW)	VD (kV)
P1	Base	-	10.81711356	10.24836163	0.008620878	0.023731669	0.844175021	33.81922053
	1	1	10.82809315	10.21280503	0.008620972	0.023731782	0.854981459	34.02753911
		2	10.82805259	10.21276746	0.008621083	0.023732155	0.854940767	34.02696536
		3	10.82810828	10.21281953	0.008620903	0.023731646	0.854996528	34.02708642
	Base	-	5.156625119	3.861042137	5.156623472	3.861033762	0.320029539	26.96343488
	2	1	5.159062323	3.859556822	5.159069139	3.859554514	0.324869318	27.16370452
		2	5.159054051	3.859550647	5.159077274	3.859560642	0.324869193	27.16367929
		3	5.159093876	3.85958088	5.159010616	3.859513341	0.324842237	27.16310182
	Base	-	2.029545474	1.368197399	3.05757638	2.127847701	0.088736672	12.54426616
	3	1	2.029889049	1.368095149	3.058369705	2.127538436	0.089864146	12.63371271
		2	2.029880156	1.368088889	3.058374619	2.127542481	0.089860103	12.63348095
		3	2.029879016	1.368088128	3.058362886	2.127534087	0.089847277	12.63266069

Table A.10 Three-phase power factor maximisation results (Scott 2) (Continued)

Train position	Case	No.	P_T (MW)	Q_T (Mvar)	P_M (MW)	Q_M (Mvar)	P_{loss} (MW)	VD (kV)
P1	Base	-	7.329556173	5.961858671	8.453650015	7.199496845	0.800691164	44.61540036
	4	1	7.33492225	5.956555861	8.460746158	7.189517439	0.813025343	44.94860563
		2	7.334894762	5.956532952	8.460669139	7.189455578	0.812920744	44.94564835
		3	7.334909314	5.95654503	8.460721205	7.189496864	0.8129874	44.94765532
P2	Base	1	10.17411935	6.943044604	0.008620878	0.023731669	0.199081029	8.109603547
	1	1	10.17501045	6.943584985	0.008620944	0.023731705	0.199726822	8.127104467
		2	10.17500583	6.943571913	0.008621016	0.023731977	0.199726173	8.127020939
		3	10.17500893	6.943585491	0.008621105	0.023732196	0.199724925	8.127925855
	Base	-	5.047625511	3.29289367	5.04762524	3.292892379	0.102984531	7.738186834
	2	1	5.047817586	3.293013635	5.047819796	3.293017578	0.103277951	7.747350122
		2	5.047836904	3.293050453	5.047792426	3.29302462	0.103261411	7.751386168
		3	5.047820439	3.293021318	5.047832661	3.29303926	0.103287649	7.749140561
	Base	-	2.014633314	1.289637472	3.022333321	1.943030329	0.038938584	3.837631675
	3	1	2.014660505	1.289651727	3.022399546	1.943073913	0.03901111	3.840228054
		2	2.014663567	1.289657645	3.022398985	1.943069426	0.039013526	3.840447677
		3	2.014661009	1.289653274	3.022398827	1.943069185	0.039011779	3.839804531
	Base	-	7.086859947	4.703471194	8.11201621	5.432880625	0.21682535	11.83032113
	4	1	7.0872464	4.703695973	8.112553071	5.433201623	0.217517401	11.84721082
		2	7.08726322	4.703722574	8.112567423	5.433242273	0.217532529	11.85046058
		3	7.087263613	4.703721179	8.11255369	5.433213118	0.217526265	11.8487577

Table A.11 Three-phase power factor maximisation results (Scott 3)

Train position	Case	No.	$V_{CF,T}$ (kV)	$V_{CR,T}$ (kV)	$V_{FR,T}$ (kV)	$V_{CF,M}$ (kV)	$V_{CR,M}$ (kV)	$V_{FR,M}$ (kV)
P1	Base	-	49.37469649	24.67609686	24.69859988	49.9986742	24.99931842	24.99935578
	1	1	49.37661286	24.69060655	24.68600685	49.99867419	24.99937494	24.99929925
		2	49.37661522	24.69058859	24.68602717	49.99867417	24.99938565	24.99928852
		3	49.37661197	24.69059736	24.68601515	49.9986742	24.99933066	24.99934354
	Base	-	49.76026619	24.87546363	24.88480266	49.76050545	24.87558329	24.88492226
	2	1	49.76033672	24.87902386	24.881313	49.76057552	24.87911913	24.88145652
		2	49.76033711	24.87901823	24.88131901	49.76057514	24.8791207	24.88145458
		3	49.7603352	24.87899533	24.88134001	49.76057815	24.87917461	24.88140368
	Base	-	49.9142519	24.95539	24.95886192	49.86715672	24.93091826	24.9362385
	3	1	49.914256	24.95648092	24.9577751	49.86717015	24.9326572	24.93451299
		2	49.91425638	24.95644528	24.95781112	49.86716992	24.93271441	24.93445556
		3	49.91425643	24.95644271	24.95781374	49.86717044	24.93268749	24.934483
	Base	-	49.6323107	24.80919851	24.82311237	49.55795552	24.77073515	24.78722058
	4	1	49.6325776	24.81553614	24.81704172	49.55847196	24.77893749	24.7795348
		2	49.63257901	24.81550129	24.81707798	49.55847582	24.77879113	24.77968502
		3	49.63257827	24.81552428	24.81705425	49.55847324	24.77890141	24.77957217
P2	Base	1	49.55962584	24.73823793	24.82144202	49.9986742	24.99931847	24.99935573
	1	1	49.55964019	24.74056258	24.81913147	49.9986742	24.99936977	24.99930442
		2	49.55964015	24.74052348	24.81917052	49.99867418	24.99934669	24.99932749
		3	49.55964028	24.74056816	24.81912598	49.99867417	24.99939474	24.99927943
	Base	-	49.79158296	24.87597739	24.91561894	49.7917909	24.87608145	24.91572282
	2	1	49.79158449	24.87687184	24.91472595	49.79179237	24.87699988	24.91480578
		2	49.79158375	24.87701278	24.91458427	49.79179247	24.8770404	24.91476539
		3	49.79158443	24.87691045	24.91468728	49.79179194	24.87708467	24.91472057

Table A.11 Three-phase power factor maximisation results (Scott 3) (Continued)

Train position	Case	No.	$V_{CF,T}$ (kV)	$V_{CR,T}$ (kV)	$V_{FR,T}$ (kV)	$V_{CF,M}$ (kV)	$V_{CR,M}$ (kV)	$V_{FR,M}$ (kV)
P2	Base	-	49.91855262	24.95155323	24.96700151	49.87728659	24.9269636	24.95032777
	3	1	49.91855275	24.95181246	24.96674241	49.87728694	24.92747352	24.94981818
		2	49.91855269	24.95188434	24.96667046	49.87728692	24.92742783	24.94986386
		3	49.91855276	24.95183669	24.96671818	49.87728693	24.92742623	24.94986546
	Base	-	49.70203935	24.82275812	24.87930756	49.65603478	24.79540734	24.8606619
	4	1	49.70204394	24.82406942	24.87800071	49.65604122	24.79702725	24.85904826
		2	49.70204349	24.82414769	24.87792199	49.65604105	24.79716175	24.85891359
		3	49.70204345	24.82413931	24.87793033	49.65604141	24.7970794	24.8589963

Table A.12 Three-phase power factor maximisation results (Scott 4)

Train position	Case	No.	TSS $V_{rail,T}$ (V)	TSS $V_{rail,M}$ (V)	Train $V_{rail,T}$ (V)	Train $V_{rail,M}$ (V)	$V_{T,train}$ (kV)	$V_{M,train}$ (kV)
P1	Base	-	5.228255243	0.00869568	58.60518401	0.000236219	19.51354776	24.99176273
	1	1	1.945108277	0.017246958	57.09116613	0.000181454	20.0720505	24.99352453
		2	1.939928673	0.022092923	57.09333147	0.000500258	20.07118086	24.9935644
		3	1.942901157	0.003306194	57.09094489	0.00014773	20.07220808	24.99259678
	Base	-	2.242731124	2.242718134	25.09448983	25.09434366	22.78569413	22.78582685
	2	1	0.976116486	0.982333268	24.95313574	24.95287154	22.95304064	22.95339479
		2	0.97759949	0.982092232	24.9531719	24.95261202	22.95274245	22.95374981
		3	0.983189463	0.967872215	24.95297737	24.9539856	22.95398764	22.95132928
	Base	-	0.849541772	1.294122416	9.457090341	14.44713989	24.18457081	23.74695386
	3	1	0.448340494	0.656699342	9.450259212	14.41710074	24.24036633	23.83425233
		2	0.458938381	0.640361853	9.450458672	14.41647633	24.23913186	23.83507583
		3	0.459640736	0.647692667	9.450522021	14.41691702	24.2389632	23.83400115

Table A.12 Three-phase power factor maximisation results (Scott 4) (Continued)

Train position	Case	No.	TSS $V_{rail,T}$ (V)	TSS $V_{rail,M}$ (V)	Train $V_{rail,T}$ (V)	Train $V_{rail,M}$ (V)	$V_{T,train}$ (kV)	$V_{M,train}$ (kV)
P1	Base	-	3.297785464	3.881565236	36.93670698	43.48926705	21.67261977	21.03680292
	4	1	1.195315469	1.308880077	36.53109691	42.86086164	21.95285623	21.38454888
		2	1.199623912	1.315492674	36.5323934	42.8664161	21.95186617	21.38152638
		3	1.196641001	1.309858647	36.53173605	42.86272782	21.95239854	21.38359402
P2	Base	1	47.73759513	0.016664353	48.35331777	0.000426671	23.68332705	24.99726111
	1	1	46.25278472	0.028934561	48.29817383	0.000582999	23.70680395	24.99778059
		2	46.27661306	0.008959463	48.29931024	0.000415031	23.70640775	24.99754703
		3	46.24956361	0.050626847	48.29797147	0.001287764	23.70686035	24.99803355
	Base	-	23.20279415	23.202693	23.49771921	23.4976167	24.36778337	24.36788968
	2	1	22.63214455	22.61745499	23.48697367	23.48643674	24.37682933	24.3771788
		2	22.5461313	22.59811854	23.48445603	23.4844044	24.37825931	24.3775915
		3	22.60888432	22.56541079	23.48621304	23.48501168	24.37722074	24.37803886
	Base	-	9.142503168	13.77940416	9.25358441	13.95111598	24.75140947	24.6256488
	3	1	8.975189043	13.45506082	9.25260477	13.94704823	24.75403187	24.63080805
		2	8.931603905	13.48217308	9.251721475	13.9478409	24.75476012	24.63034507
		3	8.960645256	13.48315996	9.252266885	13.94785945	24.75427736	24.63032886
	Base	-	32.8395974	37.74362357	33.26052528	38.22867249	24.10122421	23.96461449
	4	1	32.0006848	36.70733258	33.23921283	38.1984688	24.11447725	23.98098403
		2	31.95232925	36.6258758	33.2375715	38.19500156	24.11527141	23.98234796
		3	31.95722971	36.67614745	33.23781589	38.19704805	24.11518651	23.9815123

Table A.13 Optimal tap positions in loss minimisation (Scott)

Train position	Case	No.	Tap 1	Tap 2	Tap 3	Tap 4	Tap 5	Tap 6
P1	1	1	0.999808176	0.994578088	0.99315147	1.000017846	0.999993804	0.999928385
		2	0.999511379	0.994325651	0.99296367	0.999986219	0.999989037	0.999996538
		3	0.999635753	0.994392065	0.993101437	1.000051809	1.000134775	1.000256084
	2	1	1.016375846	1.01140402	1.004026259	1.004027379	1.011412881	1.016387524
		2	1.016334181	1.011376986	1.004038131	1.004047102	1.011455314	1.016437119
		3	1.016706799	1.011719683	1.004240209	1.004095503	1.01150296	1.016558866
	3	1	1.008179976	1.006268984	1.00275483	1.003317195	1.008323867	1.011454846
		2	1.007971145	1.005822549	1.002290011	1.003770154	1.009308857	1.012709785
		3	1.007987298	1.00577687	1.002258997	1.002738936	1.007375728	1.010425349
	4	1	1.017384868	1.011362747	1.003068449	1.001038387	1.00822652	1.014502941
		2	1.017038791	1.010861028	1.002928835	1.00117491	1.008384302	1.014816261
		3	1.017200548	1.010996217	1.002966144	1.001146901	1.008352442	1.014741301
P2	1	1	0.994548838	0.995146257	1.000211724	1.000012546	1.000009671	1.000040619
		2	0.994665749	0.995225966	1.000254437	1.000012819	1.000012223	1.000013289
		3	0.99476867	0.995282806	1.000298678	1.000003577	1.000090127	1.000048714
	2	1	0.998014354	0.998282966	1.000683817	1.000695747	0.998327493	0.998040204
		2	0.997983165	0.998269435	1.000671249	1.000682261	0.998275292	0.997991017
		3	0.998056638	0.998298236	1.000696151	1.000721447	0.998337898	0.99812711
	3	1	0.999378164	0.999477857	1.000420981	1.000498472	0.999076087	0.998905481
		2	0.999510174	0.999575975	1.000385306	1.000361231	0.998911633	0.998788799
		3	0.999401212	0.99948866	1.000409405	1.000517745	0.9991104	0.998930031
	4	1	0.996462662	0.996967138	1.000527829	1.00039045	0.996361793	0.995855646
		2	0.996885649	0.997111871	1.00064745	1.000784167	0.996921848	0.996727073
		3	0.996691001	0.997092148	1.00055586	1.00050385	0.99657289	0.996107306

Table A.14 Optimal tap positions in VUF minimisation (Scott)

Train position	Case	No.	Tap 1	Tap 2	Tap 3	Tap 4	Tap 5	Tap 6
P1	1	1	1.018022187	1.007989636	0.998349478	0.8	1.2	0.8
		2	0.999937784	0.994617336	0.993079665	1.2	0.8	1.2
		3	1.0180617	1.007999329	0.998357884	0.8	1.199999999	0.8
	2	1	0.8	0.8	0.8	0.8	0.8	0.800244382
		2	0.8	0.800053774	0.800002256	0.8	0.8	0.8
		3	0.8	0.8	0.8	0.8	0.800044075	0.800288138
	3	1	1.136565343	0.800802466	1.13062648	0.801300411	1.2	1.2
		2	0.8	1.084563267	0.8	1.199875835	1.199955279	0.800067248
		3	1.137185874	0.800342931	1.132068433	0.800007626	1.2	1.2
	4	1	1.068191171	0.800000006	1.199802383	0.8	1.199999594	1.199998706
		2	0.8	0.981922422	0.855537952	1.199999733	1.2	1.19999499
		3	1.070597474	0.800000683	1.198046858	0.80005288	1.199675779	1.199889077
P2	1	1	1.028095825	1.2	1.2	0.8	1.2	0.8
		2	0.8	0.86891616	1.020712087	1.2	0.800000002	1.177002321
		3	0.8	0.912686406	1.09073605	0.8	1.199897821	0.8
	2	1	0.8	0.800040382	0.8	0.8	0.8	0.80061964
		2	1.2	1.2	0.8	0.8	1.2	1.2
		3	0.800233417	0.800170642	0.8	0.8	0.800133246	0.800778754
	3	1	1.058321815	0.821731042	1.186203689	1.199899976	1.199712781	0.800004346
		2	0.809646942	1.08765606	0.800016218	1.199998679	1.199994939	0.800001478
		3	0.8	1.081181305	0.8	1.199049252	1.2	0.800016964
	4	1	0.823360083	1.100152338	0.8	1.199985487	1.199920669	0.8
		2	0.829179881	1.10274615	0.8	1.199923901	1.198918039	0.800252015
		3	0.838010643	1.122185407	0.800000029	0.80003202	0.800021801	1.199994827

Table A.15 Optimal tap positions in 3-phase power factor maximisation (Scott)

Train position	Case	No.	Tap 1	Tap 2	Tap 3	Tap 4	Tap 5	Tap 6
P1	1	1	0.94060107	0.950451151	0.975551354	0.999906375	0.999848631	0.999841834
		2	0.940715563	0.950512953	0.975585748	0.999888892	0.999807355	0.999876699
		3	0.94055504	0.95045952	0.975567242	0.999980439	0.999930328	0.999922362
	2	1	0.982486912	0.986476708	0.994005297	0.994048401	0.986446546	0.982473881
		2	0.982553427	0.986467383	0.99401576	0.994045764	0.986419017	0.982434714
		3	0.982316485	0.986463138	0.994054323	0.993950589	0.986593601	0.982721474
	3	1	0.994239481	0.995727579	0.998196114	0.997107669	0.993193557	0.990950655
		2	0.994367519	0.995821009	0.998256293	0.997009622	0.993107446	0.990890532
		3	0.994377676	0.99584112	0.998260402	0.997055223	0.993198661	0.990994214
	4	1	0.970394908	0.976475954	0.989230688	0.986047607	0.97022022	0.963150287
		2	0.970529157	0.976531186	0.989293473	0.986311633	0.970455471	0.963490158
		3	0.97044689	0.976511363	0.989251952	0.986112304	0.97032119	0.963230093
P2	1	1	0.999472273	0.999504144	0.995928973	0.999913881	0.999885974	0.999872486
		2	0.999362276	0.999599985	0.995995648	0.999953611	0.999888311	0.999787173
		3	0.999468022	0.999476709	0.995919807	0.999872786	0.999790218	0.99971308
	2	1	1.000092696	1.000098111	0.998440371	0.998399567	1.000049397	1.000069299
		2	0.999572449	0.999855228	0.998199151	0.998340999	0.999486509	1.00010609
		3	0.999964074	1.000004354	0.998374997	0.998254057	0.99992554	0.99989028
	3	1	1.000201567	1.00022956	0.999546133	0.999113901	1.000059248	1.000110028
		2	1.000063906	1.000088377	0.999424524	0.99919019	1.000201236	1.000196542
		3	1.000170846	1.000166317	0.999505498	0.999192928	1.000203173	1.000195752
	4	1	1.000174382	1.000105149	0.997706998	0.997164475	1.000015768	0.999847853
		2	0.999933739	0.999995876	0.997571928	0.996935548	0.999682471	0.999571472
		3	1.000027033	1.000027843	0.997585916	0.9970767	0.999851567	0.999817656

A.3.2 V/V transformer system

Table A.16 Loss minimisation results (V/V 1)

Train position	Case	No.	VUF (%)	IUF (%)	3φ PF	3φ Power (MW)	3φ Reactive (Mvar)
P1	Base	-	2.002556918	99.83890752	0.714089051	10.9146931	10.70018381
	1	1	2.000816641	99.83892121	0.71458257	10.91347347	10.68390521
		2	2.000779158	99.83892982	0.714594895	10.91347308	10.68352829
		3	2.000821652	99.83892841	0.71458095	10.91347306	10.68395431
	Base	-	0.826442373	49.70315961	0.79842974	10.32742468	7.787809079
	2	1	0.82706036	49.70289232	0.797754954	10.32595621	7.804857212
		2	0.827089389	49.70445794	0.797752431	10.32595683	7.80492557
		3	0.827063846	49.70304772	0.797754152	10.32595624	7.804878806
	Base	-	0.421508693	53.75529912	0.823464823	5.089451385	3.506632405
	3	1	0.421735024	53.76446231	0.823089461	5.08892515	3.511234738
		2	0.421744709	53.7654949	0.823086537	5.08892534	3.511273545
		3	0.421764679	53.76650456	0.823063538	5.08892376	3.511576663
	Base	-	1.40027729	51.43362294	0.762122144	15.84627847	13.46163205
	4	1	1.400956415	51.41835521	0.761510389	15.84481615	13.48617247
		2	1.400937212	51.41764032	0.761510148	15.84481615	13.48618262
		3	1.400957517	51.41840628	0.761510537	15.8448161	13.48616616
P2	Base	1	1.601666797	99.85024226	0.822512658	10.20499872	7.056499806
	1	1	1.601770998	99.85021227	0.822445486	10.20476735	7.058121314
		2	1.601770688	99.85021537	0.822445642	10.20476716	7.058117042
		3	1.60177182	99.85021516	0.822445113	10.20476726	7.058131144
	Base	-	0.7690183437	49.68554862	0.836351321	10.10457682	6.623133679
	2	1	0.769042904	49.6855466	0.836317192	10.10446356	6.623958767
		2	0.769043535	49.68557041	0.836316925	10.10446355	6.623965805

Table A.16 Loss minimisation results (V/V 1) (Continued)

Train position	Case	No.	VUF (%)	IUF (%)	3φ PF	3φ Power (MW)	3φ Reactive (Mvar)
P2		3	0.769043264	49.68556212	0.83631707	10.10446356	6.623961986
	Base	-	0.402941792	53.05198318	0.841040755	5.039104737	3.241238139
	3	1	0.402952439	53.05255215	0.841023117	5.039074938	3.24145124
		2	0.402952823	53.05258608	0.841022868	5.039074962	3.241454535
		3	0.402951643	53.05242024	0.84102271	5.039075027	3.241456653
	Base	-	1.19578484	50.28674479	0.829872132	15.22345523	10.23529008
	4	1	1.1958569	50.28722433	0.829820657	15.22319838	10.23715667
		2	1.195862939	50.28747886	0.829820682	15.22319811	10.23715548
		3	1.195856945	50.28722782	0.829820669	15.22319813	10.23715603

Table A.17 Loss minimisation results (V/V 2)

Train position	Case	No.	P_T (MW)	Q_T (Mvar)	P_M (MW)	Q_M (Mvar)	P_{loss} (MW)	VD (kV)
P1	Base	-	10.88640608	10.59386305	0.008301551	0.022852623	0.914693103	45.38185602
	1	1	10.88532618	10.57816762	0.00830212	0.022854418	0.91347347	45.37617199
		2	10.88532761	10.57779819	0.008301789	0.022853162	0.913473076	45.37565765
		3	10.88532626	10.5782183	0.008301756	0.022853332	0.913473059	45.37471069
	Base	-	5.158265329	3.869370284	5.162214311	3.889433268	0.327424677	32.40747018
	2	1	5.157497618	3.877683126	5.161444978	3.897882706	0.325956213	32.29260318
		2	5.157499123	3.87757659	5.161443336	3.89805447	0.325956827	32.29221079
		3	5.157497364	3.877678239	5.161444907	3.897907741	0.325956236	32.29241734
	Base	-	2.029569839	1.36834987	3.058249158	2.131464968	0.089451385	14.62013373
	3	1	2.029389857	1.369802553	3.05787976	2.134518168	0.08892515	14.52583047
		2	2.029389667	1.369779494	3.057881073	2.134583922	0.08892534	14.52630848

Table A.17 Loss minimisation results (V/V 2) (Continued)

Train position	Case	No.	P_T (MW)	Q_T (Mvar)	P_M (MW)	Q_M (Mvar)	P_{loss} (MW)	VD (kV)
P1		3	2.029389261	1.369860973	3.057877644	2.13479616	0.08892376	14.52215795
	Base	-	7.33648456	5.99660184	8.491302147	7.387800499	0.846278466	54.55053167
	4	1	7.335608835	6.009430897	8.490665968	7.399304975	0.844816149	54.51156576
		2	7.335607043	6.009528733	8.490666982	7.399214037	0.844816152	54.51119978
		3	7.335608237	6.009418638	8.4906657	7.399307509	0.844816105	54.51130408
P2	Base	1	10.18039676	6.965674358	0.008352293	0.022992304	0.204998719	15.64995204
	1	1	10.18016873	6.967309391	0.008352403	0.022993134	0.204767347	15.67716399
		2	10.18017181	6.967319075	0.008352281	0.02299227	0.204767164	15.67878836
		3	10.1801668	6.967311966	0.008352285	0.022992256	0.204767258	15.67805649
	Base	-	5.048124317	3.293985177	5.048856027	3.297437481	0.104576821	12.16624485
	2	1	5.048054733	3.294338345	5.048784802	3.297794603	0.104463562	12.18311821
		2	5.048054748	3.294339922	5.0487855	3.297803073	0.104463554	12.1835739
		3	5.048055086	3.294340126	5.048784921	3.297798035	0.104463556	12.18336146
	Base	-	2.014673069	1.289646845	3.022510249	1.943570434	0.039104737	5.705057254
	3	1	2.014660635	1.289698399	3.022483043	1.943690973	0.039074938	5.711437052
		2	2.01466082	1.289699267	3.022483673	1.943696698	0.039074962	5.712080068
		3	2.014660111	1.289702796	3.022483869	1.943692876	0.039075027	5.711619966
	Base	-	7.088100154	4.706638373	8.117493281	5.454088807	0.223455232	18.53092939
	4	1	7.087970824	4.707358506	8.117335731	5.455110148	0.223198376	18.56406342
		2	7.087973261	4.707338264	8.11733219	5.455125729	0.223198106	18.56429622
		3	7.087972308	4.707364357	8.11733046	5.455088918	0.223198127	18.5635257

Table A.18 Loss minimisation results (V/V 3)

Train position	Case	No.	$V_{CF,T}$ (kV)	$V_{CR,T}$ (kV)	$V_{FR,T}$ (kV)	$V_{CF,M}$ (kV)	$V_{CR,M}$ (kV)	$V_{FR,M}$ (kV)
P1	Base	-	48.30216449	24.13932669	24.16283804	49.06393523	24.53194929	24.53198594
	1	1	48.30463879	24.1461264	24.15851272	49.06449504	24.53219842	24.53229662
		2	48.3046955	24.14621456	24.15848127	49.06450652	24.53225836	24.53224816
		3	48.30463123	24.14613888	24.15849269	49.0644937	24.53221311	24.53228058
	Base	-	49.52461591	24.75761177	24.76700424	48.97509193	24.48278238	24.49230966
	2	1	49.52306629	24.75450207	24.76856431	48.9736387	24.47974446	24.49389433
		2	49.52307611	24.75458375	24.76849244	48.97361552	24.4796123	24.49400331
		3	49.52306594	24.754484	24.76858203	48.97363509	24.47973883	24.49389635
	Base	-	49.87115021	24.93383817	24.93731206	49.50760706	24.75112244	24.75648466
	3	1	49.8708143	24.93223893	24.93857538	49.5071286	24.74902853	24.75810011
		2	49.87081546	24.93223285	24.93858262	49.50712036	24.74912599	24.7579944
		3	49.87079606	24.93219959	24.93859648	49.50708616	24.74890593	24.75818027
	Base	-	49.24028688	24.61310798	24.62717909	48.22088115	24.10183144	24.11904994
	4	1	49.2379667	24.6104704	24.62749645	48.21882312	24.10087758	24.11794575
		2	49.23795487	24.61038314	24.62757188	48.21883426	24.10092158	24.11791289
		3	49.23796802	24.6104409	24.62752727	48.21882287	24.10086284	24.11796023
P2	Base	1	48.85650857	24.38607356	24.47049164	49.21365209	24.60680772	24.60684437
	1	1	48.85627219	24.38608352	24.47024556	49.21361727	24.60673699	24.60688029
		2	48.85627272	24.38611771	24.47021189	49.21361751	24.60679124	24.60682627
		3	48.85627063	24.38606189	24.47026562	49.21361709	24.60679421	24.60682287
	Base	-	49.62318796	24.79175677	24.83144473	49.08574211	24.5227984	24.5629577
	2	1	49.62311224	24.791455	24.83167084	49.0856735	24.52249384	24.56319372
		2	49.62311183	24.79145522	24.83167021	49.08567265	24.52250963	24.56317708
		3	49.62311209	24.79146292	24.83166278	49.08567307	24.52249666	24.56319047

Table A.18 Loss minimisation results (V/V 3) (Continued)

Train position	Case	No.	$V_{CF,T}$ (kV)	$V_{CR,T}$ (kV)	$V_{FR,T}$ (kV)	$V_{CF,M}$ (kV)	$V_{CR,M}$ (kV)	$V_{FR,M}$ (kV)
P2	Base	-	49.887044	24.93581358	24.95123255	49.53806537	24.75729907	24.7807712
	3	1	49.88702862	24.93563313	24.95139764	49.53804294	24.75706346	24.78098441
		2	49.8870285	24.93564362	24.95138703	49.53804248	24.75708665	24.78096075
		3	49.8870277	24.9356002	24.95142964	49.53804295	24.75709368	24.7809542
	Base	-	49.47887068	24.71110095	24.76779648	48.56697395	24.25012261	24.31688826
	4	1	49.47871066	24.71075888	24.76797866	48.56680118	24.24997572	24.31686256
		2	49.47871401	24.71079802	24.76794286	48.56679772	24.24993035	24.31690447
		3	49.47871075	24.71078389	24.76795374	48.5668012	24.24990604	24.31693226

Table A.19 Loss minimisation results (V/V 4)

Train position	Case	No.	TSS $V_{rail,T}$ (V)	TSS $V_{rail,M}$ (V)	Train $V_{rail,T}$ (V)	Train $V_{rail,M}$ (V)	$V_{T,train}$ (kV)	$V_{M,train}$ (kV)
P1	Base	-	5.582963653	0.008744328	61.07461976	0.000231806	18.72455844	24.52453485
	1	1	3.157916758	0.022712531	60.71951844	0.001930759	18.83251758	24.5266745
		2	3.133647228	0.002909069	60.7117011	0.000498092	18.83503294	24.52602877
		3	3.151142074	0.015851588	60.71960667	0.000461628	18.83242062	24.52408377
	Base	-	2.311440205	2.342889346	25.23939223	25.58471365	22.65488089	22.34910747
	2	1	3.339327741	3.360274586	25.36357414	25.71310028	22.50533373	22.19982339
		2	3.30461711	3.414875918	25.36152276	25.71603137	22.50721681	22.19696733
		3	3.347465936	3.361990332	25.36373566	25.7133151	22.50525099	22.19952563
	Base	-	0.871359871	1.33672485	9.465808561	14.56347079	24.1622977	23.55727133
	3	1	1.503456347	2.154416315	9.475794155	14.59929978	24.08611793	23.45387911
		2	1.506637503	2.107939752	9.475394116	14.599313	24.08686539	23.45325393
		3	1.517161932	2.200075497	9.47560661	14.60149185	24.08425683	23.44763958

Table A.19 Loss minimisation results (V/V 4) (Continued)

Train position	Case	No.	TSS $V_{rail,T}$ (V)	TSS $V_{rail,M}$ (V)	Train $V_{rail,T}$ (V)	Train $V_{rail,M}$ (V)	$V_{T,train}$ (kV)	$V_{M,train}$ (kV)
P1	Base	-	3.416170146	4.143672106	37.33991543	45.30990412	21.4385942	20.19151027
	4	1	4.059720472	4.098452993	37.54096562	45.47785126	21.29719311	20.09959004
		2	4.096323251	4.081328488	37.54351073	45.47609217	21.29574169	20.10047144
		3	4.073325219	4.104973984	37.54141864	45.47823197	21.29702889	20.09944575
P2	Base	1	50.84034115	0.017194998	49.09756953	0.000442666	23.3125425	24.60478257
	1	1	50.81104353	0.065864779	49.07964591	0.001751304	23.31364286	24.60422416
		2	50.78866397	0.016471982	49.07861243	0.000431327	23.31398789	24.60477353
		3	50.82494289	0.01359802	49.08023954	0.000300804	23.31342971	24.60480564
	Base	-	24.41087574	24.69018674	23.56967353	23.83954589	24.28113546	24.00625739
	2	1	24.61216302	24.89579892	23.56735792	23.83737772	24.27840069	24.00346121
		2	24.61195196	24.88546661	23.5673319	23.83698685	24.27840471	24.00362501
		3	24.60696618	24.89395638	23.56719491	23.83728203	24.27848171	24.00349158
	Base	-	9.590568884	14.54689471	9.254945611	14.04223708	24.73530751	24.45351233
	3	1	9.714833689	14.71071632	9.254198999	14.04113643	24.73354503	24.45121852
		2	9.707991252	14.69572526	9.254046841	14.04069687	24.73365196	24.4514558
		3	9.736814836	14.69095344	9.254443279	14.04068184	24.73321483	24.45152518
	Base	-	34.59317211	40.52606544	33.4046029	39.13523645	23.9851611	23.39765358
	4	1	34.80472859	40.61118801	33.40063576	39.12528233	23.98238168	23.39689958
		2	34.77920814	40.64043245	33.39998762	39.12626185	23.98276554	23.39645291
		3	34.78836927	40.65677141	33.40003891	39.12715528	23.98263521	23.39619198

Table A.20 VUF minimisation results (V/V 1)

Train position	Case	No.	VUF (%)	IUF (%)	3φ PF	3φ Power (MW)	3φ Reactive (Mvar)
P1	Base	-	2.002556918	99.83890752	0.714089051	10.9146931	10.70018381
	1	1	1.997107422	97.19985953	0.706308644	11.05088275	11.07584393
		2	1.997133676	97.256479	0.706502523	11.04783761	11.06672757
		3	1.997133637	97.25734835	0.706506351	11.04780239	11.06657255
	Base	-	0.82644237	49.70315961	0.79842974	10.32742468	7.787809079
	2	1	0.808949021	45.86759689	0.768499293	10.51806814	8.757317857
		2	0.808949011	45.86698403	0.768493065	10.51811742	8.75753226
		3	0.808949016	45.86685652	0.768491917	10.51812986	8.757574575
	Base	-	0.421508693	53.75529912	0.823464823	5.089451385	3.506632405
	3	1	0.361102475	37.93361534	0.733571253	5.484017851	5.080634407
		2	0.363255527	37.66592212	0.729929797	5.526943028	5.175549543
		3	0.361102476	37.93293092	0.733563886	5.484059658	5.08078361
	Base	-	1.40027729	51.43362294	0.762122144	15.84627847	13.46163205
	4	1	1.347445771	44.68078908	0.716844885	16.40819264	15.95927988
		2	1.347445693	44.68000875	0.716838891	16.40832371	15.95968184
		3	1.347445837	44.68672181	0.716898178	16.40737485	15.95604403
P2	Base	1	1.601666797	99.85024226	0.822512658	10.20499872	7.056499806
	1	1	1.601650389	99.85014799	0.822526505	10.20508791	7.05619422
		2	1.601649631	99.85024483	0.82252555	10.20506094	7.056200899
		3	1.601650151	99.85023717	0.822527246	10.20508709	7.056174005
	Base	-	0.7690183437	49.68554862	0.836351321	10.10457682	6.623133679
	2	1	0.750893266	44.79579348	0.798847177	10.42026465	7.846486736
		2	0.750800943	45.11109499	0.801995336	10.38987612	7.738433748
		3	0.749709312	44.74944399	0.798553358	10.41082271	7.847345782

Table A.20 VUF minimisation results (V/V 1) (Continued)

Train position	Case	No.	VUF (%)	IUF (%)	3φ PF	3φ Power (MW)	3φ Reactive (Mvar)
P2	Base	-	0.402941792	53.05198318	0.841040755	5.039104737	3.241238139
	3	1	0.341053868	36.68368697	0.746648514	5.455175668	4.860232248
		2	0.341894527	36.7323066	0.746880037	5.463003915	4.863796552
		3	0.341053889	36.68529732	0.746667553	5.455080714	4.859867592
	Base	-	1.19578484	50.28674479	0.829872132	15.22345523	10.23529008
	4	1	1.141199773	43.48605985	0.786051365	15.82552671	12.44540344
		2	1.129853403	41.88411289	0.772344106	15.95608276	13.12287268
		3	1.131543962	41.99867416	0.773370445	15.95911665	13.08215483

Table A.21 VUF minimisation results (V/V 2)

Train position	Case	No.	P_T (MW)	Q_T (Mvar)	P_M (MW)	Q_M (Mvar)	P_{loss} (MW)	VD (kV)
P1	Base	-	10.88640608	10.59386305	0.008301551	0.022852623	0.914693103	45.38185602
	1	1	10.89088649	10.54772804	0.139883982	0.444119965	1.050882751	47.11131636
		2	10.89086756	10.54768058	0.137014459	0.435703931	1.047837614	46.86674988
		3	10.89087708	10.54766943	0.136970258	0.435562321	1.04780239	46.86697294
	Base	-	5.158265329	3.869370284	5.162214311	3.889433268	0.327424677	32.40747018
	2	1	5.345434275	4.833855483	5.164362771	3.888922947	0.518068135	34.93565961
		2	5.345489987	4.83407281	5.164356783	3.888921828	0.518117424	34.93610068
		3	5.345500785	4.834114898	5.164358487	3.888922314	0.518129864	34.93622344
	Base	-	2.029569839	1.36834987	3.058249158	2.131464968	0.089451385	14.62013373
	3	1	2.409807276	2.885323831	3.058955407	2.13172416	0.484017851	24.51208365
		2	2.456949123	2.997811537	3.058969211	2.13177806	0.526943028	21.28433716
		3	2.409849951	2.885472859	3.058954454	2.131723981	0.484059658	24.51200349

Table A.21 VUF minimisation results (V/V 2) (Continued)

Train position	Case	No.	P_T (MW)	Q_T (Mvar)	P_M (MW)	Q_M (Mvar)	P_{loss} (MW)	VD (kV)
P1	Base	-	7.33648456	5.99660184	8.491302147	7.387800499	0.846278466	54.55053167
	4	1	7.885140197	8.472998603	8.500083309	7.390357486	1.40819264	61.99238367
		2	7.885239244	8.473385586	8.500114042	7.390367078	1.408323712	61.99401864
		3	7.884326335	8.469825277	8.500089554	7.390337393	1.407374854	61.98263565
P2	Base	1	10.18039676	6.965674358	0.008352293	0.022992304	0.204998719	15.64995204
	1	1	10.18059073	6.96580884	0.008357508	0.023010571	0.205087909	15.66156421
		2	10.18057449	6.965857105	0.008352463	0.022992656	0.205060937	15.66746559
		3	10.18061847	6.965904297	0.008352881	0.022994594	0.205087092	15.66869352
	Base	-	5.048124317	3.293985177	5.048856027	3.297437481	0.104576821	12.16624485
	2	1	5.350225161	4.461146279	5.04905886	3.297851167	0.420264653	20.44182297
		2	5.332228722	4.404730605	5.049050914	3.297815889	0.389876117	20.06859048
		3	5.353551474	4.515203503	5.049056458	3.297844463	0.410822713	17.9550059
	Base	-	2.014673069	1.289646845	3.022510249	1.943570434	0.039104737	5.705057254
	3	1	2.424888609	2.884354091	3.022569873	1.943701137	0.455175668	14.08797273
		2	2.427368264	2.865633506	3.022570207	1.94370143	0.463003915	16.48983207
		3	2.424795373	2.884004381	3.022571957	1.943702041	0.455080714	14.08606067
	Base	-	7.088100154	4.706638373	8.117493281	5.454088807	0.223455232	18.53092939
	4	1	7.685390467	6.892357569	8.120901261	5.472732196	0.825526712	27.08233245
		2	7.799237904	7.505822067	8.118439315	5.456848982	0.956082762	27.59182248
		3	7.818673139	7.533438447	8.1184317	5.456822905	0.95911665	27.32329989

Table A.22 VUF minimisation results (V/V 3)

Train position	Case	No.	$V_{CF,T}$ (kV)	$V_{CR,T}$ (kV)	$V_{FR,T}$ (kV)	$V_{CF,M}$ (kV)	$V_{CR,M}$ (kV)	$V_{FR,M}$ (kV)
P1	Base	-	48.30216449	24.13932669	24.16283804	49.06393523	24.53194929	24.53198594
	1	1	48.30148656	24.15073134	24.15075571	49.00246077	24.51858069	24.48388012
		2	48.30164892	24.15077365	24.15087576	49.00381046	24.48931866	24.51449184
		3	48.3016531	24.1508191	24.15083449	49.00383159	24.48934901	24.51448261
	Base	-	49.52461591	24.75761177	24.76700424	48.97509193	24.48278238	24.49230966
	2	1	49.38223127	24.6698729	24.71235843	48.93616566	24.46629079	24.46987501
		2	49.38219905	24.66986992	24.7123292	48.93615647	24.46629808	24.46985852
		3	49.38219294	24.66986953	24.71232348	48.93615454	24.466293	24.46986168
	Base	-	49.87115021	24.93383817	24.93731206	49.50760706	24.75112244	24.75648466
	3	1	49.64149486	24.71178903	24.92970584	49.44001803	24.71872313	24.72129495
		2	49.62737182	24.9027271	24.72464476	49.43484126	24.71612298	24.71871833
		3	49.64147287	24.71177807	24.9296948	49.44001133	24.71871771	24.72129367
	Base	-	49.24028688	24.61310798	24.62717909	48.22088115	24.10183144	24.11904994
	4	1	48.86826923	24.459858	24.40841125	48.11466819	24.05627908	24.05838945
		2	48.86821146	24.4598377	24.40837378	48.11464884	24.05625861	24.05839056
		3	48.86875506	24.46002275	24.40873234	48.11481443	24.05629127	24.0585235
P2	Base	1	48.85650857	24.38607356	24.47049164	49.21365209	24.60680772	24.60684437
	1	1	48.85655495	24.38728763	24.46932388	49.21365412	24.60656332	24.60709079
		2	48.85655194	24.38735202	24.46925649	49.21365733	24.60687139	24.60678594
		3	48.8565558	24.38755503	24.46905732	49.21365641	24.60686872	24.60678769
	Base	-	49.62318796	24.79175677	24.83144473	49.08574211	24.5227984	24.5629577
	2	1	49.44299925	24.6134772	24.82953755	49.0321939	24.49666767	24.5355402
		2	49.45899261	24.70601571	24.75298628	49.03707625	24.49909384	24.53799638
		3	49.44299017	24.73008659	24.71291436	49.03271169	24.49690978	24.53581589

Table A.22 VUF minimisation results (V/V 3) (Continued)

Train position	Case	No.	$V_{CF,T}$ (kV)	$V_{CR,T}$ (kV)	$V_{FR,T}$ (kV)	$V_{CF,M}$ (kV)	$V_{CR,M}$ (kV)	$V_{FR,M}$ (kV)
P2	Base	-	49.887044	24.93581358	24.95123255	49.53806537	24.75729907	24.7807712
	3	1	49.65072815	24.75694197	24.89379054	49.46798885	24.72258275	24.745411
		2	49.65012792	24.72700066	24.92313045	49.46744235	24.72230233	24.74514492
		3	49.65078182	24.75699209	24.89379409	49.46800476	24.72259277	24.74541689
	Base	-	49.47887068	24.71110095	24.76779648	48.56697395	24.25012261	24.31688826
	4	1	49.15229219	24.58132016	24.57098974	48.46569517	24.20742816	24.2583044
		2	49.04975857	24.39888221	24.65091149	48.43985136	24.18782516	24.25206327
		3	49.05568236	24.56216254	24.49354258	48.44086978	24.18831848	24.25258837

Table A.23 VUF minimisation results (V/V 4)

Train position	Case	No.	TSS $V_{rail,T}$ (V)	TSS $V_{rail,M}$ (V)	Train $V_{rail,T}$ (V)	Train $V_{rail,M}$ (V)	$V_{T,train}$ (kV)	$V_{M,train}$ (kV)
P1	Base	-	5.582963653	0.008744328	61.07461976	0.000231806	18.72455844	24.52453485
	1	1	1.580404004	8.038086613	59.75750438	0.633856735	19.16268991	24.53817754
		2	1.579812702	5.826610617	59.75887376	0.579895259	19.16226555	24.33828747
		3	1.580633676	5.817471964	59.75667887	0.579326464	19.1629351	24.33926686
	Base	-	2.311440205	2.342889346	25.23939223	25.58471365	22.65488089	22.34910747
	2	1	9.968422822	1.184037684	27.7150639	25.4857045	20.30675378	22.46501511
		2	9.962373589	1.18004933	27.71510971	25.48574606	20.30668143	22.46483008
		3	9.961145111	1.181335697	27.71511624	25.48585489	20.30666855	22.46483739
	Base	-	0.871359871	1.33672485	9.465808561	14.56347079	24.1622977	23.55727133
	3	1	50.57823844	0.787094106	10.79195736	14.56075179	22.32071742	23.58974865
		2	41.28061958	0.791648551	8.991379472	14.56223292	23.70261604	23.58733312
		3	50.57822071	0.787785119	10.79204367	14.56080423	22.32076104	23.58964514

Table A.23 VUF minimisation results (V/V 4) (Continued)

Train position	Case	No.	TSS $V_{rail,T}$ (V)	TSS $V_{rail,M}$ (V)	Train $V_{rail,T}$ (V)	Train $V_{rail,M}$ (V)	$V_{T,train}$ (kV)	$V_{M,train}$ (kV)
P1	Base	-	3.416170146	4.143672106	37.33991543	45.30990412	21.4385942	20.19151027
	4	1	11.86965892	1.413633384	42.29172171	44.83121617	18.65868898	20.43753558
		2	11.8736294	1.416027318	42.29199021	44.82972872	18.65855934	20.43832164
		3	11.83350689	1.423337684	42.28981883	44.83178705	18.65964243	20.43741775
P2	Base	1	50.84034115	0.017194998	49.09756953	0.000442666	23.3125425	24.60478257
	1	1	50.04978057	0.242451019	49.06368471	0.003130908	23.32467452	24.60229343
		2	50.00956552	0.039387411	49.0609711	0.001205918	23.32534237	24.60540448
		3	49.87694697	0.037699756	49.05535634	0.000426312	23.3273865	24.60538128
	Base	-	24.41087574	24.69018674	23.56967353	23.83954589	24.28113546	24.00625739
	2	1	99.73955358	24.26979195	25.50493816	23.85827473	23.19860658	23.98562883
		2	25.02998219	24.27819642	24.35026477	23.85613143	24.07235207	23.98795238
		3	18.07789746	24.28049269	23.46948991	23.85832269	24.38165403	23.9857211
	Base	-	9.590568884	14.54689471	9.254945611	14.04223708	24.73530751	24.45351233
	3	1	63.16136002	14.33938235	9.774055055	14.06005672	23.87368378	24.42145669
		2	89.97129412	14.34387935	10.62813531	14.06036633	23.57196999	24.42110845
		3	63.13990443	14.33750466	9.774021022	14.06015686	23.87397558	24.42148544
	Base	-	34.59317211	40.52606544	33.4046029	39.13523645	23.9851611	23.39765358
	4	1	21.07590482	35.8521624	33.85551982	38.98338503	23.98370559	23.42534505
		2	117.3857998	39.72472317	35.94788886	39.21781152	22.5481092	23.34535091
		3	40.16133502	39.73464225	32.79693512	39.2173337	24.18001003	23.34571152

Table A.24 Three-phase power factor maximisation results (V/V 1)

Train position	Case	No.	VUF (%)	IUF (%)	3φ PF	3φ Power (MW)	3φ Reactive (Mvar)
P1	Base	-	2.002556918	99.83890752	0.714089051	10.9146931	10.70018381
	1	1	1.998696161	99.83921099	0.71600527	10.92497502	10.65169404
		2	1.998674716	99.83916699	0.716005106	10.92486522	10.65159199
		3	1.998680206	99.83921422	0.716005342	10.92489253	10.65161141
	Base	-	0.826442373	49.70315961	0.79842974	10.32742468	7.787809079
	2	1	0.826552379	49.70265279	0.798691577	10.33238234	7.784499375
		2	0.826549535	49.70265407	0.798691549	10.33234703	7.78447351
		3	0.826545687	49.70265481	0.798691518	10.33229952	7.784438567
	Base	-	0.421508693	53.75529912	0.823464823	5.089451385	3.506632405
	3	1	0.421533502	53.75267673	0.823558815	5.090586783	3.50617102
		2	0.42153287	53.75264621	0.823558818	5.09058212	3.506167768
		3	0.421532417	53.7526499	0.823558816	5.090576348	3.506163818
	Base	-	1.40027729	51.43362294	0.762122144	15.84627847	13.46163205
	4	1	1.399469787	51.41354209	0.762826754	15.85890794	13.44265422
		2	1.399474651	51.41351384	0.762826765	15.85896939	13.44270582
		3	1.399479358	51.41353377	0.762826777	15.85901475	13.44274378
P2	Base	1	1.601666797	99.85024226	0.822512658	10.20499872	7.056499806
	1	1	1.601705513	99.85026102	0.822541562	10.20561389	7.056158524
		2	1.601703542	99.85025558	0.822541522	10.20560173	7.056151198
		3	1.601703787	99.85024949	0.822541293	10.20560087	7.056156674
	Base	-	0.7690183437	49.68554862	0.836351321	10.10457682	6.623133679
	2	1	0.769029594	49.68553146	0.83636148	10.10485289	6.623046912
		2	0.769029854	49.68553104	0.836361486	10.1048564	6.623049053
		3	0.769030477	49.68553122	0.836361434	10.10486372	6.623055233

Table A.24 Three-phase power factor maximisation results (V/V 1) (Continued)

Train position	Case	No.	VUF (%)	IUF (%)	3φ PF	3φ Power (MW)	3φ Reactive (Mvar)
P2	Base	-	0.402941792	53.05198318	0.841040755	5.039104737	3.241238139
	3	1	0.402944404	53.05187189	0.841045305	5.039175416	3.241223686
		2	0.402944348	53.05185106	0.841045052	5.039175138	3.241226837
		3	0.402944447	53.05188143	0.84104534	5.039175259	3.241223126
	Base	-	1.19578484	50.28674479	0.829872132	15.22345523	10.23529008
	4	1	1.195803239	50.28644589	0.829890524	15.22412824	10.23501388
		2	1.195803261	50.28644446	0.829890516	15.22412879	10.23501454
		3	1.195803181	50.28643636	0.829890519	15.22413024	10.23501542

Table A.25 Three-phase power factor maximisation results (V/V 2)

Train position	Case	No.	P_T (MW)	Q_T (Mvar)	P_M (MW)	Q_M (Mvar)	P_{loss} (MW)	VD (kV)
P1	Base	-	10.88640608	10.59386305	0.008301551	0.022852623	0.914693103	45.38185602
	1	1	10.89689176	10.54622388	0.008302114	0.022854127	0.924975019	45.54303266
		2	10.89678128	10.54611728	0.008303607	0.022862074	0.924865221	45.53450369
		3	10.89681023	10.54614504	0.008301907	0.022853473	0.924892533	45.540332
	Base	-	5.158265329	3.869370284	5.162214311	3.889433268	0.327424677	32.40747018
	2	1	5.160721569	3.867835292	5.164758072	3.887834942	0.332382341	32.60862125
		2	5.16069193	3.867813202	5.164752254	3.887830568	0.332347027	32.60714284
		3	5.160657176	3.867788385	5.164739509	3.887820492	0.332299518	32.60563547
	Base	-	2.029569839	1.36834987	3.058249158	2.131464968	0.089451385	14.62013373
	3	1	2.029908963	1.368243871	3.05905454	2.131147524	0.090586783	14.7093615
		2	2.029909742	1.368244366	3.059049069	2.131143659	0.09058212	14.70904603
		3	2.029907155	1.368242536	3.059045853	2.13114141	0.090576348	14.70858055

Table A.25 Three-phase power factor maximisation results (V/V 2) (Continued)

Train position	Case	No.	P_T (MW)	Q_T (Mvar)	P_M (MW)	Q_M (Mvar)	P_{loss} (MW)	VD (kV)
P1	Base	-	7.33648456	5.99660184	8.491302147	7.387800499	0.846278466	54.55053167
	4	1	7.341867567	5.990841439	8.498683397	7.375144742	0.858907936	54.87254879
		2	7.341906576	5.990874016	8.49870569	7.375163148	0.858969388	54.87359133
		3	7.341915013	5.990881023	8.498742563	7.375193886	0.859014748	54.87477875
P2	Base	1	10.18039676	6.965674358	0.008352293	0.022992304	0.204998719	15.64995204
	1	1	10.18122033	6.966201507	0.008352304	0.022992252	0.205613893	15.66612138
		2	10.18120737	6.966191094	0.008352585	0.022993163	0.205601735	15.66675045
		3	10.18122163	6.966259785	0.008352898	0.022994275	0.205600868	15.67144935
	Base	-	5.048124317	3.293985177	5.048856027	3.297437481	0.104576821	12.16624485
	2	1	5.048297831	3.294095674	5.049031917	3.2975458	0.104852886	12.17299011
		2	5.048298778	3.294091972	5.049033327	3.297546827	0.104856398	12.1724603
		3	5.048294199	3.294082812	5.049046797	3.297568697	0.104863722	12.17232687
	Base	-	2.014673069	1.289646845	3.022510249	1.943570434	0.039104737	5.705057254
	3	1	2.01469919	1.289660662	3.022571118	1.943610128	0.039175416	5.706340679
		2	2.014697362	1.289655614	3.022572853	1.943619098	0.039175138	5.705985223
		3	2.014699714	1.289663686	3.022571022	1.943608979	0.039175259	5.70710175
	Base	-	7.088100154	4.706638373	8.117493281	5.454088807	0.223455232	18.53092939
	4	1	7.088465077	4.706869001	8.118001166	5.454414489	0.224128236	18.54695137
		2	7.088463113	4.706859488	8.11799995	5.454409099	0.224128792	18.54598186
		3	7.088471475	4.706874413	8.117995682	5.454406066	0.224130243	18.54649744

Table A.26 Three-phase power factor maximisation results (V/V 3)

Train position	Case	No.	$V_{CF,T}$ (kV)	$V_{CR,T}$ (kV)	$V_{FR,T}$ (kV)	$V_{CF,M}$ (kV)	$V_{CR,M}$ (kV)	$V_{FR,M}$ (kV)
P1	Base	-	48.30216449	24.13932669	24.16283804	49.06393523	24.53194929	24.53198594
	1	1	48.30933189	24.15790764	24.15142484	49.06479785	24.53247001	24.53232785
		2	48.30934993	24.15785697	24.15149354	49.0648064	24.53214106	24.53266534
		3	48.30934545	24.15785707	24.15148897	49.06480518	24.53241667	24.53238851
	Base	-	49.52461591	24.75761177	24.76700424	48.97509193	24.48278238	24.49230966
	2	1	49.52501328	24.76133918	24.76367424	48.9752163	24.48648553	24.48873091
		2	49.52501657	24.76126088	24.76375582	48.97521934	24.48649103	24.48872845
		3	49.52502031	24.76129091	24.76372954	48.97522363	24.4864378	24.48878597
	Base	-	49.87115021	24.93383817	24.93731206	49.50760706	24.75112244	24.75648466
	3	1	49.87121716	24.93495151	24.93626567	49.50763199	24.75289459	24.75473746
		2	49.87121692	24.93494573	24.93627121	49.50763254	24.75288263	24.75474996
		3	49.87121711	24.93493129	24.93628584	49.50763309	24.75287599	24.75475715
	Base	-	49.24028688	24.61310798	24.62717909	48.22088115	24.10183144	24.11904994
	4	1	49.24193801	24.62020958	24.6217287	48.22260129	24.11127313	24.11132851
		2	49.24193325	24.62021131	24.6217222	48.22259493	24.1112462	24.11134909
		3	49.24193302	24.62025228	24.62168101	48.22258908	24.11125183	24.11133762
P2	Base	1	48.85650857	24.38607356	24.47049164	49.21365209	24.60680772	24.60684437
	1	1	48.85655039	24.38834849	24.46825826	49.21362677	24.60681215	24.60681461
		2	48.85655177	24.38834397	24.46826416	49.21362759	24.6068553	24.60677229
		3	48.85655112	24.38852189	24.46808559	49.21362736	24.60687284	24.60675453
	Base	-	49.62318796	24.79175677	24.83144473	49.08574211	24.5227984	24.5629577
	2	1	49.62320133	24.79258817	24.83062663	49.08574033	24.52361049	24.56214375
		2	49.62320116	24.79255867	24.83065595	49.08574003	24.52361146	24.56214248
		3	49.6232016	24.79251181	24.83070325	49.08573906	24.52369349	24.56205948

Table A.26 Three-phase power factor maximisation results (V/V 3) (Continued)

Train position	Case	No.	$V_{CF,T}$ (kV)	$V_{CR,T}$ (kV)	$V_{FR,T}$ (kV)	$V_{CF,M}$ (kV)	$V_{CR,M}$ (kV)	$V_{FR,M}$ (kV)
P2	Base	-	49.887044	24.93581358	24.95123255	49.53806537	24.75729907	24.7807712
	3	1	49.88704716	24.93604408	24.9510052	49.53806529	24.7577602	24.78030997
		2	49.88704683	24.93594257	24.95110638	49.53806507	24.75783601	24.78023394
		3	49.88704726	24.93609767	24.95095171	49.53806531	24.75774838	24.78032181
	Base	-	49.47887068	24.71110095	24.76779648	48.56697395	24.25012261	24.31688826
	4	1	49.47890888	24.7123974	24.76653809	48.56698089	24.25174292	24.31527471
		2	49.4789088	24.7123565	24.76657891	48.56698083	24.25172394	24.31529363
		3	49.47890807	24.71240092	24.76653375	48.56698087	24.25172355	24.31529405

Table A.27 Three-phase power factor maximisation results (V/V 4)

Train position	Case	No.	TSS $V_{rail,T}$ (V)	TSS $V_{rail,M}$ (V)	Train $V_{rail,T}$ (V)	Train $V_{rail,M}$ (V)	$V_{T,train}$ (kV)	$V_{M,train}$ (kV)
P1	Base	-	5.582963653	0.008744328	61.07461976	0.000231806	18.72455844	24.52453485
	1	1	2.291913901	0.033075291	59.2652557	0.00072362	19.3367397	24.52808607
		2	2.271948322	0.12174713	59.27227447	0.003185201	19.33427948	24.51778997
		3	2.273276553	0.006777285	59.27036795	0.000587063	19.33489584	24.52635597
	Base	-	2.311440205	2.342889346	25.23939223	25.58471365	22.65488089	22.34910747
	2	1	1.009362435	1.006135937	25.09490301	25.43133636	22.82335498	22.52168775
		2	1.029168907	1.0050028	25.0967254	25.43149954	22.8214869	22.52146892
		3	1.021055453	1.01818283	25.09739856	25.43264428	22.82025839	22.5204816
	Base	-	0.871359871	1.33672485	9.465808561	14.56347079	24.1622977	23.55727133
	3	1	0.462698468	0.673945934	9.458948388	14.53215767	24.21758815	23.64547582
		2	0.464528703	0.677397434	9.458975612	14.5323775	24.21763687	23.64497432
		3	0.468991843	0.679396362	9.459072409	14.5324659	24.21724113	23.64469788

Table A.27 Three-phase power factor maximisation results (V/V 4) (Continued)

Train position	Case	No.	TSS $V_{rail,T}$ (V)	TSS $V_{rail,M}$ (V)	Train $V_{rail,T}$ (V)	Train $V_{rail,M}$ (V)	$V_{T,train}$ (kV)	$V_{M,train}$ (kV)
P1	Base	-	3.416170146	4.143672106	37.33991543	45.30990412	21.4385942	20.19151027
	4	1	1.233207686	1.366037257	36.91793008	44.57561168	21.72251865	20.56223498
		2	1.233477534	1.366881718	36.91635869	44.57460583	21.72366576	20.56269806
		3	1.227633478	1.367287181	36.9162788	44.57312223	21.72398408	20.56358041
P2	Base	1	50.84034115	0.017194998	49.09756953	0.000442666	23.3125425	24.60478257
	1	1	49.32186807	0.003625621	49.04166402	0.000115016	23.33543227	24.60494336
		2	49.32601662	0.038308184	49.04162347	0.001082704	23.33538142	24.60537716
		3	49.21283498	0.054450291	49.035871	0.001546889	23.33719145	24.60555607
	Base	-	24.41087574	24.69018674	23.56967353	23.83954589	24.28113546	24.00625739
	2	1	23.8563413	24.14260006	23.55967606	23.82969046	24.28950394	24.01449904
		2	23.8746057	24.14170648	23.5603612	23.82970997	24.28920506	24.0145101
		3	23.90472791	24.08812396	23.56126331	23.82836608	24.28872762	24.01534588
	Base	-	9.590568884	14.54689471	9.254945611	14.04223708	24.73530751	24.45351233
	3	1	9.433804517	14.23723719	9.25436941	14.03865221	24.7376293	24.45818776
		2	9.498263569	14.18967189	9.255800924	14.03736314	24.73660074	24.45895805
		3	9.400222599	14.24463073	9.253541433	14.03886245	24.73817263	24.45806767
	Base	-	34.59317211	40.52606544	33.4046029	39.13523645	23.9851611	23.39765358
	4	1	33.73264454	39.43750072	33.38330697	39.10299445	23.99813282	23.41405516
		2	33.75851154	39.44955993	33.38433323	39.10350856	23.99771789	23.41386262
		3	33.72949445	39.45015692	33.3833803	39.10343869	23.99817157	23.41385904

Table A.28 Optimal tap positions in loss minimisation (V/V)

Train position	Case	No.	Tap 1	Tap 2	Tap 3	Tap 4	Tap 5	Tap 6
P1	1	1	0.991822034	0.987752932	0.989482167	1.000055682	0.999890013	0.999771923
		2	0.991597346	0.987493217	0.989371745	0.99996088	0.999912738	0.999870038
		3	0.991861676	0.98773414	0.989451242	1.000025566	1.00006515	1.000066013
	2	1	1.01629894	1.011323763	1.003964309	1.003970818	1.011421234	1.016499901
		2	1.01613875	1.011137613	1.003830414	1.00418476	1.011656237	1.016796261
		3	1.016304666	1.011333001	1.003996138	1.003977449	1.01143668	1.016539986
	3	1	1.007788713	1.00586719	1.002372347	1.003116566	1.00792212	1.010910995
		2	1.007775681	1.005745758	1.002386232	1.002935716	1.008023496	1.010925805
		3	1.008045238	1.005943549	1.002423412	1.003286169	1.008405212	1.011561409
	4	1	1.016409349	1.010277474	1.002519598	0.999756683	1.005886541	1.012047385
		2	1.016543768	1.01041542	1.002665925	0.999685037	1.00583442	1.011928249
		3	1.016410232	1.010307167	1.002574233	0.999783954	1.005906457	1.012055174
P2	1	1	0.994143562	0.99467059	0.999874629	1.000090191	1.000160398	1.000213524
		2	0.994025283	0.994601492	0.99981521	0.999998594	0.99999906	0.999999215
		3	0.994150282	0.994701586	0.999911322	0.999993439	0.999978861	0.999989727
	2	1	0.997788682	0.998069712	1.000501689	1.000518475	0.998048662	0.997778821
		2	0.997774901	0.998063204	1.000501073	1.000490969	0.997989056	0.997698627
		3	0.99776983	0.998049338	1.000488107	1.000513494	0.998029723	0.997755783
	3	1	0.999248041	0.999365962	1.000313118	1.000414101	0.998970621	0.998799695
		2	0.999222916	0.999339518	1.000295368	1.000374697	0.998893766	0.998713827
		3	0.99926826	0.999371678	1.000369363	1.000362546	0.998907155	0.998754108
	4	1	0.996735476	0.997071299	1.000520368	1.000187883	0.996021498	0.995724943
		2	0.996734322	0.997071228	1.000454381	1.000265152	0.996073022	0.995557256
		3	0.996667722	0.997014483	1.000477534	1.000309569	0.996197163	0.995802758

Table A.29 Optimal tap positions in VUF minimisation (V/V)

Train position	Case	No.	Tap 1	Tap 2	Tap 3	Tap 4	Tap 5	Tap 6
P1	1	1	0.953686506	0.959272263	0.978129635	0.968892076	1.029515076	0.938139138
		2	0.953731111	0.959332167	0.978202748	1.022539449	0.956661029	1.046525047
		3	0.953690603	0.959246398	0.97812177	1.022505502	0.956601085	1.046419364
	2	1	1.2	1.2	1.025656549	0.994840481	0.988558752	0.985468575
		2	1.2	1.2	1.025632154	0.994819024	0.988565846	0.985497264
		3	1.2	1.199999779	1.025627206	0.99482615	0.988580619	0.985479817
	3	1	1.069087767	1.2	1.199999993	0.997639072	0.994598265	0.992917217
		2	1.059323326	0.946219275	0.850012798	0.997659883	0.994544228	0.99291115
		3	1.069066851	1.2	1.2	0.99764251	0.994608435	0.992925319
	4	1	1.199999833	1.199997733	0.93425628	0.986182095	0.971828545	0.9660181
		2	1.2	1.2	0.934240335	0.986203542	0.971742385	0.965941967
		3	1.199999942	1.2	0.934400516	0.986295457	0.97186565	0.966013502
P2	1	1	0.998497398	0.998282673	0.997903182	1.000428486	1.000116255	1.000634758
		2	0.997881398	0.997907549	0.997792714	0.999897306	0.999791707	0.999791705
		3	0.997654598	0.997651537	0.997438349	0.999898257	0.999933501	1.000170473
	2	1	1.071530475	1.199999994	1.161681032	0.998816013	1.000086978	1.000093859
		2	1.2	1.2	1.000985878	0.998845741	1.000126496	1.000133663
		3	1.2	1.011340868	0.948768072	0.998845526	1.000117783	1.00011507
	3	1	0.85	1.000992366	1.109985595	0.999402395	1.000145316	1.00013929
		2	1.027246022	1.19999912	1.164705526	0.999414145	1.000172679	1.000194774
		3	0.850000139	1.001047777	1.109939114	0.999397862	1.000188612	1.000154715
	4	1	1.2	0.915334159	0.889191223	0.997565412	0.999651835	0.999663462
		2	0.85	1.04529325	1.185576112	0.9975513	0.999639078	0.99964372
		3	1.2	0.915310495	0.889243863	0.997580811	0.999667183	0.999663887

Table A.30 Optimal tap positions in 3-phase power factor maximisation (V/V)

Train position	Case	No.	Tap 1	Tap 2	Tap 3	Tap 4	Tap 5	Tap 6
P1	1	1	0.933996563	0.944528594	0.972190614	0.99984947	0.999734461	0.99970634
		2	0.934262523	0.9447677	0.972300017	1.00041432	1.000535543	1.000749485
		3	0.934234965	0.944671023	0.972296973	0.999945448	0.999902395	0.999848687
	2	1	0.98231036	0.986313844	0.993968734	0.993700335	0.98577867	0.981655573
		2	0.982496023	0.986473688	0.994107592	0.99369286	0.985799202	0.981677528
		3	0.982647971	0.986557794	0.994056366	0.993790357	0.985899361	0.981760486
	3	1	0.994295151	0.995759945	0.99820919	0.997038735	0.993062614	0.990795998
		2	0.994289736	0.995756132	0.998219043	0.997059353	0.993107349	0.990842923
		3	0.994327937	0.995788749	0.998243582	0.997071117	0.993126745	0.990874212
	4	1	0.96990094	0.97594864	0.989008202	0.984433587	0.967226772	0.959636272
		2	0.969775769	0.975849616	0.989002309	0.984479169	0.967137392	0.959631362
		3	0.969648578	0.975912915	0.988927029	0.98446395	0.967086177	0.959500726
P2	1	1	0.999584548	0.999620942	0.995976219	0.99997141	0.99993394	0.999946181
		2	0.99960306	0.999557556	0.995986852	0.9998991	0.99981052	0.999938616
		3	0.998891263	0.99907262	0.995678235	0.999869096	0.999757705	0.999540714
	2	1	1.000191463	1.00021544	0.998551901	0.99855553	1.000270597	1.000303447
		2	1.000277754	1.000320086	0.998601175	0.998553233	1.000285	1.00027863
		3	1.000526612	1.000408511	0.998681784	0.998409214	1.000192643	1.000216856
	3	1	1.000355574	1.000329197	0.999595836	0.999189535	1.000174538	1.000156007
		2	1.000593309	1.00057258	0.999766546	0.999061204	0.999964052	1.000011635
		3	1.000175731	1.000179158	0.999506106	0.999209477	1.00021027	1.000184111
	4	1	1.000181298	1.000209458	0.997748033	0.997097177	1.000003318	0.999983956
		2	1.000311604	1.000319666	0.997817611	0.997130127	1.000053831	0.999996033
		3	1.000260186	1.000254641	0.997740206	0.99713152	1.000022293	1.000026398

Appendix B

Simulation verification

B.1 Introduction

This appendix shows the verification of simulation in this study by graphically comparing the result of the proposed calculation using MATLAB with the result from the power flow study report using the C++-based RR version 13 software (by Front Range Systems Consultants, FRSC). The simulation contains train movement calculation, current-based Newton Raphson power flow calculation, and traction power supply components' models which are all verified in this comparison. A test system used in the verification is the East Corridor line, which is introduced in Chapter 6.

B.2 Comparative results for verification

In order to confirm the correctness of the simulation, the following results are collected for comparison: up-track and down-track speed profiles shown in Fig. B.1 – B.2, traction voltage profiles and grade profiles depicted in Fig. B.3 – B.4.

The speed profiles show train speed versus distance from the first to the last passenger station. The figures also include different speed limits on different parts of the track. The voltage profiles show a per-unit traction voltage of one of the trains running on the track versus train position. The curves obtained from both MATLAB and RR version 13 are similar in value and a trend. For the voltage profiles, the curves from this study primarily have the same increasing and decreasing trends as those of RR version13. Besides, at the maximum and minimum voltage points, the difference between the voltage from MATLAB and RR version 13 is less than 2%. Finally, Fig. B.5 shows a tractive force versus a train speed simulated by the proposed simulation using MATLAB and that using in the FRSC's power flow simulation report (green curve in Fig. B.5-b).

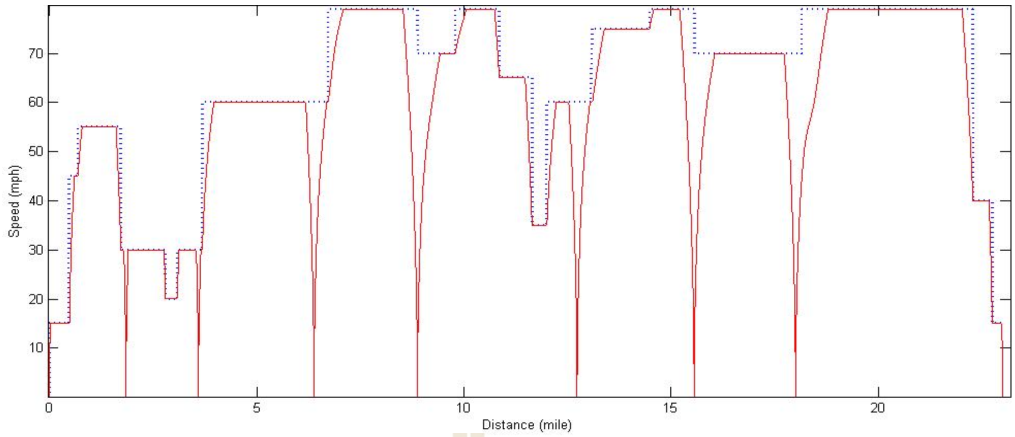

(a)

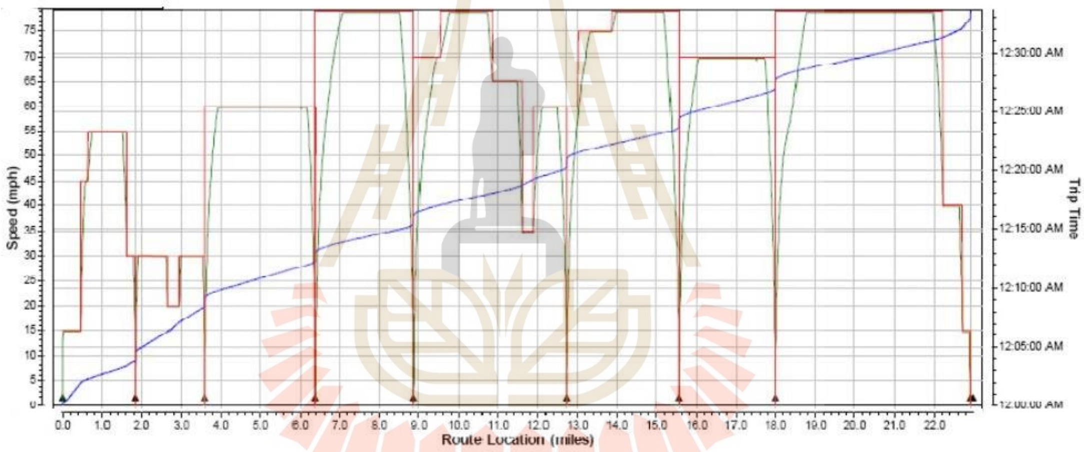

(b)

Fig. B.1 East Corridor line's up-track speed profile

(a) MATLAB, (b) RR version 13

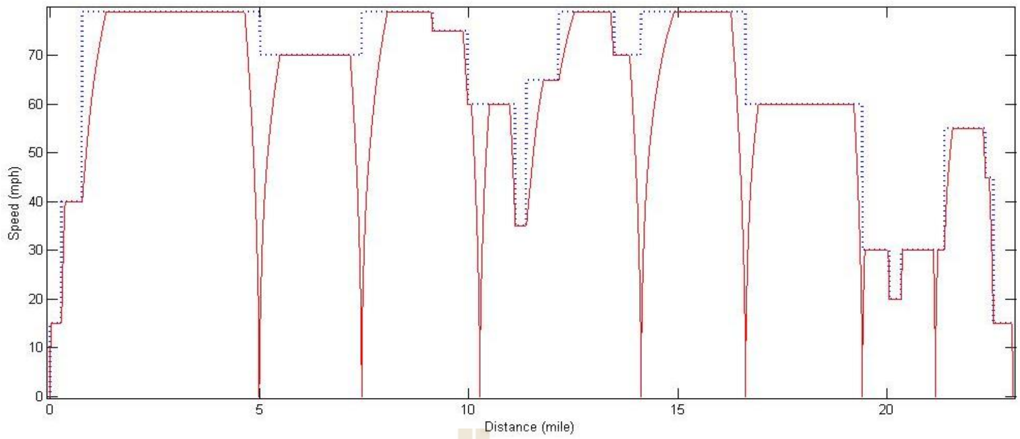

(a)

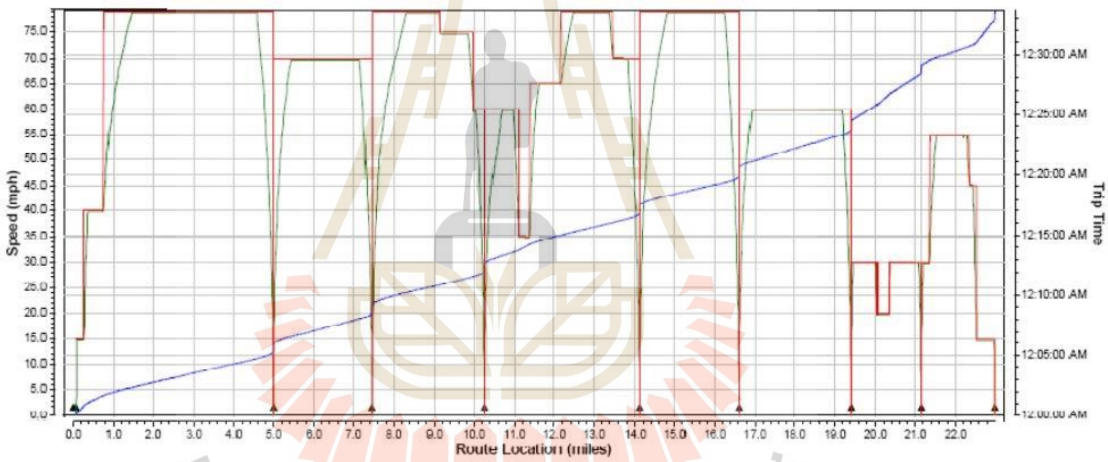

(b)

Fig. B.2 East Corridor line's down-track speed profile

(a) MATLAB, (b) RR version 13

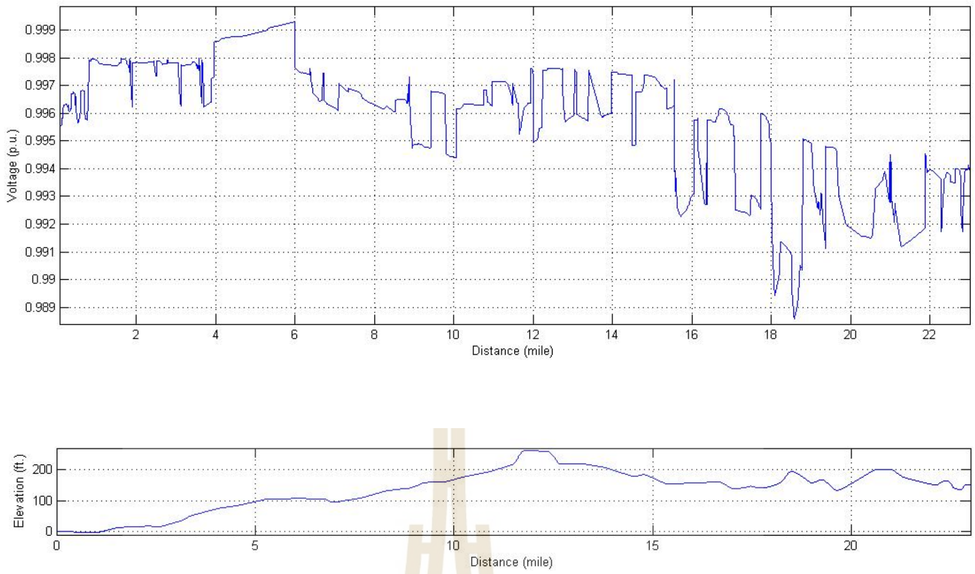

(a)

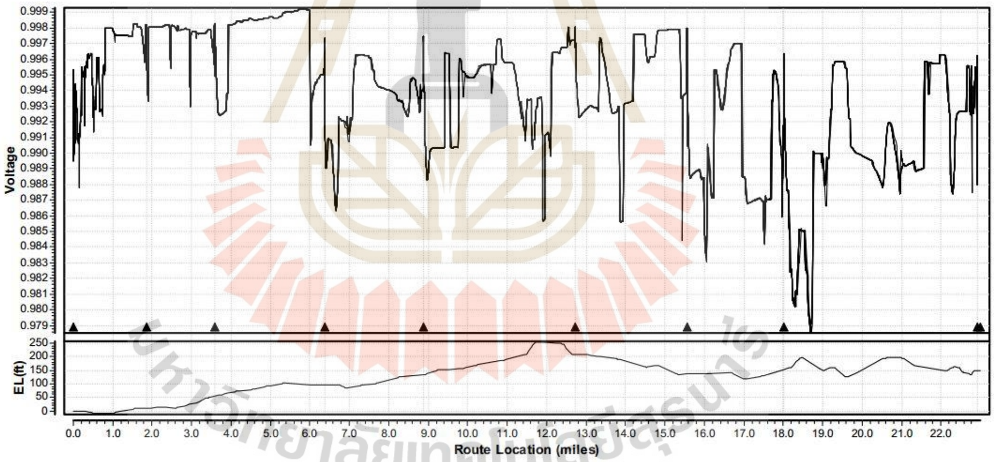

(b)

Fig. B.3 East Corridor line's up-track traction voltage and grade profile

(a) MATLAB, (b) RR version 13

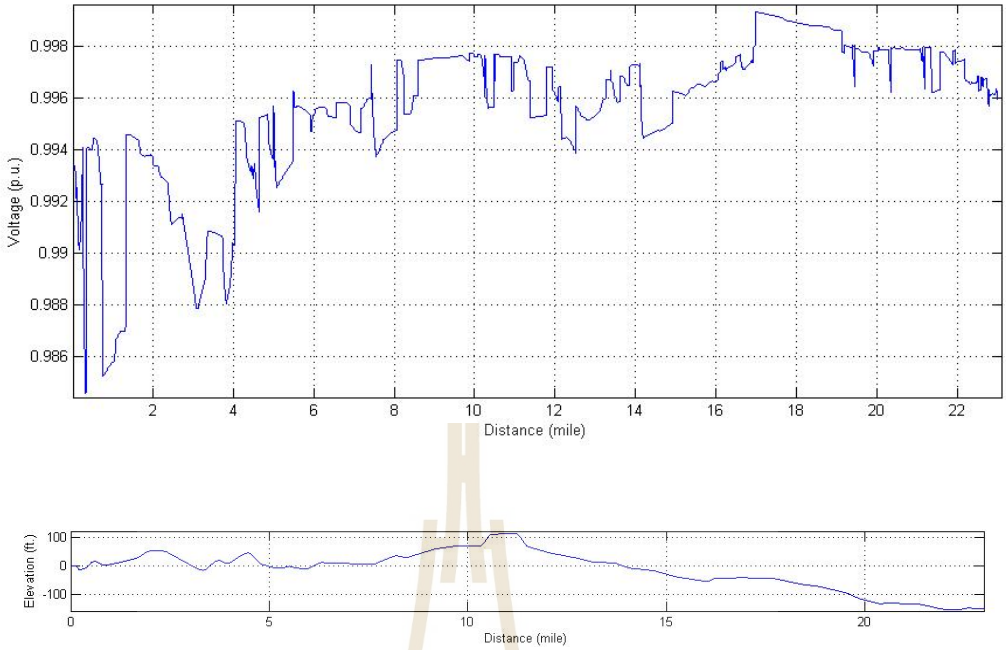

(a)

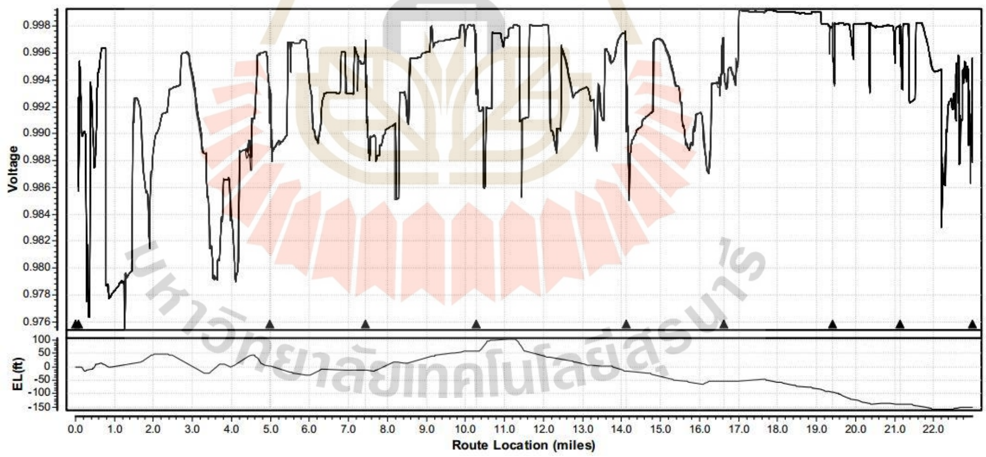

(b)

Fig. B.4 East Corridor line’s down-track traction voltage and grade profile

(a) MATLAB, (b) RR version 13

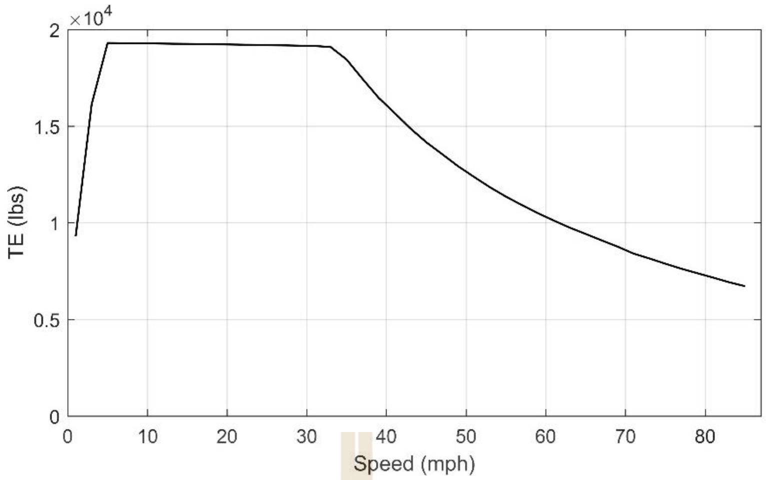

(a)

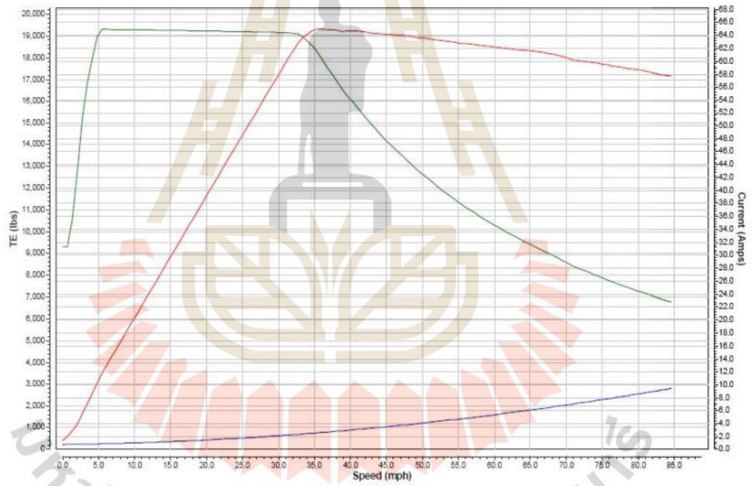

(b)

Fig. B.5 Tractive effort curve

(a) MATLAB, (b) RR version 13

Appendix C

Train movement calculation

C.1 Introduction

This appendix describes a calculation method of train motion. Kinetic quantities are also obtained from the method such as speed, acceleration rate, distance, etc. Most importantly, the required tractive power or train load can be calculated; it plays an essential role in the load estimation part of the RPC optimal sizing procedure in Chapter 6.

C.2 Train movement calculation

The train movement calculation is carried out by the Newton's second law of motion. Forces acted on a train, as depicted in Fig. C.1, are composed of a propelling force and resistive forces: the only propelling force of a train is tractive force (F_T), and the resistive forces are a rolling resistive force, an aerodynamic drag force, and a gradient force (F_{grad}). An amalgamation of a rolling resistive, an aerodynamic drag force, and other resistive forces (if any), F_R, is summarised as Davis's equation. Therefore, the motion equation is obtained as shown in (C.1) where M_{eff} is the effective mass, M_t is the tare mass, λ_w is the rotary allowance, M_L is the freight or passenger load, θ is the angle of track inclination, a is the train acceleration rate, g is the acceleration rate due to gravity (9.8 m/s^2), [A B C] are Davis's coefficients, and v is the train speed.

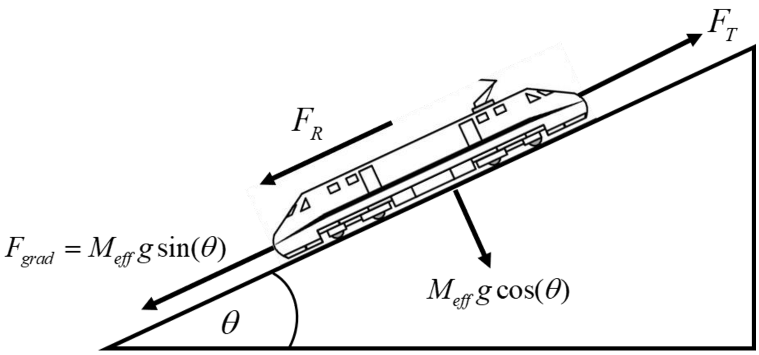

Fig. C.1 Free body diagram of a train on an inclined track

(Adapted from: Kritsada Mongkoldee, Uthen Leeton, and Thanatchai Kulworawanichpong, 2016)

$$\begin{aligned} F_T - F_R - F_{grad} &= M_{eff}\, a \\ F_R &= A + Bv + Cv^2 \\ F_{grad} &= M_{eff}\, g \sin(\theta) \\ M_{eff} &= M_t (1 + \lambda_w) + \mathrm{M}_L \end{aligned} \tag{C.1}$$

Considering a train travelling from one station to another station, the modes of motion are mainly divided into 4 modes: accelerating mode, cruising mode (maintaining a constant speed), coasting mode (a train moving without tractive effort), and braking mode (braking to a stop). The coasting mode is not taken into consideration in this study. Fig. C.2 shows the speed profile of the mentioned modes. With the known forces and mass, ones can calculate the instantaneous acceleration rate, speed, and train position in specified time step. Those speed and position are updated in every time step Δt as shown in (C.2). Then, the train's tractive power consumption is obtained by the tractive force, speed, and energy conversion efficiency (η); see (C.3). The total required train power (P_T) is the sum of the tractive power and auxiliary power (P_{aux}), which is other electricity consumption on a train such as lighting, air-conditioning system, etc. However, regenerative braking power or negative electrical power fed back to a supply system is neglected. Instead, braking energy is assumed to dissipate in braking resistors.

$$\begin{aligned} v_{i+1} &= v_i + a\Delta t \\ s_{i+1} &= s_i + v_i\Delta t + \frac{1}{2}a\Delta t^2 \end{aligned} \tag{C.2}$$

$$P_T = \frac{F_T v}{\eta} + P_{aux} \tag{C.3}$$

In case of multiple passenger stations and/or multiple trains, the movement calculation is performed using the same calculation method.

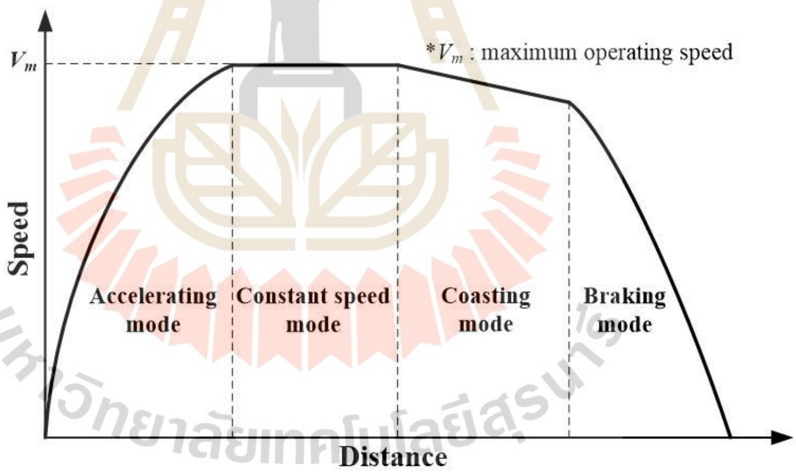

Fig. C.2 Speed curve with the modes of motion

(Kritsada Mongkoldee, Uthen Leeton, and Thanatchai Kulworawanichpong, 2016)

Appendix D

Optimisation result comparison

D.1 Introduction

This appendix shows the results of the study case simulation in Chapter 6 using PSO and GA for comparison in terms of optimal searching performance. According to the following results, PSO is proved to have better performance in global minimum search. In addition to the optimisation comparison, the selection of penalty factors (γ) embedded in the objective function is described in this Appendix.

D.2 Comparative results and discussion

RPC operation points (modulation indices and phase angles of converters), unbalance factors, and power factors after compensation using PSO and GA are shown in Table D.1 – D.2 for V/V transformer case and D.3 – D.4 for Scott transformer case. Besides, optimal sizes in MVA and optimal compensating powers are summarised in Table D.5 – D.6 for V/V transformer case and D.7 – D.8 for Scott transformer case. Both optimisation methods can find the optimal RPC size; however, PSO can achieve lower optimal sizes with shorter execution time per iteration (less computational burden per iteration). It is noted that the C phase's power factors after compensation obtained from PSO are equal to the targeted values in all cases while those from GA are somewhat higher than the targeted values. Therefore, PSO gives the result in a way that RPC uses less reactive compensation in the higher-loaded side. The correctness of the RPC's optimal operation points is also verified by both methods nearly converging to the same global minima.

Another aspect for comparison is convergence of optimal solutions. Fig. D.1 - D.4 show convergence characteristic of both PSO and GA in case 1 (Max. ΔP, ΔQ, ΔS and $PF^{*} \geq 0.95$) as an example. In other cases, the convergence curves closely resemble those of the example in these figures. For both methods, the function values are huge, up to 10^{10}, owing to constraint penalties. Then until around the 40^{th} iteration, the values are greatly reduced because almost all of the constraints are satisfied. After the 100^{th} iteration or generation, the values start to settle and gradually converge to the optimal solutions. At this stage, the function values of PSO decrease more continuously than those of GA.

Table D.1 Comparative results of power quality between PSO and GA (V/V, PF* ≥ 0.95)

Case		Optimisation method	m_α	m_β	δ_α (degree)	δ_β (degree)	*VUF*/ *IUF* (%)	cos(φ_A)	cos(φ_B)	cos(φ_C)
1	Max. ΔP, ΔQ, ΔS	PSO	0.732	0.900	26.308	89.602	0.628/38.424	0.950	-0.978	0.950
		GA	0.732	0.901	26.037	89.832	0.573/35.106	0.961	-0.983	0.953
	Max. P, Q, S	PSO	0.765	0.850	27.800	88.353	0.222/12.698	0.996	0.983	0.950
		GA	0.766	0.849	27.465	88.656	0.248/14.195	0.999	0.977	0.953
2	Max. ΔP, ΔQ, ΔS	PSO	0.710	0.962	24.180	89.503	0.818/34.359	0.951	-0.987	0.950
		GA	0.714	0.962	23.999	89.649	0.801/33.737	0.963	-0.987	0.950
	Max. P, Q, S	PSO	0.756	0.885	25.779	88.463	0.403/15.624	0.997	0.953	0.950
		GA	0.759	0.885	25.894	88.358	0.392/15.237	0.998	0.960	0.950

Table D.2 Comparative results of power quality between PSO and GA (V/V, PF* ≥ 0.90)

Case		Optimisation method	m_α	m_β	δ_α (degree)	δ_β (degree)	*VUF*/ *IUF* (%)	cos(φ_A)	cos(φ_B)	cos(φ_C)
1	Max. ΔP, ΔQ, ΔS	PSO	0.735	0.885	27.180	88.805	0.817/49.209	0.900	-0.980	0.900
		GA	0.741	0.885	27.150	88.827	0.858/52.183	0.935	-0.972	0.902
	Max. P, Q, S	PSO	0.762	0.835	27.604	88.483	0.333/18.556	0.990	0.954	0.900
		GA	0.763	0.838	27.362	88.717	0.335/18.822	0.997	0.954	0.915
2	Max. ΔP, ΔQ, ΔS	PSO	0.726	0.943	26.280	87.774	1.320/55.137	0.900	-0.967	0.900
		GA	0.723	0.944	24.896	88.910	1.044/43.542	0.956	-0.987	0.907
	Max. P, Q, S	PSO	0.755	0.867	26.108	88.102	0.510/19/354	0.995	0.943	0.90
		GA	0.757	0.869	26.607	87.656	0.463/17.647	0.993	0.957	0.901

Table D.3 Comparative results of power quality between PSO and GA (Scott, PF* ≥ 0.95)

Case		**Optimisation method**	$\boldsymbol{m_\alpha}$	$\boldsymbol{m_\beta}$	$\boldsymbol{\delta_\alpha}$ **(degree)**	$\boldsymbol{\delta_\beta}$ **(degree)**	***VUF/ IUF*** **(%)**	**cos(φ_A)**	**cos(φ_B)**	**cos(φ_C)**
1	Max. ΔP, ΔQ, ΔS	PSO	0.773	0.846	-8.258	91.646	0.241/14.577	0.999	0.980	0.950
		GA	0.772	0.855	-7.523	90.994	0.260/15.875	0.999	0.997	0.955
	Max. P, Q, S	PSO	0.809	0.801	-4.499	87.888	0.219/12.451	0.996	0.975	0.950
		GA	0.813	0.805	-4.586	87.978	0.213/12.256	0.998	0.979	0.963
2	Max. ΔP, ΔQ, ΔS	PSO	0.773	0.908	-9.522	90.000	0.570/24.061	0.998	-0.999	0.950
		GA	0.773	0.905	-10.545	90.830	0.397/16.714	0.998	0.999	0.960
	Max. P, Q, S	PSO	0.798	0.822	-6.698	86.871	0.078/2.966	0.963	0.963	0.950
		GA	0.821	0.822	-6.612	86.901	0.231/8.983	0.990	0.974	0.954

Table D.4 Comparative results of power quality between PSO and GA (Scott, PF* ≥ 0.90)

Case		Optimisation method	m_α	m_β	δ_α (degree)	δ_β (degree)	*VUF/ IUF* (%)	cos(φ_A)	cos(φ_B)	cos(φ_C)
1	Max. ΔP, ΔQ, ΔS	PSO	0.772	0.840	-7.215	90.807	0.392/23.574	0.999	0.999	0.900
		GA	0.772	0.850	-6.073	89.814	0.522/31.725	0.999	-0.999	0.904
	Max. P, Q, S	PSO	0.793	0.786	-4.571	87.899	0.221/12.068	0.974	0.943	0.900
		GA	0.787	0.791	-4.603	87.910	0.142/7.765	0.963	0.944	0.916
2	Max. ΔP, ΔQ, ΔS	PSO	0.772	0.893	-8.560	89.301	0.799/33.394	0.999	-0.999	0.900
		GA	0.773	0.895	-8.609	89.329	0.780/32.650	0.999	-0.999	0.908
	Max. P, Q, S	PSO	0.807	0.797	-6.819	87.012	0.332/12.375	0.975	0.941	0.900
		GA	0.782	0.799	-6.804	86.878	0.143/5.208	0.935	0.927	0.900

Table D.5 Comparative results of compensating power between PSO and GA (V/V, PF* ≥ 0.95)

Case		Optimisation method	$S_{Optimal}$ (MVA)		$P_{Transfer}$ (MW)		$Q_{com,\alpha}$ (MVAR)		$Q_{com,\beta}$ (MVAR)	
			Full	**Partial**	**Full**	**Partial**	**Full**	**Partial**	**Full**	**Partial**
1	Max. ΔP, ΔQ, ΔS	PSO	19.37	16.11	4.05	2.04	-2.34	-2.24	8.80	7.79
		GA	19.37	16.24	4.05	2.20	-2.34	-2.24	8.80	7.81
	Max. P, Q, S	PSO	12.85	9.87	0.69	0.29	0.29	0.16	6.39	4.93
		GA	12.85	9.899	0.69	0.504	0.29	0.22	6.39	4.92
2	Max. ΔP, ΔQ, ΔS	PSO	28.83	23.97	5.89	3.15	-3.40	-3.399	13.16	11.56
		GA	28.83	23.98	5.89	3.27	-3.40	-3.26	13.16	11.54
	Max. P, Q, S	PSO	19.12	14.56	1.03	1.0299	0.47	0.00025	9.51	7.20
		GA	19.12	14.58	1.03	0.966	0.47	0.127	9.51	7.22

Table D.6 Comparative results of compensating power between PSO and GA (V/V, PF* ≥ 0.90)

Case		Optimisation method	$S_{Optimal}$ (MVA)		$P_{Transfer}$ (MW)		$Q_{com,\alpha}$ (MVAR)		$Q_{com,\beta}$ (MVAR)	
			Full	**Partial**	**Full**	**Partial**	**Full**	**Partial**	**Full**	**Partial**
1	Max. ΔP, ΔQ, ΔS	PSO	19.37	14.40	4.05	1.46	-2.34	-2.11	8.80	7.05
		GA	19.37	14.47	4.05	1.499	-2.34	-1.802	8.80	7.079
	Max. P, Q, S	PSO	12.85	8.60	0.69	0.372	0.29	0.007	6.39	4.286
		GA	12.85	8.91	0.69	0.53	0.29	0.065	6.39	4.422
2	Max. ΔP, ΔQ, ΔS	PSO	28.83	21.55	5.89	1.88	-3.40	-2.70	13.16	10.61
		GA	28.83	21.93	5.89	2.711	-3.40	-2.837	13.16	10.622
	Max. P, Q, S	PSO	19.12	12.897	1.03	0.78	0.47	0.00	9.51	6.40
		GA	19.12	12.94	1.03	0.475	0.47	0.0598	9.51	6.451

Table D.7 Comparative results of compensating power between PSO and GA (Scott, PF* ≥ 0.95)

Case		Optimisation method	$S_{Optimal}$ (MVA)		$P_{Transfer}$ (MW)		$Q_{com,\alpha}$ (MVAR)		$Q_{com,\beta}$ (MVAR)	
			Full	**Partial**	**Full**	**Partial**	**Full**	**Partial**	**Full**	**Partial**
1	Max. ΔP, ΔQ, ΔS	PSO	15.25	12.88	4.05	3.91	0.00	0.00	6.46	5.12
		GA	15.25	13.06	4.05	3.57	0.00	0.00	6.46	5.46
	Max. P, Q, S	PSO	7.96	5.25	0.69	0.60	2.76	2.55	3.92	2.55
		GA	7.96	5.55	0.69	0.65	2.76	2.70	3.92	2.70
2	Max. ΔP, ΔQ, ΔS	PSO	22.79	19.57	5.89	4.51	0.00	0.00	9.76	8.68
		GA	22.79	19.72	5.89	4.99	0.00	0.00	9.76	8.50
	Max. P, Q, S	PSO	11.99	8.31	1.03	0.88	4.07	2.76	5.91	4.06
		GA	11.99	8.30	1.03	0.90	4.07	3.56	5.91	4.05

Table D.8 Comparative results of compensating power between PSO and GA (Scott, PF* ≥ 0.90)

Case		Optimisation method	$S_{Optimal}$ (MVA)		$P_{Transfer}$ (MW)		$Q_{com,\alpha}$ (MVAR)		$Q_{com,\beta}$ (MVAR)	
			Full	Partial	Full	Partial	Full	Partial	Full	Partial
1	Max. ΔP, ΔQ, ΔS	PSO	15.25	11.99	4.05	3.42	0.00	0.00	6.46	4.89
		GA	15.25	12.10	4.05	2.88	0.00	0.00	6.46	5.32
	Max. P, Q, S	PSO	7.96	4.13	0.69	0.61	2.76	1.97	3.92	1.97
		GA	7.96	4.49	0.69	0.62	2.76	1.78	3.92	2.16
2	Max. ΔP, ΔQ, ΔS	PSO	22.79	18.08	5.89	4.06	0.00	0.00	9.76	8.08
		GA	22.79	18.31	5.89	4.08	0.00	0.00	9.76	8.19
	Max. P, Q, S	PSO	11.99	6.44	1.03	0.96	4.07	3.07	5.91	3.07
		GA	11.99	6.52	1.03	0.89	4.07	2.20	5.91	3.14

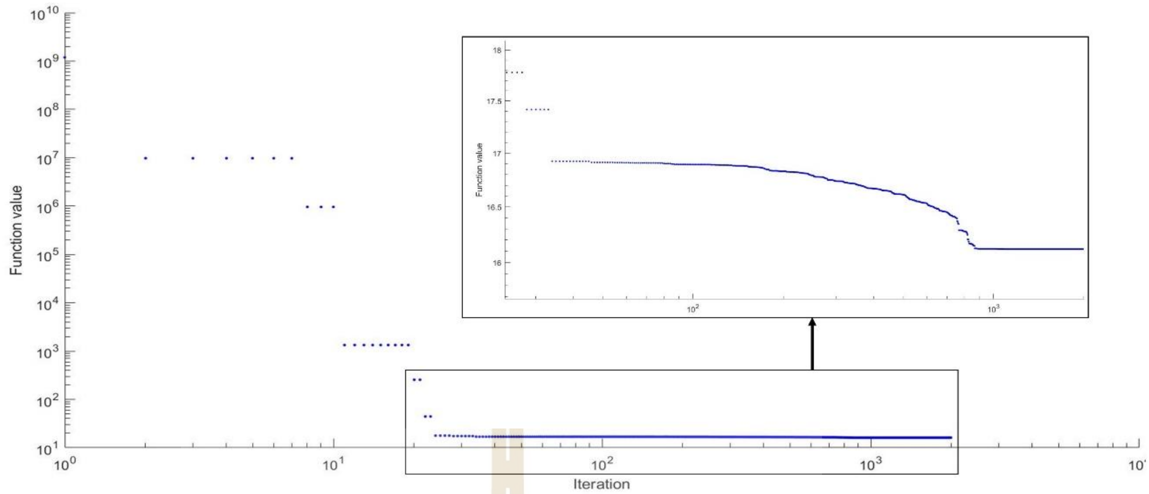

Fig. D.1 PSO's convergence curve in V/V transformer case 1 (Max. ΔP, ΔQ, ΔS and $PF^{*} \geq 0.95$)

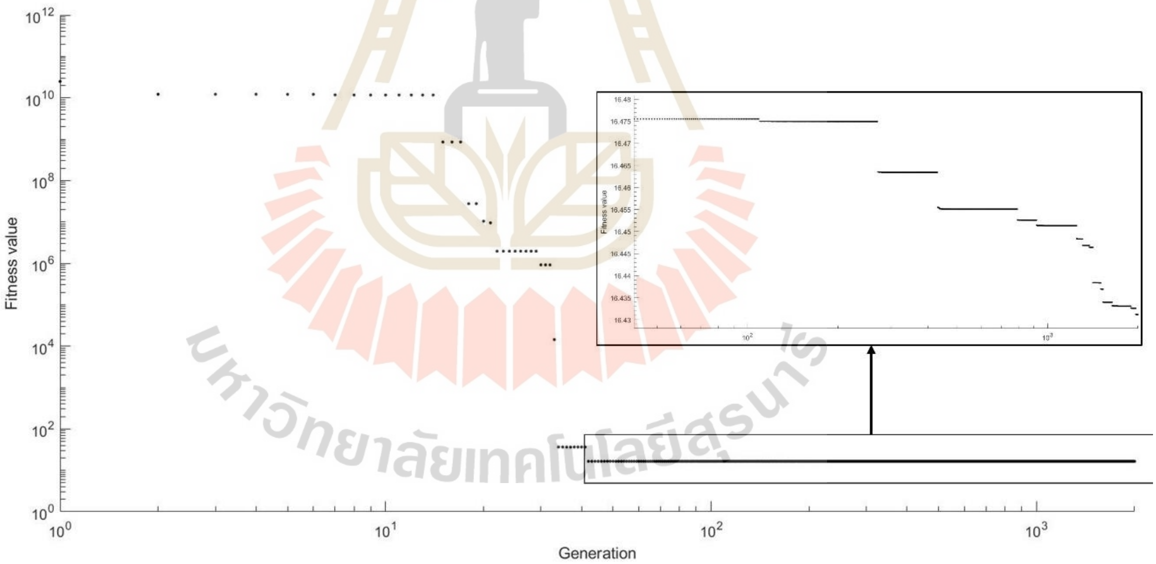

Fig. D.2 GA's convergence curve in V/V transformer case 1 (Max. ΔP, ΔQ, ΔS and $PF^{*} \geq 0.95$)

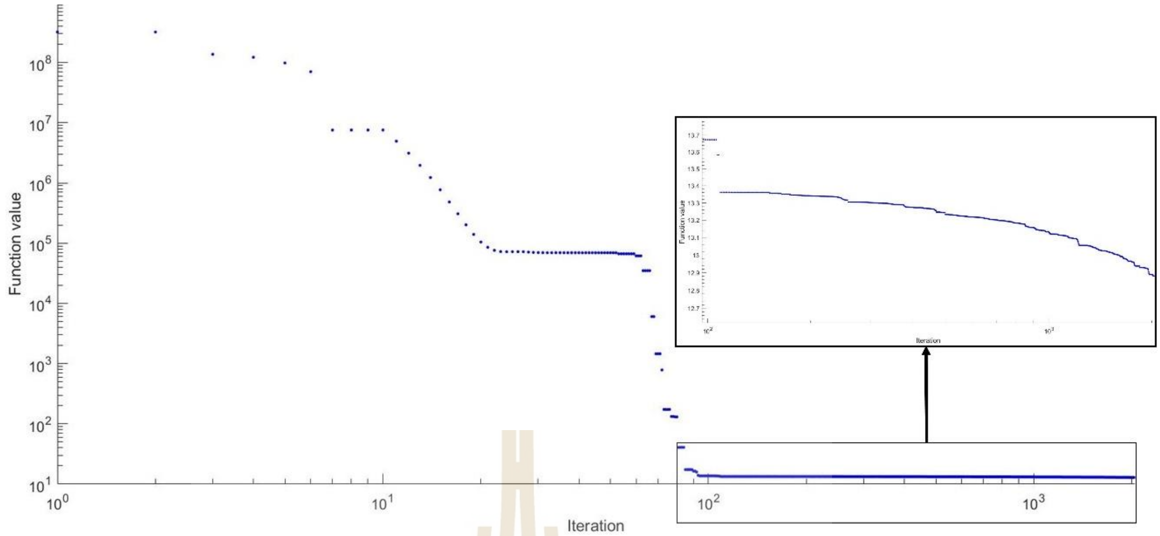

Fig. D.3 PSO's convergence curve in Scott transformer case 1 (Max. ΔP, ΔQ, ΔS and $PF^{*} \geq 0.95$)

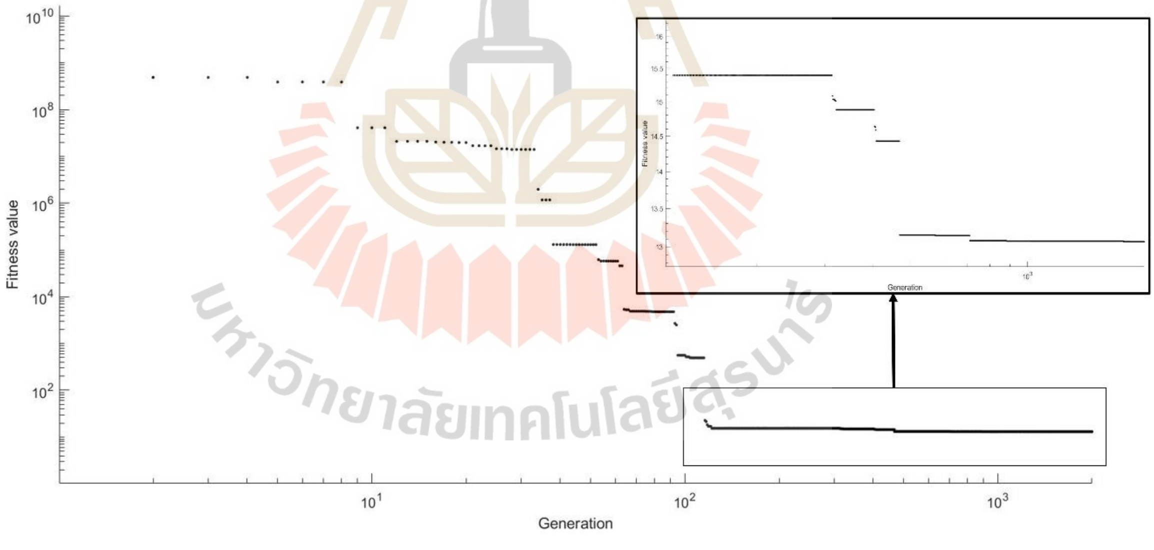

Fig. D.4 GA's convergence curve in Scott transformer case 1 (Max. ΔP, ΔQ, ΔS and $PF^{*} \geq 0.95$)

D.3 Optimisation parameters

D.3.1 Particle swarm optimisation

Swarm size:	25
Tolerance function value:	10^{-30}
Self-adjusted weight (y_1):	0.5
Social-adjusted weight (y_2):	1.6
Inertia range (W):	[0.40 – 0.80]
Maximum iteration:	6000
Stall iteration limit:	500

Note: the above parameters are adopted from the study proposed by Dai, Liu, and Li (2011).

D.3.2 Genetic algorithm optimisation

Population size:	50
Tolerance function value:	10^{-30}
Crossover fraction:	0.5
Elite count:	3
Maximum generation:	6000
Stall generation limit:	500

Note: the GA's population size doubles the swarm size of PSO by virtue of faster calculation and searching.

D.4 Penalty factor selection

This section describes how the penalty factors (γ_1 and γ_2) used in the objective function for the RPC size optimisation are selected. The penalty factors are divided into 5 levels; the PSO optimisation with the parameters specified in D.3 is performed 10 times in each level. This selection process uses case 1 with V/V transformer (max. ΔP, ΔQ, ΔS and $PF^* \geq 0.95$) from the simulation case study in Chapter 6 for repeated optimisation tests, shown in Table D.9 – D.13.

The results are summarised in Table D.14. The penalty factors $\gamma_1 = 10^{-3}$ and $\gamma_2 = 10^{10}$ result in the least average function value, the lowest minimum function value, and the lowest maximum function value among all the tested penalty levels. Accordingly, $\gamma_1 = 10^{-3}$ and $\gamma_2 = 10^{10}$ are appropriate and selected for the problem in this thesis.

Table D.9 Repeated optimisation test for $\gamma_1 = 10^{-7}$ and $\gamma_2 = 10^{3}$

No.	Iteration	Function value	m_1	m_2	γ_1	γ_2
1	1415	16.13891282	0.801992	0.987737	0.446858	1.574206
2	2053	16.17928069	0.801797	0.98633	0.439832	1.580139
3	6000	16.33011103	0.801424	0.983188	0.423668	1.593839
4	6000	16.21867601	0.801667	0.985314	0.43468	1.584498
5	1176	16.150879	0.801924	0.987257	0.444473	1.576219
6	1150	16.12815037	0.802068	0.988252	0.449397	1.572066
7	1000	16.10996882	0.802272	0.98958	0.455875	1.566613
8	6000	16.30970174	0.80146	0.983526	0.42544	1.592334
9	1112	16.11218269	0.802235	0.989346	0.454742	1.567566
10	6000	16.52020104	0.801191	0.980619	0.409905	1.605562
Min.	1000	16.10996882	0.801191	0.980619	0.409905	1.566613
Ave.	3190.6	16.21980642	0.801803	0.986115	0.438487	1.581304
Max	6000	16.52020104	0.802272	0.98958	0.455875	1.605562
SD	2434.925744	0.131432948	0.000362	0.002927	0.014961	0.012671

Table D.10 Repeated optimisation test for $\gamma_1 = 10^{-5}$ and $\gamma_2 = 10^5$

No.	Iteration	Function value	m_1	m_2	γ_1	γ_2
1	2608	16.13767392	0.802	0.987792	0.447127	1.573979
2	1066	115714.6002	0.85	0.988159	0.444483	1.576536
3	1188	16.11995433	0.802141	0.988735	0.451765	1.570071
4	6000	16.33618079	0.801414	0.983091	0.423157	1.594274
5	6000	16.37565022	0.801354	0.982489	0.419976	1.596978
6	6000	16.26773897	0.801544	0.984282	0.429377	1.588992
7	2021	16.10799228	0.804765	0.990284	0.459006	1.563962
8	1769	16.11715606	0.802171	0.98893	0.452719	1.569268
9	5831	16.17310182	0.801822	0.986513	0.440754	1.579359
10	6000	16.21597037	0.801676	0.985377	0.435001	1.584226
Min.	1066	16.10799228	0.801354	0.982489	0.419976	1.563962
Ave.	3848.3	16.2057132	0.806889	0.986565	0.440336	1.579765
Max	6000	16.37565022	0.85	0.990284	0.459006	1.596978
SD	2272.287103	0.100182311	0.01518	0.002656	0.013141	0.011105

Table D.11 Repeated optimisation test for $\gamma_1 = 10^{-3}$ and $\gamma_2 = 10^{10}$

No.	Iteration	Function value	m_1	m_2	γ_1	γ_2
1	5375	16.25905	0.801563	0.984452	0.4302522	1.58825
2	6000	16.17347	0.80182	0.986502	0.4406975	1.579407
3	2433	16.16606	0.801851	0.986733	0.4418567	1.578428
4	6000	16.2317	0.801631	0.98502	0.4331774	1.58577
5	1731	16.12221	0.802119	0.988591	0.4510606	1.570664
6	6000	16.21121	0.801689	0.98549	0.4355777	1.583737
7	3303	16.17646	0.801808	0.986412	0.4402473	1.579788
8	6000	16.15489	0.801903	0.98711	0.4437439	1.576834
9	5338	16.20753	0.8017	0.985579	0.4360325	1.583352
10	1726	16.10798	0.80521	0.990398	0.4595054	1.563538
Min.	1726	16.10798	0.801563	0.984452	0.4302522	1.563538
Ave.	4390.6	16.18106	0.80213	0.986629	0.4412151	1.578977
Max	6000	16.25905	0.80521	0.990398	0.4595054	1.58825
SD	1868.33	0.047198	0.001094	0.001767	0.0087108	0.007357

Table D.12 Repeated optimisation test for $\gamma_1 = 10^5$ and $\gamma_2 = 10^{15}$

No.	Iteration	Function value	m_1	m_2	γ_1	γ_2
1	121.991098	5536	16.17059233	0.801832	0.98659	0.44114
2	23.43935552	901	5.99E+15	0.85	0.96303	0.541052
3	151.6700121	6000	16.45074671	0.80126	0.981464	0.41449
4	148.0318286	6000	16.42257788	0.801298	0.981833	0.416475

Table D.12 Repeated optimisation test for $\gamma_1 = 10^5$ and $\gamma_2 = 10^{15}$ (Continued)

No.	Iteration	Function value	m_1	m_2	γ_1	γ_2
5	144.8599131	6000	16.39001283	0.801476	0.982289	0.418899
6	162.0834456	6000	16.62612196	0.801109	0.979468	0.403565
7	141.8751799	6000	16.29091959	0.801496	0.983853	0.427148
8	55.30700334	2619	16.12859407	0.802064	0.988228	0.449282
9	24.75424399	1147	16.1153908	0.811421	0.992001	0.466405
10	144.4608963	6000	16.38368871	0.801343	0.982373	0.419357
Min.	23.43935552	901	16.1153908	0.801109	0.96303	0.403565
Ave.	111.8472976	4620.3	16.33096054	0.80733	0.982113	0.439781
Max	162.0834456	6000	16.62612196	0.85	0.992001	0.541052
SD	54.94932871	2164.41283	0.169880068	0.015317	0.007674	0.040227

Table D.13 Repeated optimisation test for $\gamma_1 = 10^{10}$ and $\gamma_2 = 10^{20}$

No.	Iteration	Function value	m_1	m_2	γ_1	γ_2
1	84.92720925	6000	16.1639714	0.801861	0.9868	0.442196
2	67.84799015	4833	16.18726471	0.801767	0.986104	0.438695
3	94.42112016	6000	16.35991834	0.801377	0.982723	0.421215
4	93.58162109	6000	16.40942487	0.801311	0.982011	0.417429
5	101.5641112	6000	16.50629575	0.801205	0.980782	0.410792
6	90.10843371	5310	16.50581789	0.801204	0.980787	0.410823
7	86.54900408	6000	16.44676551	0.832946	0.990098	0.441688
8	102.512715	6000	16.46536478	0.803111	0.981359	0.413808
9	42.2706722	2889	16.16076084	0.801875	0.986907	0.442729
10	96.03317599	6000	16.32601785	0.801431	0.983255	0.424017
Min.	42.2706722	2889	16.16076084	0.801204	0.980782	0.410792
Ave.	85.98160528	5503.2	16.35316019	0.804809	0.984083	0.426339
Max	102.512715	6000	16.50629575	0.832946	0.990098	0.442729
SD	18.26973781	1002.674623	0.138397981	0.009903	0.003191	0.013576

Table D.14 Repeated optimisation test summary

γ_1	γ_2	Ave. function value	Min. function value	Max. function value	SD
10^{-7}	10^3	16.21981	16.10997	16.52020	0.131433
10^{-5}	10^5	16.20571	16.10799	16.37565	0.100182
10^{-3}	10^{10}	16.18106	16.10798	16.25905	0.047198
10^5	10^{15}	16.33096	16.11539	16.62612	0.169880
10^{10}	10^{20}	16.35316	16.16076	16.50630	0.138398

Appendix E

Simulation programmes

E.1 Introduction

This appendix lists and describes the MATLAB codes used in the simulation: the train movement simulation, the optimal RPC sizing in Chapter 6, and the tap-changing AT investigation in Chapter 5.

E.2 Train movement simulation programmes

The following file list is used in the train movement simulation throughout this thesis.

(i) Main_EC.m (Main programme): this file runs the main programme by calling other files that constitute the whole programme.

```
TerDist_EC = 37.00690706e3;
idx_service_EC = [1 1];
Tstep = 0.05;
uService_EC = [10*60      1    % departure time Train no.
        25*60     2
        40*60    3
        55*60    4
        70*60    5
        85*60    6
        100*60    7
        115*60   8
        130*60   9
        145*60   10
        160*60   11
        175*60   12
        190*60   13
        ];

dService_EC = [4*60  14  % departure time       Train no.
        19*60     15
        34*60     16
        49*60     17
        64*60     18
        79*60     19
        94*60     20
        109*60    21
        124*60    22
```

```
        139*60    23
        154*60    24
        169*60    25
        184*60    26
        ];

t = 0;
count_EC=1;
for k=1:26
    tr_EC(k) = TRAINMOVE('EastCorridor');
    if k<=13
        tr_EC(k) =
tr_EC(k).setJourney('East_corridor_up',Tstep);
    else
        tr_EC(k) =
tr_EC(k).setJourney('East_corridor_dn',Tstep);
    end
    tr_EC(k) = tr_EC(k).init;
    tr_EC(k).idx_Stn = 1;
    tr_EC(k).Time = 0;
    tr_EC(k).Timer_STNstop = 0;
end

T = [t];
for i=1:26
    if i<=13
      S_EC(i,1) = 0;
    else
      S_EC(i,1) = TerDist_EC;
    end
    Sp_EC(i,1) = 0;
    Vs_EC(i,1) = 0;
    Pt_EC(i,1) = 0;
    Qt_EC(i,1) = 0;
    St_EC(i,1) = 0;
    TE_EC(i,1) = 0;
end
H_up_EC = [0];
H_dn_EC = [0];
SinQ_up_EC = [0];
SinQ_dn_EC = [0];
a_int_EC = [0];
V_diff_up_EC = [0];
dis_diff_up_EC = [0];
V_diff_dn_EC = [0];
dis_diff_dn_EC = [0];
Total_FR_up_EC = [0];
Total_FR_dn_EC = [0];
trTAB_EC{1} = [];
```

```
Train_num_EC{1} = [0;0];

while t<13000
    t = t + Tstep;
    count_EC=count_EC+1;

    if (t>=uService_EC(idx_service_EC(1),1)-1e-
3)&&(t<=uService_EC(idx_service_EC(1),1)+1e-
3)&&(idx_service_EC(1)<=size(uService_EC,1))
        k = uService_EC(idx_service_EC(1),2);
        tr_EC(k) =
tr_EC(k).setJourney('East_corridor_up',Tstep);
        tr_EC(k).status = 1; % Status = 1: in service
        idx_service_EC(1) = idx_service_EC(1) + 1;
        if (idx_service_EC(1)>size(uService_EC,1))
            idx_service_EC(1) = size(uService_EC,1);
        end
        tr_EC(k).idx_Stn = 1;
        tr_EC(k).Timer_STNstop = 0;
        DISP = ['Track 1, Train number: ',num2str(k),'
departs'];
        disp(DISP);
        pause(1);
    end

    if (t>=dService_EC(idx_service_EC(2),1)-1e-
3)&&(t<=dService_EC(idx_service_EC(2),1)+1e-
4)&&(idx_service_EC(2)<=size(dService_EC,1))
        k = dService_EC(idx_service_EC(2),2);
        tr_EC(k) =
tr_EC(k).setJourney('East_corridor_dn',Tstep);
        tr_EC(k).status = 1;               % Status = 1:
in service
        idx_service_EC(2) = idx_service_EC(2) + 1;
        if (idx_service_EC(2)>size(dService_EC,1))
            idx_service_EC(2) = size(dService_EC,1);
        end
        tr_EC(k).idx_Stn = 1;
        tr_EC(k).Timer_STNstop = 0;
        DISP = ['Track 2, Train number: ',num2str(k),'
departs'];
        disp(DISP);
        pause(1);
    end

    for k=1:26
        if tr_EC(k).status==1
            tr_EC(k) = tr_EC(k).perfcalc(t,k);
        elseif tr_EC(k).status==0
```

```
            tr_EC(k) = tr_EC(k).waiting;
        elseif tr_EC(k).status==2
            tr_EC(k) = tr_EC(k).terminate;
        end
    end

    trTAB_EC_c = [];
    Tr_count_EC_up = 0;
    Tr_count_EC_dn = 0;
    for k=1:26
        if tr_EC(k).status==1
            if tr_EC(k).Dir==1
            trTAB_EC_c = [trTAB_EC_c; k tr_EC(k).posi
tr_EC(k).Ptr tr_EC(k).Qtr];
            Tr_count_EC_up = Tr_count_EC_up+1;
            else
            trTAB_EC_c = [trTAB_EC_c; k (TerDist_EC-
tr_EC(k).posi) tr_EC(k).Ptr tr_EC(k).Qtr];
            Tr_count_EC_dn = Tr_count_EC_dn+1;
            end
        end
    end
    trTAB_EC{count_EC} = trTAB_EC_c;
    Train_num_EC{count_EC} = [Tr_count_EC_up;
Tr_count_EC_dn];
    T = [T;t];
        for i=1:26
          if i<=13
            S_EC(i,count_EC) = tr_EC(i).posi;
          else
            S_EC(i,count_EC) = TerDist_EC-tr_EC(i).posi;
          end
            Sp_EC(i,count_EC) = tr_EC(i).speed;
            Vs_EC(i,count_EC) = tr_EC(i).Vset;
            Pt_EC(i,count_EC) = tr_EC(i).Ptr;
            Qt_EC(i,count_EC) = tr_EC(i).Qtr;
            TE_EC(i,count_EC) = tr_EC(i).TE;
            H_up_EC(count_EC) = tr_EC(1).H;
            H_dn_EC(count_EC) = tr_EC(14).H;
            a_int_EC(count_EC) = tr_EC(1).a_int;
            SinQ_up_EC(count_EC) = tr_EC(1).SinQ;
            SinQ_dn_EC(count_EC) = tr_EC(14).SinQ;
            V_diff_up_EC(count_EC) = tr_EC(1).V_diff;
            dis_diff_up_EC(count_EC) = tr_EC(1).dis_diff;
            V_diff_dn_EC(count_EC) = tr_EC(14).V_diff;
            dis_diff_dn_EC(count_EC) =
tr_EC(14).dis_diff;
            Total_FR_up_EC(count_EC) = tr_EC(1).Total_FR;
```

```
                Total_FR_dn_EC(count_EC) =
tr_EC(14).Total_FR;
          end

end

figure(1)
subplot(411),plot(T/60,Sp_EC(1,:)*3.6)
axis([0 120 0 150])
xlabel('Time (minute)');ylabel('Speed (km/h)');
subplot(412),plot(T/60,Sp_EC(2,:)*3.6)
axis([0 120 0 150])
xlabel('Time (minute)');ylabel('Speed (km/h)');
subplot(413),plot(T/60,Sp_EC(3,:)*3.6)
axis([0 120 0 150])
xlabel('Time (minute)');ylabel('Speed (km/h)');
subplot(414),plot(T/60,Sp_EC(4,:)*3.6)
axis([0 120 0 150])
xlabel('Time (minute)');ylabel('Speed (km/h)');

figure(2)
subplot(411),plot(T/60,Sp_EC(14,:)*3.6)
axis([0 120 0 150])
xlabel('Time (minute)');ylabel('Speed (km/h)');
subplot(412),plot(T/60,Sp_EC(15,:)*3.6)
axis([0 120 0 150])
xlabel('Time (minute)');ylabel('Speed (km/h)');
subplot(413),plot(T/60,Sp_EC(16,:)*3.6)
axis([0 120 0 150])
xlabel('Time (minute)');ylabel('Speed (km/h)');
subplot(414),plot(T/60,Sp_EC(17,:)*3.6)
axis([0 120 0 150])
xlabel('Time (minute)');ylabel('Speed (km/h)');


figure(4)
plot(T/60,S_EC/1000);
xlabel('Time (minute)');ylabel('Distance (km)');
axis([0 230 0 37.00690706])

figure(5)
subplot(411),plot(T/60,Pt_EC(1,:)*1e-6)
axis([0 120 0 5])
xlabel('Time (minute)');ylabel('Train power (MW)');
subplot(412),plot(T/60,Pt_EC(2,:)*1e-6)
axis([0 120 0 5])
xlabel('Time (minute)');ylabel('Train power (MW)');
subplot(413),plot(T/60,Pt_EC(3,:)*1e-6)
axis([0 120 0 5])
```

```
xlabel('Time (minute)');ylabel('Train power (MW)');
subplot(414),plot(T/60,Pt_EC(4,:)*1e-6)
axis([0 120 0 5])
xlabel('Time (minute)');ylabel('Train power (MW)');

figure(6)
subplot(411),plot(T/60,Pt_EC(14,:)*1e-6)
axis([0 120 0 5])
xlabel('Time (minute)');ylabel('Train power (MW)');
subplot(412),plot(T/60,Pt_EC(15,:)*1e-6)
axis([0 120 0 5])
xlabel('Time (minute)');ylabel('Train power (MW)');
subplot(413),plot(T/60,Pt_EC(16,:)*1e-6)
axis([0 120 0 5])
xlabel('Time (minute)');ylabel('Train power (MW)');
subplot(414),plot(T/60,Pt_EC(17,:)*1e-6)
axis([0 120 0 5])
xlabel('Time (minute)');ylabel('Train power (MW)');

figure(9)
subplot(211),plot(S_EC(1,:)/1000,Vs_EC(1,:)*3.6,S_EC(2,:)
/1000,Vs_EC(2,:)*3.6,S_EC(3,:)/1000,Vs_EC(3,:)*3.6,S_EC(4
,:)/1000,Vs_EC(4,:)*3.6)
xlabel('Distance (km)');ylabel('Speed (km/h)');
axis([0 37.00690706 0 150])
subplot(212),plot(TerDist_EC/1000-
S_EC(14,:)/1000,Vs_EC(14,:)*3.6,TerDist_EC/1000-
S_EC(15,:)/1000,Vs_EC(15,:)*3.6,TerDist_EC/1000-
S_EC(16,:)/1000,Vs_EC(16,:)*3.6,TerDist_EC/1000-
S_EC(17,:)/1000,Vs_EC(17,:)*3.6)
xlabel('Distance (km)');ylabel('Speed (km/h)');
axis([0 37.00690706 0 150])

figure(10)
plot(S_EC(1,:)*0.621371/1000,Vs_EC(1,:)*3.6*0.621371,'b:'
,'LineWidth',2);
hold on
plot(S_EC(1,:)*0.621371/1000,Sp_EC(1,:)*3.6*0.621371,'r')
;
xlabel('Distance (mile)'); ylabel('Speed (mph)');

figure(11)
plot((TerDist_EC-
(S_EC(14,:)))*0.621371/1000,Vs_EC(14,:)*3.6*0.621371,'b:'
,'LineWidth',2);
hold on
plot((TerDist_EC-
(S_EC(14,:)))*0.621371/1000,Sp_EC(14,:)*3.6*0.621371,'r')
;
```

```
xlabel('Distance (mile)'); ylabel('Speed (mph)');

figure(12)
plot(S_EC(1,:)*0.621371/1000,H_up_EC*3.28084)
xlabel('Distance (mile)'); ylabel('Elevation (ft.)');
axis([0 23 -10 270])
grid on;

figure(13)
plot((TerDist_EC-
(S_EC(14,:)))*0.621371/1000,H_dn_EC*3.28084)
xlabel('Distance (mile)'); ylabel('Elevation (ft.)');
axis([0 23 -160 120])
grid on;
```

(ii) TRAINMOVE.m: this file defines the class and functions for the train movement programme.

```
classdef TRAINMOVE
    properties
        v1;  % Cornor speed 1 (km/h)
        v2;  % Cornor speed 2 (km/h)
        Mtare;  % Tare mass (kg)
        P_Aux;  % Train auxiliary power (W)
        acc;    % Accelerating rate (m/s^2)
        dec;    % Decelerating rate (m/s^2)
        mode;   % Mode of operation
                %   0: station-stop mode
                %   1: running mode
                %    -1: braking-for-station-stop mode
        psgstn; % Passenger Station Data (km,s)
        status
        Dir
        Vset
        TerDist
        fgradprof
        SP_cmd; % Train's travelling speed command
        idx_Stn;  % Station index
        idx_PS;   % Power supply index
        Tservice; % Service time
        volt;     % Train voltage
        volt_c
        Ptr;      % Train real power (W)
        Qtr;      Train reactive power (var)
        PFtr;       % Train power factor
        Eff_total;  % Overall efficiency
```

```
        TE_max;  % Maximum tractive effort (N)
        BE_max;  % Maximum braking effort (N)
        acc_max; % Maximum accerelating rate (m/s^2)
        dec_max; % Maximum decelerating rate (m/s^2)
        Time;    % Simulated time
        Timer_STNstop;  % Timer for station stop
        dT;             % Time step
        posi;  % Train position from the last stop (m)
        speed;    % Train speed (m/s)
        a;        % Train acceleration
        TE;       % Train's tractive effort (N)
        TR_coeff; % Train resistance coefficient
                  % TR = TR_1 + TR_2*u + TR_3*u^2
        SinQ      % Gredient
        H         % elevation
        a_int     % instantaneous acc
        TEprof    % TE profile
        dis_diff  % distance error at station stop
        V_diff    % speed error at station stop
        Total_FR  % Total resistive force: Grade + other
resistances
    end

    methods
        function obj = TRAINMOVE(fname)  % Constructor
            [obj.v1, obj.v2, obj.Mtare, obj.acc, obj.dec,
obj.TR_coeff,...
             obj.P_Aux, obj.TE_max,
obj.BE_max,obj.Eff_total, obj.PFtr] = feval(fname);
        end

        function obj = setJourney(obj,fservice,Tstep)

[psgstn,direction,SpeedCommand,TerDist,fgradprof, TEprof]
= feval(fservice);
            obj.psgstn = psgstn; % passenger stop info
            obj.SP_cmd = SpeedCommand; % speed command
            obj.dT = Tstep;       % time step
            obj.Dir = direction; % service direction
            obj.TerDist = TerDist;  % service distance
            obj.fgradprof = fgradprof; % gradient track
profile
            obj.TEprof = TEprof; % TE profile
        end

        function obj = init(obj)
            obj.speed = 0;
            obj.TE = 0;
```

```
            obj.posi = 0;
            obj.mode = 1;
            obj.Ptr = 0;
            obj.Qtr = 0;
            obj.idx_Stn = 1;
            obj.status = 0;
            obj.Vset = 0;
            obj.volt = 0;
            obj.volt_c = 0;
            obj.SinQ = 0;
            obj.H = 0;
            obj.a_int = 0;
            obj.V_diff = 0;
            obj.dis_diff = 0;
            obj.Total_FR = 0;
        end

        function obj = waiting(obj)
                obj.speed = 0;
                obj.posi = 0;
                obj.TE = 0;
                obj.Ptr = 0;
                obj.Qtr = 0;
                obj.volt = 0;
                [SinQ] =
feval(obj.fgradprof,obj.posi,obj.Dir,obj.TerDist);
                obj.SinQ = SinQ;
                obj.H = obj.H;
                obj.a_int = 0;
                obj.Total_FR = 0;
        end

        function obj = terminate(obj)
                obj.speed = 0;
                obj.posi = obj.TerDist;
                obj.TE = 0;
                obj.Ptr = 0;
                obj.Qtr = 0;
                obj.volt = 0;
                obj.status = 2;
                [SinQ] =
feval(obj.fgradprof,obj.posi,obj.Dir,obj.TerDist);
                obj.SinQ = SinQ;
                obj.H = obj.H;
                obj.a_int = 0;
                obj.Total_FR = 0;
        end
```

```
        function obj = perfcalc(obj,t,Train_num)
            obj.Time = t;
            idx = obj.idx_Stn;
            u = obj.speed;
            s = obj.posi;
            TE_max = obj.TE_max;
            v1 = obj.v1;
            v2 = obj.v2;
            dT = obj.dT;
            Meff = (1+obj.psgstn(idx,3))*obj.Mtare;
            ukph = u*3.6;
            TR = obj.TR_coeff(1) + obj.TR_coeff(2)*ukph +
obj.TR_coeff(3)*ukph^2;
            TE_set = TE_track(obj.TEprof,ukph);
            TE = TE_set;
            [SinQ] =
feval(obj.fgradprof,s,obj.Dir,obj.TerDist);
            obj.SinQ = SinQ;
            Fgrad = Meff*9.81*SinQ;
            obj.Total_FR = TR +  Fgrad;
            V_set = fspeed(obj.SP_cmd,s);

            obj.Vset = V_set;
            dist2next = obj.psgstn(idx+1,1);

%****************** station stop mode ******************
            if obj.mode==0  % station stop
                obj.Timer_STNstop = obj.Timer_STNstop +
dT;
                obj.speed = 0;
                obj.posi = dist2next;
                obj.TE = 0;
                obj.a_int = 0;
                obj.H = obj.H;
                obj.Ptr = obj.P_Aux;
                obj.Qtr = obj.Ptr/0.8*sqrt(1-0.8^2);
                if obj.Timer_STNstop>=obj.psgstn(idx+1,2)
                    obj.mode = 1;   % running mode
                    obj.Timer_STNstop = 0;
                    obj.idx_Stn = obj.idx_Stn + 1;
                end
%**************** braking mode **********************
            elseif obj.mode==-1% braking for station stop
                a = obj.dec;
                TE = 0;
                v = u + a*dT;
                ds = u*dT + 0.5*a*(dT)^2;
                s = s + ds;
```

```
                if obj.Dir==1
                    obj.H = obj.H + ds*obj.SinQ;
                else
                    obj.H = obj.H - ds*obj.SinQ;
                end
                obj.a_int = a;
                obj.speed = v;
                obj.posi = s;
                obj.TE = TE;
                Pdrive = TE*v/obj.Eff_total;
                obj.Ptr = obj.P_Aux + Pdrive;
                obj.Qtr = (Pdrive/obj.PFtr*sqrt(1-
obj.PFtr^2))+(obj.P_Aux/0.8*sqrt(1-0.8^2));
                if obj.Ptr<obj.P_Aux
                obj.Ptr = obj.P_Aux;
                obj.Qtr = obj.P_Aux/0.8*sqrt(1-0.8^2);
                end

                if (abs(dist2next-s)<0.5)||(ukph<4)
                  obj.dis_diff = dist2next - s;
                  obj.V_diff = ukph;
                  obj.speed = 0;
                  obj.posi = dist2next;
                  obj.TE = 0;
                  obj.a_int = 0;
                  obj.Ptr = obj.P_Aux;
                  obj.Qtr = obj.Ptr/0.8*sqrt(1-0.8^2);
                  obj.mode = 0;
                    if obj.Dir==1
                      DISP = ['***Track 1, Train number:
',num2str(Train_num),' arrived at station number: ',
num2str(obj.idx_Stn+1),' ***'];
                      disp(DISP);
                    else
                      DISP = ['***Track 2, Train number:
',num2str(Train_num),' arrived at station number: ',
num2str(obj.idx_Stn+1),' ***'];
                      disp(DISP);
                    end
                end

            else        % running mode
%******************** running mode *********************
                    if V_set-u>=0.01 % accelerating mode
                        a = obj.acc; %(V_set-u)/dT;
                        TE = Meff*a + TR + Fgrad;
                    if TE>TE_set
                        TE = TE_set;
```

```
                        a = (TE - TR - Fgrad)/Meff;
                    end

                    elseif V_set-u<=-0.01
                        a = obj.dec;
                        TE = 0;
                    else
                        a = 0;
                        TE = TR + Fgrad;
                        if TE<0
                           TE = 0;
                        end
                    end

                [Dslow, Slow_mode] =
fslowdown(obj.SP_cmd,s,V_set,obj.dec);
                if (Slow_mode==1)&&(ukph>20)
                    a = obj.dec;
                    TE = 0;
                end

                v = u + a*dT;
                ds = u*dT + 0.5*a*(dT)^2;
                s = s + ds;
                if obj.Dir==1
                    obj.H = obj.H + ds*obj.SinQ;
                else
                    obj.H = obj.H - ds*obj.SinQ;
                end
                obj.speed = v;
                obj.a_int = a;
                obj.posi = s;
                obj.TE = TE;
                Pdrive = TE*v/obj.Eff_total;
                obj.Ptr = obj.P_Aux + Pdrive;
                obj.Qtr = (Pdrive/obj.PFtr*sqrt(1-
obj.PFtr^2))+(obj.P_Aux/0.8*sqrt(1-0.8^2));
                if obj.Ptr<obj.P_Aux
                obj.Ptr = obj.P_Aux;
                obj.Qtr = obj.P_Aux/0.8*sqrt(1-0.8^2);
                end

                    [BrakeSig] =
BrakeCheck(dist2next,u,s,dT,obj.dec);
                    if BrakeSig==1
                        obj.mode = -1;
                    end
```

```
                end
%********Check for Service Termination****************
                if obj.posi>=obj.TerDist
                    obj.posi = obj.TerDist;
                    obj.Ptr = 0;
                    obj.Qtr = 0;
                    obj.status = 2;  % status = 2: train
terminated
                    if obj.Dir==1
                      DISP = ['---Track 1, Train number:
',num2str(Train_num),' terminated---'];
                      disp(DISP);
                    else
                      DISP = ['---Track 2, Train number:
',num2str(Train_num),' terminated---'];
                      disp(DISP);
                    end
                end
            end
        end
end
```

(iii) EastCorridor.m: this file contains the East Corridor line train parameters.

```
function [v1, v2, Mtare, acc, dec, TR_coeff, P_AUX,
TE_max, BE_max, Eff_total, PFtr] = EastCorridor

v1 = 70; %km/h
v2 = 90;
Mtare = (176200+14750)*0.453592; %kg

acc = 2.5*0.44704; % mph/s to m/s^2
dec = -2.5*0.44704; % mph/s to m/s^2

TR_coeff = [893.55  11.283  0.5407]; % speed (km/h)
P_AUX = 4*35e3;   % Auxliary power (W) 35 kW per car
PFtr = 0.8;  % Original PFtr = 1.0;
TE_max = 4.44822*19304;
BE_max = 4.44822*19304;
Eff_total = 0.93*0.87; %Mechanical x Electrical
efficiency

return
```

(iv) East_corridor_dn.m: this file contains the passenger stations, the speed command, and the tractive effort profile for down-track service.

```
function
[psgstn,direction,SpeedCommand,TerDist,fgradprof, TEprof]
= East_corridor_dn()

TerDist = 37.00690706e3;

fgradprof = 'trackprof_EC';  % gradient track profile

% Passenger Station Distance (to be stopped)
psgstn = [0e3               35    0.0   % DIA
          8.035424999e3     35    0.0   % 72nd and Himalaya
(Highpoint) option 2
          11.97373727e3     35    0.0   % 64th Avenue Station
option 1
          16.51829543e3     35    0.0   % 40th and airport
          22.71760921e3     35    0.00  % Peoria
          26.73455971e3     35    0.00  % Central Park
Boulevard
          31.22455878e3     35    0.00  % Colorado Boulevard
          34.0360279e3      35    0.00  % 40th and 40th
          37.00690706e3     35    0.00  % Denver Union
Station
          ];

direction = 2;  % up direction = 1, down direction = 2

SpeedCommand = [0e3             24.1401/3.6
                0.437986652e3   24.1401/3.6
                0.437996652e3   64.3736/3.6
                1.23281333e3    64.3736/3.6
                1.23291333e3    127.13786/3.6
                8.065804933e3   127.13786/3.6
                8.065904933e3   112.6538/3.6
                11.97363727e3   112.6538/3.6
                11.97373727e3   127.13786/3.6
                14.70778635e3   127.13786/3.6
                14.70778735e3   120.7005/3.6
                16.05163764e3   120.7005/3.6
                16.05164764e3   96.5604/3.6
                17.87982408e3   96.5604/3.6
                17.87983408e3   56.3269/3.6
                18.31437794e3   56.3269/3.6
                18.31447794e3   104.60713/3.6
                19.55521605e3   104.6071/3.6
```

```
                19.55531605e3     127.13786/3.6
                21.66320829e3     127.13786/3.6
                21.66330829e3     112.6538/3.6
                22.71750921e3     112.6538/3.6
                22.71760921e3     127.13786/3.6
                26.73454971e3     127.13786/3.6
                26.73455971e3     96.5604/3.6
                31.22454878e3     96.5604/3.6
                31.22455878e3     48.2802/3.6
                32.26717733e3     48.2802/3.6
                32.26727733e3     32.186/3.6
                32.71806555e3     32.186/3.6
                32.71807555e3     48.2802/3.6
                34.38187515e3     48.2802/3.6
                34.38197515e3     88.5137/3.6
                35.96073573e3     88.5137/3.6
                35.96083573e3     72.4203/3.6
                36.26157268e3     72.4203/3.6
                36.26167268e3     24.1401/3.6
                37.00690706e3     24.1401/3.6
                37.00790706e3     0
                ];

TEprof = [  1.60934      41417.37642
            4.82802      71736.44394
            8.0467       85868.43888
            11.26538     85828.4049
            14.48406     85788.37092
            17.70274     85748.33694
            20.92142     85703.85474
            24.1401      85654.92432
            27.35878     85605.9939
            30.57746     85557.06348
            33.79614     85503.68484
            37.01482     85445.85798
            40.2335      85388.03112
            43.45218     85325.75604
            46.67086     85263.48096
            49.88954     85196.75766
            53.10822     84938.7609
            56.3269      82060.76256
            59.54558     77599.1979
            62.76426     73302.21738
            65.98294     69805.91646
            69.20162     66216.20292
            72.4203      63026.82918
            75.63898     60282.27744
            78.85766     57497.69172
```

```
                82.07634      55042.27428
                85.29502      52658.02836
                88.5137       50509.5381
                91.73238      48565.66596
                94.95106      46706.31
                98.16974      45002.64174
                101.38842     43370.145
                104.6071      41924.4735
                107.82578     40443.21624
                111.04446     39006.44118
                114.26314     37409.5302
                117.48182     36275.2341
                120.7005      35069.76648
                123.91918     33922.12572
                127.13786     32890.13868
                130.35654     31871.4963
                133.57522     30803.9235
                136.7939      29896.48662];

return
```

(v) East_corridor_up.m: this file contains the passenger stations, the speed command, and the tractive effort profile for up-track service.

```
function
[psgstn,direction,SpeedCommand,TerDist,fgradprof, TEprof]
= East_corridor_up()


TerDist = 37.00690706e3;

fgradprof = 'trackprof01'; % gradient track profile

% Passenger Station Distance (to be stopped) % position
(km)      Dwell time (s)        Psg Factor
psgstn = [0e3                35   0.0  % Denver Union Station
          2.970879167e3      35   0.0  % 40th and 40th
          5.782348278e3      35   0.0
          10.27234736e3      35   0.0  % Central park
boulevard
          14.28929786e3      35   0.00 % Peoria
          20.48861163e3      35   0.00 % 40th and airport
          25.03316979e3      35   0.00 % 64th Avenue Station
option 1
```

```
          28.97148206e3    35   0.00 % 72nd and Himalaya
(Highpoint) option 2
          37.00690706e3    35   0.00  % DIA
          ];

direction = 1; % up direction = 1, down direction = 2

SpeedCommand = [0e3                24.1401/3.6
                0.77570432e3       24.1401/3.6
                0.77571432e3       72.4203/3.6
                1.104507206e3      72.4203/3.6
                1.105507206e3      88.5137/3.6
                2.772659596e3      88.5137/3.6
                2.772759596e3      48.2802/3.6
                4.499652656e3      48.2802/3.6
                4.499752656e3      32.186/3.6
                4.967824442e3      32.186/3.6
                4.967924442e3      48.2802/3.6
                5.935257547e3      48.2802/3.6
                5.935357547e3      96.5604/3.6
                10.82119097e3      96.5604/3.6
                10.82129097e3      127.13786/3.6
                14.29559864e3      127.13786/3.6
                14.29569864e3      112.6538/3.6
                15.75863547e3      112.6538/3.6
                15.75873547e3      127.13786/3.6
                17.46459738e3      127.13786/3.6
                17.46469738e3      104.6071/3.6
                18.73743942e3      104.6071/3.6
                18.73753942e3      56.3269/3.6
                19.3191981e3       56.3269/3.6
                19.3192981e3       96.5604/3.6
                21.08226075e3      96.5604/3.6
                21.08236075e3      120.7005/3.6
                23.30150474e3      120.7005/3.6
                23.30160474e3      127.13786/3.6
                25.03588544e3      127.13786/3.6
                25.03598544e3      112.6538/3.6
                29.21430714e3      112.6538/3.6
                29.21440714e3      127.13786/3.6
                35.85923755e3      127.13786/3.6
                35.85933755e3      64.3736/3.6
                36.60608593e3      64.3736/3.6
                36.60609593e3      24.1401/3.6
                37.00690706e3      24.1401/3.6
                37.00790706e3      0
                ];
```

```
TEprof = [  1.60934     41417.37642
            4.82802     71736.44394
            8.0467      85868.43888
            11.26538    85828.4049
            14.48406    85788.37092
            17.70274    85748.33694
            20.92142    85703.85474
            24.1401     85654.92432
            27.35878    85605.9939
            30.57746    85557.06348
            33.79614    85503.68484
            37.01482    85445.85798
            40.2335     85388.03112
            43.45218    85325.75604
            46.67086    85263.48096
            49.88954    85196.75766
            53.10822    84938.7609
            56.3269     82060.76256
            59.54558    77599.1979
            62.76426    73302.21738
            65.98294    69805.91646
            69.20162    66216.20292
            72.4203     63026.82918
            75.63898    60282.27744
            78.85766    57497.69172
            82.07634    55042.27428
            85.29502    52658.02836
            88.5137     50509.5381
            91.73238    48565.66596
            94.95106    46706.31
            98.16974    45002.64174
            101.38842   43370.145
            104.6071    41924.4735
            107.82578   40443.21624
            111.04446   39006.44118
            114.26314   37409.5302
            117.48182   36275.2341
            120.7005    35069.76648
            123.91918   33922.12572
            127.13786   32890.13868
            130.35654   31871.4963
            133.57522   30803.9235
            136.7939    29896.48662];

return
```

(vi) TE_track.m: this file contains the code that tracks the tractive effort from the specification.

```
function TE = TE_track(XV,v)

ind = find(XV(:,1)>v);

if length(ind)==0
    TE = XV(length(XV(:,2),2));
else
    h = ind(1);
    if h==1
        TE = XV(1,2);
    else
        TE = XV(h-1,2) + (v - XV(h-1,1))*(XV(h,2)-XV(h-
1,2))/(XV(h,1)-XV(h-1,1));
    end
end

return
```

(vii) trackprof_EC.m: this file contains the route's grade profile and calculates the slope angle.

```
function [SinQ] = trackprof_EC(s,direction,TerDist)

SH = [  0           0
        0.120700539 0
        0.418489494 0
        0.426414277 0
        0.482802154 0.54
        0.650136992 -0.54
        0.662938564 -0.54
        0.745234386 -0.54
        0.77571432  -0.54
        0.791868685 -0.54
        0.833626195 -0.45
        0.873859708 -0.26
        0.914093221 -0.07
        1.046071335 0.03
        1.105507206 0.03
        1.189327025 0.03
        1.287472412 -0.03
        1.37129223  0.03
        1.448406463 0.03
```

```
1.480715194 0.03
1.585261367 0.03
1.62549488  0.12
1.665728393 0.32
1.707485902 0.51
1.90712947  0.61
2.147006551 0.61
2.43808992  0.61
2.478323433 0.53
2.520080943 0.36
2.560314456 0.2
2.624931916 0.11
2.772759596 0.11
2.940399233 0.11
2.970879167 0.11
3.170522734 0.11
3.414971805 0.11
3.657896879 0.11
3.698130392 0.07
3.738363905 -0.02
3.778597417 -0.1
4.145575823 -0.14
4.185809336 0
4.226042849 0.29
4.268105157 0.58
4.288831513 0.69
4.499752656 0.69
4.538462172 0.69
4.739629736 0.69
4.967924442 0.69
5.008157955 0.82
5.050220264 1
5.090453777 1.19
5.394643518 1.28
5.421770659 1.17
5.436401028 1.17
5.47663454  0.95
5.510467267 0.74
5.516868053 0.74
5.539423204 0.63
5.627815013 0.63
5.751868344 0.63
5.782348278 0.63
5.935357547 0.63
6.017348569 0.63
6.051181296 0.63
6.144449894 0.63
6.282828795 0.63
```

```
6.553185809 0.63
6.593419322 0.58
6.635176832 0.48
6.675410344 0.38
6.75587737  0.33
7.25483389  0.33
7.295067403 0.36
7.335300915 0.44
7.375534428 0.52
7.792499925 0.56
7.906799678 0.56
7.962882756 0.56
8.064380937 0.56
8.473116852 0.56
8.513350364 0.44
8.555107874 0.22
8.595341387 -0.01
9.662443876 0.1
9.704201386 -0.1
9.742910902 -0.07
9.784668411 -0.04
9.791373997 -0.03
9.876413013 -0.03
10.03429907 -0.03
10.24186742 -0.03
10.27234736 -0.03
10.82129097 -0.03
10.86152448 -0.29
10.90175799 -0.81
10.94199151 -1.33
11.03373611 -1.59
11.0852472  -1.25
11.13492949 -0.56
11.18644058 0.13
11.67411952 0.47
11.71435303 0.46
11.75458655 0.43
11.79634406 0.39
12.284023   0.37
12.32425651 0.44
12.36449002 0.56
12.40472354 0.68
13.25938089 0.74
13.2996144  0.66
13.33984791 0.5
13.38008143 0.33
14.25881792 0.25
14.28929786 0.25
```

14.29569864	0.25
14.33593216	0.38
14.37616567	0.65
14.41639918	0.91
14.81385752	1.04
14.85409103	0.88
14.89432455	0.57
14.93455806	0.25
15.34359877	0.1
15.75873547	0.1
15.7925682	0.19
15.79896899	0.19
15.8392025	0.39
15.87943601	0.59
15.92271752	0.69
16.00166055	0.69
16.36863895	0.69
16.40887247	0.65
16.44910598	0.57
16.48933949	0.5
17.45159101	0.47
17.46469738	0.47
17.50645489	0.51
17.54516441	0.61
17.57869233	0.71
17.58692192	0.71
17.67226573	0.76
18.29497078	0.76
18.4254249	0.76
18.47510719	1.3
18.52661828	2.38
18.57812937	3.46
18.66042519	4
18.69242912	4
18.73753942	4
18.80368088	3.31
18.86951754	1.93
18.9353542	0.55
19.12707298	-0.14
19.7192981	-0.14
19.88815693	-0.14
19.94454481	-0.7
19.99940869	-1.82
20.05549177	-2.94
20.10883165	-3.5
20.25361134	-3.5
20.30512243	-2.91
20.35480472	-1.73

```
20.40631581 -0.55
20.4581317  0.04
20.48861163 0.04
20.85559004 0.04
20.89399475 0.04
20.91502591 -0.03
20.93605706 -0.18
20.95525942 -0.33
21.08236075 0.4
21.40270485 -0.4
21.48621987 -0.4
22.1186785  -0.4
22.15891202 -0.4
22.19914553 -0.47
22.24120784 -0.6
22.28144135 -0.74
22.29911971 -0.8
23.30160474 -0.8
23.34183825 -0.58
23.38359576 -0.13
23.42382928 0.32
23.4610148  0.54
23.72801902 0.54
23.77953011 0.25
23.83104119 -0.34
23.84567156 -0.92
23.88102829 -0.92
24.59730673 -1.21
24.63754025 -1
24.67929776 -0.56
24.71953127 -0.11
25.00268986 0.1
25.03316979 0.1
25.93598544 0.1
26.77631722 0.1
26.8278283  -0.15
26.8775106  -0.66
26.92902169 -1.16
27.33318561 -1.42
27.3843919  -1.09
27.43437899 -0.44
27.44260857 0.22
27.48589008 0.22
27.97996981 0.54
28.02172732 0.58
28.06196083 0.67
28.10219434 0.75
28.16345901 -0.79
```

```
28.94100213 0.79
28.97148206 0.79
29.21440714 0.79
29.28207259 1.23
29.34790925 2.13
29.4140507  3.03
29.49756572 3.48
29.60546469 2.57
29.62466705 2.57
29.75024438 0.76
29.8773457  -1.06
30.4342141  -1.96
30.52108191 -1.41
30.59667214 -0.31
30.60642572 -0.31
30.69329353 0.79
30.8463028  1.34
30.94749618 0.7
30.99748328 -0.58
31.04899436 -0.58
31.15049254 -1.86
31.39494161 -2.5
31.49643979 -1.84
31.59793797 -0.52
31.69913136 0.79
31.99539631 1.45
33.03963885 1.45
33.09114994 1.23
33.14113703 0.79
33.19264812 0.36
33.45172756 0.14
33.49196107 0.08
33.53371858 -0.03
33.5739521  -0.15
33.7559173  -0.21
33.81718197 -0.48
33.87814184 -1.04
33.9394065  -1.59
34.19848594 -1.87
34.23871946 -1.64
34.28047697 -1.18
34.32071048 -0.73
35.55514781 -0.5
35.6051349  -0.14
35.65664599 0.58
35.70815707 1.29
35.77399373 1.65
35.85933755 1.65
```

```
        35.90109506 1.33
        35.9251742  0.69
        35.94132857 0.69
        35.98156208 0.05
        36.09586183 -0.27
        36.12634177 -0.87
        36.14249613 -2.08
        36.1571265  -2.08
        36.18760644 -3.28
        36.25527189 -3.88
        36.28575182 -3.33
        36.31623176 -2.23
        36.34701649 -1.12
        36.56891041 -0.57
        36.60609593 -0.57
        36.63169907 0.19
        36.65760702 1.71
        36.68321016 3.24
        36.73655005 4
        36.75575241 3.33
        36.77678356 2
        36.79750992 0.67
        36.85389779 0
        36.88437773 0
        37.00690706 0
     ];

if direction==1

    ind = find(SH(:,1)>s*1e-3);

  if length(ind)==0
    SinQ = 0;
  else
    hx = ind(1);
    dH = SH(hx,2) - SH(hx-1,2);
    dS = SH(hx,1) - SH(hx-1,1);
    tanQ = ((dH)/(dS))*((s*1e-3)-SH(hx-1,1))+SH(hx-1,2);
    tanQ = tanQ/100;
    SinQ = tanQ/sqrt(1+tanQ^2);
  end

else

    ind = find(SH(:,1)<(TerDist-s)*1e-3);
  if length(ind)==0
    SinQ = 0;
  else
```

```
    hx = ind(end);
    dH = SH(hx,2) - SH(hx+1,2);
    dS = SH(hx,1) - SH(hx+1,1);
    tanQ = ((dH)/(dS))*(((TerDist-s)*1e-3)-
SH(hx,1))+SH(hx,2);
    tanQ = tanQ/100;
    SinQ = tanQ/sqrt(1+tanQ^2);
  end

end

return
```

(viii) fspeed.m: this file tracks the command speed from the speed command profile.

```
function v = fspeed(XV,x)

ind = find(XV(:,1)>x);

if length(ind)==0
    v = XV(length(XV(:,2),2));
else
    h = ind(1);
    v = XV(h-1,2) + (x - XV(h-1,1))*(XV(h,2)-XV(h-
1,2))/(XV(h,1)-XV(h-1,1));
end

return
```

(ix) fslowdown.m: this file detects braking points and calculates braking distance in order to keep the speed below the specified limits.

```
function [Dslow, Slow_mode] = fslowdown(XV,x,Vc,a)

    ind = find(XV(:,1)>x);
    if length(ind)==0
        Vn = XV(end,2);
    else
        h = ind(2);
        Vn = XV(h,2);
    end
        if (Vc>Vn)
```

```
            Dslow = (Vn^2-Vc^2)/(2*a);
         else
            Dslow = -1;
         end

         if (XV(h,1)-x)<Dslow
             Slow_mode = 1;
         else
             Slow_mode = 0;
         end
return
```

(x) BrakeCheck.m: this file detects braking points and calculates braking distance in order to stop at a passenger station.

```
function [BrakeSig] = BrakeCheck(D2N,V,S,dT,a)

   while V>0
                 ds = V*dT + 0.5*a*(dT)^2;
                 V = V + a*dT;
                 S = S + ds;
    end
  dis_diff = D2N-S;
  if abs(dis_diff)<1
      BrakeSig = 1;
  else
      BrakeSig = 0;
  end

return
```

E.3 Optimal RPC sizing programmes

The following file list is used in the optimal sizing procedure.

(i) main_optimal_sizing_PSO.m: this file contains the code that runs the MATLAB's PSO toolbox for RPC sizing optimisation.

```
%% Main code for minimising the fitness function using
PSO
ObjFcn = @LoadFlow;
nvars = 4;
% For Scott transformer
lb = [0.700 0.700    -10*pi/180  80*pi/180];
ub = [1.000 1.000     1*pi/180   91*pi/180];

% For V/V transformer
% lb = [0.70  0.70    20*pi/180  80*pi/180];
% ub = [1.00  1.00    31*pi/180  91*pi/180];

y1 = 0.5;
y2 = 1.6;

options = optimoptions('particleswarm','SwarmSize',25,...
%'Display','iter','PlotFcn','pswplotbestf',...
'StallIterlimit',500,'TolFun',1e-
30,'SelfAdjustment',y1,'SocialAdjustment',y2,...
'ObjectiveLimit',1e-
10,'InitialSwarmSpan',2000,'InertiaRange',[0.4,0.8],'MinF
ractionNeighbors',0.25,...
'MaxIter',6000);

[x,fval,exitflag,output] =
particleswarm(ObjFcn,nvars,lb,ub,options);
```

(ii) main_optimal_sizing_GA.m: this file contains the code that runs the MATLAB's GA toolbox for RPC sizing optimisation.

```
%% Main code for minimising the fitness function using GA
(Genetic Algorithm)
ObjFcn = @LoadFlow;
nvars = 4;
% For Scott transformer
LB = [0.700 0.700    -10*pi/180  80*pi/180];
UB = [1.000 1.000     1*pi/180   91*pi/180];
```

```
 % For V/V transformer
% LB = [0.70  0.70    20*pi/180  80*pi/180];
% UB = [1.00  1.00    31*pi/180  91*pi/180];

options = gaoptimset(@ga);
options =
gaoptimset(options,'Generations',6000,'PopulationSize',50
,'TolFun',1e-30,'PopInitRange',[-
0.20;1.6],'CrossoverFraction',0.5,'EliteCount',3,'StallGe
nLimit',500);
options = gaoptimset(options,'PlotFcns',
{@gaplotbestf},...
    'MutationFcn',{[@mutationadaptfeasible] [1] [1]});

[x,fval,exitflag,output,population,scores] =
ga(ObjFcn,nvars,[],[],[],[],LB,UB,[],[],options);
```

(iii) Supply_parameter.m: this file contains the East Corridor line's traction power supply system parameters.

```
function Supply_parameter(VA,VB,VC,a1,a2)

global NTRACK Jss1 Jss2 Yss1 Yss2 Zoh ZBase SBase VBase
Zshc YRE_ballast JBase
SBase=1e6;
VBase=25e3;
ZBase=VBase^2/SBase;
JBase=SBase/VBase;
NTRACK=2;

Zoh=(1/ZBase)*[0.248+1.024i 0 0;
    0 0.1648+0.6709i 0;
    0 0 0.311+1.356i]/1.60934;
Yse=0;
ZRE_ballast=0.5;
YRE_ballast=ZBase/ZRE_ballast*[0 0 0;0 1 0;0 0 0];

SCC=500e6; % Short circuit capacity
Zshc=(115e3)^2/SCC;
f=60; % frequency (Hz)

%For Scott transformer
Rp=0; % Resistance in primary side(ohm)
Rs=0; % Resistance in secondary side(ohm)
X1=0.07*((115e3)^2/10e6);
```

```
Ls=1e-3; % Inductance in secondary side(H)
Zp=(Rp+X1*1j);
Zs=(Rs+(2*pi*f*Ls)*1j);
ZA=Zp;
ZB=Zp/2;
ZC=Zp/2;

A = (2*VA-VB-VC)/(2*a1);
D = (VC-VB)/a2;
F = (4*ZA+ZB+ZC+8*Zs*a1^2)/(16*a1^2);
G = (4*ZA+ZB+ZC)/(16*a1^2);
H = (ZB+ZC)/(4*a2^2);
J = (ZB+ZC+2*Zs*a2^2)/(4*a2^2);

Jss1=(1/JBase)*(1/(G+F))*(A/2)*[1;0;-1];
Yss1 = ZBase*[F/(F^2-G^2) -1/(F-G) G/(F^2-G^2);
    -1/(F-G) (2/(F-G))+NTRACK*Yse -1/(F-G);
    G/(F^2-G^2) -1/(F-G) F/(F^2-G^2)];

Jss2=(1/JBase)*(1/(H+J))*(D/2)*[1;0;-1];
Yss2 = ZBase*[J/(J^2-H^2) -1/(J-H) H/(J^2-H^2);
    -1/(J-H) (2/(J-H))+NTRACK*Yse -1/(J-H);
    H/(J^2-H^2) -1/(J-H) J/(J^2-H^2)];

%For V/V transformer
% a=115/25;
% R1=0; % Resistance in primary side(ohm)
% R2=0; % Resistance in secondary side(ohm)
% Rm=1.3824e8;
% X1=0.07*((115e3)^2/10e6);
% X2=0;
% Xm=1i*2*pi*60*800.68;
% Zm=Rm*Xm/((Rm+Xm)*a^2);
% Zpts=(R1/a^2)+1i*(X1/a^2);
% Z1=(Zpts*Zm/(Zpts+Zm))+(R2+1i*X2);
% Y1=1/Z1;
% Y2=Y1;
% Jss1=(1/JBase)*((VA-VB)/a)/Z1*[1;0;-1];
% Jss2=(1/JBase)*((VC-VB)/a)/Z1*[1;0;-1];
%
% Yss1=ZBase*[Y1 -Y1 0;
%     -Y1 Y1+Y2+NTRACK*Yse -Y2;
%      0 -Y2 Y2];
% Yss2 = Yss1;

return
```

(iv) Network_config.m: this file contains line data and bus data for power flow calculation.

```
function [Ldata,Bdata]= Network_config()

global Tnum NB Tbus NTRACK TV0mag TV0angle
%*******************************************************
% Max. Different power case (double load)
NB = 9;

Ldata = [3  1  8.368568000000000
         3  1  8.368568000000000
         2  6  0.981483071096597
         6  4  10.444830928903402
         2  7  1.537859748138578
         7  4  9.888454251861422
         4  5  7.081096000000001
         4  5  7.081096000000001
         5  8  1.773780820337215
         5  9  2.696575610897414];

Bdata = [1   0                 0                     0
         2   0                 0                     0
         3   0                 0                     2
         4   0                 0                     2
         5   0                 0                     2
         6   3.221270883537118  2.415953162652837    3
         7   0.422691837804576  0.317018878353432    3
         8   3.109445842094624  2.332084381570967    3
         9   1.242532803790648  0.931899602842986    3];

NTRACK = 2;
Tnum = [0 4];
Tbus = [6 7 8 9];
Tphase = [1 3];
Mphase = [2 4 5 6 7 8 9];

%*******************************************************
% % Max. Different power case (triple load)
% NB = 9;
%
% Ldata = [3  1  8.368568000000000
%          3  1  8.368568000000000
%          2  6  0.981483071096597
%          6  4  10.444830928903402
%          2  7  1.537859748138578
%          7  4  9.888454251861422
```

```
%           4  5  7.081096000000001
%           4  5  7.081096000000001
%           5  8  1.773780820337215
%           5  9  2.696575610897414];
%
% Bdata = [1  0                  0                  0
%           2  0                  0                  0
%           3  0                  0                  2
%           4  0                  0                  2
%           5  0                  0                  2
%           6  4.759303427183076  3.569477570387306  3
%           7  0.473670528834820  0.355252896626115  3
%           8  4.583012119841060  3.437259089880794  3
%           9  1.711176948949800  1.283382711712350  3];
%
% NTRACK = 2;
% Tnum = [0 4];
% Tbus = [6 7 8 9];
% Tphase = [1 3];
% Mphase = [2 4 5 6 7 8 9];
%*******************************************************
% % % Max. power case (double load)
% NB = 10;
%
% Ldata = [3  7  4.712675287771896
%           7  1  3.655892712228104
%           3  6  0.238372879336459
%           6  1  8.130195120663542
%           2  4  11.426314
%           2  8  7.253335254300037
%           8  4  4.172978745699962
%           4  9  3.980865626629737
%           9  5  3.100230373370263
%           4  5  7.081096000000001
%           5 10  8.691501779294116];
%
% Bdata = [1  0                  0                  0
%           2  0                  0                  0
%           3  0                  0                  2
%           4  0                  0                  2
%           5  0                  0                  2
%           6  0.239984388918013  0.179988291688510  3
%           7  3.314647307413686  2.485985480560264  3
%           8  3.017009810846273  2.262757358134704  3
%           9  1.739704307441183  1.304778230580887  3
%          10  0.150914628735838  0.113185971551878  3];
%
% NTRACK = 2;
```

```
% Tnum = [2 3];
% Tbus = [6 7 8 9 10];
% Tphase = [1 3 6 7];
% Mphase = [2 4 5 8 9 10];
%********************************************************
% % Max. power case (triple load)
% NB = 10;
%
% Ldata = [3  7  4.712389757959241
%          7  1  3.656178242040760
%          3  6  0.236864353199367
%          6  1  8.131703646800633
%          2  4  11.426314
%          2  8  7.263542523345162
%          8  4  4.162771476654838
%          4  9  3.980599354748093
%          9  5  3.100496645251908
%          4  5  7.081096000000001
%          5 10  8.691546548727079];

% Bdata = [1  0                  0                  0
%          2  0                  0                  0
%          3  0                  0                  2
%          4  0                  0                  2
%          5  0                  0                  2
%          6  0.247769014433248  0.185826760824936  3
%          7  4.901661416080969  3.676246062060725  3
%          8  4.455271419583055  3.341453564687290  3
%          9  2.531774389948317  1.898830792461237  3
%         10  0.150899719758562  0.113174789818922  3];
%
% NTRACK = 2;
% Tnum = [2 3];
% Tbus = [6 7 8 9 10];
% Tphase = [1 3 6 7];
% Mphase = [2 4 5 8 9 10];

%******************************************************
TV0mag=zeros(3*NB,1);
TV0angle=zeros(3*NB,1);

%For Scott transformer
for u=1:NB
    for p=1:length(Tphase)
        if (u==Tphase(p))
        TV0mag(3*u-2,1)= 1.00;
        TV0mag(3*u-1,1)= 0.01;
        TV0mag(3*u,1)= -1.00;
```

```
        TV0angle(3*u-2,1)= 0;
        TV0angle(3*u-1,1)= 0;
        TV0angle(3*u,1)= 0;
        end
    end

    for q=1:length(Mphase)
        if (u==Mphase(q))
        TV0mag(3*u-2,1)= 1.00;
        TV0mag(3*u-1,1)= 0.01;
        TV0mag(3*u,1)= -1.00;
        TV0angle(3*u-2,1)= pi/2;
        TV0angle(3*u-1,1)= pi/2;
        TV0angle(3*u,1)= pi/2;
        end
    end
end

%For V/V transformer
% for u=1:NB
%     for p=1:length(Tphase)
%         if (u==Tphase(p))
%         TV0mag(3*u-2,1)= 1.00;
%         TV0mag(3*u-1,1)= 0.01;
%         TV0mag(3*u,1)= -1.00;
%         TV0angle(3*u-2,1)= pi/6;
%         TV0angle(3*u-1,1)= pi/6;
%         TV0angle(3*u,1)= pi/6;
%         end
%     end
%
%     for q=1:length(Mphase)
%         if (u==Mphase(q))
%         TV0mag(3*u-2,1)= 1.00;
%         TV0mag(3*u-1,1)= 0.01;
%         TV0mag(3*u,1)= -1.00;
%         TV0angle(3*u-2,1)= pi/2;
%         TV0angle(3*u-1,1)= pi/2;
%         TV0angle(3*u,1)= pi/2;
%         end
%     end
% end

return
```

(v) LoadFlow.m: this file is the main programme to execute power flow calculation.

```
function [SRPC_out]=LoadFlow(x)

global TV0mag TV0angle NB Yss1 Yss2 Jss1 Jss2 Zshc VBase
JBase ZBase
m1 = x(1);
m2 = x(2);
delta1 = x(3);
delta2 = x(4);
t = [1 1 1 1 1 1] ; % Set all AT's taps to 1
Vgrid = 115e3;
Vtrac = 50e3;
a1=(sqrt(3)/2)*(Vgrid/Vtrac);
a2=Vgrid/Vtrac;
ph=exp(2*pi*1j/3);
va=Vgrid/sqrt(3);
vb=Vgrid*(ph^2)/sqrt(3);
vc=Vgrid*(ph)/sqrt(3);

%RPC
aRPC = Vtrac/3e3;
Zcom1 = 1j*52.3599;
Zcom2 = 1j*52.3599;
VDC = 11000;
Zcom1_mag = abs(Zcom1);
Zcom1_ang = angle(Zcom1);
Zcom2_mag = abs(Zcom2);
Zcom2_ang = angle(Zcom2);
Icom1 = (0.5*m1*VDC*aRPC/(sqrt(2)*Zcom1_mag))*cos(delta1-
Zcom1_ang)+1j*(0.5*m1*VDC*aRPC/(sqrt(2)*Zcom1_mag))*sin(d
elta1-Zcom1_ang);
Icom2 = (0.5*m2*VDC*aRPC/(sqrt(2)*Zcom2_mag))*cos(delta2-
Zcom2_ang)+1j*(0.5*m2*VDC*aRPC/(sqrt(2)*Zcom2_mag))*sin(d
elta2-Zcom2_ang);
Vcom1 =
(0.5*m1*VDC*aRPC/(sqrt(2)))*cos(delta1)+1j*(0.5*m1*VDC*aR
PC/(sqrt(2)))*sin(delta1);
Vcom2 =
(0.5*m2*VDC*aRPC/(sqrt(2)))*cos(delta2)+1j*(0.5*m2*VDC*aR
PC/(sqrt(2)))*sin(delta2);
VpccA(1,1)=va;
VpccB(1,1)=vb;
VpccC(1,1)=vc;
error_V(1,1)=1;
s=1;
```

```
 while (error_V(s,1)>=1e-6)
    TV0mag=[];
    TV0angle=[];

Supply_parameter(VpccA(s,1),VpccB(s,1),VpccC(s,1),a1,a2);
    [Ldata,Bdata]=Network_config;
    build_ybus(Ldata,Zcom1,Zcom2,t);
    k=0;
    [G,H]=Cal_Jbus(Bdata,Icom1,Icom2);
    F=[G;H];
    max_err=max(abs(F));

    while (max_err>=1e-6)
        [A,B,C,D]=Cal_Jacobian(Bdata);
        J=[A B;C D];
        dV=inv(J)*F;
        dV_mag=dV(1:3*NB,1);
        dV_angle=dV(3*NB+1:6*NB);
        TVmag=TV0mag-dV_mag;
        TV0mag=TVmag;
        TVangle=TV0angle-dV_angle;
        TV0angle=TVangle;
        k=k+1;
        [G,H]=Cal_Jbus(Bdata,Icom1,Icom2);
        F=[G;H];
        max_err=max(abs(F));
        max_error(k,1)=max_err;
    end

    VD = 0;

    for u=1:NB
        TVCmag(u,1)=TV0mag(3*u-2,1)*VBase/1e3; % kV
        TVRmag(u,1)=TV0mag(3*u-1,1)*VBase; % V
        TVFmag(u,1)=TV0mag(3*u,1)*VBase/1e3; % kV

        TVCangle(u,1)=TV0angle(3*u-2,1);
        TVRangle(u,1)=TV0angle(3*u-1,1);
        TVFangle(u,1)=TV0angle(3*u,1);
    end

    for u=1:NB
        if TVCmag(u,1)<0
            TVCmag(u,1)=abs(TVCmag(u,1));
            TVCangle(u,1)=TVCangle(u,1)+pi;
        end
        if TVRmag(u,1)<0
            TVRmag(u,1)=abs(TVRmag(u,1));
```

```
            TVRangle(u,1)=TVRangle(u,1)+pi;
        end
        if TVFmag(u,1)<0
            TVFmag(u,1)=abs(TVFmag(u,1));
            TVFangle(u,1)=TVFangle(u,1)+pi;
        end

        VD = VD + abs(1e3*TVCmag(u,1)-(Vtrac/2)) +
abs(TVRmag(u,1)) + abs(1e3*TVFmag(u,1)-(Vtrac/2));

    end

    TVC=TVCmag.*cos(TVCangle)+1i*TVCmag.*sin(TVCangle);
    TVR=TVRmag.*cos(TVRangle)+1i*TVRmag.*sin(TVRangle);
    TVF=TVFmag.*cos(TVFangle)+1i*TVFmag.*sin(TVFangle);

    % For Scott transformer
    It = -
Yss1*(1/ZBase)*[TVC(1)*1e3;TVR(1);TVF(1)*1e3]+Jss1*JBase;
    Im = -
Yss2*(1/ZBase)*[TVC(2)*1e3;TVR(2);TVF(2)*1e3]+Jss2*JBase;
    ITC = It(1); ITR = It(2); ITF = It(3);
    IMC = Im(1); IMR = Im(2); IMF = Im(3);
    IA= ITC/(2*a1)-ITF/(2*a1);
    IB=(-1/(4*a1))*ITC+(1/(4*a1))*ITF-
(1/(2*a2))*IMC+(1/(2*a2))*IMF;
    IC=(-1/(4*a1))*ITC+(1/(4*a1))*ITF+(1/(2*a2))*IMC-
(1/(2*a2))*IMF;

    % For V/V transformer
%     It = -
Yss1*(1/ZBase)*[TVC(1)*1e3;TVR(1);TVF(1)*1e3]+Jss1*JBase;
%     Im = -
Yss2*(1/ZBase)*[TVC(2)*1e3;TVR(2);TVF(2)*1e3]+Jss2*JBase;
%     ITC = It(1); ITR = It(2); ITF = It(3);
%     IMC = Im(1); IMR = Im(2); IMF = Im(3);
%     Ip1 = (1/(2*a))*(ITC-ITF);
%     Ip2 = (1/(2*a))*(IMC-IMF);
%     IA = Ip1;
%     IB = -Ip1-Ip2;
%     IC = Ip2;

    Z=Zshc;
    Va=va-1j*Z*IA;
    Vb=vb-1j*Z*IB;
    Vc=vc-1j*Z*IC;
    VpccA(s+1,1)=Va;
    VpccB(s+1,1)=Vb;
```

```
    VpccC(s+1,1)=Vc;
    error_V(s+1,1)=max([abs(VpccA(s+1,1)-VpccA(s,1))
abs(VpccB(s+1,1)-VpccB(s,1)) abs(VpccC(s+1,1)-
VpccC(s,1))]);
    s=s+1;
end

Vab=Va-Vb;
Vbc=Vb-Vc;
Vca=Vc-Va;
V0=(1/3)*(Va+Vb+Vc);
V1=(1/3)*(Va+ph*Vb+Vc*(ph)^2);
V2=(1/3)*(Va+Vb*(ph)^2+Vc*ph);
Vp=(1/3)*(Vab+ph*Vbc+Vca*(ph)^2);
Vn=(1/3)*(Vab+Vbc*(ph)^2+Vca*ph);
I0=(1/3)*(IA+IB+IC);
I1=(1/3)*(IA+ph*IB+IC*(ph)^2);
I2=(1/3)*(IA+IB*(ph)^2+IC*ph);
VUF = abs(V2/V1)*100;
IUF = abs(I2/I1)*100;
SA = Va*conj(IA);
SB = Vb*conj(IB);
SC = Vc*conj(IC);
S3p = SA + SB + SC;
ST = TVC(1)*1e3*conj(ITC) + TVR(1)*conj(ITR) +
TVF(1)*1e3*conj(ITF);
SM = TVC(2)*1e3*conj(IMC) + TVR(2)*conj(IMR) +
TVF(2)*1e3*conj(IMF);
pf3p = real(S3p)/abs(S3p);
pfA = sign(imag(SA))*real(SA)/abs(SA);
pfB = sign(imag(SB))*real(SB)/abs(SB);
pfC = sign(imag(SC))*real(SC)/abs(SC);
pft = sign(imag(ST))*real(ST)/abs(ST);
pfm = sign(imag(SM))*real(SM)/abs(SM);

%*********************************************************
*****************
% Max. Different power case (double load)
PTtotal = 0;
PMtotal = Bdata(6,2)+Bdata(7,2)+Bdata(8,2)+Bdata(9,2);
QTtotal = 0;
QMtotal = Bdata(6,3)+Bdata(7,3)+Bdata(8,3)+Bdata(9,3);
QT = 0.0802e-6;
QM = 6.4584;
PT = 0.0291e-6;
PM = 8.0985;
P_Hdiff = 0.5*8.0985;
```

```
%**************************************************************
****************
% % Max. Different power case (triple load)
% PTtotal = 0;
% PMtotal = Bdata(6,2)+Bdata(7,2)+Bdata(8,2)+Bdata(9,2);
% QTtotal = 0;
% QMtotal = Bdata(6,3)+Bdata(7,3)+Bdata(8,3)+Bdata(9,3);
% QT = 0.0805e-6;
% QM = 9.7578;
% PT = 0.0293e-6;
% PM = 11.775;
% P_Hdiff = 0.5*11.7754;

%
%**************************************************************
****************
% % % Max. power case (double load)
% PTtotal = Bdata(6,2)+Bdata(7,2);
% PMtotal = Bdata(8,2)+Bdata(9,2)+Bdata(10,2);
% QTtotal = Bdata(6,3)+Bdata(7,3);
% QMtotal = Bdata(8,3)+Bdata(9,3)+Bdata(10,3);
% QT = 2.7592;
% QM = 3.9207;
% PT = 3.5783;
% PM = 4.9614;
% P_Hdiff = 0.5*1.38312;

%**************************************************************
****************
% % Max. power case (triple load)
% PTtotal = Bdata(6,2)+Bdata(7,2);
% PMtotal = Bdata(8,2)+Bdata(9,2)+Bdata(10,2);
% QTtotal = Bdata(6,3)+Bdata(7,3);
% QMtotal = Bdata(8,3)+Bdata(9,3)+Bdata(10,3);
% QT = 4.0692;
% QM = 5.9073;
% PT = 5.2027;
% PM = 7.2628;
% P_Hdiff = 0.5*2.06005;
%**************************************************************
****************

QTmax = QT;
QMmax = QM;
Ploss = (real(S3p)/1e6)-(PTtotal+PMtotal);

Stransfer1 = ((TVC(1)-TVF(1))*1e3)*conj(Icom1-
((1/Zcom1)*(TVC(1)-TVF(1))*1e3));
```

```
Stransfer2 = ((TVC(2)-TVF(2))*1e3)*conj(Icom2-
((1/Zcom2)*(TVC(2)-TVF(2))*1e3));
Sum_power = Stransfer1+Stransfer2;
SC1 = 1e-
6*sqrt((max(abs(real(Stransfer1)),abs(real(Stransfer2))))
^2+(max(imag(Stransfer1),imag(Stransfer2)))^2);
SC2 = 1e-
6*sqrt((max(abs(real(Stransfer1)),abs(real(Stransfer2))))
^2+(max(imag(Stransfer1),imag(Stransfer2)))^2);
sRPC = SC1 + SC2;
sRPC_full = 2*sqrt((P_Hdiff)^2+(QMmax)^2);

ic1 = 0; ic2 = 0; ic3 = 0; ic4 = 0; ic5 = 0; ic6 = 0; ic7
= 0; ic8 = 0; ic9 =0; ic10 = 0;

SRPC_out = sRPC; % target
g1 =  1e-3;%1e-3;
g2 =  1e10;%1e6;

if (abs(real(Sum_power))>10)
    SRPC_out = SRPC_out + g1*abs(real(Sum_power))^2;
    ic1 = 1;
end

if (abs(real(Stransfer1))> P_Hdiff*1e6)
    SRPC_out = SRPC_out + g1*(abs(real(Stransfer1))-
P_Hdiff*1e6)^2;
    ic2 = 1;
end

if
((imag(Stransfer1)>=1e6*QTmax)||(imag(Stransfer1)<0*1e6*Q
Tmax))
    SRPC_out = SRPC_out + g1*(abs(1e6*QTmax-
imag(Stransfer1)))^2;
    ic3 = 1;
end

if
((imag(Stransfer2)>=1*1e6*QMmax)||(imag(Stransfer2)<0*1e6
*QMmax))
    SRPC_out = SRPC_out + g1*(abs(1e6*QMmax-
imag(Stransfer2)))^2;
    ic4 = 1;
end

if (imag(ST)<0)
    SRPC_out = SRPC_out + g1*(imag(ST))^2;
```

```
    ic5 = 1;
end

if (imag(SM)<0)
    SRPC_out = SRPC_out + g1*(imag(SM))^2;
    ic6 = 1;
end

if (VUF>2.0)
    SRPC_out = SRPC_out + g2*(VUF)^2;
    ic7 = 1;
end

if (abs(pfA)<0.90)
    SRPC_out = SRPC_out + g2*(abs(pfA))^-2;
    ic8 = 1;
end

if (abs(pfB)<0.90)
    SRPC_out = SRPC_out + g2*(abs(pfB))^-2;
    ic9 = 1;
end

if (abs(pfC)<0.90)
    SRPC_out = SRPC_out + g2*(abs(pfC))^-2;
    ic10 = 1;
end
```

(vi) YATcal.m: this file calculates the AT's admittance matrix.

```
function Yat = YATcal(t)

global ZBase

Zg = (0.015/2)*((50e3)^2/2e6)*1j;
Zm =(101.4+1j*279.1)*1e8;

M = Zg+((t-1)/(t+1))*(t/(t+1))*Zm;
N = ((t-1)/(t+1))*Zm;
P = Zm + 2*Zg;
Q = Zg + (t/(t+1))*Zm;
R = -Zg+((t-1)/(t+1))*(1/(t+1))*Zm;
S = Zg + (1/(t+1))*Zm;

YAT1 = (1/M + 1/Q)/(P/Q - N/M);
YAT2 = (-2/M)/(P/Q - N/M);
YAT3 = (1/M - 1/Q)/(P/Q - N/M);
```

```
YAT4 = (P + N)/(N*Q - M*P);
YAT5 = (-2*P)/(N*Q - M*P);
YAT6 = (P - N)/(N*Q - M*P);
YAT7 = (1/R + 1/S)/(N/R - P/S);
YAT8 = (-2/R)/(N/R - P/S);
YAT9 = (1/R - 1/S)/(N/R - P/S);

Yat=ZBase*[YAT1  YAT2  YAT3
           YAT4  YAT5  YAT6
           YAT7  YAT8  YAT9];
end
```

(vii) Cal_Jbus.m: this file creates J-bus for power flow calculation.

```
function [G,H]=Cal_Jbus(Bdata,Icom1,Icom2)

global Ybus Jss1 Jss2 TV0mag TV0angle NB JBase

Vmag=TV0mag;
Vangle=TV0angle;
Ymag=abs(Ybus);
Yangle=angle(Ybus);

Icom1_x = (1/JBase)*real([Icom1; 0; -Icom1]);
Icom1_y = (1/JBase)*imag([Icom1; 0; -Icom1]);
Icom2_x = (1/JBase)*real([Icom2; 0; -Icom2]);
Icom2_y = (1/JBase)*imag([Icom2; 0; -Icom2]);

s=real(Jss1);
t=imag(Jss1);
s2=real(Jss2);
t2=imag(Jss2);
G = zeros(NB,1);
H = zeros(NB,1);

for k=1:NB
    Sx=Bdata(k,2);
    Sy=Bdata(k,3);
    A=Vmag(3*k-2,1)*cos(Vangle(3*k-2,1))-Vmag(3*k-
1,1)*cos(Vangle(3*k-1,1));
    B=Vmag(3*k-2,1)*sin(Vangle(3*k-2,1))-Vmag(3*k-
1,1)*sin(Vangle(3*k-1,1));
    X=(Vmag(3*k-2,1))^2+(Vmag(3*k-1,1))^2-2*Vmag(3*k-
2,1)*Vmag(3*k-1,1)*cos(Vangle(3*k-2,1)-Vangle(3*k-1,1));

    for h=1:3
        ih=3*k-3+h;
```

```
        G(ih,1)=0;
        H(ih,1)=0;
        for u=1:NB
            for m=1:3
                im=3*u-3+m;

G(ih,1)=G(ih,1)+Ymag(ih,im)*Vmag(im,1)*cos(Yangle(ih,im)+
Vangle(im,1));

H(ih,1)=H(ih,1)+Ymag(ih,im)*Vmag(im,1)*sin(Yangle(ih,im)+
Vangle(im,1));
            end
        end
        if k==1
            G(ih,1)=G(ih,1)-s(ih,1)-Icom1_x(ih,1);
            H(ih,1)=H(ih,1)-t(ih,1)-Icom1_y(ih,1);
        end
        if k==2
            G(ih,1)=G(ih,1)-s2(ih-3,1)-Icom2_x(ih-3,1);
            H(ih,1)=H(ih,1)-t2(ih-3,1)-Icom2_y(ih-3,1);
        end
        if h==1
            G(ih,1)=G(ih,1)+(Sx*A+Sy*B)/X;
            H(ih,1)=H(ih,1)+(Sx*B-Sy*A)/X;
        elseif h==2
            G(ih,1)=G(ih,1)-(Sx*A+Sy*B)/X;
            H(ih,1)=H(ih,1)-(Sx*B-Sy*A)/X;
        end
    end
end

return
```


(viii) Cal_Jacobian.m: this file creates Jacobian matrix for power flow calculation.

```
function [J1,J2,J3,J4]=Cal_Jacobian(Bdata)

global Ybus TV0mag TV0angle NB

Vmag=TV0mag;
Vangle=TV0angle;
Ymag=abs(Ybus);
Yangle=angle(Ybus);
J1 = zeros(3*NB,3*NB);
J2 = zeros(3*NB,3*NB);
```

```
J3 = zeros(3*NB,3*NB);
J4 = zeros(3*NB,3*NB);

for k=1:NB
    Sx=Bdata(k, 2);
    Sy=Bdata(k,3);
    X=(Vmag(3*k-2,1))^2+(Vmag(3*k-1,1))^2-2*Vmag(3*k-
2,1)*Vmag(3*k-1,1)*cos(Vangle(3*k-2,1)-Vangle(3*k-1,1));
    N=Vmag(3*k-2,1)*(Sx*cos(Vangle(3*k-
2,1))+Sy*sin(Vangle(3*k-2,1)))-Vmag(3*k-
1,1)*(Sx*cos(Vangle(3*k-1,1))+Sy*sin(Vangle(3*k-1,1)));
    M=Vmag(3*k-2,1)*(Sx*sin(Vangle(3*k-2,1))-
Sy*cos(Vangle(3*k-2,1)))-Vmag(3*k-
1,1)*(Sx*sin(Vangle(3*k-1,1))-Sy*cos(Vangle(3*k-1,1)));

    for u=1:NB
        for h=1:3
            ih=3*k-3+h;
            for m=1:3
                im=3*u-3+m;

J1(ih,im)=Ymag(ih,im)*cos(Yangle(ih,im)+Vangle(im,1));
                J2(ih,im)=-
Ymag(ih,im)*Vmag(im,1)*sin(Yangle(ih,im)+Vangle(im,1));

J3(ih,im)=Ymag(ih,im)*sin(Yangle(ih,im)+Vangle(im,1));

J4(ih,im)=Ymag(ih,im)*Vmag(im,1)*cos(Yangle(ih,im)+Vangle
(im,1));
                if (u==k)&(h==1)&(m==1)

J1(ih,im)=J1(ih,im)+(X*(Sx*cos(Vangle(3*k-
2,1))+Sy*sin(Vangle(3*k-2,1)))-N*(2*Vmag(3*k-2,1)-
2*Vmag(3*k-1,1)*cos(Vangle(3*k-2,1)-Vangle(3*k-
1,1))))/(X^2);
                    J2(ih,im)=J2(ih,im)+(X*Vmag(3*k-
2,1)*(-Sx*sin(Vangle(3*k-2,1))+Sy*cos(Vangle(3*k-2,1)))-
N*(2*Vmag(3*k-2,1)*Vmag(3*k-1,1)*sin(Vangle(3*k-2,1)-
Vangle(3*k-1,1))))/(X^2);

J3(ih,im)=J3(ih,im)+(X*(Sx*sin(Vangle(3*k-2,1))-
Sy*cos(Vangle(3*k-2,1)))-M*(2*Vmag(3*k-2,1)-2*Vmag(3*k-
1,1)*cos(Vangle(3*k-2,1)-Vangle(3*k-1,1))))/(X^2);
                    J4(ih,im)=J4(ih,im)+(X*Vmag(3*k-
2,1)*(Sx*cos(Vangle(3*k-2,1))+Sy*sin(Vangle(3*k-2,1)))-
M*(2*Vmag(3*k-2,1)*Vmag(3*k-1,1)*sin(Vangle(3*k-2,1)-
Vangle(3*k-1,1))))/(X^2);
                elseif (u==k)&(h==1)&(m==2)
```

```
                    J1(ih,im)=J1(ih,im)+(-
X*(Sx*cos(Vangle(3*k-1,1))+Sy*sin(Vangle(3*k-1,1)))-
N*(2*Vmag(3*k-1,1)-2*Vmag(3*k-2,1)*cos(Vangle(3*k-2,1)-
Vangle(3*k-1,1)))))/(X^2);
                    J2(ih,im)=J2(ih,im)+(-X*Vmag(3*k-
1,1)*(-Sx*sin(Vangle(3*k-1,1))+Sy*cos(Vangle(3*k-
1,1)))+N*(2*Vmag(3*k-2,1)*Vmag(3*k-1,1)*sin(Vangle(3*k-
2,1)-Vangle(3*k-1,1)))))/(X^2);
                    J3(ih,im)=J3(ih,im)+(-
X*(Sx*sin(Vangle(3*k-1,1))-Sy*cos(Vangle(3*k-1,1)))-
M*(2*Vmag(3*k-1,1)-2*Vmag(3*k-2,1)*cos(Vangle(3*k-2,1)-
Vangle(3*k-1,1)))))/(X^2);
                    J4(ih,im)=J4(ih,im)+(-X*Vmag(3*k-
1,1)*(Sx*cos(Vangle(3*k-1,1))+Sy*sin(Vangle(3*k-
1,1)))+M*(2*Vmag(3*k-2,1)*Vmag(3*k-1,1)*sin(Vangle(3*k-
2,1)-Vangle(3*k-1,1)))))/(X^2);
                elseif (u==k)&(h==2)&(m==1)
                    J1(ih,im)=J1(ih,im)-
((X*(Sx*cos(Vangle(3*k-2,1))+Sy*sin(Vangle(3*k-2,1)))-
N*(2*Vmag(3*k-2,1)-2*Vmag(3*k-1,1)*cos(Vangle(3*k-2,1)-
Vangle(3*k-1,1)))))/(X^2));
                    J2(ih,im)=J2(ih,im)-((X*Vmag(3*k-
2,1)*(-Sx*sin(Vangle(3*k-2,1))+Sy*cos(Vangle(3*k-2,1)))-
N*(2*Vmag(3*k-2,1)*Vmag(3*k-1,1)*sin(Vangle(3*k-2,1)-
Vangle(3*k-1,1)))))/(X^2));
                    J3(ih,im)=J3(ih,im)-
((X*(Sx*sin(Vangle(3*k-2,1))-Sy*cos(Vangle(3*k-2,1)))-
M*(2*Vmag(3*k-2,1)-2*Vmag(3*k-1,1)*cos(Vangle(3*k-2,1)-
Vangle(3*k-1,1)))))/(X^2));
                    J4(ih,im)=J4(ih,im)-((X*Vmag(3*k-
2,1)*(Sx*cos(Vangle(3*k-2,1))+Sy*sin(Vangle(3*k-2,1)))-
M*(2*Vmag(3*k-2,1)*Vmag(3*k-1,1)*sin(Vangle(3*k-2,1)-
Vangle(3*k-1,1)))))/(X^2));
                elseif (u==k)&(h==2)&(m==2)
                    J1(ih,im)=J1(ih,im)-((-
X*(Sx*cos(Vangle(3*k-1,1))+Sy*sin(Vangle(3*k-1,1)))-
N*(2*Vmag(3*k-1,1)-2*Vmag(3*k-2,1)*cos(Vangle(3*k-2,1)-
Vangle(3*k-1,1)))))/(X^2));
                    J2(ih,im)=J2(ih,im)-((-X*Vmag(3*k-
1,1)*(-Sx*sin(Vangle(3*k-1,1))+Sy*cos(Vangle(3*k-
1,1)))+N*(2*Vmag(3*k-2,1)*Vmag(3*k-1,1)*sin(Vangle(3*k-
2,1)-Vangle(3*k-1,1)))))/(X^2));
                    J3(ih,im)=J3(ih,im)-((-
X*(Sx*sin(Vangle(3*k-1,1))-Sy*cos(Vangle(3*k-1,1)))-
M*(2*Vmag(3*k-1,1)-2*Vmag(3*k-2,1)*cos(Vangle(3*k-2,1)-
Vangle(3*k-1,1)))))/(X^2));
                    J4(ih,im)=J4(ih,im)-((-X*Vmag(3*k-
1,1)*(Sx*cos(Vangle(3*k-1,1))+Sy*sin(Vangle(3*k-
```

```
1,1)))+M*(2*Vmag(3*k-2,1)*Vmag(3*k-1,1)*sin(Vangle(3*k-
2,1)-Vangle(3*k-1,1))))/(X^2));
                end
            end
        end
    end
end

return
```

(ix) build_ybus.m: this file creates Y-bus for power flow calculation.

```
function build_ybus(Ldata,Zcom1,Zcom2,t)

global NB Yss1 Yss2 Zoh Ybus Yat NTRACK YRE_ballast ZBase

Ybus=zeros(3*NB,3*NB);
if Ldata==0
nline = 0;
else
nline=size(Ldata,1);
end

for u=1:nline
    m=Ldata(u,1);
    n=Ldata(u,2);
    Ytemp=(1/Ldata(u,3))*inv(Zoh);
    YRE_ballast_half= (YRE_ballast/2)*Ldata(u,3);
    Ybus(3*m-2:3*m,3*n-2:3*n)=Ybus(3*m-2:3*m,3*n-2:3*n)-
Ytemp;
    Ybus(3*n-2:3*n,3*m-2:3*m)=Ybus(3*m-2:3*m,3*n-2:3*n);
    Ybus(3*m-2:3*m,3*m-2:3*m)=Ybus(3*m-2:3*m,3*m-
2:3*m)+Ytemp+YRE_ballast_half;
    Ybus(3*n-2:3*n,3*n-2:3*n)=Ybus(3*n-2:3*n,3*n-
2:3*n)+Ytemp+YRE_ballast_half;
end
ATbus = [3 4 5];
for u=1:NTRACK
    for v=1:length(ATbus)
        m = ATbus(v);
        Yat = YATcal(t(v));
        Ybus(3*m-2:3*m,3*m-2:3*m)=Ybus(3*m-2:3*m,3*m-
2:3*m)+Yat;
    end
end
Yrpc1 = ZBase*[1/Zcom1  0   -1/Zcom1 ;
                  0      0        0 ;
```

```
                -1/Zcom1   0     1/Zcom1];

Yrpc2 = ZBase*[1/Zcom2   0    -1/Zcom2 ;
                    0      0         0 ;
                -1/Zcom2   0     1/Zcom2];

Ybus(1:3,1:3)=Ybus(1:3,1:3)+Yss1+Yrpc1;
Ybus(4:6,4:6)=Ybus(4:6,4:6)+Yss2+Yrpc2;

return
```

E.4 Tap-changing AT programmes

The following file list is used in the tap-changing AT investigation.

(i) Tap_changing_test.m: this file is the main programme, varying tap positions and collecting the results of Part 1 in Chapter 5.

```
int_tap = 0.7;
f_tap = 1.4;
step = 0.01;
count = ((f_tap-int_tap)/step)+1;
tap1(1) = int_tap;
tap2(1) = int_tap;
tap3(1) = int_tap;
tap4(1) = int_tap;
tap5(1) = int_tap;
tap6(1) = int_tap;
Output = [];
x = [tap1(1) tap2(1) tap3(1) tap4(1) tap5(1) tap6(1)];

for i=1:count

[Output]=atpflow2(x);
VUF(i) = Output(1); % 1 = VUF (%)
IUF(i) = Output(2); % 2 = IUF (%)
pf3p(i) = Output(3); % 3 = three-phase power factor
pft(i) = Output(4); % 4 = Teaser power factor
pfm(i) = Output(5); % 5 = Main power factor
Ploss(i) = Output(6); % 6 = Power losses (MW)
P3p(i) = Output(7); % 7 = Three-phase power (MW)
Q3p(i) = Output(8); % 8 = Three-phase reactive power
(Mvar)
PT(i) = Output(9); % 9 = Teaser power (MW)
QT(i) = Output(10); % 10 = Teaser reactive power (Mvar)
```

```
PM(i) = Output(11); % 11 = Main power (MW)
QM(i) = Output(12); % 12 = Main reactive power (Mvar)
VD(i) = Output(13); % 13 = Voltage deviation (V)
VTCRmag(i) = Output(14); % 14 = TSS Teaser voltage
magnitude (CR) (kV)
VTCRang(i) = Output(15); % 15 = TSS Teaser voltage angle
(CR) (degree)
VMCRmag(i) = Output(16); % 16 = TSS Main voltage
magnitude (CR) (kV)
VMCRang(i) = Output(17); % 17 = TSS Main voltage angle
(CR) (degree)
VTFRmag(i) = Output(18); % 18 = TSS Teaser voltage
magnitude (FR) (kV)
VTFRang(i) = Output(19); % 19 = TSS Teaser voltage angle
(FR) (degree)
VMFRmag(i) = Output(20); % 20 = TSS Main voltage
magnitude (FR) (kV)
VMFRang(i) = Output(21); % 21 = TSS Main voltage angle
(FR) (degree)
VTCFmag(i) = Output(22); % 22 = TSS Teaser voltage
magnitude (CF) (kV)
VTCFang(i) = Output(23); % 23 = TSS Teaser voltage angle
(CF) (degree)
VMCFmag(i) = Output(24); % 24 = TSS Main voltage
magnitude (CF) (kV)
VMCFang(i) = Output(25); % 25 = TSS Main voltage angle
(CF) (degree)
VTrail(i) = Output(26); % 26 = TSS Teaser rail voltage
(V)
VMrail(i) = Output(27); % 27 = TSS Main rail voltage (V)
VtrT_rail(i) = Output(28); % 28 = Teaser train rail
voltage (V)
VtrM_rail(i) = Output(29); % 29 = Main train rail voltage
(V)
VtrTmag(i) = Output(30); % 30 = Teaser train voltage
magnitude (kV)
VtrTang(i) = Output(31); % 31 = Teaser train voltage
anglee (degree)
VtrMmag(i) = Output(32); % 32 = Main train voltage
magnitude (kV)
VtrMang(i) = Output(33); % 33 = Main train voltage anglee
(degree)
IC_Tmag(i) = Output(34); % 34 = IC_T mag
IR_Tmag(i) = Output(35); % 34 = IR_T mag
IF_Tmag(i) = Output(36); % 34 = IF_T mag
IC_Mmag(i) = Output(37); % 34 = IC_M mag
IR_Mmag(i) = Output(38); % 34 = IR_M mag
IF_Mmag(i) = Output(39); % 34 = IF_M mag
```

```
tap1(i+1) = tap1(i) + step;
tap2(i+1) = tap2(i) + step;
tap3(i+1) = tap3(i) + step;
tap4(i+1) = tap4(i) + step;
tap5(i+1) = tap5(i) + step;
tap6(i+1) = tap6(i) + step;
x = [tap1(i+1) tap2(i+1) tap3(i+1) tap4(i+1) tap5(i+1)
tap6(i+1)];

end

tap1 = tap1(1:end-1);
tap2 = tap2(1:end-1);
tap3 = tap3(1:end-1);
tap4 = tap4(1:end-1);
tap5 = tap5(1:end-1);
tap6 = tap6(1:end-1);
tap = tap1;

LabPos = 'north';
figure(1)
plot(tap,VUF)
grid on
ylabel('VUF (%)');
xlabel('tap setting');
axis([int_tap f_tap min(VUF)*0.99 max(VUF)*1.01]);
print('-f1','VUF','-dpng')
savefig('VUF.fig')

figure(2)
plot(tap,IUF)
grid on
ylabel('IUF (%)');
xlabel('tap setting');
axis([int_tap f_tap min(IUF)*0.99 max(IUF)*1.01]);
print('-f2','IUF','-dpng')
savefig('IUF.fig')

figure(3)
plot(tap,pf3p)
grid on
ylabel('three-phase power factor');
xlabel('tap setting');
axis([int_tap f_tap min(pf3p)*0.99 max(pf3p)*1.01]);
print('-f3','3p_PF','-dpng')
savefig('3p_PF.fig')
```

```
figure(4)
plot(tap,Ploss)
grid on
ylabel('Ploss (MW)');
xlabel('tap setting');
axis([int_tap f_tap min(Ploss)*0.99 max(Ploss)*1.01]);
print('-f4','Ploss','-dpng')
savefig('Ploss.fig')

figure(5)
plot(tap,P3p)
grid on
ylabel('Three phase power (MW)');
xlabel('tap setting');
axis([int_tap f_tap min(P3p)*0.99 max(P3p)*1.01]);
print('-f5','3p_P','-dpng')
savefig('3p_P.fig')

figure(6)
plot(tap,Q3p)
grid on
ylabel('Three phase reactive power (Mvar)');
xlabel('tap setting');
axis([int_tap f_tap min(Q3p)*0.99 max(Q3p)*1.01]);
print('-f6','3p_Q','-dpng')
savefig('3p_Q.fig')

figure(7)
plot(tap,PT)
grid on
ylabel('Teaser power (MW)');
xlabel('tap setting');
axis([int_tap f_tap min(PT)*0.99 max(PT)*1.01]);
print('-f7','T_P','-dpng')
savefig('T_P.fig')

figure(8)
plot(tap,QT)
grid on
ylabel('Teaser reactive power (Mvar)');
xlabel('tap setting');
axis([int_tap f_tap min(QT)*0.99 max(QT)*1.01]);
print('-f8','T_Q','-dpng')
savefig('T_Q.fig')

figure(9)
plot(tap,PM)
grid on
```

```
ylabel('Main power (MW)');
xlabel('tap setting');
axis([int_tap f_tap min(PM)*0.99 max(PM)*1.01]);
print('-f9','M_P','-dpng')
savefig('M_P.fig')

figure(10)
plot(tap,QM)
grid on
ylabel('Main reactive power (Mvar)');
xlabel('tap setting');
axis([int_tap f_tap min(QM)*0.99 max(QM)*1.01]);
print('-f10','M_Q','-dpng')
savefig('M_Q.fig')

figure(11)
plot(tap,VD/1e3)
grid on
ylabel('Voltage deviation (kV)');
xlabel('tap setting');
axis([int_tap f_tap min(VD/1e3)*0.99 max(VD/1e3)*1.01]);
print('-f11','VD','-dpng')
savefig('VD.fig')

figure(12)
plot(tap,VTCRmag,tap,VTFRmag)
grid on
ylabel('Teaser TSS voltage (kV)');
xlabel('tap setting');
legend('C-R','F-R','Location',LabPos);
axis([int_tap f_tap
min(min(VTCRmag)*0.99,min(VTFRmag)*0.99)
max(max(VTCRmag)*1.01,max(VTFRmag)*1.01)]);
print('-f12','T_TSS_Voltage','-dpng')
savefig('T_TSS_Voltage.fig')

figure(13)
plot(tap,VTCFmag)
grid on
ylabel('C-F Teaser TSS voltage (kV)');
xlabel('tap setting');
axis([int_tap f_tap min(VTCFmag)*0.99
max(VTCFmag)*1.01]);
print('-f13','CF_T_TSS_Voltage','-dpng')
savefig('CF_T_TSS_Voltage.fig')

figure(14)
plot(tap,VMCRmag,tap,VMFRmag)
```

```
grid on
ylabel('Main TSS voltage (kV)');
xlabel('tap setting');
legend('C-R','F-R','Location',LabPos);
axis([int_tap f_tap
min(min(VMCRmag)*0.99,min(VMFRmag)*0.99)
max(max(VMCRmag)*1.01,max(VMFRmag)*1.01)]);
print('-f14','M_TSS_Voltage','-dpng')
savefig('M_TSS_Voltage.fig')

figure(15)
plot(tap,VMCFmag)
grid on
ylabel('C-F Main TSS voltage (kV)');
xlabel('tap setting');
axis([int_tap f_tap min(VMCFmag)*0.99
max(VMCFmag)*1.01]);
print('-f15','CF_M_TSS_Voltage','-dpng')
savefig('CF_M_TSS_Voltage.fig')

figure(16)
plot(tap,VTrail,tap,VMrail)
grid on
ylabel('TSS rail voltage (V)');
xlabel('tap setting');
legend('Teaser','Main','Location',LabPos);
axis([int_tap f_tap
min(min(VTrail)*0.99,min(VMrail)*0.99)
max(max(VTrail)*1.01,max(VMrail)*1.01)]);
print('-f16','TSS_RailVoltage','-dpng')
savefig('TSS_RailVoltage.fig')

figure(17)
plot(tap,VtrT_rail,tap,VtrM_rail)
grid on
ylabel('Train rail voltage (V)');
xlabel('tap setting');
legend('Teaser','Main','Location',LabPos);
axis([int_tap f_tap
min(min(VtrT_rail)*0.99,min(VtrM_rail)*0.99)
max(max(VtrT_rail)*1.01,max(VtrM_rail)*1.01)]);
print('-f17','TrainRailVoltage','-dpng')
savefig('TrainRailVoltage.fig')

figure(18)
plot(tap,VtrTmag,tap,VtrMmag)
grid on
ylabel('Train voltage (kV)');
```

```
xlabel('tap setting');
legend('Teaser','Main','Location',LabPos);
axis([int_tap f_tap
min(min(VtrTmag)*0.99,min(VtrMmag)*0.99)
max(max(VtrTmag)*1.01,max(VtrMmag)*1.01)]);
print('-f18','TrainVoltage','-dpng')
savefig('TrainVoltage.fig')

figure(19)
plot(tap,IC_Tmag,tap,IR_Tmag,tap,IF_Tmag)
grid on
ylabel('I_{T} (A)');
xlabel('tap setting');
legend('IC','IR','IF','Location',LabPos);
axis([int_tap f_tap
min(min(IC_Tmag)*0.99,min(IR_Tmag)*0.8)
max(max(IC_Tmag)*1.01,max(IF_Tmag)*1.01)]);
print('-f19','IT','-dpng')
savefig('IT.fig')

figure(20)
plot(tap,IC_Mmag,tap,IR_Mmag,tap,IF_Mmag)
grid on
ylabel('I_{M} (A)');
xlabel('tap setting');
legend('IC','IR','IF','Location',LabPos);
axis([int_tap f_tap
min(min(IC_Mmag)*0.99,min(IR_Mmag)*0.8)
max(max(IC_Mmag)*1.01,max(IF_Mmag)*1.01)]);
print('-f20','IM','-dpng')
savefig('IM.fig')
```

(ii) main_TCAT_PSO. m: this file contains the code that runs the MATLAB's PSO toolbox for the AT's tap-changing optimisation.

```
%% Main code for minimising the fitness function using
PSO
ObjFcn = @LoadFlow_TCAT;
nvars = 6;
lb = [0.7 0.7 0.7 0.7 0.7 0.7];
ub = [1.4 1.4 1.4 1.4 1.4 1.4];

options =
optimoptions('particleswarm','SwarmSize',25,'Display','it
er','PlotFcn','pswplotbestf',...
```

```
    'StallIterlimit',50,'TolFun',1e-
3,'SelfAdjustment',0.5,'SocialAdjustment',1.6,...
    'ObjectiveLimit',1e-
10,'InitialSwarmSpan',2000,'InertiaRange',[0.4,0.8],'MinF
ractionNeighbors',0.25,...
    'MaxIter',6000);

[x,fval,exitflag] =
particleswarm(ObjFcn,nvars,lb,ub,options);
```

(iii) Supply_parameter_TCAT.m: this file contains the case study's traction power supply system parameters.

```
function Supply_parameter_TCAT(VA,VB,VC,a1,a2)

global NTRACK Tnum Jss1 Jss2 Yss1 Yss2 Zoh ZBase SBase
VBase Zshc YRE_ballast JBase
SBase=1e6;
VBase=25e3;
ZBase=VBase^2/SBase;
JBase=SBase/VBase;

NTRACK = 1;
Tnum = [2 0];
ZRE_ballast = 0.5;
YRE_ballast = ZBase/ZRE_ballast*[0 0 0;0 1 0;0 0 0];
Zoh=(1/ZBase)*[0.1192+0.7522i 0 0;
    0 0.1648+0.6709i 0;
    0 0 0.2036+0.8847i];

f=50; % frequency (Hz)
SCC=2.7e9; % Short circuit capacity
Zscc=(230e3)^2/SCC;
Rscc=Zscc/sqrt(1+(20)^2);
Xscc=sqrt(Zscc^2-Rscc^2);
Zsvc=(Rscc+1j*Xscc);
Zshc=Zsvc+(0.013+1j*0.039)*0;
Yse=1/4;
% For Scott transformer
Rp=0.01; % Resistance in primary side(ohm)
Rs=0.2; % Resistance in secondary side(ohm)
Lp=2.6526e-4; % Inductance in primary side(ohm)
Ls=2.6526e-3; % Inductance in secondary side(ohm)
Zp=(Rp+(2*pi*f*Lp)*1j);
Zs=(Rs+(2*pi*f*Ls)*1j);
ZA=Zp;
```

```
ZB=Zp/2;
ZC=Zp/2;

A = (2*VA-VB-VC)/(2*a1);
D = (VB-VC)/a2;
F = (4*ZA+ZB+ZC+8*Zs*a1^2)/(16*a1^2);
G = (4*ZA+ZB+ZC)/(16*a1^2);
H = (ZB+ZC)/(4*a2^2);
J = (ZB+ZC+2*Zs*a2^2)/(4*a2^2);

Jss1=(1/JBase)*(1/(G+F))*(A/2)*[1;0;-1];
Yss1 = ZBase*[F/(F^2-G^2) -1/(F-G) G/(F^2-G^2);
    -1/(F-G) (2/(F-G))+NTRACK*Yse -1/(F-G);
    G/(F^2-G^2) -1/(F-G) F/(F^2-G^2)];

Jss2=(1/JBase)*(1/(H+J))*(D/2)*[1;0;-1];
Yss2 = ZBase*[J/(J^2-H^2) -1/(J-H) H/(J^2-H^2);
    -1/(J-H) (2/(J-H))+NTRACK*Yse -1/(J-H);
    H/(J^2-H^2) -1/(J-H) J/(J^2-H^2)];

% For V/V transformer
% Rp=0.01; % Resistance in primary side(ohm)
% Rs=0.2; % Resistance in secondary side(ohm)
% Lp=2.6526e-4; % Inductance in primary side(ohm)
% Ls=2.6526e-3; % Inductance in secondary side(ohm)
% Zp=(Rp+(2*pi*f*Lp)*1j);
% Zs=(Rs+(2*pi*f*Ls)*1j);
% ze = 0;
% A = (Zp/(4*a^2))+(Zs/2);
% B = Zp/(4*a^2);
% Jss1=(1/JBase)*((VA-VB)/(2*a*(A+B)))*[1;0;-1];
% Yss1 = ZBase*(1/((A+B)*(2*ze+A-B)))*[A+ze  -A-B    B-ze
%      -A-B   2*(A+B)  -A-B
%      B-ze   -A-B    A+ze];
%
% Jss2=(1/JBase)*((VC-VB)/(2*a*(A+B)))*[1;0;-1];
% Yss2 = ZBase*(1/((A+B)*(2*ze+A-B)))*[A+ze  -A-B    B-ze
%      -A-B   2*(A+B)  -A-B
%      B-ze   -A-B    A+ze];

return
```

(iv) Network_config_TCAT.m: this file contains line data and bus data for power flow calculation.

```
function [Ldata,Bdata]=Network_config_TCAT()

global Tnum NB Tbus NTRACK TV0mag TV0angle

NB = 10;
%Trains are next to the TSS. P1
% Ldata = [3   9   5
%            9   4   5
%            4   5   10
%            5   1   10
%            2   6   10
%            6   7   10
%            7  10   5
%           10  8   5];

%Trains are next to the TSS. P2
Ldata = [3   4   10
         4   5   10
         5   9   5
         9   1   5
         2   10  5
        10  6   5
         6   7   10
         7   8   10];

PT = 7;
PM = 8;
PFt = 0.85;
PFm = 0.85;
P_T = PT;
Q_T = PT*sqrt(1-PFt^2)/PFt;
P_M = PM;
Q_M = PM*sqrt(1-PFm^2)/PFm;
Bdata = [1      0        0           0
         2      0        0           0
         3      0        0           2
         4      0        0           2
         5      0        0           2
         6      0        0           2
         7      0        0           2
         8      0        0           2
         9      P_T      Q_T         3
        10      P_M      Q_M         3];
```

```
NTRACK = 1;
Tnum = [2 0];
Tbus = [9 10];

TV0mag=zeros(3*NB,1);
TV0angle=zeros(3*NB,1);
Tphase = [1 3 4 5 9];
Mphase = [2 6 7 8 10];

%For Scott transformer
for u=1:NB
    for p=1:length(Tphase)
        if (u==Tphase(p))
        TV0mag(3*u-2,1)= 1.00;
        TV0mag(3*u-1,1)= 0.01;
        TV0mag(3*u,1)= -1.00;
        TV0angle(3*u-2,1)= 0;
        TV0angle(3*u-1,1)= 0;
        TV0angle(3*u,1)= 0;
        end
    end

    for q=1:length(Mphase)
        if (u==Mphase(q))
        TV0mag(3*u-2,1)= 1.00;
        TV0mag(3*u-1,1)= 0.01;
        TV0mag(3*u,1)= -1.00;
        TV0angle(3*u-2,1)= -pi/2;
        TV0angle(3*u-1,1)= -pi/2;
        TV0angle(3*u,1)= -pi/2;
        end
    end
end

%For V/V transformer
% for u=1:NB
%     for p=1:length(Tphase)
%         if (u==Tphase(p))
%         TV0mag(3*u-2,1)= 1.00;
%         TV0mag(3*u-1,1)= 0.01;
%         TV0mag(3*u,1)= -1.00;
%         TV0angle(3*u-2,1)= pi/6;
%         TV0angle(3*u-1,1)= pi/6;
%         TV0angle(3*u,1)= pi/6;
%         end
%     end
%
%     for q=1:length(Mphase)
```

```
%           if (u==Mphase(q))
%           TV0mag(3*u-2,1)= 1.00;
%           TV0mag(3*u-1,1)= 0.01;
%           TV0mag(3*u,1)= -1.00;
%           TV0angle(3*u-2,1)= pi/2;
%           TV0angle(3*u-1,1)= pi/2;
%           TV0angle(3*u,1)= pi/2;
%           end
%       end
% end

return
```

(v) LoadFlow_TCAT.m: this file is the main programme to execute power flow calculation.

```
function [Op_output]=LoadFlow_TCAT(x)

global TV0mag TV0angle NB Yss1 Yss2 Jss1 Jss2 Zshc VBase
JBase ZBase
t = x;
Vgrid = 230e3;
Vtrac = 50e3;
a1=(sqrt(3)/2)*(Vgrid/Vtrac);
a2=Vgrid/Vtrac;
a=Vgrid/Vtrac;
ph=exp(2*pi*1j/3);
va=Vgrid/sqrt(3);
vb=Vgrid*(ph^2)/sqrt(3);
vc=Vgrid*(ph)/sqrt(3);
VpccA(1,1)=va;
VpccB(1,1)=vb;
VpccC(1,1)=vc;
error_V(1,1)=1;
s=1;
while (error_V(s,1)>=1e-6)
    TV0mag=[];
    TV0angle=[];

Supply_parameter_TCAT(VpccA(s,1),VpccB(s,1),VpccC(s,1),a1
,a2); % use 'a' for V/V transformer
    [Ldata,Bdata]=Network_config_TCAT;
    build_ybus_TCAT(Ldata,t);
    k=0;
    [G,H]=Cal_Jbus_TCAT(Bdata);
    F=[G;H];
```

```
    max_err=max(abs(F));

    while (max_err>=1e-6)
        [A,B,C,D]=Calc_Jacobian_TCAT(Bdata);
        J=[A B;C D];
        dV=inv(J)*F;
        dV_mag=dV(1:3*NB,1);
        dV_angle=dV(3*NB+1:6*NB);
        TVmag=TV0mag-dV_mag;
        TV0mag=TVmag;
        TVangle=TV0angle-dV_angle;
        TV0angle=TVangle;
        k=k+1;
        [G,H]=Cal_Jbus_TCAT(Bdata);
        F=[G;H];
        max_err=max(abs(F));
        max_error(k,1)=max_err;
    end

    VD = 0;

    for u=1:NB
        TVCmag(u,1)=TV0mag(3*u-2,1)*VBase/1e3; % kV
        TVRmag(u,1)=TV0mag(3*u-1,1)*VBase; % V
        TVFmag(u,1)=TV0mag(3*u,1)*VBase/1e3; % kV

        TVCangle(u,1)=TV0angle(3*u-2,1);
        TVRangle(u,1)=TV0angle(3*u-1,1);
        TVFangle(u,1)=TV0angle(3*u,1);
    end

    for u=1:NB
        if TVCmag(u,1)<0
            TVCmag(u,1)=abs(TVCmag(u,1));
            TVCangle(u,1)=TVCangle(u,1)+pi;
        end
        if TVRmag(u,1)<0
            TVRmag(u,1)=abs(TVRmag(u,1));
            TVRangle(u,1)=TVRangle(u,1)+pi;
        end
        if TVFmag(u,1)<0
            TVFmag(u,1)=abs(TVFmag(u,1));
            TVFangle(u,1)=TVFangle(u,1)+pi;
        end

        VD = VD + abs(1e3*TVCmag(u,1)-(Vtrac/2)) +
abs(TVRmag(u,1)) + abs(1e3*TVFmag(u,1)-(Vtrac/2));
```

```
    end

    TVC=TVCmag.*cos(TVCangle)+1i*TVCmag.*sin(TVCangle);
    TVR=TVRmag.*cos(TVRangle)+1i*TVRmag.*sin(TVRangle);
    TVF=TVFmag.*cos(TVFangle)+1i*TVFmag.*sin(TVFangle);

    % For Scott transformer
    It = -
Yss1*(1/ZBase)*[TVC(1)*1e3;TVR(1);TVF(1)*1e3]+Jss1*JBase;
    Im = -
Yss2*(1/ZBase)*[TVC(2)*1e3;TVR(2);TVF(2)*1e3]+Jss2*JBase;
    ITC = It(1); ITR = It(2); ITF = It(3);
    IMC = Im(1); IMR = Im(2); IMF = Im(3);
    IA= ITC/(2*a1)-ITF/(2*a1);
    IB=(-1/(4*a1))*ITC+(1/(4*a1))*ITF+(1/(2*a2))*IMC-
(1/(2*a2))*IMF;
    IC=(-1/(4*a1))*ITC+(1/(4*a1))*ITF-
(1/(2*a2))*IMC+(1/(2*a2))*IMF;

    % For V/V transformer
%     Is1 = Jss1*JBase -
Yss1*(1/ZBase)*[TVC(1)*1e3;TVR(1);TVF(1)*1e3];
%     Is2 = Jss2*JBase -
Yss2*(1/ZBase)*[TVC(2)*1e3;TVR(2);TVF(2)*1e3];
%     I_1C = Is1(1); I_1R = Is1(2); I_1F = Is1(3);
%     I_2C = Is2(1); I_2R = Is2(2); I_2F = Is2(3);
%     Ip1 = (1/(2*a))*(I_1C-I_1F);
%     Ip2 = (1/(2*a))*(I_2C-I_2F);
%     IA = Ip1;
%     IB = -Ip1-Ip2;
%     IC = Ip2;

    Z=Zshc;
    Va=va-Z*IA;
    Vb=vb-Z*IB;
    Vc=vc-Z*IC;
    VpccA(s+1,1)=Va;
    VpccB(s+1,1)=Vb;
    VpccC(s+1,1)=Vc;
    error_V(s+1,1)=max([abs(VpccA(s+1,1)-VpccA(s,1))
abs(VpccB(s+1,1)-VpccB(s,1)) abs(VpccC(s+1,1)-
VpccC(s,1))]);
    s=s+1;
end

Vab=Va-Vb;
Vbc=Vb-Vc;
Vca=Vc-Va;
```

```
V0=(1/3)*(Va+Vb+Vc);
V1=(1/3)*(Va+ph*Vb+Vc*(ph)^2);
V2=(1/3)*(Va+Vb*(ph)^2+Vc*ph);
Vp=(1/3)*(Vab+ph*Vbc+Vca*(ph)^2);
Vn=(1/3)*(Vab+Vbc*(ph)^2+Vca*ph);
I0=(1/3)*(IA+IB+IC);
I1=(1/3)*(IA+ph*IB+IC*(ph)^2);
I2=(1/3)*(IA+IB*(ph)^2+IC*ph);
VUF = abs(V2/V1)*100;
IUF = abs(I2/I1)*100;
S3p = Va*conj(IA)+Vb*conj(IB)+Vc*conj(IC);
ST = TVC(1)*1e3*conj(ITC) + TVR(1)*conj(ITR) +
TVF(1)*1e3*conj(ITF);
SM = TVC(2)*1e3*conj(IMC) + TVR(2)*conj(IMR) +
TVF(2)*1e3*conj(IMF);
pf3p = real(S3p)/abs(S3p);
pft = real(ST)/abs(ST);
pfm = real(SM)/abs(SM);
Ploss = (real(S3p)/1e6)-(Bdata(9,2)+Bdata(10,2));
Op_output = 1/pf3p; %Select variables for minimisation
```

(vi) YATcal.m: this file calculates the AT's admittance matrix.

The code is the same as that of YATcal.m in the optimal RPC sizing programme.

(vii) Cal_Jbus_TCAT.m: this file creates J-bus for power flow calculation.

```
function [G,H]=Cal_Jbus_TCAT(Bdata)

global Ybus Jss1 Jss2 TV0mag TV0angle NB

Vmag=TV0mag;
Vangle=TV0angle;
Ymag=abs(Ybus);
Yangle=angle(Ybus);

s=real(Jss1);
t=imag(Jss1);
s2=real(Jss2);
t2=imag(Jss2);
G = zeros(NB,1);
H = zeros(NB,1);

for k=1:NB
    Sx=Bdata(k,2);
    Sy=Bdata(k,3);
```

```
    A=Vmag(3*k-2,1)*cos(Vangle(3*k-2,1))-Vmag(3*k-
1,1)*cos(Vangle(3*k-1,1));
    B=Vmag(3*k-2,1)*sin(Vangle(3*k-2,1))-Vmag(3*k-
1,1)*sin(Vangle(3*k-1,1));
    X=(Vmag(3*k-2,1))^2+(Vmag(3*k-1,1))^2-2*Vmag(3*k-
2,1)*Vmag(3*k-1,1)*cos(Vangle(3*k-2,1)-Vangle(3*k-1,1));

    for h=1:3
        ih=3*k-3+h;
        G(ih,1)=0;
        H(ih,1)=0;
        for u=1:NB
            for m=1:3
                im=3*u-3+m;

G(ih,1)=G(ih,1)+Ymag(ih,im)*Vmag(im,1)*cos(Yangle(ih,im)+
Vangle(im,1));

H(ih,1)=H(ih,1)+Ymag(ih,im)*Vmag(im,1)*sin(Yangle(ih,im)+
Vangle(im,1));
            end
        end
        if k==1
            G(ih,1)=G(ih,1)-s(ih,1);
            H(ih,1)=H(ih,1)-t(ih,1);
        end
        if k==2
            G(ih,1)=G(ih,1)-s2(ih-3,1);
            H(ih,1)=H(ih,1)-t2(ih-3,1);
        end
        if h==1
            G(ih,1)=G(ih,1)+(Sx*A+Sy*B)/X;
            H(ih,1)=H(ih,1)+(Sx*B-Sy*A)/X;
        elseif h==2
            G(ih,1)=G(ih,1)-(Sx*A+Sy*B)/X;
            H(ih,1)=H(ih,1)-(Sx*B-Sy*A)/X;
        end
    end
end

return
```

(viii) Cal_Jacobian_TCAT.m: this file creates Jacobian matrix for power flow calculation.

The code is the same as that of Cal_Jacobian.m in the optimal RPC sizing programme.

(ix) build_ybus_TCAT.m: this file creates Y-bus for power flow calculation.

```
function build_ybus_TCAT(Ldata,t)

global NB Yss1 Yss2 Zoh Ybus Yat NTRACK YRE_ballast

Ybus=zeros(3*NB,3*NB);
if Ldata==0
nline = 0;
else
nline=size(Ldata,1);
end

for u=1:nline
    m=Ldata(u,1);
    n=Ldata(u,2);
    Ytemp=(1/Ldata(u,3))*inv(Zoh);
    YRE_ballast_half= (YRE_ballast/2)*Ldata(u,3);
    Ybus(3*m-2:3*m,3*n-2:3*n)=Ybus(3*m-2:3*m,3*n-2:3*n)-
Ytemp;
    Ybus(3*n-2:3*n,3*m-2:3*m)=Ybus(3*m-2:3*m,3*n-2:3*n);
    Ybus(3*m-2:3*m,3*m-2:3*m)=Ybus(3*m-2:3*m,3*m-
2:3*m)+Ytemp+YRE_ballast_half;
    Ybus(3*n-2:3*n,3*n-2:3*n)=Ybus(3*n-2:3*n,3*n-
2:3*n)+Ytemp+YRE_ballast_half;
end
ATbus = [3 4 5 6 7 8];
for u=1:NTRACK
    for v=1:length(ATbus)
        m = ATbus(v);
        Yat = YATcal(t(v));
        Ybus(3*m-2:3*m,3*m-2:3*m)=Ybus(3*m-2:3*m,3*m-
2:3*m)+Yat;
    end
end

Ybus(1:3,1:3)=Ybus(1:3,1:3)+Yss1;
Ybus(4:6,4:6)=Ybus(4:6,4:6)+Yss2;

return
```

BIOGRAPHY

Kritsada Mongkoldee was born on November 13, 1992 in Lampang, Thailand. He earned the Bachelor's Degree in Electrical Engineering from Suranaree University of Technology (SUT) in 2015. Then, he continued his doctoral degree in Electrical Engineering at School of Electrical Engineering, Institute of Engineering at Suranaree University of Technology. His expertise and field of research include railway electrification, power system analysis, and power quality in electrified railway.